Towards very high energy density insulated Rare-EarthBaCuO magnets

André-Julien Vialle

THÈSE

Pour obtenir le grade de

DOCTEUR DE L'UNIVERSITÉ GRENOBLE ALPES

Spécialité : GENIE ELECTRIQUE

Arrêté ministériel : 25 mai 2016

Présentée par

André-Julien VIALLE

Thèse dirigée par **Pascal TIXADOR**
et codirigée par **Arnaud BADEL**, CNRS

préparée au sein du **Laboratoire Institut Néel**
dans **l'École Doctorale Electronique, Electrotechnique, Automatique, Traitement du Signal (EEATS)**

Vers des aimants isolés en Terre-Rare-BaCuO à très haute densité énergétique

Towards very high energy density insulated Rare-EarthBaCuO magnets

Thèse soutenue publiquement le **24 mai 2022**,
devant le jury composé de :

Monsieur Thierry KLEIN
PROFESSEUR DES UNIVERSITES, Institut Néel, Président
Monsieur Carmine SENATORE
PROFESSEUR DES UNIVERSITES, Université de Genève, Rapporteur
Monsieur Marc DHALLE
PROFESSEUR ASSOCIE, Université de Twente, Rapporteur
Monsieur Alexandre TORRE
INGENIEUR, CEA Cadarache, Examinateur
Monsieur Arnaud BADEL
CHARGE DE RECHERCHE, G2Elab, Encadrant de thèse
Monsieur Pascal TIXADOR
PROFESSEUR DES UNIVERSITES, G2Elab, Directeur de thèse
Monsieur Frédérick FOREST
INGENIEUR, Sigmaphi, Invité
Monsieur Francois REPTIN
INGENIEUR, DGA, Invité

Acknowledgements

Je souhaite en premier lieu remercier mes encadrants Arnaud et Pascal. Merci pour votre confiance, votre disponibilité et votre encadrement au quotidien. Je vous remercie également pour votre soutien, ainsi que vos nombreux conseils et remarques qui ont rendu ce travail si passionnant et enrichissant. Enfin, je vous suis grandement reconnaissant d'avoir pu rendre ce projet de doctorat possible.

Je tiens maintenant à remercier chaleureusement les membres du jury pour m'avoir fait l'honneur d'évaluer mes travaux ainsi que pour l'intérêt qu'ils ont portés à cette thèse.

Un grand merci également à mes camarades de thèse Alex et Blandine avec qui j'ai partagé mon quotidien. Merci pour tous les bons moments passés ensemble qui ont rendu ces années de travail si agréables.

Merci Momo pour m'avoir toujours apporté un appui sans faille durant tout mon cursus, et pour avoir toujours répondu présent lorsque qu'il fallait réaliser des boitiers électroniques.

Mes remerciements vont aussi envers à Guillaume DONNIER-VALENTIN pour avoir accepté que je consacre la totalité de mon temps à ce projet de doctorat.

Enfin, je tiens à remercier ma famille de m'avoir encouragé et d'avoir cru en moi durant toutes ces années. Et pour finir, un très grand merci à ma compagne Pauline, pour son soutien constant, sa patience et tout ce qu'elle m'apporte dans la vie de tous les jours.

Table of contents

General Introduction

High Temperature Superconductors are the key solution for the development of superconducting magnets with fields far above the limit imposed by conventional Low Temperature Superconducting (23.5 T with Nb_3Sn at 1.8 K). HTS REBCO conductors (Rare-Earths-BaCuO) are the most promising. They make it possible to design coils with very high energy densities, as they combine high critical current densities under strong magnetic field and very high mechanical strength. This makes them particularly interesting for the generation of high magnetic fields.

For some years now, REBCO-coated conductor tapes have been available in sufficient lengths for the realization of large-scale devices, and the first high-temperature superconducting (HTS) magnets have appeared, especially for high field [1, 2, 3]. However, REBCO magnets are not yet widespread. There are still many failures and even if some realizations present impressive performances in terms of magnetic field and current density, they do not fully use the material performances. This is because the implementation of REBCO materials remains difficult, first of all due to the risk of destructive thermal runaway. Indeed, REBCO tapes are thermally very stable and the propagation speed of dissipative zones is slow (a few cm/s). They present at the same time local millimetric variations of their critical current. This leads to a risk of destructive localized thermal runaway due to local overstepping of the critical current at the defects positions.

Protection strategies for REBCO windings are therefore a major topic of study, with the aim to guarantee safe operating conditions for these magnets. In recent years, new winding strategies have emerged to tackle these protection problems. Non-insulated and metal insulated windings, where the absence of insulation between turns enables the current to flow from one turn to the other so that the current can bypass the turns where dissipation occurs, have been successfully introduced [4, 5, 6]. These innovative winding technologies provide a combination of operating stability and protection in the event of a dissipative state. However, these protection methods can present other problems and are limited in terms of dynamics, making them impractical for fast transient applications such as SMES (Superconducting Magnetic Energy Storage).

This PhD work focuses specifically on insulated REBCO windings and is conducted in the framework of the BOSSE project. The objective is the realization of a high energy density SMES with high power output. This is not the first program dedicated to the realization of a SMES in Grenoble. A previous SMES of 800 kJ realized with the first generation of HTS BSCCO superconductors and entirely cooled by conduction was realized in 2009. In the continuity of this work, the BOSSE magnet for "BObine Supraconductrice pour le Stockage d'Energie" aims at developing a new SMES of 1 MJ by emphasizing the high energy density and the compactness of the device thanks to the spectacular performances of REBCO superconductors. The 12 T magnet is cooled by liquid helium and achieves a specific energy density of 20 kJ/kg for the superconducting winding, nearly double the current world record of 13 kJ/kg.

After a brief introduction to the phenomenon of superconductivity and superconducting materials, the first chapter focuses on REBCO materials. The properties and specificities that distinguish them from other superconducting materials used in the development of high field magnets are highlighted. Then, the different technical challenges to be met in the realization of REBCO windings are exposed. These include the winding itself, the splices, the management of mechanical stresses as well as the protection problems.

Our research team has been working for several years on the protection of REBCO insulated windings. It was established in previous works that reliable protection against thermal runaway can be achieved

through a highly sensitive detection system that provides early detection of the occurrence of a dissipative zone. The main difficulty of this strategy is the need to detect a small variation of the voltage signal, embedded in a much higher magnitude signal (inductive voltage due to the magnet load) often very noisy since the coil can be compared to an antenna. Chapter II presents an in-depth analysis of the transient electromagnetic behavior of REBCO insulated coils. This study was conducted experimentally and numerically on a highly instrumented test coil, enabling a detailed interpretation of the measured voltages.

The third chapter is dedicated to the works conducted on the BOSSE solenoid. After a short introduction on SMES, the description of the BOSSE solenoid and the history of the project until the beginning of this PhD work are presented. Then, the tests of the Double Pancake (DP) prototype in self and background magnetic field are presented. They aimed to evaluate the critical current and confirm the design. In order to validate the electromagnetic performance of the 21 DPs, each of them is tested in liquid helium up to its rated current. The performances of the 17 DPs already tested and validated are also presented. Finally, the tests and results of 2 preliminary assemblies of 3 and 5 DPs are presented. These assemblies have been tested with two different protection philosophies in order to validate the protection strategies of the device at full scale.

Finally, based on the knowledge gained from these new developments, the last chapter proposes a new high-performance REBCO coil design with conduction cooling capability. First, the design, fabrication, and testing of a simplified, partially impregnated insulated prototype pancake with conductive cooling capability are presented. This pancake consists of a single REBCO conductor insulated by a polyimide coating and uses the so-called edge impregnation concept. Following this promising initial result, we then present the design of a larger high-performance insulated REBCO pancake with conductive cooling capability for a high magnetic field insert.

Chapter I:
Superconductivity and REBCO for magnets

Summary

This chapter is a brief introduction to superconductivity and more specifically to the use of REBCO high temperature superconductors for magnets. The most relevant characteristics of superconductivity for large scale applications will be briefly presented in section 1. The specific properties of REBCO HTS materials, with their advantages and drawbacks, will be presented in section 2. Finally, the last section is devoted to the technical challenges to be met for the realization of REBCO magnets.

I.1 Characteristics of the superconducting state

I.1.1 Discovery of the superconducting state

The phenomenon of superconductivity was discovered in 1911. The liquefaction of helium at 4.2 K in 1908 by the physicist Heike Kamerlingh Onnes allowed him to discover by chance the superconducting state of mercury in April 1911 [7]. He then improved the precision of his experiment to obtain on October 26, 1911 an experimental measurement of the unmeasurable resistivity of mercury (Fig.1).

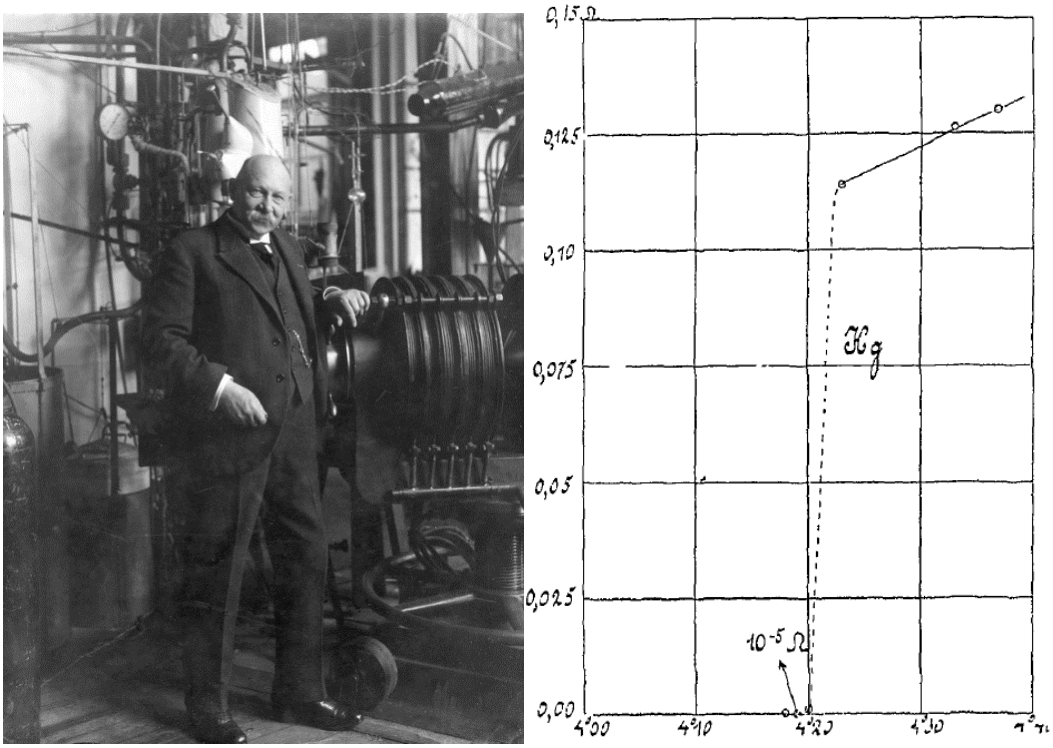

Fig. 1. Professor Dr Heike Kamerlingh Onnes on the left and the resistivy of mercury versus temperature measured by K.Onnes's team in October 1911 on the right.

Superconductivity appears when some metals or alloys are cooled to very low temperatures. It is characterized by specific electrical, magnetic and quantum properties. The temperature at which the material becomes superconducting is called critical temperature (T_c).

Throughout the history of superconductivity, chemists and physicists have been striving to discover and develop superconducting materials with improved performances: with higher critical temperatures but also with higher current carrying capabilities even under high magnetic field [8]. For most superconducting materials, colloquially referred as "classical" or "conventional" superconductors, T_c is below 30 K, which requires cooling with liquid helium. These materials are usually in the form of metal alloys.

The continuous search for materials with ever higher critical temperatures lead to a breakthrough at the end of the 80's with the discovery of a new family of superconducting materials, which became referred

as “High Temperature Superconductors”. Fig. 2 shows the evolution of the critical temperatures of the discovered superconductors until recent years.

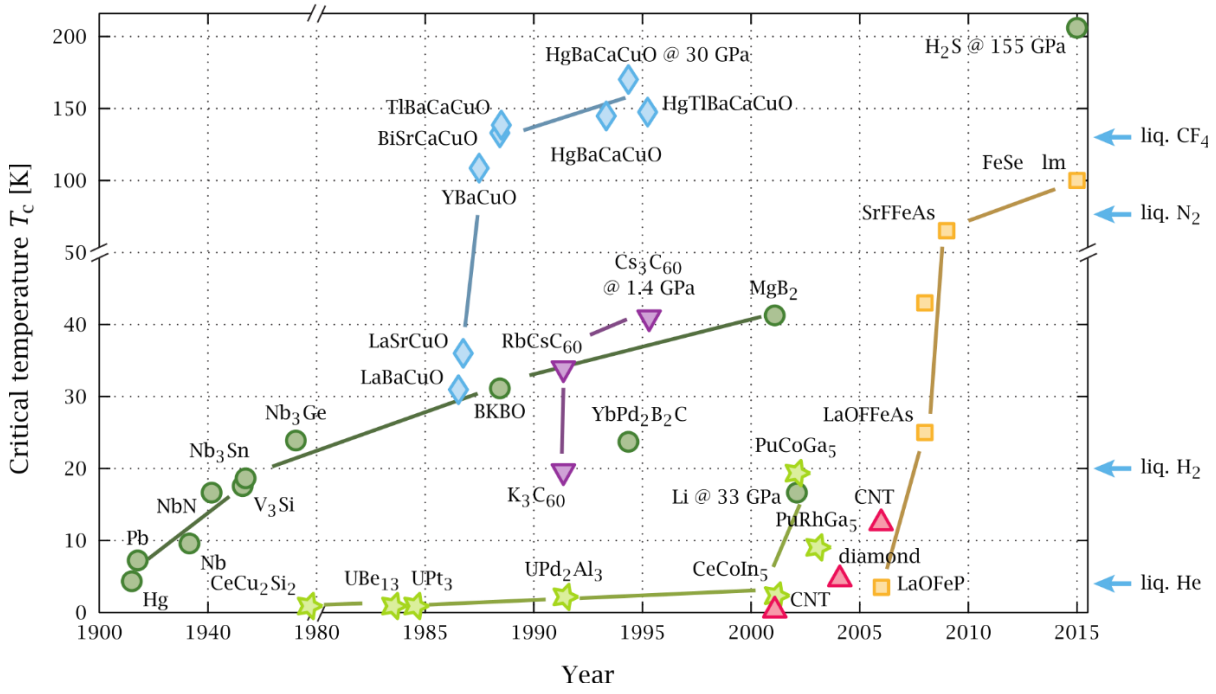

Fig. 2. Superconductor critical temperature as a function of their year of discovery [8].

I.1.2 The two main properties of the superconducting state

Superconductivity is a state of matter in which a remarkable combination of electrical and magnetic properties is found. Unlike conventional conductors, superconductors exhibit zero static resistivity under certain magnetic field and temperature conditions. It offers no resistance to the flow of an electrical current that can pass through the material without dissipating energy by Joule effect.

Another famous property is perfect diamagnetism, but only under very specific magnetic field conditions. This field expulsion phenomenon is called the Meissner effect, after the physicist who first observed it in 1933. Indeed, for weak external magnetic field, the field is “expelled” from the material as surface currents are cancelling it. Nevertheless, this phenomenon disappears above a certain critical field, which is usually quite low (few hundreds of mT) so that it does not have practical use in large scale applications.

I.1.3 Two types of superconductors

Superconductors may be grouped into two families, depending on what happen when the material is submitted to a magnetic field high enough that the Meissner effect disappears. For Type I materials, beyond the critical value H_c at which Meissner effect disappears, the superconducting state is lost abruptly in the whole material.

Type II superconductors on the contrary show the Meissner state up to a first critical field H_{c1}, where parts of the material remain superconducting beyond it, up to a second critical field called H_{c2} [9] (Fig. 3). Between H_{c1} and H_{c2} the magnetic flux starts to penetrate in the material in a way that will be described more in the next part. H_{c2} can be very large (several Teslas or even tens of Teslas).

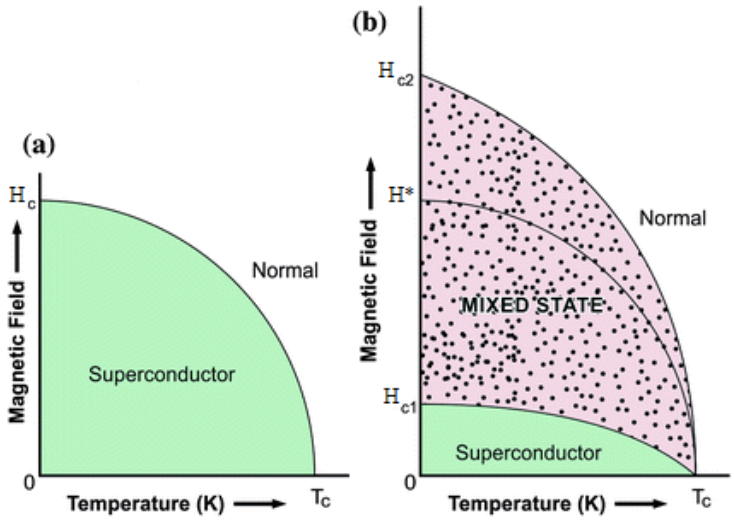

Fig. 3. Phase diagrams for the two types of superconductors: (a) type I superconductors, (b) type II superconductors. Inspired by [9].

In practice, type II superconductors cannot be used up to H_{c2}, they are limited by the irreversibility field, denoted H* (Fig. 3 b). Above this irreversibility field the lossless transport carrying capability is lost, even though the material is still superconducting. Fig. 4 shows the irreversibility fields of the most commonly used superconducting conductors in magnet manufacturing [10]. In the next part, we will see that this phenomenon is associated with vortices, vortex pinning and critical current.

Thanks to their larger domain of operation (both in terms of applied field and temperature), Type II superconductors have made it possible to use superconductivity for high magnetic field applications, for magnetic resonance imaging (MRI) and Nuclear Magnetic Resonance (NMR) among others. That is why in the rest of this work, we will focus only on this type of superconductor and their behavior in the mixed state.

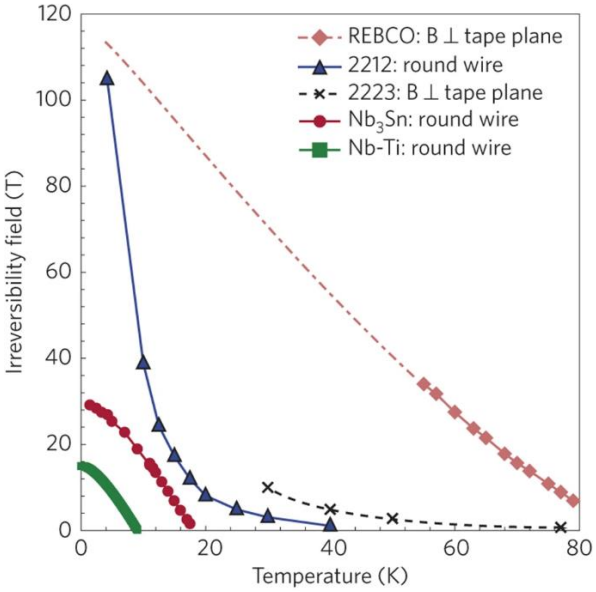

Fig. 4. Data at 4.2 K on the upper critical field or irreversibility field for the most commonly used superconducting conductors in magnet manufacturing. The great opportunities offered by REBCO at temperatures well above 4 K are clear [10].

I.1.4 Mixed state: vortices dynamics for type II superconductors

When the magnetic field exceeds H_{c1} in type II superconductors, a state of minimum energy can exist where the magnetic field penetrate locally through vortices. The cores of these vortices are like columns or tubes through the sample and are in the normal state. Each vortex carries a quantum of flux ($\Phi_0 = h/(2e) \approx 2\times10^{-15}$ Wb) that follows the magnetic field orientation (Fig. 5).

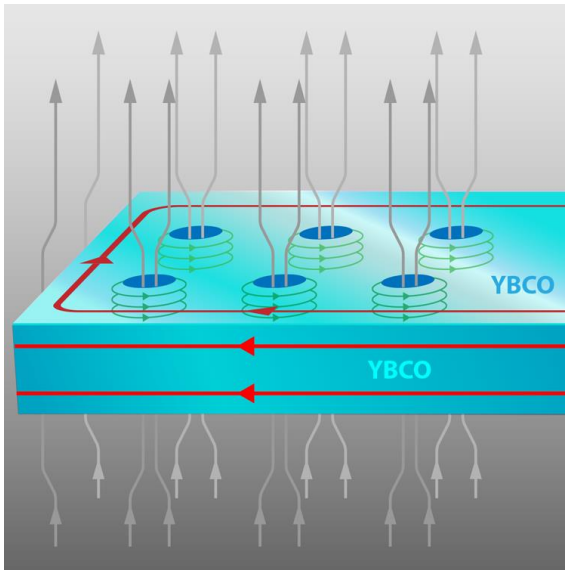

Fig. 5. Representation of the mixed state. A magnetic field (shown in grey) penetrates through vortices: a kind of non-superconducting "tunnel" through which a quantum of magnetic flux passes. Supercurrents (in green) around the vortex cores shield the rest of the material.

The existence of this trade-off between Superconducting and Normal state in the form of vortices was proposed by Abrikosov in 1952 [11]. This phenomenon can be visualized with a magnetic powder over a superconductor in the mixed state.

In the mixed state, even if the field expulsion and diamagnetism no longer exist, the electric current can flow in the parts that remain superconducting. However, the vortices may interact with the current flow and their movement due to Lorenz force causes dissipation. Non dissipative state can thus only be reached if the vortices are immobilized. The critical current density J_c is the one that creates a Lorentz force high enough to displace the vortices.

As the vortices interact with each other, forming a lattice, it only takes a few of them to be blocked to freeze the whole lattice. The vortex pinning can be due to microstructural defects in the material, which occur naturally (crystal joints) and/or can be introduced on purpose during the fabrication to enhance the critical current.

I.1.5 Critical surfaces

In practical large scale applications of Type II superconductors, current transport must be lossless and it is essential to know the limits of the non-dissipative domain of operation. That domain is limited by three quantities defining a critical surface beyond which the material goes to a dissipative state, characterized by the appearance of an electric field: The critical temperature (T_c), the irreversibility magnetic field (H_{irr} or H*), and the critical current density (J_c). T_c is intrinsic to the material whereas H_{irr} as well as J_c are more dependent on the fabrication process [12]. These parameters define the critical surface below which the material is in a non-dissipative state and beyond which it becomes dissipative. Fig. 6 shows some examples of critical surfaces for different superconductors.

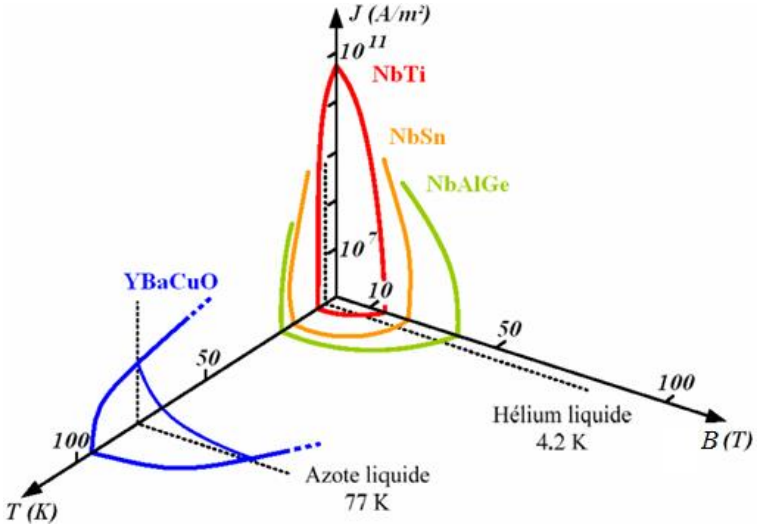

Fig. 6. Critical surfaces of different superconductors [12].

I.1.6 Power Law E(J)

The behavior of vortices and their motion as a function of J, B, and T is complex to describe and is not the subject of this PhD. From an electrical point of view, the transport of a current density J in a superconductor generates the movement of vortices or the vibration of their lattice. It is accompanied by the creation of an electric field (E (V/m)). This electrical behavior is illustrated in Fig. 7.

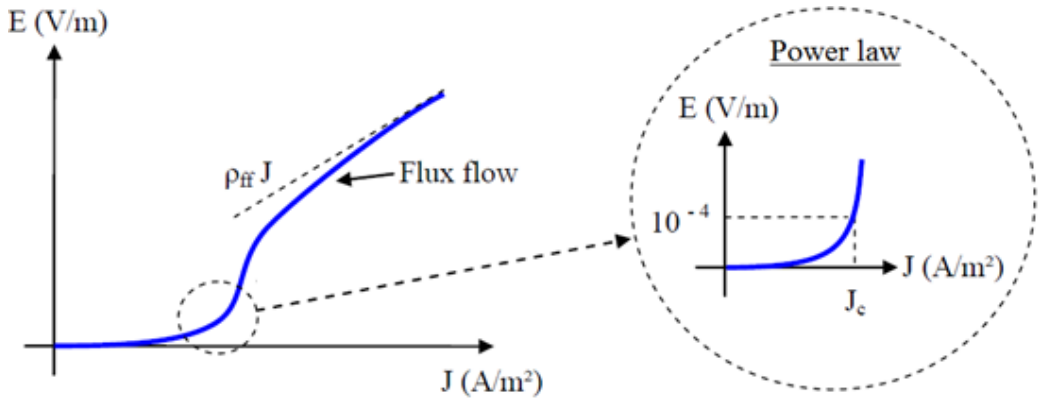

Fig. 7. Characteristic E (J) of a superconductor.

Two operating regimes can be observed in the E(J) characteristic of a superconductor. An exponential part and an almost linear part called Flux Flow. The Flux Flow regime appears when the current density J exceeds significantly the critical value J_c. The vortices are moving freely in the superconductor, causing dissipation and an electrical field which is proportional to the current density, like in the case of the normal state. For this reason, the coefficient of proportionality is usually called "flux flow resistivity". Because the dissipation in this regime is very high, the temperature cannot remain stable so devices do not usually operate in this regime. The use of a superconductor is of interest only for current densities J lower or close to J_c. This corresponds to the first part of the E(J) characteristic, which can be found empirically to follow a power law (Eq. 1). As the E(J) relationship is continuous, the "limit" J_c is defined arbitrarily. The usual criterion E_c criterion is 1 µV/cm for HTS, and often only 0.1 µV/cm for LTS conductors. In any case, as soon as *n* is large enough (greater than 30), the value chosen for E_c has little influence on the value of the estimated critical current density.

$$E(J) = E_c * \left(\frac{J}{J_c}\right)^n$$

Equation 1

E and J the electric field and the current density going through the superconductor respectively, E_c the critical field criterion, *n* the power law index. The value of *n* depends not only on the material and its manufacture but also on T_c and H_c.

The critical current density is then unambiguously defined. This law represents well the electrical behavior of practical superconducting materials for current densities close to J_c (Fig. 8).

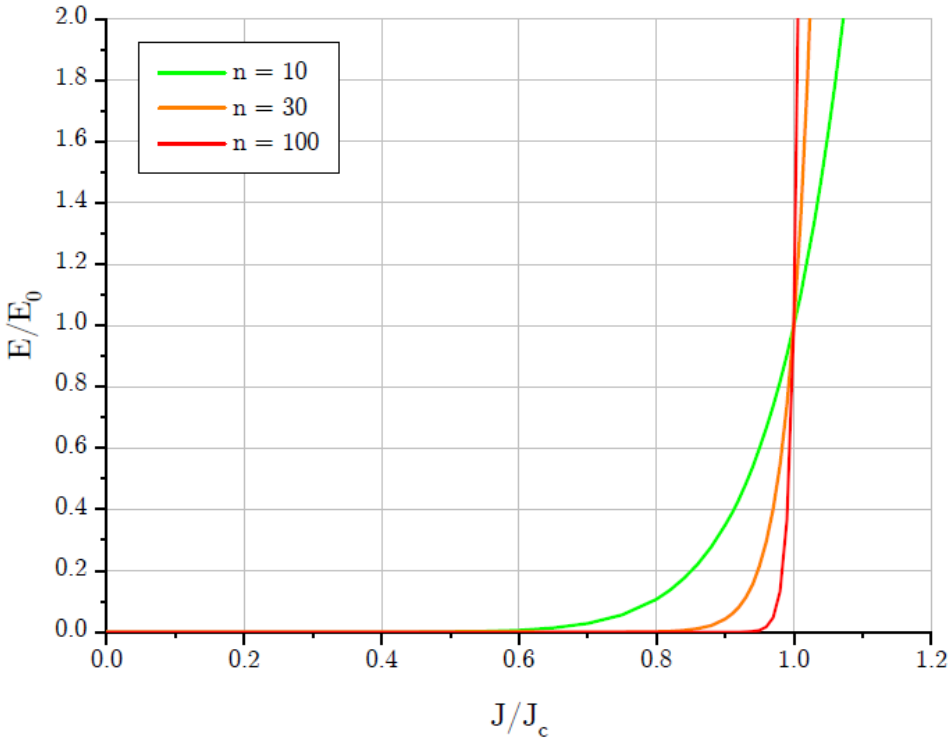

Fig. 8. Power Law fitting from experimental results on a short sample characterization.

I.1.7 Macroscopic behavior

If the power law fits well numerical simulation, it is not convenient for analytical consideration. The Critical State Model (CSM) was proposed for analytical approach. The CSM is based on an approximation of the E(J) relationship by step function. This results into a binary distribution of the local current density inside the superconductor, which becomes either zero or ± J_c (Fig. 9). In Maxwell's equations, this translates into:

$$\overrightarrow{rot}\vec{B} = \mu_0 \vec{J_c}$$

Or $\overrightarrow{rot}\vec{B} = 0$

Equation 2

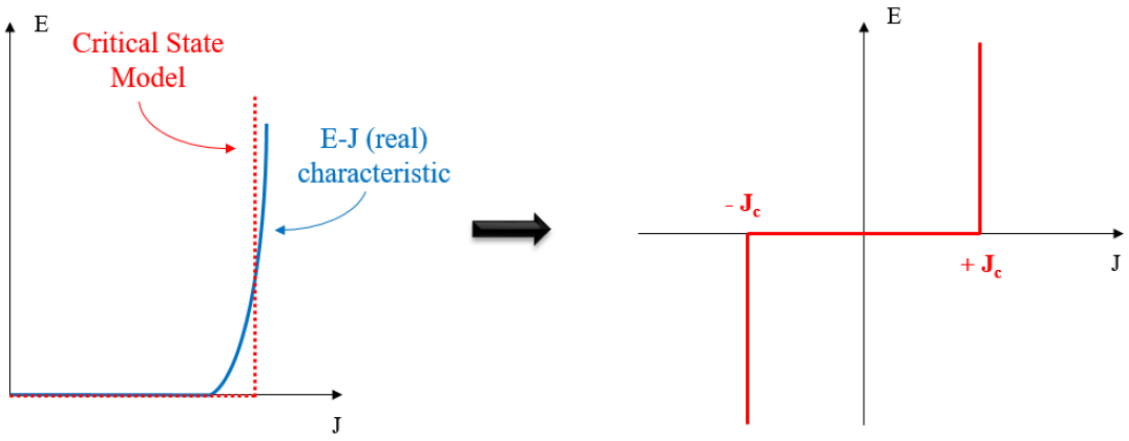

Fig. 9. E(J) relation versus Critical State Model

Fig. 10 is a simple example that can be derived from the CSM hypotheses to understand what happens in a superconducting ring when it is exposed to a current variation. From (1) to (2), the transport current increases from zero to a certain amplitude value (2). The current starts to enter the superconductor from the edges with a local current density equal to $+J_c$. If we stay in (2), the current remains in the external ring leaving the central part free of any current. Then the transport current decreases from (2) to (4) passing through 0 (3). Since only critical values of current density ± J_c can exist inside the superconducting material, the current starts to penetrate inside the material from the edges but with the value of $-J_c$. In (3), when the transport current is zero, there are still current densities inside the material. Practically, a closed current loop has formed. This feature is called hysteresis. Finally, from (3) to (4), the $-J_c$ current densities become predominant inside the material.

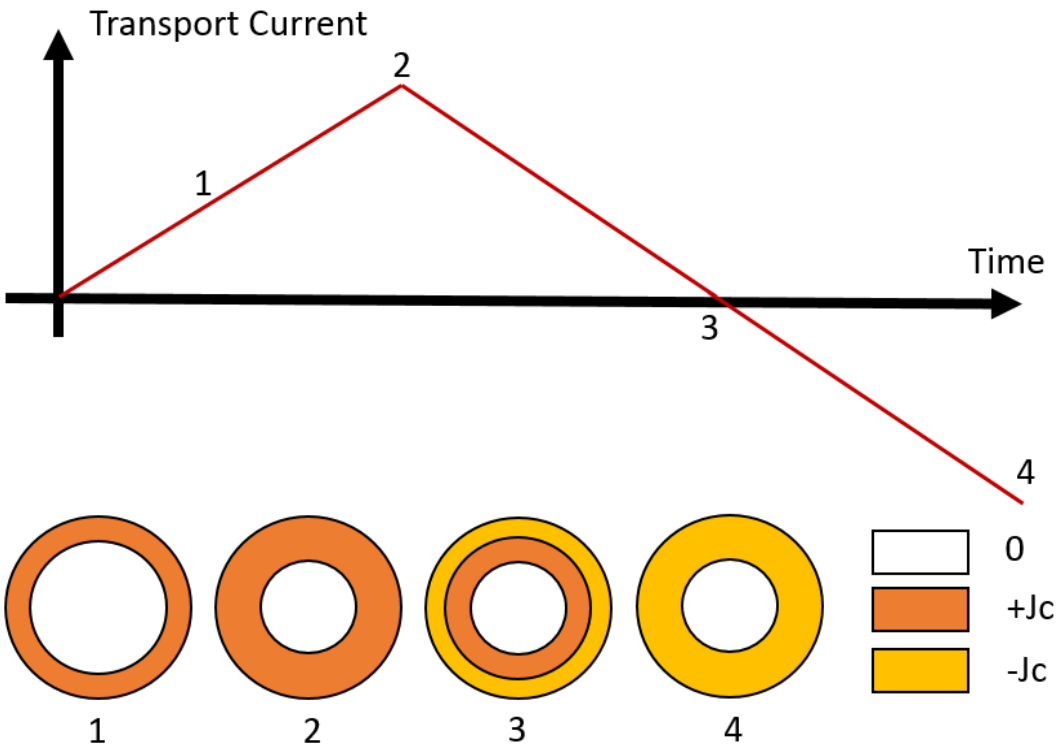

Fig. 10. Distribution of the critical current density inside a superconducting wire during a current variation

From a macroscopic point of view, this simple model offers an easy and intuitive understanding of superconductivity. This model can be further simplified by assuming that the critical current density is independent of the magnetic induction value B (it is then called “Bean model”). However, the discontinuity of this model makes it difficult to use in most numerical solvers. Paradoxically, a more exact description of the continuous E(J) relationship is easier to account for in numerical solvers and gives more accurate results, that is the reason why it is preferred all throughout chapter II.

I.1.8 Transient losses

As seen above, superconducting materials have a hysteretic behavior, and thus transient losses, usually referred as AC losses. Such losses will occur when time-varying transport current is imposed (as presented above) but also in case of time-varying applied magnetic field, due to the induced currents: the so-called screening currents.

Fig. 11, the polarity of these screening currents is indicated by the + and - signs. Shielded by the screening currents, the interior of the sample (blue area) sees no magnetic field variation. If the magnetic field continues to increase steadily Fig. 11 b), the screening currents penetrate deeper into the sample. As the screening currents progress through the sample, the energy used for de-pinning and shifting the flux lines generates dissipation in the form of heat.

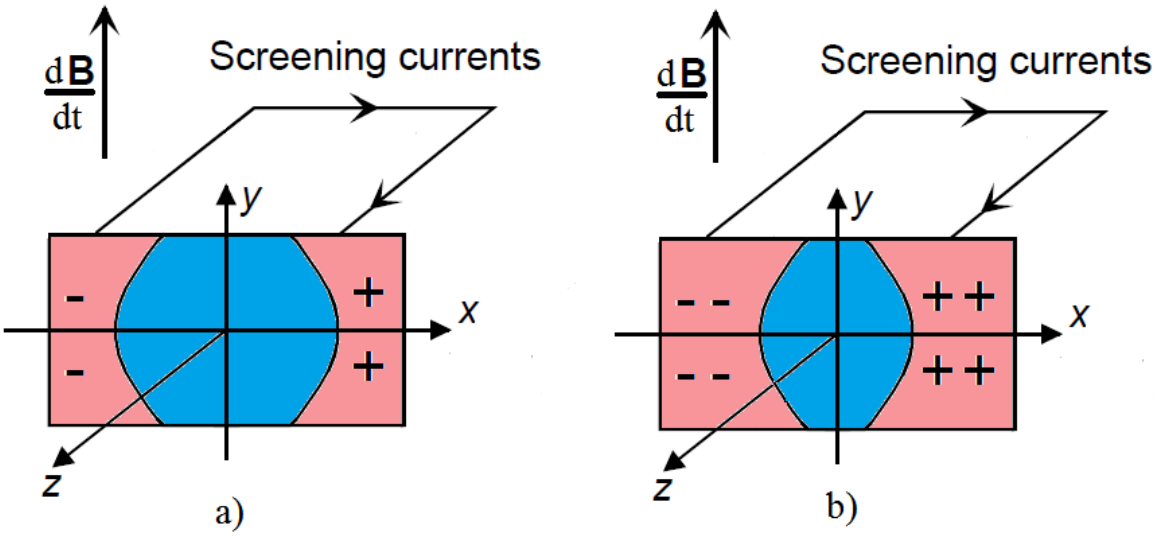

Fig. 11. Simplified description of the screening current penetration in a variable external magnetic field in a superconducting material.

In our models, this dissipation is represented by the E(J) relationship. For a given current cycle, the total energy dissipation can be estimated following Eq. 3.

$$Q_{ac} = \int E * J * dt$$

Equation 3

Where Q_{ac} is the energy dissipation per unit of volume, E is the electric field and J the current density.

I.2 The main superconductors used for magnets

Superconducting materials are very numerous as shown in Fig. 2, but only a few of them can be used and implemented. We distinguish two classes of superconducting materials: the so-called "Low Temperature Superconductors" (LTS) and the "High Temperature Superconductors" (HTS). Fig. 12 shows the main conductors used in the manufacture of magnets.

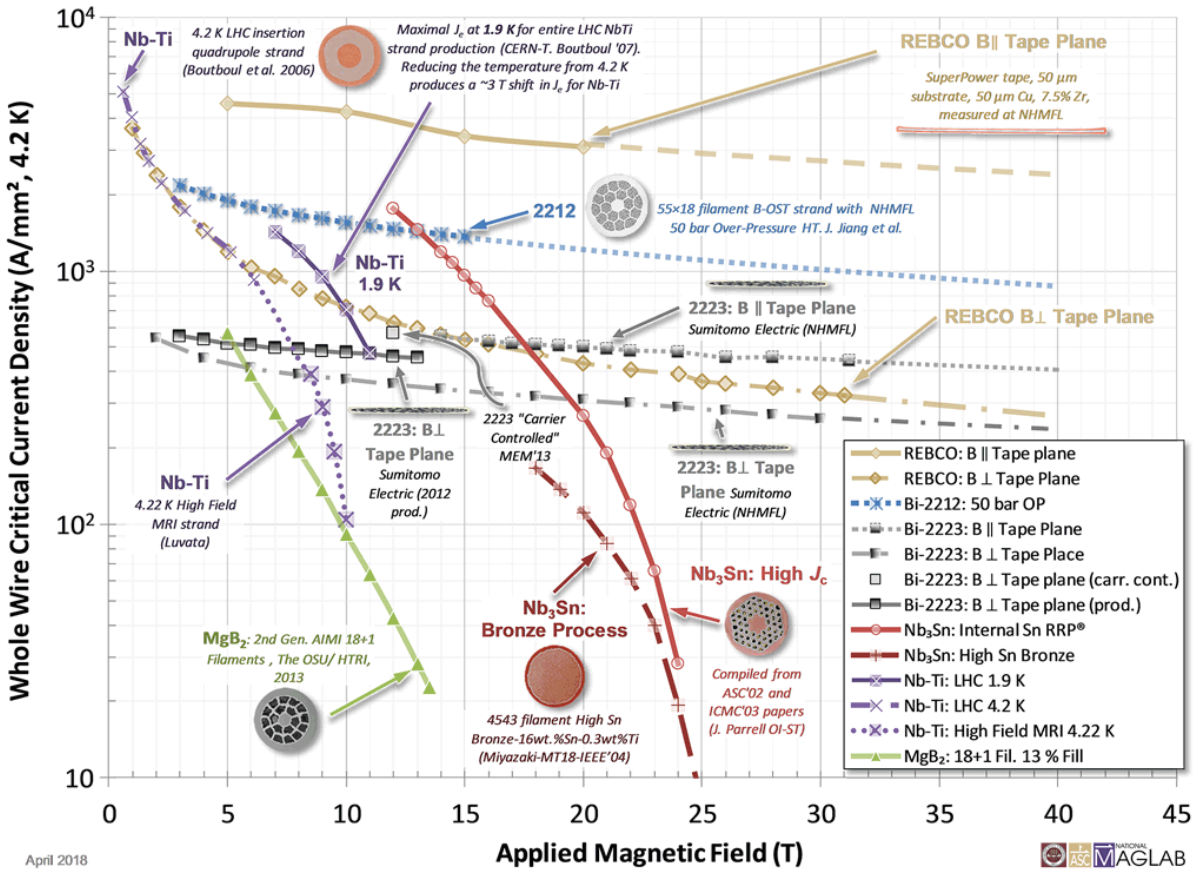

Fig. 12. Critical current density of commercialized superconductors at 4.2 K according to the magnetic field, taken from [13].

LTS magnets, made of NbTi and /or Nb_3Sn conductors are the most common. The development and manufacture of these magnets began in the 1960s in many laboratories. Their technology is very well mastered and has enabled the expansion of commercial applications such as MRI. They are also used in the manufacture of scientific instruments for large-scale scientific projects such as particle accelerators at the Large Hadron Collider or nuclear fusion at ITER. However, these conductors cannot be used above a magnetic field of 12 T for NbTi and 24 T for Nb_3Sn at 1.8 K.

The discovery of so-called HTS superconducting materials is more recent. They were discovered in 1986 when J.G. Bednorz and K.A Muller discovered lanthanum barium copper oxide (LaBaCuO) [14] superconducting at 35 K. Thus, HTS conductors are generally defined as superconductors with T_c higher than about 30 K. Their high T_c has opened the possible way to a much wider range of practical applications and it becomes possible to design less expensive cryogenic systems since the use of liquid helium is no longer mandatory. Liquid nitrogen, which has a boiling point at atmospheric pressure of 77 K, can be used in some applications such as the Superconducting Fault Current Limiter (SCFCL). On the other hand, in the context of the realization of high magnetic field magnets, even if we would be interested in operating at temperatures above 20 K from the point of view of cryogenic cost and ease of use, these HTS magnets generally operate at temperatures below 20 K. This is to maximize the performance of these materials since it is mainly their high H_c (>24 T) and J_c at low temperature that make them suitable for the fabrication of magnets generating high magnetic fields. One of the particularities of HTS is that they are anisotropic materials with a polycrystalline structure. Their superconducting properties are not the same in all magnetic field orientations, which makes the implementation of these materials more complex.

Regarding HTS superconductors, two are commercially available in forms suitable for magnet design: BSCCO (Bismuth Strontium Calcium Copper Oxide) and REBCO (Rare Earth Barium Copper Oxide) where RE can be Yttrium (Y), Gadolinium (Gd), or another rare earth. BSCCO superconductors are said to be of first generation and REBCO of second generation.

I.2.1 NbTi

Among the LTS, NbTi (an alloy of niobium and titanium Fig. 13) has a critical temperature of 9.5 K and a critical field of 10 T at 4.2 K. Its critical field can reach 12 T when the operating temperature is lowered to 1.8 K. These conductors are found in the form of multifilament wires made from NbTi/Cu composites. It is the most widely used superconductor. The NbTi conductor is mechanically resistant and easy to manufacture in long lengths (kilometer lengths), and its processing is very well mastered. These conductors for magnets have reliable performance and are cost-effective (some $1/kA/m). However, as NbTi can only be used at magnetic fields up to about 10T, it is not suitable for higher field magnets, for which another Nb-based LTS superconductor, Nb_3Sn, is preferred.

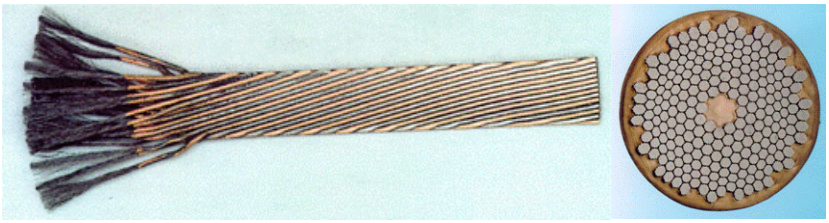

Fig. 13. On the left, a Rutherford cable composed of several NbTi wires. A cross section of an NbTi wire on the right, where the filaments are embedded in a copper stabilizer, which protects the conductors during a transition (quench) to the normal state.

I.2.2 Nb3Sn

Nb_3Sn (intermetallic of niobium and tin Fig. 14) has a critical temperature of 18 K and a critical field of 24 T at 4.2 K. Even if its performance is superior to that of NbTi, its brittle nature in tensile stress and extreme sensitivity to strain make it more complex to implement. Moreover, their fabrication is more complex, requiring a homogeneous and demanding heat treatment to obtain excellent superconducting properties. This more complex elaboration process impacts the price, about 5 time that of NbTi.

Fig. 14. Nb3Sn cable.

I.2.3 BSCCO

Bismuth based copper-oxide superconductors (Fig. 15), discovered in 1988 [15], were the first HTS to become available for applications. They come in two compounds, Bi2212 (flat or round tape conductor) and Bi2223 (flat tape conductor only) with T_c of 85 K and 110 K respectively. The upper critical field H_{c2} in Bi2212 polycrystalline samples at 4.2 K was measured to be 200 ± 25 T (cf. 168 ± 26 T for REBCO polycrystalline samples) [16].

Nevertheless, Bi-2212 reaches a very high J_{eng} of 2500 A/mm² at 20 T and 4.2 K and a little more than 1000 A/mm² for Bi-2223 at 5 T in transverse magnetic field (worst case) at 4.2 K.

These conductors also require complex heat treatment [10]. They are made of a superconducting ceramic placed in a silver matrix to let oxygen penetrate the conductor during the heat treatment. This silver matrix leads to several disadvantages for its use. They are quite expensive ($100/kA/m), with small prospects of price reduction due to the expensive base materials.

Silver being soft, the intrinsic mechanical strength of these conductors is of the order of 100 to 180 MPa, which limits their use for the generation of high magnetic fields. Nevertheless, the conductor can be strengthened by adding a mechanical reinforcement and reach values up to 300 MPa [17]. It should be noted that round conductors are isotropic in contrast to tapes which can be advantageous for cabling.

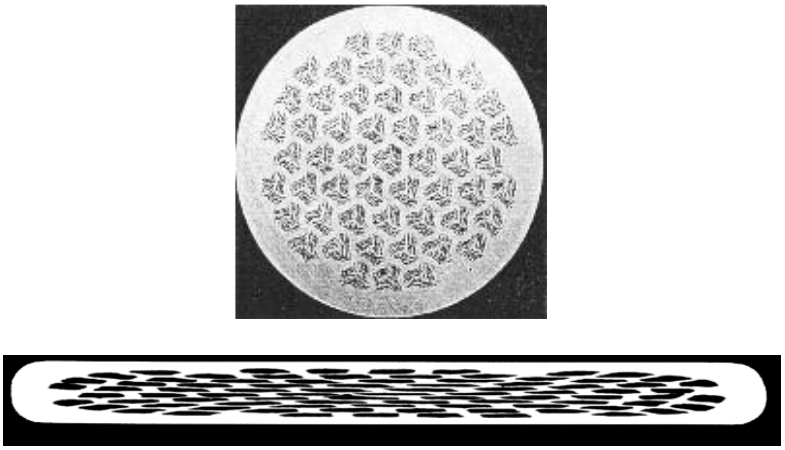

Fig. 15. BSCCO wires.

I.2.4 HTS REBCO Superconductors

REBCO stands for Rare Earth BaCuO. It has a T_c around 92 K, with small variations depending on the Rare Earth used (Y, Gd and Eu are commonly found). It is only found in tape form due to its manufacturing process. To achieve high current density, a biaxial texture is required. The advantages of REBCO tapes lie mainly in their good current carrying capabilities under very high magnetic fields (with an H_{c2} greater than 100 T at 4.2 K [18]) due to a high magnetic pinning energy much higher than that of bismuth-based superconducting oxides. It also has the ability to withstand high longitudinal tensile stress.

REBCO HTS tapes having the highest potential for ambitious future magnets, it is the type of conductor used throughout this PhD work. That is the reason why it will be described in more details in the following parts.

I.2.4.1 Architecture and manufacturing of REBCO tapes

REBCO so-called second generation conductors are coated conductors (CC). CCs are composed of several layers (Fig. 16). The basis is a flexible metal substrate on which one or more textured buffer layers are applied. Then, an epitaxial REBCO layer is deposited, followed by a metallization layer (silver or silver alloy). The bare tape may be finally surrounded by a metallic copper shunt depending on the intended use.

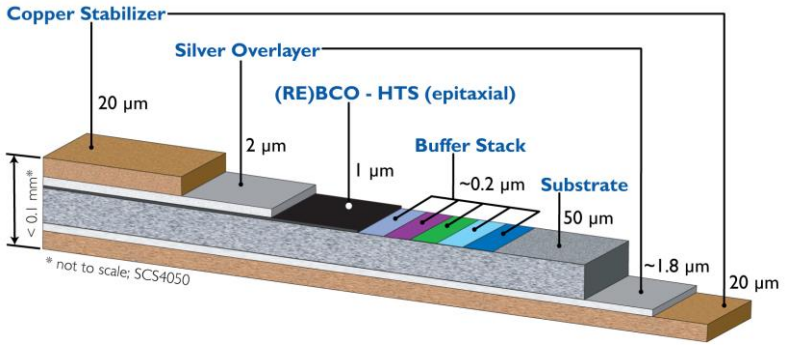

Fig. 16. Architecture of a typical REBCO tape. [19]

There are two main routes for the fabrication of these tapes. The RABiTs process, where the substrate is textured (Nickel Tungsten alloy), and the IBAD process with a non-textured substrate (Hastelloy) on which a textured buffer layer is grown [20].

- The substrate can have a thickness of 30 to 100 µm, remaining flexible. The substrate is the part of the tape that withstand the applied mechanical stress.
- The buffer layers have a total thickness of about 1 µm. They are made of MgO or LZO and aim to isolate the superconducting layer from the substrate to avoid any risk of chemical pollution or oxidation. They also enable to adapt the crystallographic properties and to improve (or even create in the case of IBAD) the texturing necessary for REBCO deposition. The REBCO layer itself is typically between 1 and 4 µm thick
- The silver overlayer has almost no chemical interaction with the REBCO layer and enables a better current injection in the superconducting layer, it is typically a few µm thick.

Finally, the whole tape can be covered with a copper stabilizer, acting as thermal shunt and decreasing linear resistance, which help reduce thermal runaway in case the tape becomes dissipative. These REBCO superconducting tapes are produced in different widths, typically 12 mm but some manufacture output widths as wide as 40 mm. These tapes are often sliced to create narrower conductors, typically 4 or 6 mm. The overall thickness is about 100-150 micrometers. Fig. 17 shows a schematic view of a REBCO tape production line at the manufacturer SuperOx (the tape supplier used for most of this PhD), using the IBAD manufacturing process.

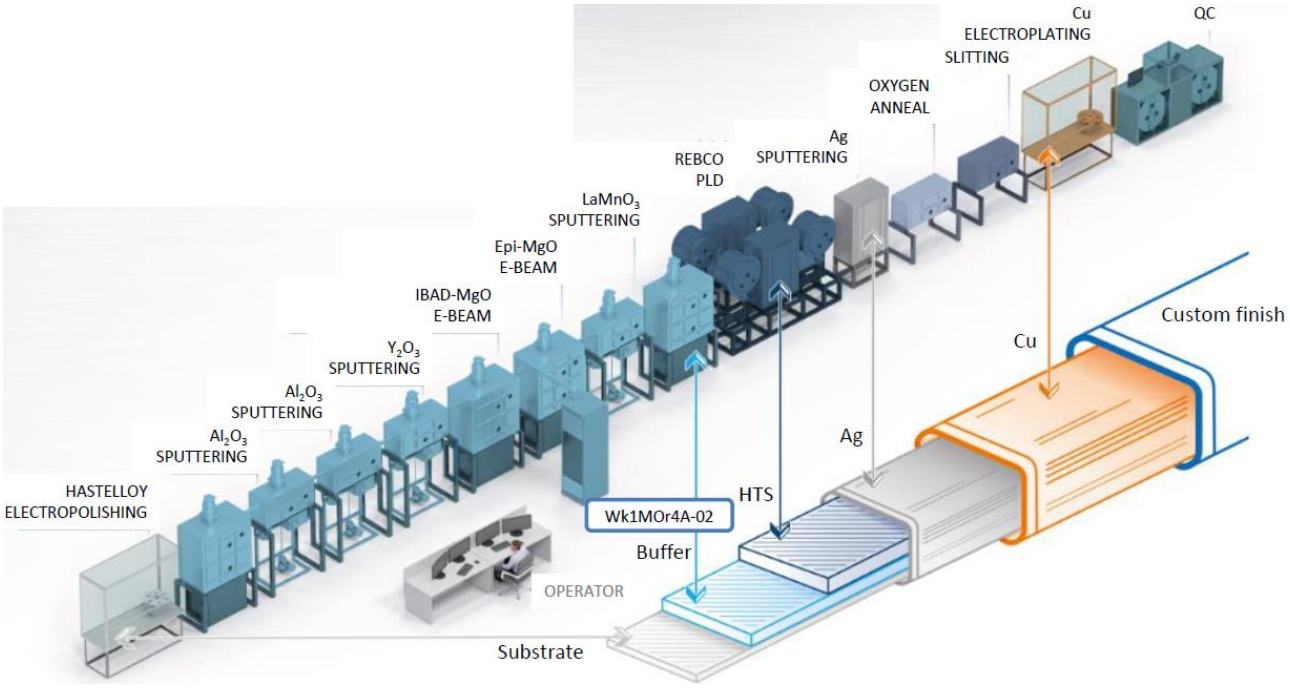

Fig. 17. Production line of a REBCO tape at the manufacturer SuperOx [21].

The superconducting layer crystallographic structure is highly anisotropic and its superconducting properties vary strongly with the direction of the magnetic field. Indeed, like all copper oxide-based compounds, REBCO material owes its superconducting characteristics to the presence of CuO_2 plane. The critical current density is much higher in the CuO_2 texturing plane (ab) than along the (c) axis perpendicular to it. Thus, in order to have good superconducting properties capable of carrying a high current density, an almost perfect crystallographic orientation of the grains is necessary (it must be better than 5° in plane). The crystal lattice of YBaCuO is shown in Fig. 18.

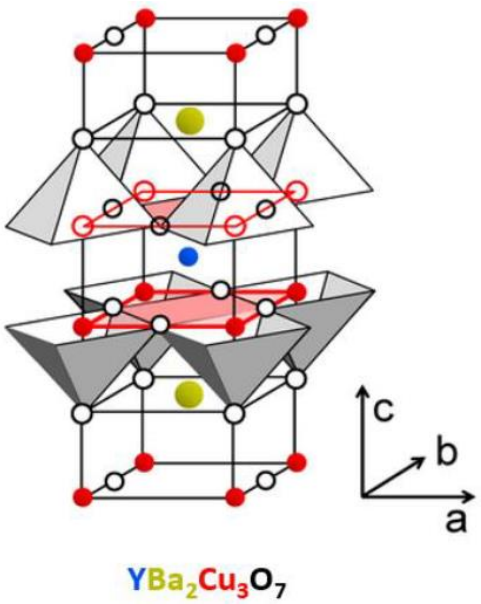

Fig. 18. Crystalline lattice of YBa2Cu3O7.

I.2.4.2 Conductor cost

The cost of REBCO conductors (100 €/kA/m at 77 K, 0 T) remains high at present and is an obstacle to the development of widespread power applications such as transformers, high power cables, fault current limiters, or for storage applications such as SMES (Superconducting Magnetic Energy Storage). For such application in power systems, a price below 50€/kA/m would be desired [22]. The cost of these conductors is mainly due to a significant investment in production infrastructure and also due to the low manufacturing yield. Indeed, the difficulty lies in maintaining a homogeneous performance over a long length during the manufacturing process, without a single drop. This is why the most typical lengths found on the market are between 50 m and 250 m even if the recent feasibility of manufacturing kilometer lengths has been demonstrated. These lengths are in real contrast with the lengths available for LTS where tens or even hundreds of kilometers can be fabricated in a single piece and complicate their use in large devices.

Manufacturers are striving to process longer lengths and improve conductor performance without increasing production costs, in an effort to lower the overall cost of REBCO conductors. Indeed, even if the price per unit length has not really decreased for more than a decade the cost per unit length of transported kA (€/kA/m) has decreased significantly due to performance boost.

In any case, in order to correctly estimate the additional cost of designing a device using a REBCO HTS conductor, it is necessary to take into account the global cost of the hypothetic LTS device with identical performances. This includes capital cost of the cryostat, the current leads, and cooling system -liquid helium or cryocooler- as well as the running cost of the device over their service life. Indeed, in a high field magnet (>18 T), we will see that REBCO conductors show excellent performances in terms of critical current and mechanical stress at temperatures ranging from 4.2 K to 30 K even under a high transverse magnetic field (>10 T) where for example a Nb_3Sn conductor should work at 2.2 K. This leads to saving on cryostat size, cooling system power consumption and so on. Therefore, the use of REBCO conductor can become competitive in high magnetic field coil manufacturing.

I.2.5 REBCO tapes properties

The purpose of this section is to describe the strengths and weaknesses of REBCO tape electromagnetic and mechanical properties, focusing on their use in high magnetic field applications.

I.2.5.1 A high current density in high magnetic field

Although many superconducting devices have been successfully realized with BSCCO superconductors, even at high fields [2], REBCO conductor offer higher current densities, which enables more ambitious designs, especially under very high magnetic fields (Fig. 12). In terms of J_c the REBCO has a clear advantage of more than an order of magnitude over the BSCCO and although the J_c values of the NbTi and Nb_3Sn conductors are high at low magnetic inductions, these drop rapidly below 1000 A/mm² at 11 T (at 1.9 K) for the NbTi and 17 T (at 4.2 K) for the Nb_3Sn due to their low irreversibility fields. For this reason, with a $J_c(B)$ characteristic surpassing all other superconducting conductors, even at operating temperatures ranging from 4.2 to 77 K, REBCOs are therefore the preferred candidates for new generation high field magnets capable of producing 25 T and more. In Fig. 19, an example of $I_c(B)$ data with artificial pinning (B//c) for different operating temperature from manufacturer Fujikura [23].

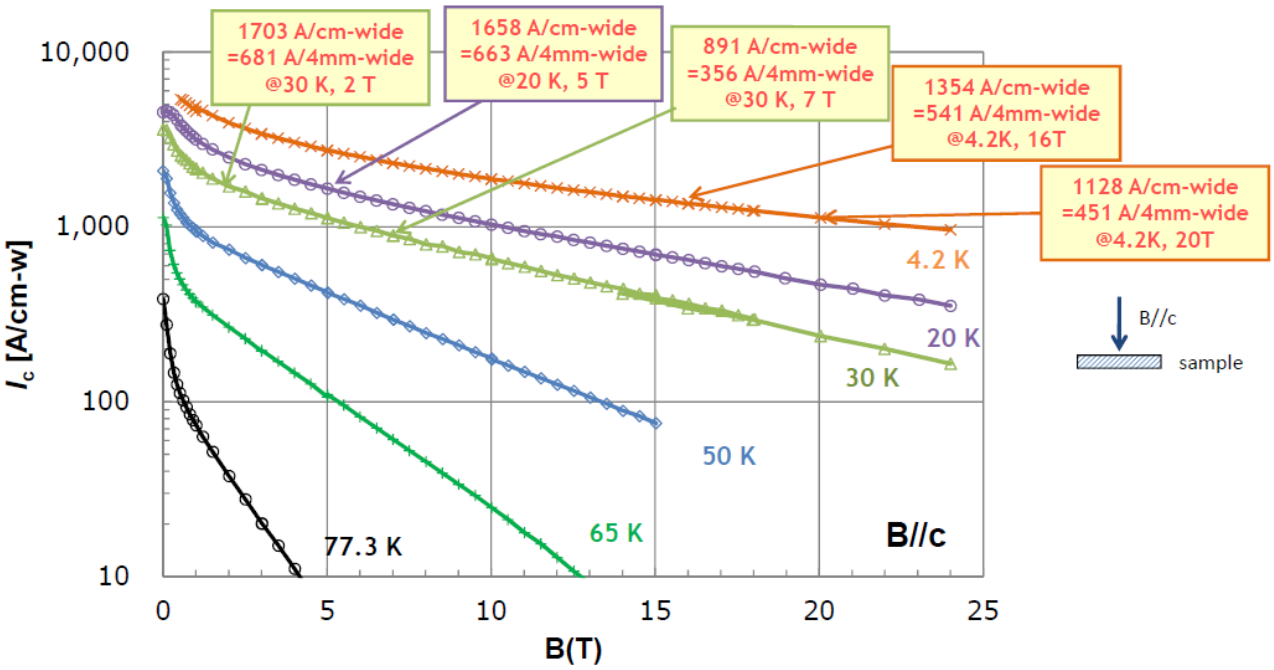

Fig. 19. Typical I_c in transverse magnetic field of a REBCO tape produced by Fujikura for different operating temperatures [23].

I.2.5.2 Strong anisotropy of I_c

Due to their flat shape and thus to the crystallographic orientation of the grains of the REBCO layer, the superconducting properties of these conductors are very anisotropic depending on the direction of the magnetic field they are exposed to. This anisotropy affects the critical current density J_c of the conductor. The J_c is maximal when the magnetic field direction is parallel to the tape (ab plane θ = 0 °) and decreases with the field incident angle to reach a minimum when the magnetic field is perpendicular to the tape (c axis θ = 90 °) as shown in Fig. 20.

Parameters such as the operating temperature, the magnetic field and the pinning landscape influence the shape of the peak formed by $I_c(\theta)$. In order to broaden this peak, artificial pinning centers (APCs) can be introduced in the REBCO layer by adding precipitates such as barium zirconate (BZO) nanocolumn. We notice in Fig 20, where the samples with and without APCs were compared for different magnetic fields, a broadening of the ab plane peak with the BZO additions leading to a higher current from 5° to 20°. Moreover, the critical current of commercial coated conductors covers a wide range of values at 4.2 K, in magnetic field, depending on their manufacturing process (Fig. 21).

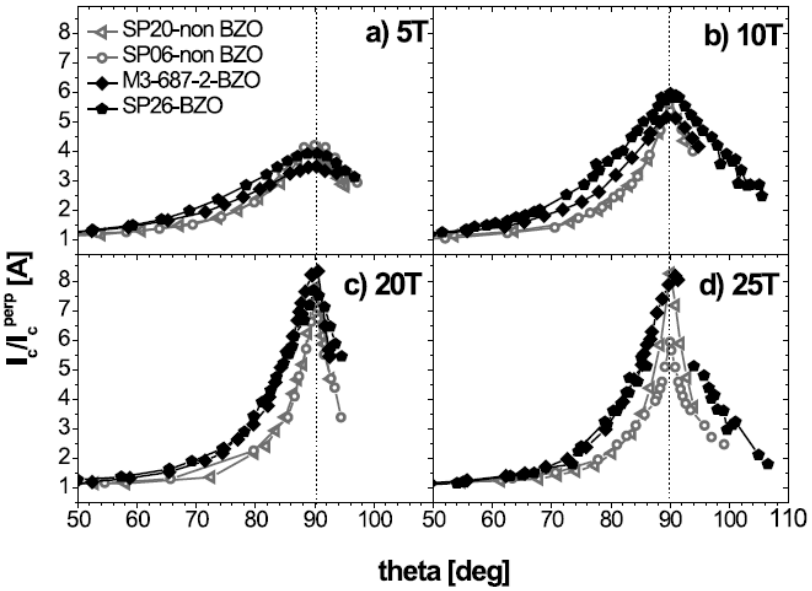

Fig. 20. Reduced critical current I_c/I_c^{perp}, versus angle for the REBCO at 4.2 K (a) 5 T, (b) 10 T, (c) 20 T and (d) 25 T [24].

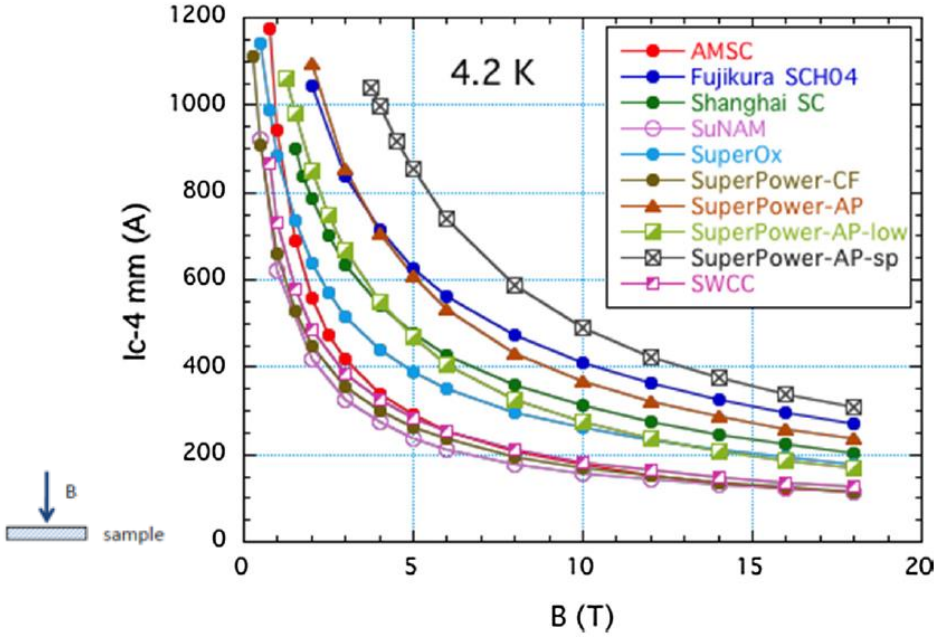

Fig. 21. Overview of field dependence of I_c for several 4 mm commercial coated conductors (field perpendicular to c-axis) [25].

This anisotropy complicates the design of REBCO high field magnets. Indeed, in a solenoid, the conductor is not exposed to the same magnetic field orientation depending on its position in the magnet. The ends of the magnets see a larger transverse component of the magnetic field due to the radial component of the self-field and therefore have smaller critical current density. Therefore, it is essential to know the anisotropic specifics of a REBCO conductor as a function of its manufacturer and these operating conditions in order to consider safety margins when designing a magnet.

I.2.5.3 Screening current and magnetic field drift

When any superconductor is exposed to varying magnetic field, screening currents are automatically induced within it to generate an opposite magnetic field. These screening currents and their effect called SCIF (Screening Current Induced Field), pose two major problems for superconducting magnets. First, a reduction of the central magnetic field and second, a temporal drift of the magnetic field due to the relaxation of these currents.

The disturbances generated by the screening currents are typical of monofilament superconductors and, as seen in I.1.8, the hysteretic AC losses are due to these screening currents. SCIF contributions are indeed conditioned by the effective size and shape of the conductors. They are typically much reduced by making twisted multifilament conductors, but this technique is impossible to implement at present with REBCO superconductors which are Coated tapes.

Screening currents in REBCO tapes will establish mostly in the wide flat surface of the tape. They are induced by the radial component of the magnet's self-field (Fig. 22). For this reason, the SCIF contributions vary deeply with the position. At the magnet center, they are of the same order of magnitude than those which would be found in typical multifilament conductors where the size of a filament is about 6 µm, while at the extremities, they will become 2 to 3 orders of magnitude bigger [22].

As shown in Fig. 22, the field of the solenoid induces mainly SCIFs at the coil extremities which generate a magnetic field B_s (in blue). This field B_s is opposite to the magnetic field B_c (in red) which corresponds to the magnetic field generated by the coil transport current. B_s can reach up to 18 % [26] of the B_c field which strongly reduces the central magnetic field B_0. It should be noted that the impact of SCIFs is also very dependent on the form factor of the solenoid coil. For example, the impact will be less for a thin and long solenoid with ends far from the center of the solenoid [26, 27].

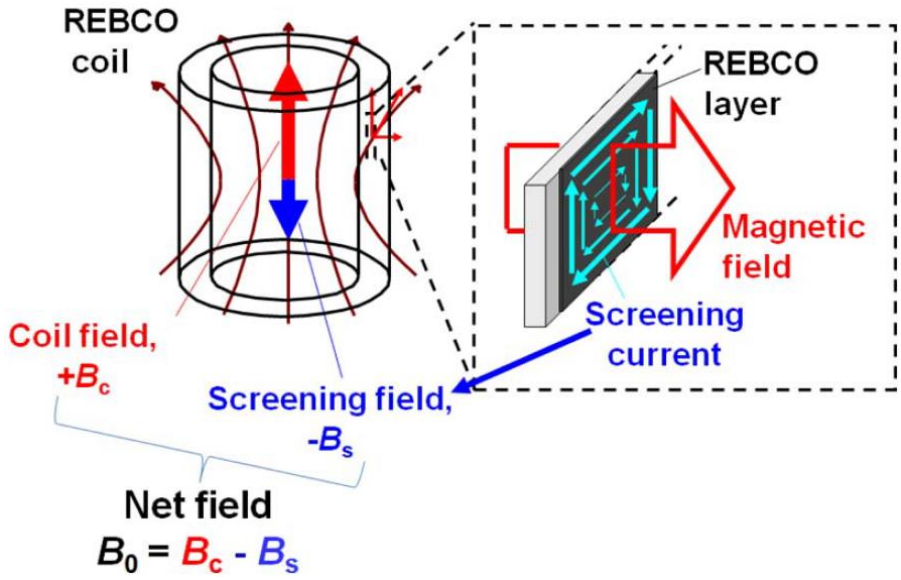

Fig. 22. SCIF effect in a REBCO coil [28].

The reduction in magnetic field at the center of a solenoid could be compensated for by optimizing the magnet at the design stage with these considerations. However, the temporal drift of these SCIFs complicates the matter. The resulting magnetic relaxation at the center of the solenoid that decrease logarithmically with

time and prevents the use of REBCO conductors for applications that require very homogeneous and stable magnetic fields over long periods of time (0.01 ppm/h max for NMR). Also, potentially higher operating temperatures for superconductors increase the magnitude of magnetization drift. This phenomenon is apparent in Fig 23 (a). The current ramp charging a REBCO coil is suspended at different currents for 1 hour. The magnetic relaxation B_s indicated by the dashed arrows is clearly visible at each current plateau and results in a positive time drift that leads to a time increase in the field B_0. Note also in Fig. 23 (b) that the closer the transport current in the coil approaches its critical current, the faster the magnetic drift.

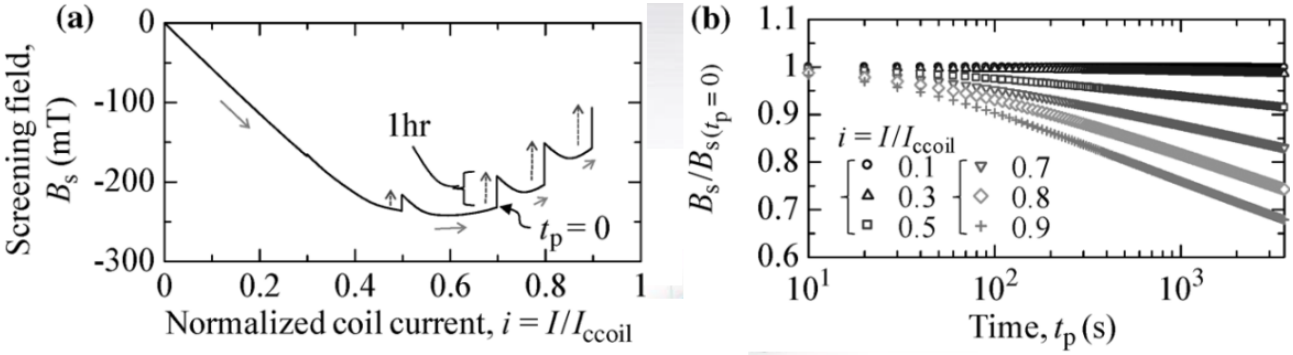

Fig. 23. Magnetic relaxation of a REBCO coil at 4.2 K as a function of normalized current i=0 to 0,9 (298 A) at i=0.1, 0.3, 0.5, 0.7, 0.8 and 0.9 [27].

It is possible to minimize the impact of SCIF in several ways. We will not list these solutions exhaustively here, but among them, the simplest is to apply current overshoot. That is, to increase the current a few percent above the rated value at the end of the ramp, before going back to the rated current [28]. An opposite sheet of current is formed at the upper and lower ends of the REBCO tape width. In a way, this forms flux barriers that reduce the external field applied to the conductor and decrease the relaxation. Thus, the magnetic field drift is greatly reduced (Fig. 24).

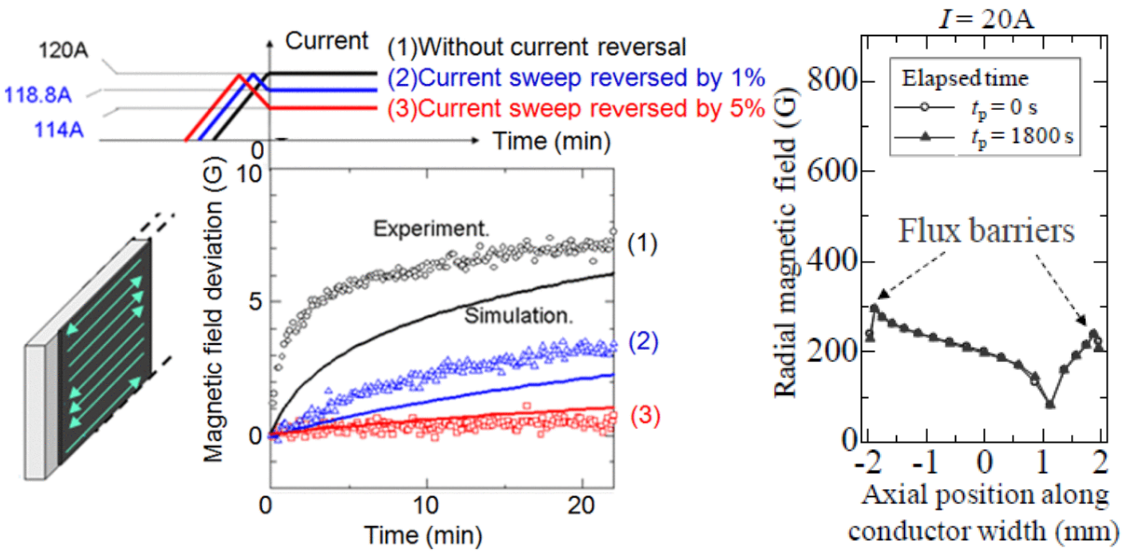

Fig. 24. To the left: (1) Magnetic field drift without current overshoot, (2) Magnetic field drift with a current overshoot of 1%, (3) Magnetic field drift with a current overshoot of 5% [27]. To the right: Magnetic field distribution at 20 A in the superconductor in the innermost layer of the upper coil end obtained by numerical simulation [28].

The method known as "demagnetization" makes it possible to reduce the screening field amplitude as well as its temporal drift. It consists in using current sweep cycles. The current is ramped up and down several times around the rated current value, with the amplitude of the ramp decreasing with time. However, this method requires a significant overshoot of the rated coil current. For REBCO magnets with a high magnetic field and therefore a high hoop stress, excessive overshoot of the coil current is not possible.

At last, since the intensity of the magnetic field induced by SCIF is proportional to the width of the tape another solution to minimize SCIF would be to act on the tape architecture and adopt the multifilament superconducting conductor method by subdividing the REBCO layer [29]. The striation process can be performed by laser striation, chemical etching, mechanical cutting, substrate undercutting or patterning. Fig. 25 compares the time evolution during 10 000 s of the shielding current loops induced by electromagnetic induction in a REBCO "monofilament" pancake and a REBCO "four-filament" pancake after a ramp-up of the magnetic field at 30 K. The magnetic field generated by the SCIFs of the multifilament pancake decreases much faster than the pancake made with a single conductor ("monofilament").

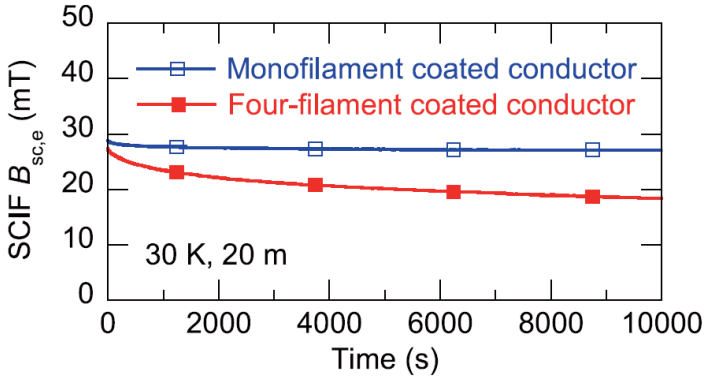

Fig. 25. Illustration of the temporal evolution of the current lines in a REBCO conductor wound into a single pancake coil: (a) t = 0 and (b) t = 10,000 s [29].

Nevertheless, these processes are expensive and very technical to implement over long lengths. In addition, the filaments created by the striation of the tape always remain in contact with each other through the resistive layers of the REBCO tape. This results in coupling interactions between the filaments, as screening currents can flow from one filament to another through the resistive layers making up the tape. Therefore, the coupling of the filaments created by the tape striation is counterproductive because it partially cancels the effect of the subdivision. To reduce this effect and decouple the filaments it would be necessary to twist the tape along their path to limit the length of the magnetization loops. However, this is complicated to implement in practical applications, and can lead to decreases in the critical current (mechanically, and electromagnetically).

I.2.5.4 Critical current inhomogeneity and risks of local thermal runaway

One key feature of REBCO tapes is that the critical current distribution along REBCO tapes is inhomogeneous. Variations of 10-20% can be observed using a continuous magnetic measurement at 77 K [30, 31] (Fig. 26). Indeed, the manufacturing process that makes possible the homogeneous crystallographic growth of REBCO is complicated to keep constant during the fabrication of the lengths. As a result, the tapes have very local (millimeter-scale) portions where the critical current is lower, which may affect the performance and reliability of the magnets.

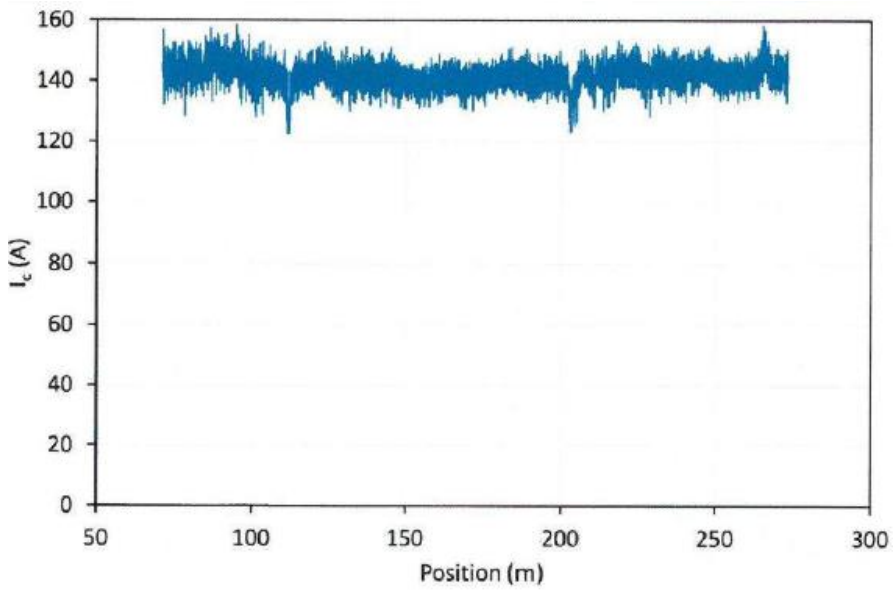

Fig. 26. Critical current variations along a SuperOx 4 mm wide REBCO tape at 77 K.

The other characteristics of these tapes compounding the inhomogeneity of critical current is their high thermal stability and slow thermal runaway propagation speed. This propagation speed is often called NZPV for Normal Zone Propagation Velocity similarly to LTS, even though in REBCO the material is not really in normal state at the propagation front. The NZPV of REBCO HTS tapes is in the range of a few cm/s, depending on the operating current density, while it can be more than 100 m/s for LTS wires. This is due to the difference in temperature margin of HTS and LTS materials, leading to an increase in the Minimum Quench Energy (MQE: the minimum energy required to initiate a quench) by several orders of magnitude. In addition, the copper stabilizer cross-section of a REBCO tape is much smaller than that of an LTS wire, which does not facilitate the propagation of dissipative zones by thermal conductivity.

This large thermal stability due to a high temperature margin has a strong influence on REBCO magnets quench behavior as we will describe in section I.3.3.1.2.

I.2.5.5 Electromechanical characteristics

I.2.5.5.1 Longitudinal stress and strain limits

Mechanical characteristics are very important for high magnetic fields to fully exploit the high current densities of these conductors. REBCO conductors fabricated with a Hastelloy substrate exhibit a high critical mechanical stress value at cryogenic temperature, up to 800 MPa in tensile stress along the longitudinal direction [32]. These REBCO conductors made with nickel substrates have critical mechanical stress values below 450 MPa [33] and are therefore less predisposed to the fabrication of high magnetic field coils.

The longitudinal stress applied to conductors causes them to strain. Beyond a certain strain limit of the conductor, its critical current deteriorates irreversibly. However, the maximum mechanical stress that a conductor can withstand before reaching its strain limit depends on the stiffness of the conductor used.

As shown in Fig. 27 (a), the stiffness of REBCO tapes enables them to achieve a much higher critical longitudinal tensile stress than BSCCO or Nb3Sn wires. This makes them more suitable for the manufacture of high field magnets. REBCO reaches just over 800 MPa where the I_c of Nb3Sn and Bi2223 drops sharply to 230 and 440 MPa respectively. Concerning the strain limit of these conductors Fig. 27 (b), the REBCO tapes show the highest strain limit (0.45%) with an almost constant critical current, while BSCCO and Nb3Sn see their critical current decrease sharply at much lower strain values (around 0.3%). However, while REBCO tapes have high mechanical performance in the longitudinal direction, the other mechanical properties are much less favorable as we will see in the next section. We do not mention the exceptional mechanical performance of NbTi because of its low critical field (see I.2.1).

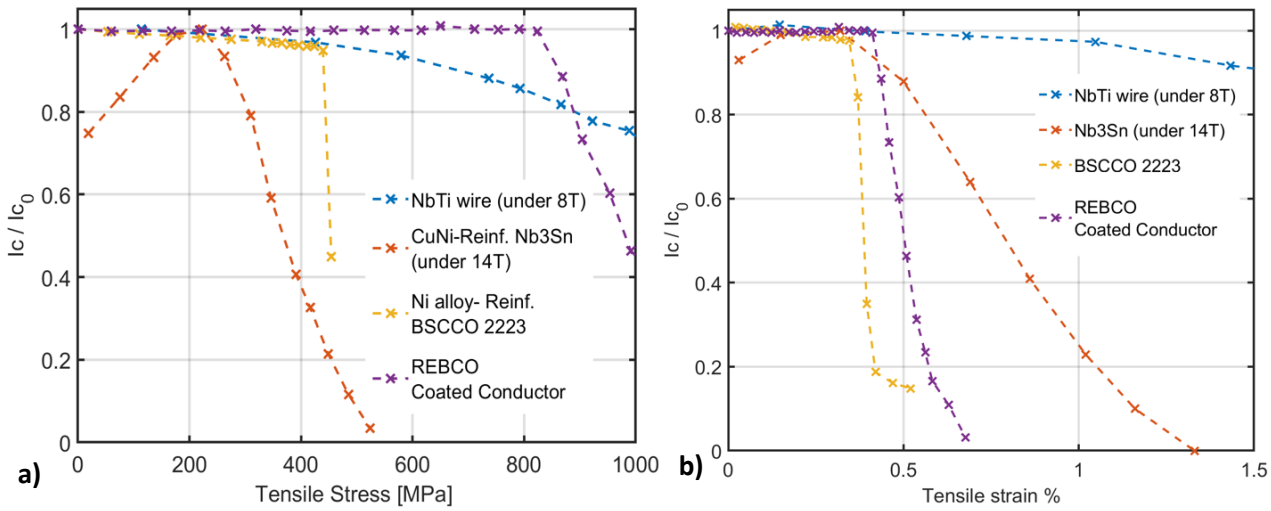

Fig. 27. Normalized critical current versus irreversibility limits of mechanical stress (a) and strain (b).

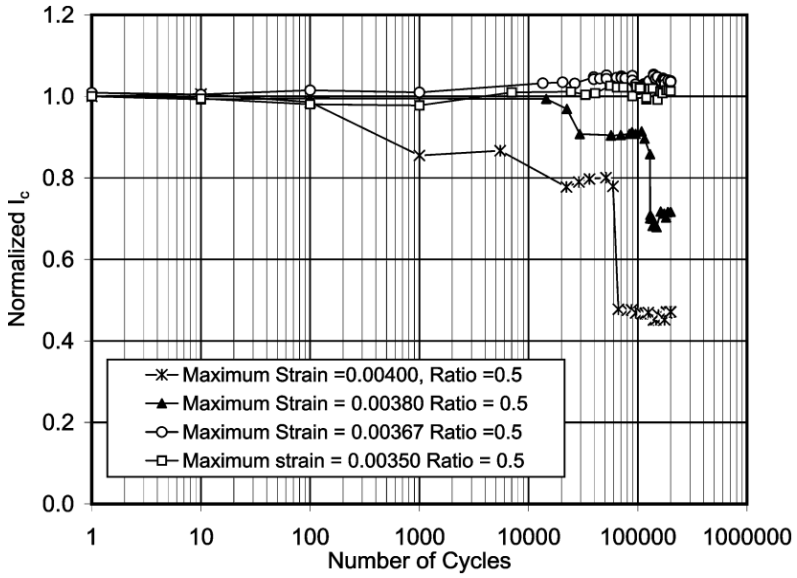

Fig. 28. Effect on normalized critical current of strain cycles applied to SuperPower® REBCO tapes [34].

Similarly, the effect of cyclic loads on the critical current of REBCO conductors is an equally important parameter to consider in magnet design. Indeed, magnets designed to generate strong magnetic fields are subject to repeated loading and unloading cycles throughout their lifetime, resulting in conductor fatigue due to electromagnetic forces. It has been shown in Fig. 28 that the conductor's critical current can progressively deteriorate depending on the level of strain reached and the number of cycles performed [34]. The maximum strain of a magnet must therefore be defined with care.

I.2.5.5.2 Impact of the conductor's architecture

The irreversible strain limit of a REBCO conductor under mechanical stress beyond which the superconducting layer is damaged (and consequently its critical current), is mainly determined by the conductor architecture. The hastelloy substrate of these conductors is a very stiff material with a high Young's modulus of 217 GPa. It can almost single-handedly support the hoop stress and limit the strain of the REBCO layer. However, REBCO superconducting tapes are made of several layers of materials with different Young's moduli. In addition to the Hastelloy substrate, there is a thick layer of copper to thermally stabilize and protect the magnet in case of thermal runaway. The Young's modulus of copper (124 GPa) is almost twice as low as that of Hastelloy. It therefore plays only a small role in the mechanical strength of REBCO conductors subjected to longitudinal stresses. A high copper thickness will tend to weaken the critical mechanical tensile strength of the conductor [35]. Therefore, the maximum stress that the conductor can absorb before reaching its critical strain limit will be lower. Thus, it is important when designing a conductor to evaluate its equivalent Young's modulus (E_{eq}) so that the hoop stress of the magnet does not exceed the permissible strain of the REBCO layer. E_{eq} can be estimated using the law of mixtures below:

$$E_{eq} = \frac{E_1.S_1 + E_2.S_2 + \cdots + E_n.S_n}{S_1 + S_2 + \cdots + S_n}$$

Equation 4

With E and S corresponding respectively to the Young's modulus and the surface areas of the materials composing the conductor (Fig. 29). The indices correspond to the number of materials composing the conductor.

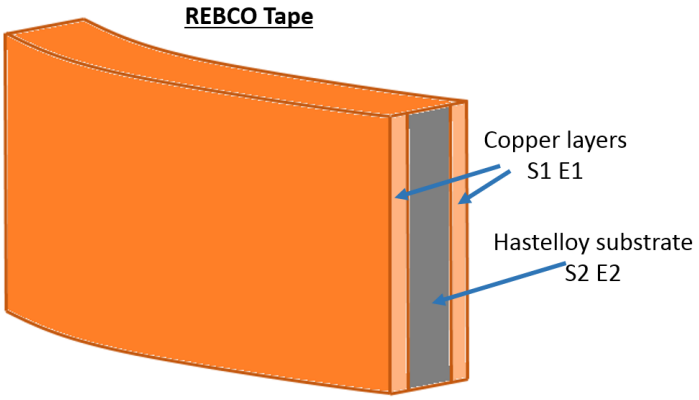

Fig. 29. Schematic diagram of a REBCO tape to evaluate its equivalent longitudinal Young modulus E_{eq}. E1 and S1 correspond to the Young's modulus and cross-section of copper, respectively. E2 and S2 correspond to the Young's modulus and cross-section of hastelloy.

I.2.5.5.3 Delamination: transverse stress and impregnation problem

The architecture of REBCO tapes can be seen as a stack of several layers that must remain bonded to ensure the superconducting properties of the conductor. As soon as one of the layers peels off or breaks (especially the brittle REBCO/buffer layer), which is called delamination, the performance of the REBCO tape deteriorates significantly. We find in Fig. 30 the different common stresses that can cause delamination. Note that the mechanical limits of REBCO conductors are also very anisotropic. We have discussed and highlighted the incredible performance of REBCO tapes in longitudinal tension previously but when transverse forces are applied to the conductor, the critical stresses have a much lower value: 10-100 MPa. In addition, the shear, cleavage, and peel limit stresses, which severely damage the critical current of the tape if exceeded, are so low that they should clearly be avoided when designing a REBCO magnet. These types of stresses, make epoxy impregnation of REBCO coils difficult because the differential stresses generated during cooling easily delaminate the tape and thus its performance. We will deal more specifically with the impregnation of REBCO coils in chapter IV.

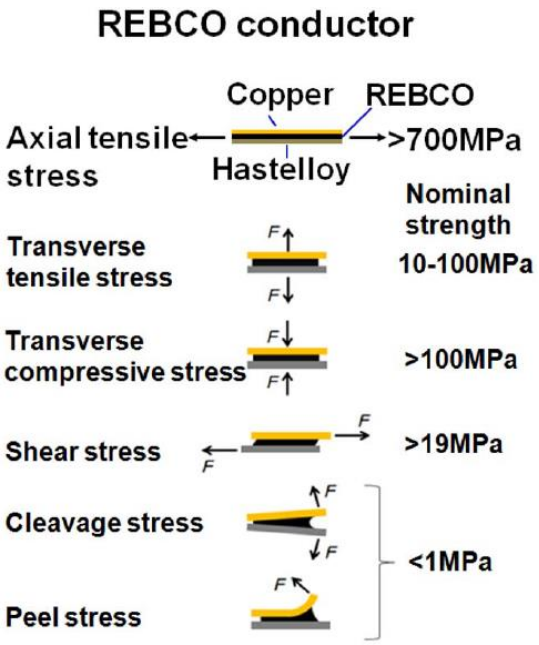

Fig. 30. Stress limits for a coated conductor under various mechanical constraints [28].

I.3 Technical challenges for winding REBCO coil

I.3.1 Impact of short unit length of REBCO tapes

I.3.1.1 Coil winding techniques

The most common winding technique for usual superconducting coils, which are using LTS, is layered winding. This is due to their large unit lengths (> 1 km) which make it possible to wind the entire coil with a single length of superconductor (or a few tens of meters). The conductor is wound onto the mandrel of the coil turn by turn, and layer by layer, each layer being wound on top of the previous one from the innermost

to the outermost (Fig. 31 left). In addition, layer winding is facilitated by the quasi-isotropic mechanical properties of these conductors (that is especially true for NbTi).

Using REBCO tapes, layered winding is less frequent, for several reasons.

- First, the unit lengths currently available on the market rarely exceed 200 m, which would require many junctions in the winding.
- Second, the management of mechanical stress is more complex with layer winding. As discussed in section I.2.5.5.1, REBCO conductors are sensitive to strain, so their critical current decreases if the irreversible strain limit is exceeded. During winding, the main sources of strain are due to conductor bending. For a tape, bending stresses occur along two directions: along the conductor axis ("easyway bending") or perpendicular to the conductor axis ("hardway bending"). Since the tape is much wider than it is thick, hardway bending generates a much higher inner stress than easyway bending. In order not to damage the superconducting layer, it is therefore important to respect a minimum bending radius for both bending directions. The minimum bending radius for hardway bending is of the order of a meter (for a 12 mm wide tape), and of the order of a centimeter for easyway bending [36]. In the case of layer winding hardway bending is necessary for each turn which is not ideal, especially for small bore magnets (inner bore diameter < 50 mm [37]).

For these reasons, REBCO coils are often produced in Single Pancake (SP) or Double Pancake (DP) assemblies (Fig. 31 right). These sub-assemblies are then interconnected by means of resistive connections (soldered or pressed contacts) to form the final magnet.

To make a SP, the tape is wound on itself on an inner mandrel until the desired number of turns is reached. One of the advantages is that such winding is relatively simple to do, and junctions are found outside of the winding itself, at the inner and outer diameter. Still, the assembly of SPs is tricky, especially their inner electrical interconnection. This is due to the difficult accessibility (mandrel, flange) at the winding inner radius once the winding is complete.

To overcome this drawback, DPs can be manufactured. If the tape is long enough and the mandrel inner diameter is sufficient to satisfy the critical hardway bending of the tape, the two pancakes are wound sequentially, starting from the center of the tape length, which is placed at the inner diameter layer jump (Fig. 32). This has the advantage of eliminating the inner junction between 2 pancakes and limits the number of resistive joints during magnet assembly. Electrical interconnections between DPs are manageable since they are located only at the outer diameter, where there is more room.

If the mandrel diameter is too small or the conductor length is insufficient to satisfy the required number of turns of the 2 pancakes, a quasi-Double Pancake can be made, starting from a splice between two REBCO lengths. The 2 lengths are electrically connected by soldering with for example a piece of copper integrated in the mandrel and/or superconducting bridges. SPs and DPs with inner splices also permit windings with smaller inner diameters than layered windings. In any case, the DPs must be interconnected and an assembly of DPs require multiple connection joints to make a magnet. Therefore, it is essential that these splices have reproducible low electrical resistance as well as high mechanical strength to minimize the impact of these splices on the performance of a given superconducting device.

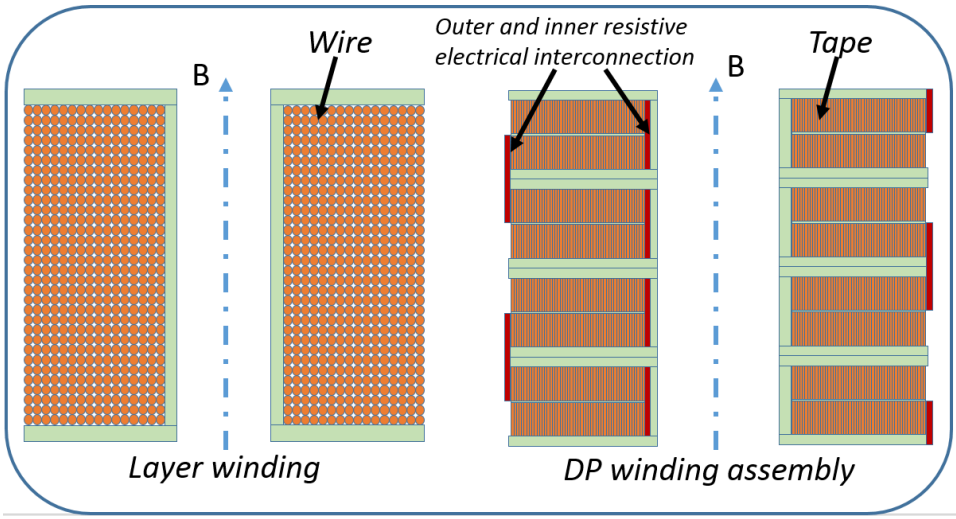

Fig. 31.Left: a layer winding made with a round wire. Right: a Pancake winding made with a REBCO tape.

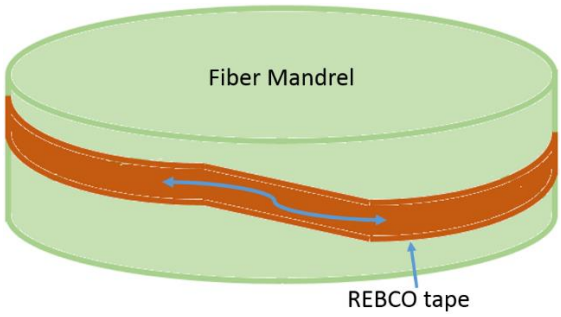

Fig. 32. Beginning of a DP winding with an internal twist.

I.3.1.2 REBCO tape splices

Superconducting or very low resistance splices are very well mastered with LTS using, for example, magnetoforming. Resistances down to 10^{-13} ohms [38] enable the devices to operate in persistent mode. However, such cold pressed joints processes are impossible with REBCO HTS because the REBCO ceramic layer is very brittle, and the surface is very often partially deoxidized. The electrical connections between REBCO tapes, made by mean of pressed or soldered contacts, are therefore always significantly resistive. The "soldered" solution is most often preferred because it obtains better results in terms of electrical joint resistance. Soldered connections between REBCO tapes are made using low temperature soldering (<250°C) because of their extreme sensitivity to high temperatures and deoxygenation. Indeed, the performance of the superconducting layer and thus the critical current degrades with the duration and the temperature of the heat treatment [39]. In addition, the heat treatment also causes a significant increase in the resistivity of the splices (Fig. 33).

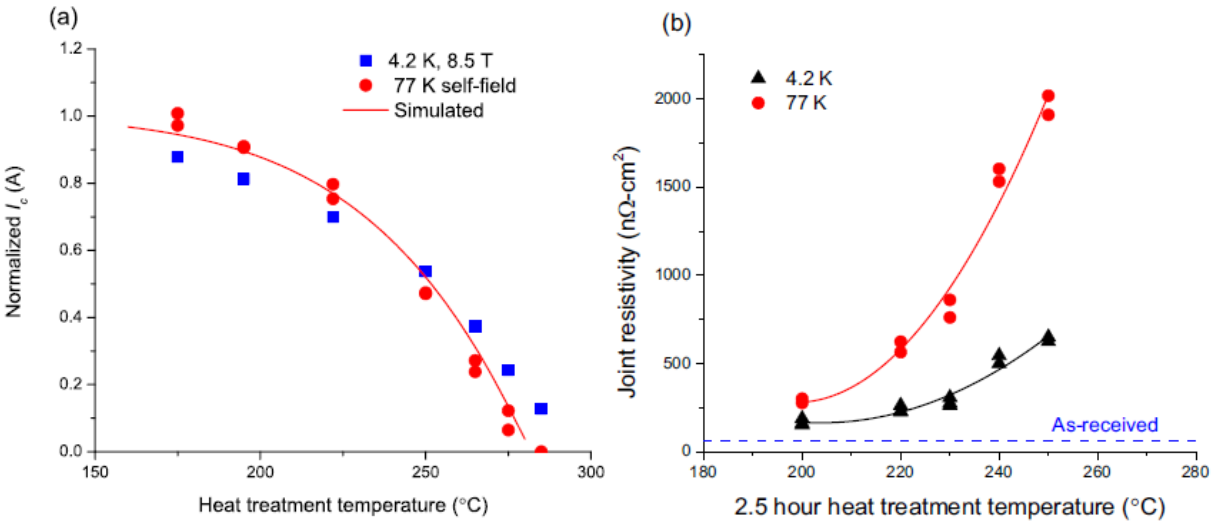

Fig. 33. (a) Normalized Ic of REBCO samples heat-treated for 2 h at different temperatures in air. Ic measures at 77 K in self-field and at 4.2 K in 8.5 T field perpendicular to ab plane are presented. (b) Joint resistivity versus heat treatment temperature for 2.5 h of heat treatment [39].

Several joint configurations can be made, including bridge joints and lap joints. Bridge joints are particularly useful for the inner or outer connections of pancakes discussed in the previous paragraph. They can be made with parallel joints or multiple perpendicular joints (Fig. 34 (a), (b)). Lap joints (Fig. 35) are useful for joining two lengths end to end to increase the effective length of a pancake. The resistance value of the joint depends on several factors such as the strength and thickness of the different materials making up the layers of the tape (Ag, buffer layers, Cu, substrate), the resistance and thickness of the soldering material, the cleaning of the surfaces, and finally the pressure exerted on the joint during soldering [22]. The lowest joint resistances at 4.2 K are obtained with face-to-face soldered REBCO layers where splices resistances between 13.4 nΩ.cm² and 151 nΩ.cm² are measured depending on the manufacturer [40]. As soon as the substrate is sandwiched between the REBCO layers, such as in a Face-to-Back tape configuration, the joint resistance increases by at least a factor of 8. However, the joint with Face-to-Face REBCO layers is not always possible in the realization of a magnet and can also lead to mechanical problems inside a winding (gaps between turns, REBCO layer reversal with respect to the inner winding radius). All these parameters must be taken into account in order to decide which contact type to use, according to the rated current of the application and the need for magnetic field stability.

The resistance of these splices prevent the operation of a magnet in persistent mode for some applications. Superconducting junctions using melting diffusion and oxygenation annealing (350 h at 500 °C) between 2 REBCO tapes have been realized with joint resistances lower than 10^{-17} Ω [41]. For this purpose, laser drilled microholes on the surface of the REBCO tapes have been made to serve as conduits for oxygen during annealing. However, even if the success of this process suggests a good prospect for fully persistent magnets, the fabrication process of such joints is currently still too complex to be scaled up by magnet manufacturers.

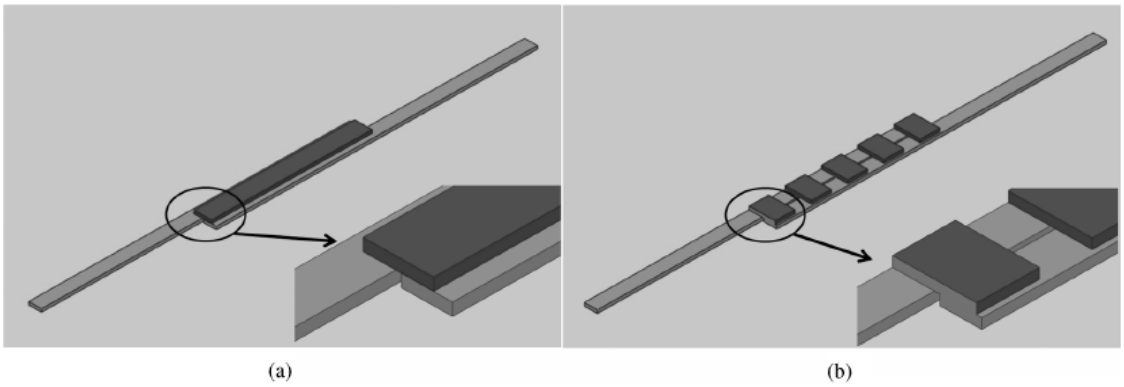

Fig. 34. (a) Parallel joint (b) Perpendicular joint. [42]

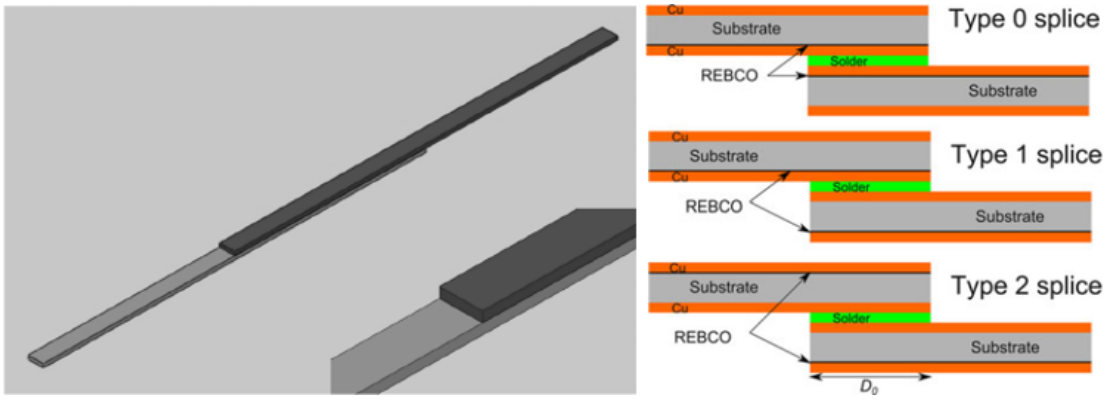

Fig. 35. Lap joints [40,42]

I.3.2 Mechanical stress on REBCO conductor in solenoids

The mechanical design is of extreme importance for any magnet. The design must ensure that the conductor withstands the high stress and strain without degradation of its superconducting properties. For a long time, the main concerns for HTS magnets were not mechanical as electric properties were not reliable enough. Today the performance and reliability achieved by manufacturers in long length REBCO tapes in terms of critical current, even under high transverse magnetic fields, mean that REBCO magnets can reach their hoop stress limits. Therefore, it is necessary to precisely estimate the stress on the conductor during magnet operation to define operating limits avoiding excessive strain, which could degrade the current carrying capabilities of the REBCO ceramic layer as mentioned in part I.2.5.5. In particular, radial stress, which is in the transverse direction with regards to the conductor, must be kept very small so as not to delaminate the tape, as discussed in part I.2.5.5.3.

However, accurately estimating the mechanical stress distribution in a winding is not straightforward. It depends on the winding fabrication technique as well as the conductor structure (I.2.5.5.2). Two analytical formulas can be used for easy but rough calculation of the stress induced by Lorentz forces:

- The BJR formula in which each turn acts independently without interacting with each other. With J the current density in the turn, B the axial magnetic field, and R the turn radius. This model is

interesting thanks to its simplicity but has meaning only in winding configurations were the turns tend to naturally separate from each other.

- In Wilson's formula [43], or its more complete form defined in Arp [44], the turns of the solenoid are on the contrary considered attached to each other. The solenoid body is then considered as a homogeneous solid subjected to a volume density of Lorentz force. It must be noted than Wilson's analytical formula does not take into account complex multi-body winding structures and is always a first cut approximation.

This PhD focuses specifically on insulated REBCO windings. Thus, due to the risk of conductor delamination, our REBCO windings are wound in a dry manner, that is to say without impregnation. Therefore, considering the above assumptions, the evaluation of the stress distribution in an unimpregnated winding should intuitively approach the BJR calculation since the winding turns are rather independent from each other, and can separate under the influence of Lorentz forces or thermal contraction. However, in reality, we can suspect that under the influence of electromagnetic forces and under certain configurations, the turns will still interact and support each other.

Let’s consider the BOSSE solenoid configuration (see part III.2.2 Final design of the BOSSE solenoid) as an example of a circumferential mechanical stress calculation. Fig. 36 shows the calculations of the mechanical stress distribution in the winding of a central pancake of the solenoid according to a calculation hypothesis in BJR or Wilson, as well as the radial stress for the Wilson hypothesis (The radial stress in BJR hypothesis being by principle zero). We notice that the hoop stress calculation is much higher at the inner radius of the winding in BJR than in Wilson and much lower at the outer radius in BJR than in Wilson. In Wilson hypothesis, we observe that the radial stress calculation indicates a negative stress which means that the winding is subjected to compressive forces. From this we understand that the turns will support each other, whether they are glued to each other or not, and thus that the independent-turn hypothesis (BJR) is invalid, even for such a dry winding.

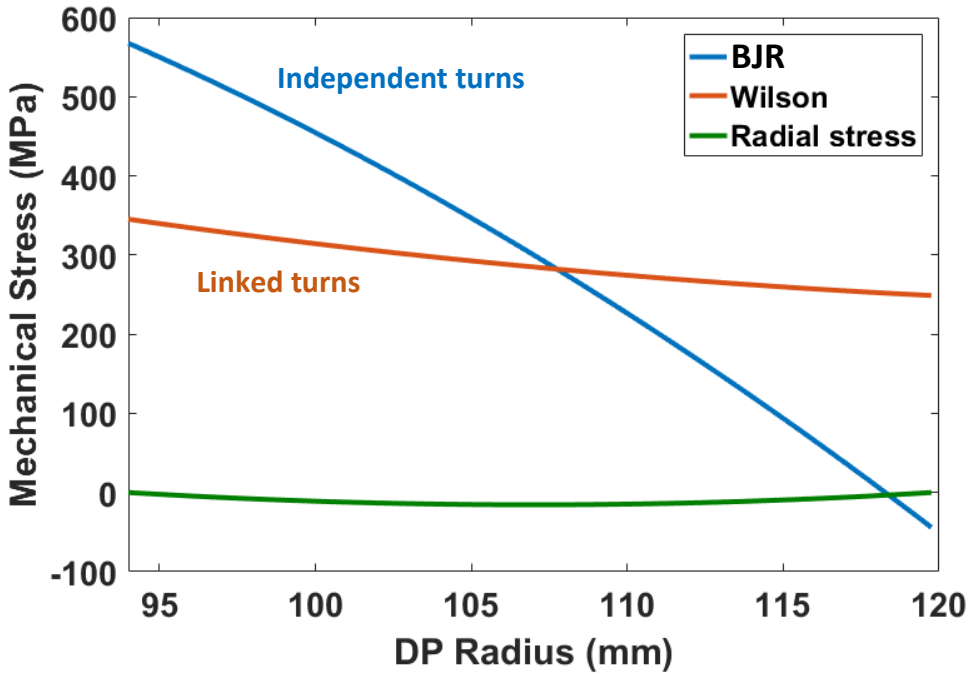

Fig. 36. Comparison of circumferential mechanical stress distribution in a central pancake of the BOSSE solenoid for 1 MJ storage according to BJR and Wilson. The radial stress is calculated with the Wilson’s formula.

The mechanical behavior of a solenoid depends on its geometry, the structure of the conductor but also if it operates in self-field or in a background magnetic field. We can see in the example Fig. 37 that a configuration with a thick solenoid (or which operates in a magnetic background field) gives at the inner radius a higher hoop stress with the Wilson hypothesis than the BJR. In such case, the radial stress is positive: the inner turns are pulled outwards by the outer turns, which can only happen if the turns are actually glued together. Of course, for a non-impregnated (dry) winding, there cannot be such radial tensile stress between turns, so that the actual behavior would be closer to the BJR hypothesis. In case of an impregnated winding (turns glued together), in this configuration the radial tensile stress reaches almost 100 MPa, which would surely lead to REBCO tape delamination.

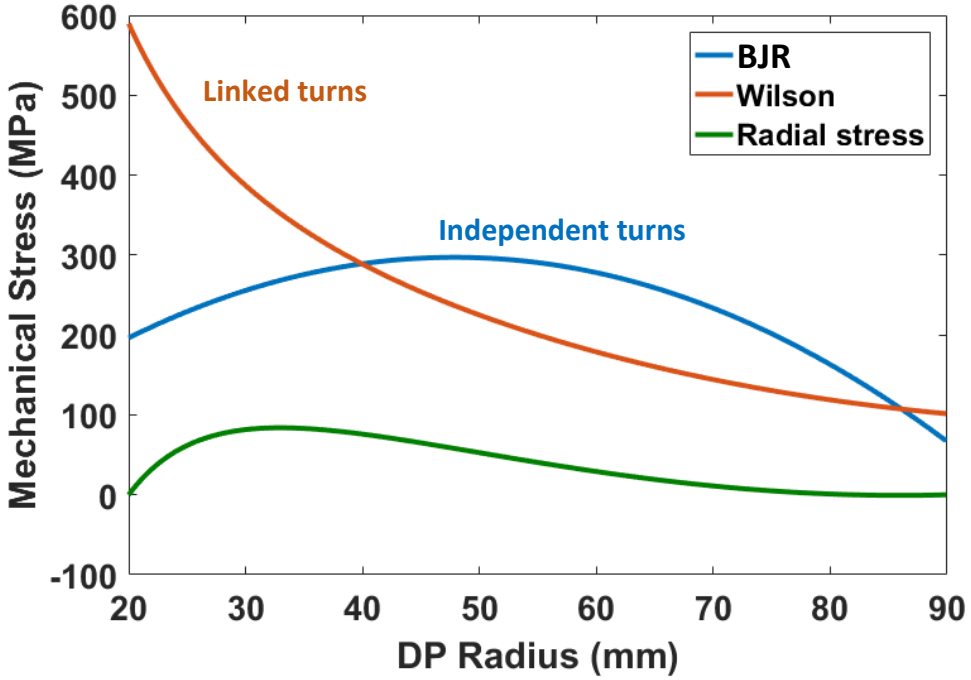

Fig. 37. Comparison of circumferential mechanical stress distribution and positive radial stress for a thick solenoid.

More detailed calculations about mechanical behavior can only be conducted knowing the specific coil structures. Such discussions will be presented in chapter III and chapter IV.

I.3.3 Protection of REBCO superconducting magnets

I.3.3.1 Is there a need to protect an HTS magnet?

I.3.3.1.1 Usual superconducting magnet protection philosophy

In general, Superconducting Magnets need to be protected against quench, or rather local thermal runaway in the case of REBCO magnets. In such event the magnet operation becomes impossible and the current must go back to zero. The magnet protection design aims at limiting the temperature increase in the winding during its discharge. There are two protection strategies for superconducting magnets:

- *Active protection* where a dedicated system detects the quench and activate a protection scheme (either to dissipate energy in the coil volume or discharge stored energy in an external dump resistance).
- *Passive protection* where quench is not monitored and the protection requirements are fulfilled by design of the magnet itself.

In both cases, the magnet protection requirements are traditionally defined by the adiabatic hot spot criterion (maximum temperature not to be exceeded) (Eq. 5). The hot spot criterion is used to estimate the energy that a winding can absorb before reaching T_{max}.

$$\int_{T_0}^{T_{max}} \frac{C\ dT}{\rho} = \int_{0}^{t_0} J^2\ dt$$

Equation 5

Here *C* and *ρ* are the specific heat and resistivity of the conductor respectively, and *J* is the current density in the conductor cross-section. T_0 and T_{max} are the initial and maximum acceptable temperature of the conductor and t_0 is the time at which the magnet is fully discharged. Note that *ρ* is not trivial to define precisely as in a first time the conductor is still superconducting, even though dissipative. The hypothesis generally assumed is that *ρ* the equivalent electrical resistivity of the conductor without its superconducting part. This leads to a pessimistic estimate of T_{max} since the energy dissipation is lower between the operating temperature of the winding and its critical temperature. Naturally, this assumption works best for LTS magnets, where the difference between the magnet Operating Temperature and its Critical Temperature remain small.

I.3.3.1.2 Case of REBCO magnets

Unlike LTS magnets, where conductor stability is one of the key factors in the design of these magnets, the high stability of REBCO conductors makes it very unlikely that a transition will occur. Conductor movements in the winding caused by electromagnetic forces or other short term energy deposition due to external events cannot cause accidental thermal runaway. Thermal runaway can only happen due to local overstepping of the critical current, either because of intrinsic critical current inhomogeneities over the length of the superconducting REBCO tape or a local damage in the winding. The initiation and small-range-propagation of dissipative zones inside a REBCO insulated winding leads to irreversible local damage if the coil is not protected. We speak of "localized thermal runaway" forming what is called a "hot spot". Such mechanisms were extensively studied in our group [45, 46, 47].

This thermal runaway protection issue is made even worse considering the high critical current densities found in REBCO tapes. The energy dissipated per volume being much higher than in other conductors, the temperature may rise rapidly up to the melting temperature of the conductor if it is not detected and protected quickly (Fig. 38).

To solve this issue, one could consider that these magnets could simply operate with sufficiently large current margins relative to the $I_c(B)$ characterization of the conductor at a given temperature, and dispense with any protection scheme. But this raises the issue of the conductor cost and device performances, since it would lead to severe overdesign.

In consequence, detecting and protecting against thermal runaway phenomena in REBCO windings remain as major issue and will be one of the important topics of this PhD work.

Fig. 38. Melting of the conductor after the appearance of an unprotected hot spot in an REBCO insulated magnet.

I.3.3.2 Passive protection strategy

Passive protection does not require a detection device. It relies on the windings resistance increase to shut down the power source and initiate the current discharge. This type of protection is commonly used in LTS coils where the propagation of the resistive zone extends rapidly (quench, see section I.2.5.4). The current discharge may occur in the winding itself for coils with relatively low specific energy [48].

Parallel connections of winding segments with number dump resistors (Fig. 39) can be used to ensure a faster discharge of the current, remove some energy from the winding and thus limit the heating. Another advantage of subdividing the windings is that the magnetic coupling between the elements create a domino effect of quench on the subdivided windings. This is because the current in the other windings increases rapidly, which causes the entire winding to quench. Diodes can be added to prevent current from flowing through the dump resistances when charging the magnet.

In any case, in very high-energy / high-current-density magnets, passive protection is usually not enough and active protection methods are preferred. Passive protection is not suitable for REBCO magnets due to the slow propagation of dissipating area (see section I.3.3.1.2).

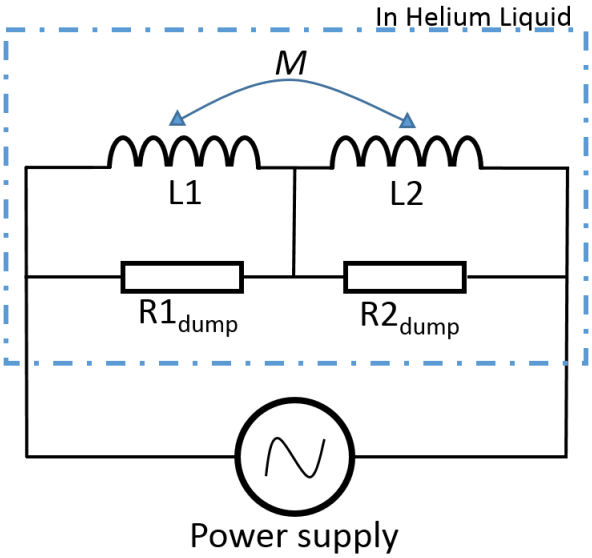

Fig. 39. Electrical circuit of a passive protection. Inspired by [48].

I.3.3.3 Active protection strategy: detection and protection

Active protection is defined by the need to detect the quench or thermal runaway event, in order to trigger an external protection device to release the stored magnetic energy, either in an external dump resistance or by diffusing the energy by means of heaters inside the coil volume and thus avoid a destructive thermal runaway.

I.3.3.3.1 Detection of quench or thermal runaway

To detect the occurrence of a hot spot in a superconducting magnet, the classical method is to detect the resistive voltage that results from the dissipating area. This can be done by cancelling the inductive voltage, by means of a Wheatstone bridge configuration as in Fig. 40, where the inductive components of the two halves magnet cancel each over. This method may however underestimate the total dissipation as dissipative voltages appearing on both halves would cancel each other. This is why in chapter II and the rest of this work, the use of pick up coils will be preferred.

In any case, detection of thermal runaway is much more complex in a REBCO magnet than in an LTS magnet because, as we have seen in part I.2.5.4, thermal runaway in REBCO magnets does not propagate quickly. The change in the measured voltage signal is therefore not as obvious as that of an LTS magnet going into quench. This means that for effective protection of a REBCO magnet it is necessary to detect a low dissipating voltage in an often very noisy electromagnetic environment, which is not straightforward. Moreover, as it was observed in the transition voltage, it can be confused with signals of the same order of magnitude such as transient voltages due to magnetization of the conductor or wire movements, which disturbs the detection. Early detection of thermal runaway is the method that is developed in our team for REBCO magnet protection so this approach will be extensively covered in this work, both in chapter II and III.

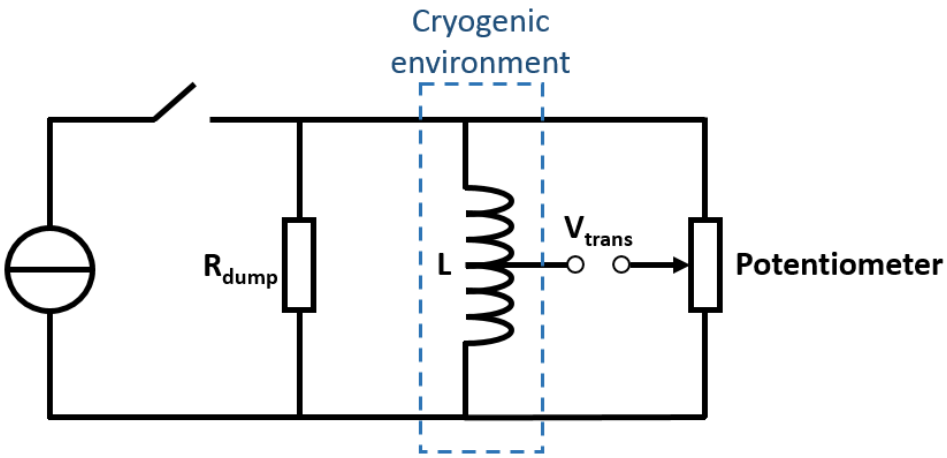

Fig. 40. Electrical circuit of a balanced bridge.

Other means of hot spot detection are still being studied to ensure faster and more reliable detections of thermal runaway in REBCO coils; such as the use of optical fibers, LTS co-wound wire or the modification of the tape along its length coupled with a Hall effect sensor [49, 50, 51].

I.3.3.3.2 Protection discharge

In all cases, once the thermal runaway is detected, the magnet protection can be triggered. One of the most commonly used solutions is to automatically discharge the stored magnetic energy into an external dump resistance (Fig. 41). The dump resistance must be sized to ensure a sufficiently fast discharge to limit the heating of the hot spot ($\tau = L/ R_{dump}$, L: inductance of the coil, R_{dump}: resistance of the dump resistance). However, the dielectric strength of the magnet must also be taken into account and the reduction of τ is then limited by the inductance of the coil: $V_{max} = R_{dump} . I$ (where I is the operating current). In addition, as there is always a delay of a few milliseconds between detection and triggering of the protection, it is important to adapt the thickness of the stabilizing copper of the REBCO tape in relation to the calculation of T_{max} for the conductor in order to save precious milliseconds.

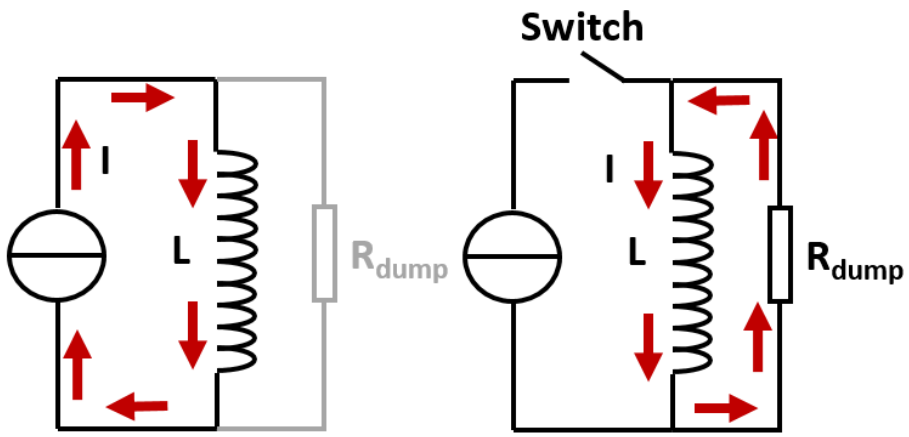

Fig. 41. Electrical circuit of an active protection using a dump resistance. At left: normal operation. At right: fault mode.

Another active protection system can be used with heater elements placed in the winding. As soon as a transition is detected, the heater elements placed inside the winding are activated, quickly enabling a large volume of the winding to return to the resistive state. This helps to dissipate the energy of the magnet in a volume sufficient to limit the increase in temperature. However, this solution is more complex to implement in REBCO HTS and requires very powerful heaters. Indeed, the high critical temperature of REBCO conductors as well as their high thermal stability compared to LTS, implies that the temperature of the coils must be increased significantly in order for a sufficiently large fraction of the winding to transition to the normal state. For example, the 32 T NHMFL magnet using this protection means requires a battery network of the order of 50 kW for all heaters combined [52].

I.3.3.3.3 Hot spot mitigation efforts and conclusion

Mitigation efforts that involve increasing the NZPV of the conductors [53, 54] or increasing the thermal conductivity [55] of the windings are being studied. These solutions all aim at improving the development of the dissipative zone in the coil volume to facilitate the hot spot detection. However, the hot spot issue persists and these solutions also present significant drawbacks such as important modifications of the tape architecture or complicated implementation.

To reduce the probability of a hot spot appearing, one technique is to wind a two-tape bundle conductor [56]. In this way, the probability of a sudden drop in I_c due to inhomogeneities in tape performance or local damage at the same location is greatly limited and the current can be shared between the two tapes. This also has the advantage of improving the effective use of the coil cross section as the number of insulation layers is reduced.

In summary, protecting an insulated REBCO magnet from thermal runaway during a resistive transition is not straightforward. This is only possible with a sensitive transition detection device coupled with active protection. Since the active protection strategy for insulated REBCO magnets is made difficult by the need to obtain a very sensitive detection of hot spots, different approaches having an impact on the winding philosophy have been imagined. Non-insulated or metal-insulated windings have been developed to approach a self-protected REBCO magnet.

I.3.3.4 Non-Insulated and Metal-as-insulation REBCO windings protection

As the name suggests, a non-insulated REBCO coil has no electrical insulation between the turns. This enables the current to flow through adjacent turns as soon as a normal zone appears and thus limits thermal runaway due to a hot spot. This winding method has been shown to be effective against thermal runaway [57]. Tests of non-insulated REBCO coils have been performed at 4.2 K and have demonstrated self-protection even if the source current is maintained for a long time after the quench occurs. In Fig. 42, it can be seen that after a quench to 486 A, the non-insulated coil tested in [58] is able to withstand a current almost as high for over 30 s. In this way, passive coil protection is achieved.

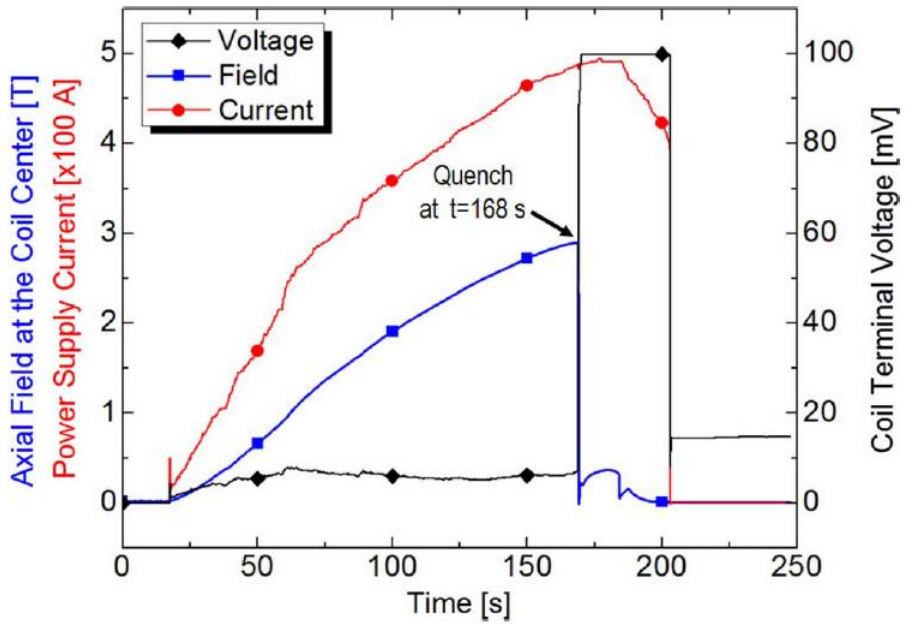

Fig. 42. Overcurrent test results of the REBCO coil at 4.2 K [58].

However, these windings have some drawbacks. Since there is electrical contact between turns, the magnet charge or discharge time constants are slow. In fact, the inductive voltage due to a rapid increase or decrease in the current can become greater than the equivalent turn to turn resistance, which causes the current to short-circuit the turns instead of following the superconducting spiral path. The poor current distribution within the winding also leads to unbalanced axial forces that can result in mechanical damage to the coil.

Moreover, since the current distribution is not precisely controlled turn by turn as in an insulated coil, this has an impact on the magnetic field map of the magnet both in terms of spatial homogeneity and temporal stability. Fig. 43 shows the magnetic behavior as a function of a linear increase in current up to 80 A of seven REBCO coils ranging from an insulated coil (coil 1) to a completely non-insulated coil (coil 7) [59]. The magnetic field of coil 1 increases almost linearly with the current. Since the conductor is insulated, the current cannot bypass the winding. The 1% field error is due to the screening currents as explained in section I.2.5.3. In contrast, for the non-insulated coil 7, the magnetic field does not increase linearly with current at all and a sharp decrease in magnetic field is observed.

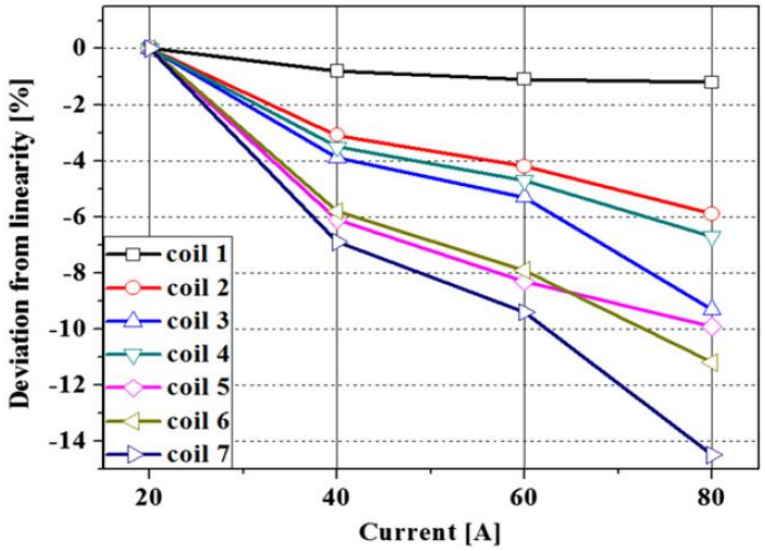

Fig. 43. Magnetic field deviation versus a linear increase in current for 7 REBCO coils ranging from insulated coil (coil 1) to fully uninsulated one (coil 7) [59].

Another winding alternative has been developed in order to maintain the advantage of self-protection but also to reduce the charge or discharge time constants. This is the Metal-as-Insulation winding. By winding a metal tape with the REBCO tape, the contact resistance between each turn is increased. As a result, the charge or discharge time constant is reduced (Fig. 44) and the quality of the magnetic field is also improved (Fig. 43: coil 2 is co-wound with stainless steel). Of course, in order to have the most favorable effect on these two parameters, it is necessary to use a metal that is as resistive as possible.

The performance in terms of magnetic field and time constant is therefore improved, but not as good as for an insulated winding. Moreover, as discussed in I.2.5.5.2 and depending on the thickness and the material used for the co-winding, the Metal-as-Insulation winding has the advantage of resisting high mechanical stress.

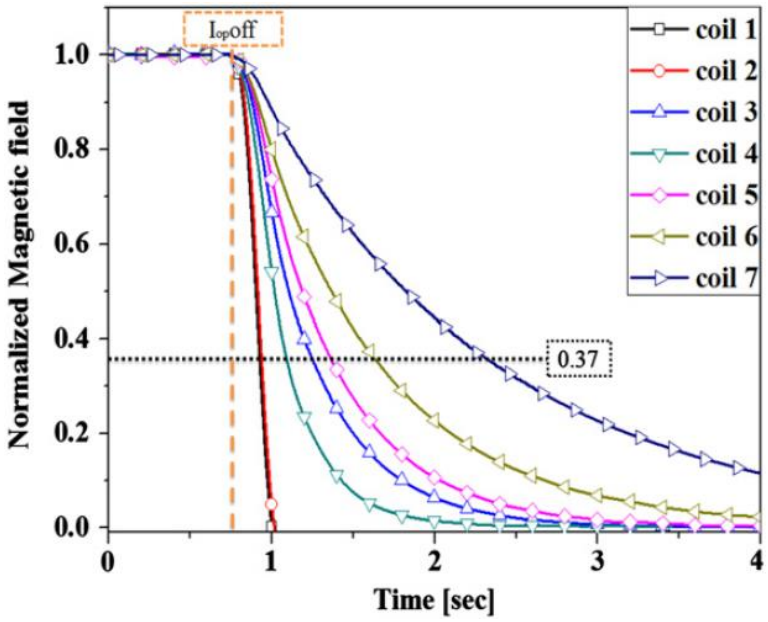

Fig. 44. Discharge test of 7 REBCO coils ranging from insulated coil (coil 1) to fully uninsulated one (coil 7) [59].

I.4 Conclusion

In this chapter basic knowledge required to understand this PhD work was introduced, starting with the phenomenon of superconductivity and its remarkable properties. Different superconductors used in the fabrication of magnets were described with a particular attention to REBCO conductors since they are at the heart of this work. The description of the architecture of these different LTS and HTS conductors as well as their properties highlights the advantages of REBCO conductors for their use in the design and realization of high magnetic field magnets. Starting from the proven techniques used in LTS magnets, a parallel is made with REBCO conductors in order to highlight that conventional approaches cannot be directly transposed to REBCO magnets, due to their complex electromagnetic and electromechanical anisotropic characteristics.

One of the main concerns is to develop reliable protection for these magnets in case of thermal runaway, which is a prerequisite for their large-scale use. Our team has been working on a protection approach based on early dissipative voltage detection to protect insulated REBCO windings [60]. However, the realization of a reliable sensitive detection is complex due to the transient electromagnetic behavior of REBCO conductors during current variations which makes their behavior particularly difficult to predict and complicates the detection of a dissipative zone. An in-depth experimental and numerical study of these transient behaviors is presented in the next chapter to further our understanding of REBCO tape magnet behavior and help determine protection thresholds.

Chapter II:
Transient voltages and energy balance in REBCO insulated magnet: experimental and numerical studies

Summary

Different approaches are investigated today to protect a rare earth–barium–copper oxide (REBCO) coil against local thermal runaway, what is commonly called a 'Quench'. Metal Insulated Coil or No-Insulated coil have been successfully introduced. However, these protections method may show other issues and are limited in terms of dynamics, making them impractical for fast applications such as SMES. In our group, protection based on early dissipative voltage detection followed by current discharge was proposed as a method to protect REBCO insulated test coils. J. Cicéron tested this method successfully during his PhD, using pick-up coils to compensate inductive coil voltage and gain in sensitivity, applying it successfully to test coils with engineering current density in the range of kA/mm². However, we will see that achieving reliable sensitive detection is complex due to the presence of transient voltage due to the hysteretic current distribution in REBCO tape width, which makes the measured signal hard to interpret. This issue of "compensated voltage drift" was first identified by J. Cicéron, and numerical modeling was later developed during the PhD of B. Rozier in order to understand it. Here, we will investigate further the phenomena related to transient current in REBCO coils by combining experiments and modelling. A small REBCO coil, well characterized and instrumented with three different pick-up coils, will be used as reference. It includes notably a co-wound pick-up whose magnetic coupling with the REBCO winding is close to perfect. The post processing and analysis of the numerical simulation results obtained for that reference coil makes it possible to discriminate, in the transient coil voltage, the contribution due to transient losses (generating heat) and that of the coil inductance variation. The resulting evaluation of the REBCO coil inductance and its variations is validated by the analysis of the pick-up coil signals. From a practical point of view, this work shows the possibility to have very sensitive early detection of thermal runaway if the threshold is adjusted based on the expected coil compensated voltage drift. The interest of using insulated high-strength co-wound reinforcement tape as pick-up coil is also highlighted.

II.1 Motivation

II.1.1 Context

As discussed at the end of chapter I, insulated REBCO windings are known to be difficult to protect in case of local thermal runaway. Our research team has been studying insulated REBCO coils for many years, with a particular interest in their protection against the hot spot phenomenon. The high current densities in REBCO magnets as well as the non-propagation of a dissipative spot imposes a very low threshold voltage for the detection, in the millivolt range, to maintain minimal dissipation.

Important work on modeling the thermal runaway phenomenon in insulated REBCO windings has been done by B. Rozier and A. Badel [61, 62, 63]. These models have shown that a sensitive dissipative voltage detection technique can give a sufficient warning to protect an HTS coil using an external dump resistance, even in the case of a high local critical current drop. When applied to a specific magnet design, these models can be used to determine the detection threshold and protection schemes for safe operation.

As an example, Fig 45 shows the quench modeling studies conducted to effectively protect the upgrade to 30 T of the existing 25 T cryogen-free magnet (25 T CSM) at the High Field Laboratory for Superconducting Materials. This model shows that the discharge must occur before the dissipation exceeds a few mV, even with modest current densities (here 199.8 A/mm²). It can be understood that for higher operating current densities the acceptable threshold value will decrease, so that the level of dissipation is kept low enough. Moreover, for a given current density, the added benefit of having a lower detection threshold is that the reaction delay can be longer and reach hundreds of milliseconds or even a few seconds. This time can be used for treating the voltage to avoid false positives due to noise or turns movement. In Fig. 45, between the time the dissipation voltage exceeds 12 mV and the time thermal runaway cannot be controlled, about 1 s has elapsed, which is sufficient to initiate a discharge. The response time can be doubled if the threshold is set at 5mV, become more than 10 s if the threshold is set at 2 mV, and reach 1 minute for 1mV.

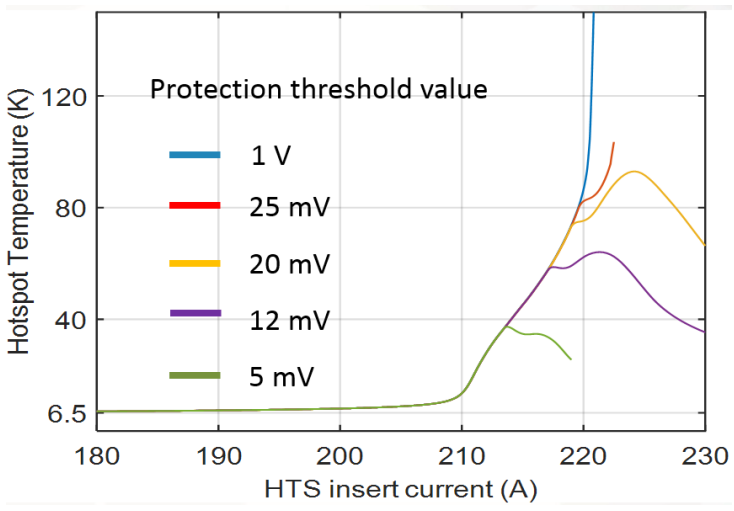

Fig. 45. Dissipating voltage evolution for various protection discharge thresholds [62].

In practice, this small hot spot detection voltage, ranging from a few hundreds of µV to a few mV, must be extracted from the voltage across the magnet. This is not straightforward because the inductive

voltage when ramping up the magnet is often several orders of magnitude higher than the voltage related to the onset of a thermal runaway. The electromagnetic noise itself is often higher in amplitude than the signal of interest. Therefore, in order to detect only the resistive component of a potential hot spot and to gain detection sensitivity, the inductive component of the voltage during magnet charging must be removed from the protection signal.

This has been successfully achieved by J. Ciceron. In his experimental work, it was showed that pickup coils can be used to detect the onset of thermal runaway of insulated REBCO magnets in a sensitive manner and ensure their protection, making it possible to set detection thresholds in the millivolt range. However, the first experimental tests also highlighted the existence of a voltage drift on the detection signal when the current is varying, making the detection of dissipative behavior more complex. Numerical modelling work conducted by B. Rozier established that this drifting of measured voltage was related to the variation of the current distribution in the conductor. The voltage signal useful for the detection of the dissipative behavior must therefore be studied more deeply in order to improve the understanding of the REBCO coil's transient behavior, in order to better interpret the signals used for thermal runaway detection.

II.1.2 Protection strategy for insulated REBCO coils

Fig. 46 shows the electrical test circuit of an insulated REBCO coil. In red the REBCO coil and in blue the compensation coil. In normal operation, the power DC switch is closed. The coil is charged to its current and when desired, the DC power switch is opened to discharge the coil into the dump resistance.

A voltage divider bridge is added on the pickup coil signal to adjust the compensated voltage V_{det} to completely cancel the inductive component (Eq. 6). Practically, the fact that the compensated voltage is always close to 0 makes it possible to use the highest sensitivity for the signal acquisition. The charging time depends on the power supply voltage and the inductance of the coil.

If a thermal runaway is detected during the charging of the magnet (compensated voltage exceeds a predefined threshold) then the energy of the coil is also quickly transferred and dissipated into the dump resistance by automatically opening the switch and thus avoiding a destructive thermal runaway.

This system gives us high protection responsiveness for our insulated REBCO coils and enables to initiate the discharge in less than 20 ms. The value of the dump resistance is defined according to the desired discharge speed ($\tau = L/R$) and the dielectric strength of the coil's insulation. The voltage is highest ($R_d I_0$) at the start of the discharge.

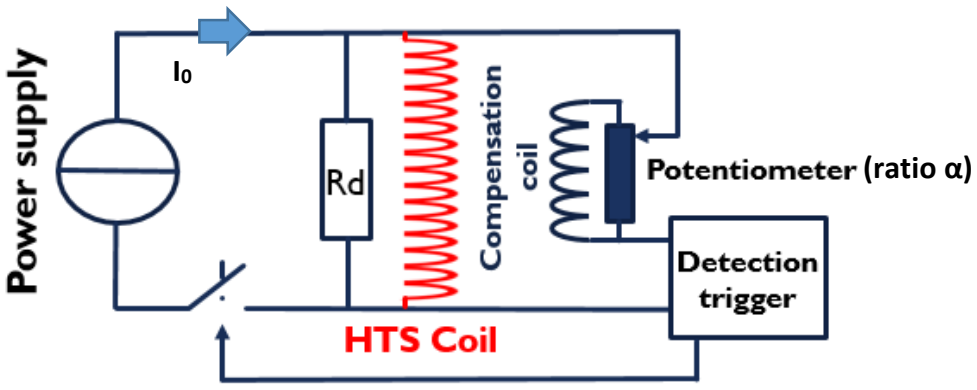

Fig. 46. Electrical circuit to test our superconducting coils.

$$V_{det} = V_{sc} - \alpha . V_{pickup}$$

Equation 6

With V_{det} the detection voltage, V_{sc} the voltage across the superconducting coil, α the coefficient to adjust the potentiometer and cancel the inductive voltage of the coil and V_{pickup} the voltage across the pickup coil.

The size of the pick-up coil must be sufficient to obtain a slightly higher voltage than that of the REBCO coil to obtain the highest possible sensitivity. In order to minimize the size of the pickup coil, it should be placed close to the superconducting coil to ensure good magnetic coupling (Fig. 47).

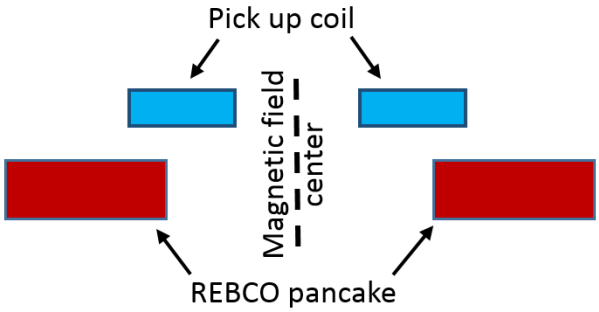

Fig. 47. Magnetic coupling between a superconducting REBCO pancake and its pick up coil.

Instead of measuring the compensated voltage obtained by an analogical voltage subtraction, an algorithm could be used to subtract the REBCO and pick up coil voltages independently measured. However, in that case the acquisition system caliber has to be set higher so that the two measurement channels do not saturate, which leads to a great loss of signal sensitivity.

II.1.3 Transient voltage and compensated voltage drift

The challenge with such pick-up-based compensation is that the compensated voltage has transient components. A voltage signal recorded on a small insulated REBCO coil during a current ramp is shown in Fig 48. Despite a constant current ramp rate, an increase in the voltage across the coil is observed. This could be interpreted as a resistive part that develops in the winding, when the current increases in the coil. However, this evolution is not caused by steady-state dissipation as the signal rapidly goes back to zero as soon as the current reaches a plateau, as it was already discussed in [46, 60, 64]. The evolution is due to electromagnetic phenomena characterized by the current density redistribution, which affects the inductance. Indeed, the classical definition of an inductance, assuming a homogeneous current density distribution, is not applicable in the case of superconducting magnets, especially REBCO ones.

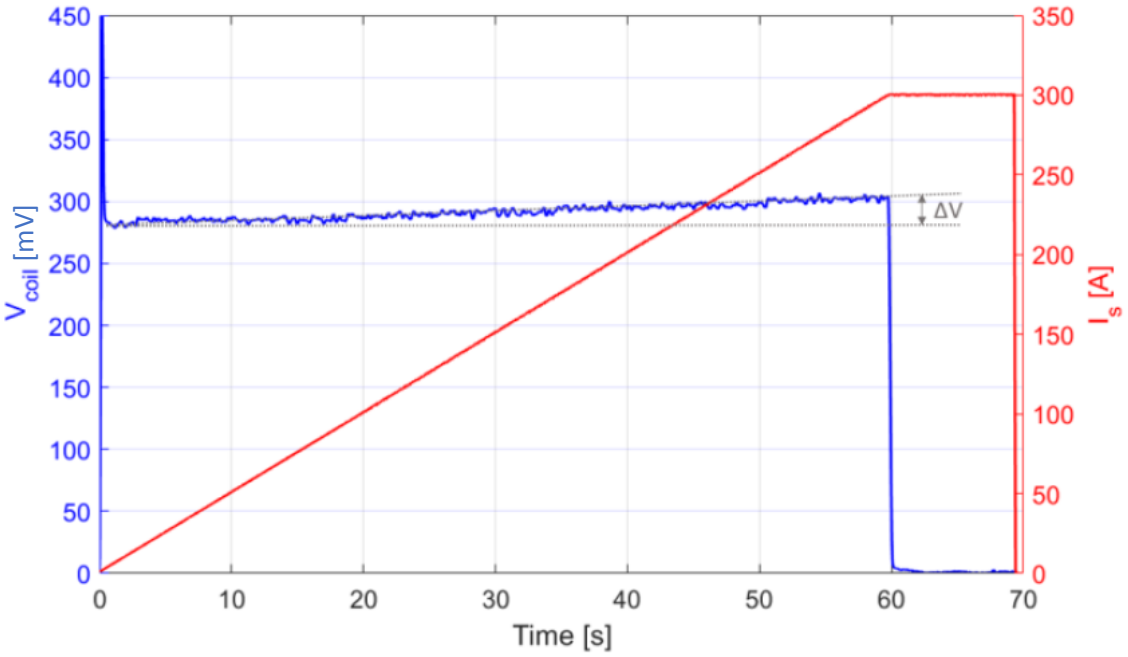

Fig. 48. Voltage across a small insulated REBCO coil during a current ramp.

If the compensation bridge is adjusted to cancel out the REBCO coil inductive voltage at low level of current, the compensated signal starts from zero but then "drifts" when the current increases and may overstep the low threshold values required to protect the coil.

These transient phenomena are shown in Fig. 49 where we see the recorded compensated voltage signal used to detect and protect one of the BOSSE project double pancakes during a current ramp [60]. We notice on this graph the difference of the compensated voltage signal as a function of the current increase between a first current ramp (blank state) in blue and a second one with a higher current target in red. The two current ramps are performed at the same speed, yet the voltage increase is lower for the second ramp. We also notice that as soon as the previously reached current is exceeded, a sudden and rapid increase of the compensated voltage occurs at 600 A. Around 630 A, the slope decreases and the signal goes back to the same trend as the first current ramp. This hysteretic behavior, observed first by J. Cicéron [65] appeared from the start as related to the magnetization of superconducting tapes. In the framework of B. Rozier's PhD, a numerical model was developed to reproduce that behavior, and was successful to reproduce it qualitatively at small scale. From these model results, it appeared clearly that this behavior is related to the inhomogeneous distribution of current density in the tape width and its variation with current amplitude and time.

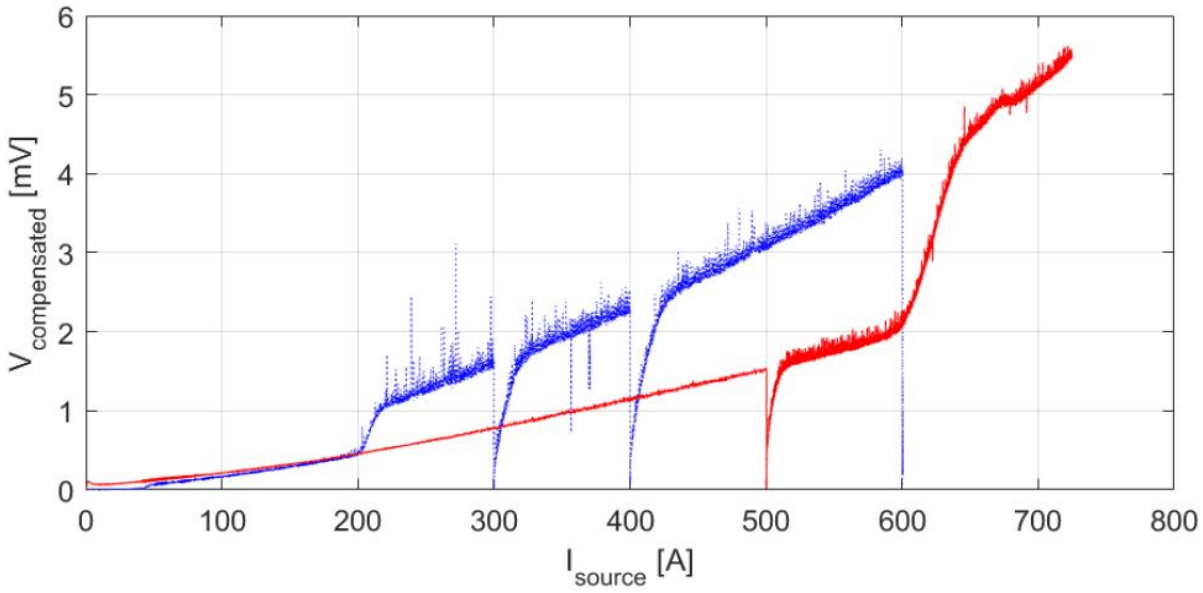

Fig. 49. Compensated voltage signal recorded on a BOSSE double pancake. The blue curve represents the first current ramp after cooling (1 A/s up to 600 A with some plateaus in between) and the red curve corresponds to the second current ramp (same speed but higher current target) - The sudden voltage drops at 0 V correspond to the current plateaus.

This difference between the first ramp trend and the second one (and following) is problematic in terms of protection and complicates the interpretation of the signal. Indeed, this sudden break in the compensated voltage slope could be interpreted mistakenly as the onset of a thermal runaway leading to trigger the protection system uselessly. Moreover, even if this behavior is known and expected, the detection system is in a way blind during the whole duration of the transient, as the sudden variation of the compensated voltage can be up to an order of magnitude higher than the detection threshold range. It is thus clear that it must be taken into account in the detection scheme.

II.1.4 Aim of this work

The aim of this chapter is to develop a better understanding of the transient phenomena in terms of the different contributions, either inductive or dissipative. As previously mentioned, such transient voltages can confuse the detection of a dissipative phenomenon and must therefore be anticipated. For that we will establish the energy balance of a small insulated REBCO coil throughout charge and discharge cycles, and compare the modelling results with experimental data. The test coil is instrumented with three different compensation coils to discriminate the nature of the different contributions to the coil voltage. The first is a pick up coil co-wound with the pancake to get a nearly “perfect” magnetic coupling [66, 67], able to cancel completely the inductive component of the coil signal, the second one is a solenoidal pick up coil close to the studied pancake with a partial coupling, the last one is a Rogowski coil placed at the output of the current source and therefore fully magnetically decoupled.

The chapter is organized as follows. First, the experimental setup will be described, as well as the numerical simulation input data and hypothesis. In a second part, the REBCO coil signals are studied. The model is used to establish the energy balance of the coil and a voltage decomposition is proposed to materialize the distinction that can be made between dissipative and inductive contributions to the transient

coil voltage. This distinction is supported in a third part by experimental results using the compensation coils. Then, an experimental ramping up to runaway is carried out on purpose to investigate protection enhancement. Finally, we will discuss other magnetic behaviors that were visualized during these experiments, before concluding and talking about the perspectives.

II.2 Experimental and Numerical setup

II.2.1 REBCO coil design and experimental setup

The test coil is a single pancake (Fig. 50), which is wound with two tapes in parallel: an insulated REBCO tape (135 µm thick tape, from SuperOx®) and a 30 µm thick *Durnomag*® tape. Both tapes are 6 mm wide. The superconducting tape is made of 60 µm of Hastelloy® C-276 substrate, with 17.5 µm of copper on both sides the tape, and 40 µm of polyamide insulation. The co-wound and REBCO pancake coils have 32 turns. The REBCO coil's current leads are a copper mandrel for the inner diameter and a copper crescent for the outer diameter (Fig.50). Both current leads are soldered at 180°C with InSn at superconducting pancake extremities. The main parameters of the REBCO coil are summarized in Tab. 1.

TABLE 1: REBCO COIL AND PICKUP COILS

SuperOx Tape 6 mm wide 135 µm thick with Polyamide insulation.	
Durnomag® tape 6 mm wide 30 µm thick.	
I_c (77 K sf (100 µV/m))	210 A
32 turns	
Inner diameter	40 mm
Outer diameter	51 mm
Inductance	63.37 µH
Durnomag pickup coil coupling	≅ 1 (32 turns)
Copper pickup coil coupling	≅ 0.36 (340 turns)
Rogowski coil coupling	= 0 (2000 turns)

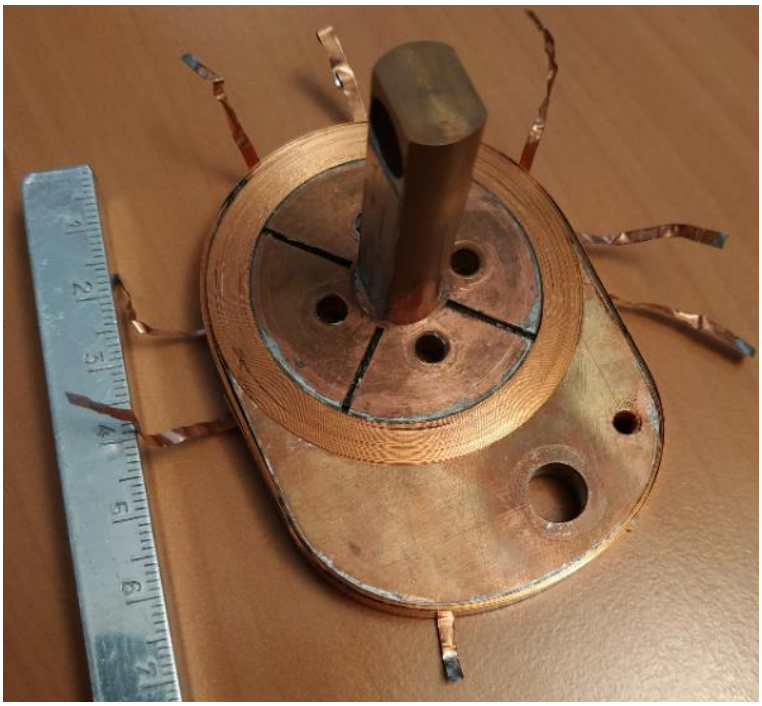

Fig. 50. Single insulated REBCO pancake with a co-wound pick-up coil.

Voltage taps are placed on the copper current leads, the superconducting tape and the *Durnomag*® tape. In order to avoid over thicknesses inside the coil and the risk of local critical current degradation, the voltages taps are made using a thin copper tape (0.05 mm thick and 2 mm wide). They are not soldered on the superconducting tape. Each is directly wrapped around the REBCO tape and soldered on itself to form a loop, the winding tension ensuring the good contact between voltage tap and REBCO tape. The current source is controlled through a LabVIEW program. All voltage signals are acquired using an oscilloscope with differential inputs.

As mentioned previously we use three pick up coils with different magnetic coupling to the REBCO coil.

The one obtained with the co-wound metallic tape is maximal, in the 0.97 to 0.99 range (see section II.4.1). It is made by a co-wound *Durnomag*® tape alloy from Laminerie Matthey S.A. Its properties are close to those of hastelloy, with a high resistivity (70 µOhm.cm) limiting the eddy currents distorting the signal.

The second is a copper solenoid just below the magnet, with a coupling coefficient in the 0.362 to 0.358 range (see section II.4.1), similar to what we could achieve in a real system.

The third one is a torus put on the external current lead (a Rogowski coil). With no coupling at all, it will give us an exact image of the current variation di/dt.

The whole system is schematically described Fig. 51.

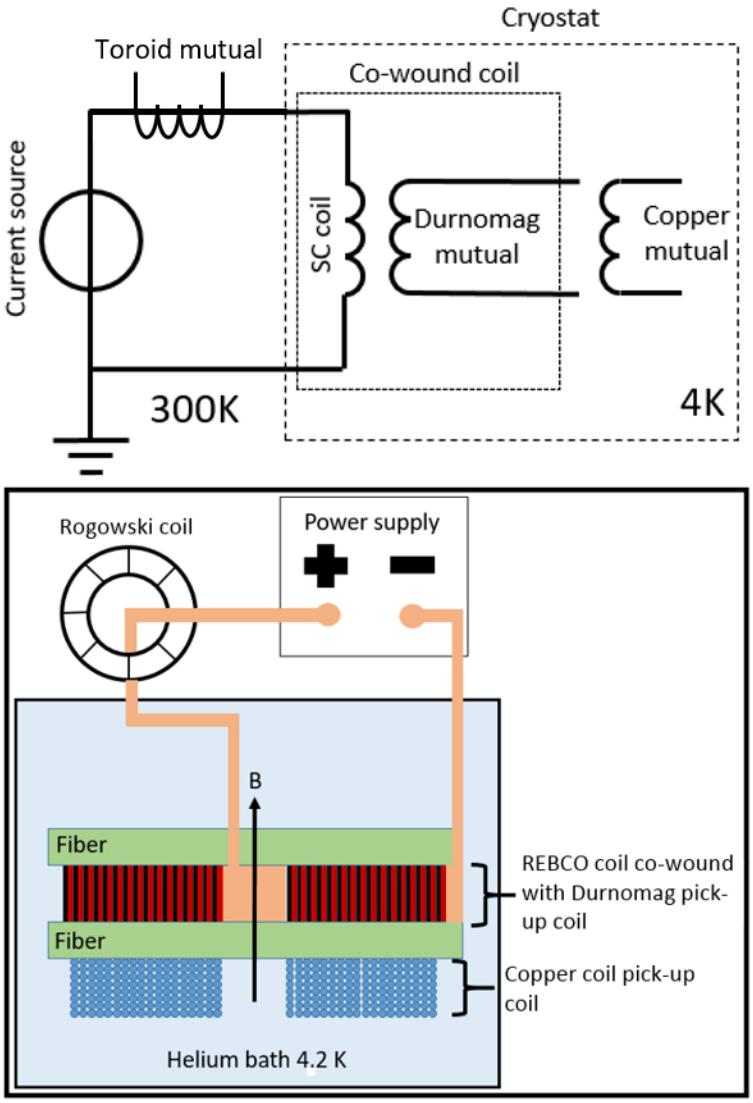

Fig. 51. Electrical circuit (at the top) and a schematic of the experiment (at the bottom).

The experiments are all performed in liquid helium at 4.2 K, with no background field. In order to amplify phenomena due to the current distribution variation inside the superconducting tape, our tests are carried out with fast current ramps of 20 A/s. Fast current ramps also minimize the influence of current leads heating. The discharge is even faster at 100 A/s to minimize burnout risk when ramping up to the critical current.

II.2.2 Numerical model definition and simulation parameters

The model enables to establish the current distribution in the REBCO tape in every turn of the coil. It is a two-dimensional (2D) axisymmetric transient model, developed in Java and implemented in a numerical platform called Mipse (Modelling of Interconnected Power Systems) [68] in development since many years at G2Elab. It is a multi-method platform dedicated to numerical computations which offers more flexibility than commercial computation software. This model uses the so-called J-formulation coupled with a PEEC approach [69] based on a generalization of the partial element equivalent circuit method to compute the

local distribution of the current density inside the REBCO insulated coils. The use of a 2D axisymmetry and the integral method formulation requires a very light mesh compared to a more traditional 3D approach with FEM: only the superconducting layer has to be discretized. The transient version of this formulation, taking into account the REBCO non-linear behavior, was developed by B. Rozier in her PhD work, and was already used for the calculation of the current distribution in superconducting coils [70].

The E-J constitutive equation is a power law with an adjustable index value *n* (set here at 25 based on tape characterization). We assume that this *n* value is a constant, because the impact of small variations in a realistic range is negligible. Trusting the temperature stability of our experimental setup, the temperature is assumed constant at 4.2 K since it is in a liquid helium bath.

The critical current density $J_c(B,\theta)$ then depends only on field amplitude (B) and angle (ϑ) (Fig. 52). We use data from [71], relevant to the SuperOx REBCO conductor used in our experiment, with an adjustment coefficient applied to all data to adjust the surface to the properties of the tape actually used in our coil. In addition, the variations of J_c, along the length of the conductor due to its inhomogeneous performance are neglected.

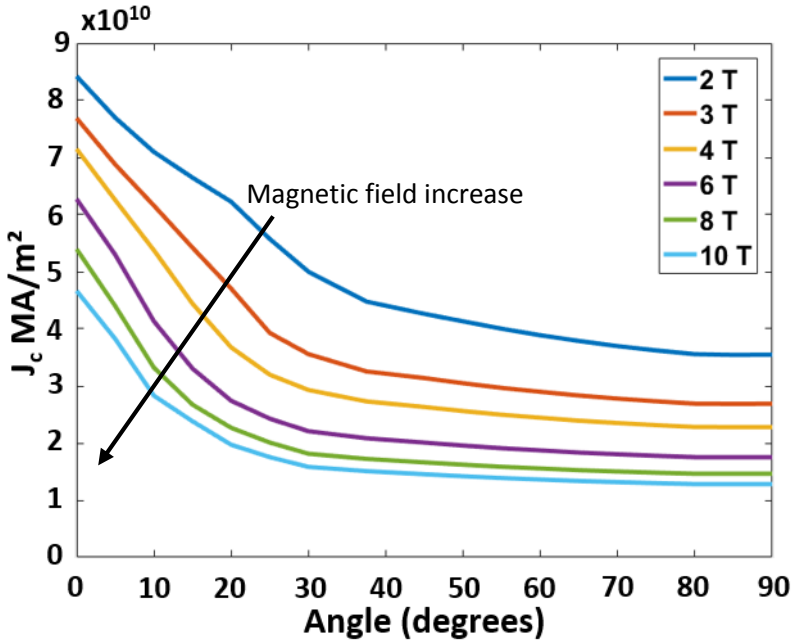

Fig. 52. Reduced critical current density versus angle for REBCO tape for different magnetic field.

The REBCO pancake is modelled based on the coil dimensions as measured after winding (Fig. 53). The turns of the coil are represented by line-segments corresponding to the tape width. Each turn is discretized in 50 elements. No current sharing between the conducting layers of the conductor is considered, the current flows through the superconducting layer only. That assumption is valid at low level of electric field where current sharing is negligible. The current flows only in the superconducting layer as long as the critical current value is not exceeded. Beyond this limit, the model is no longer valid.

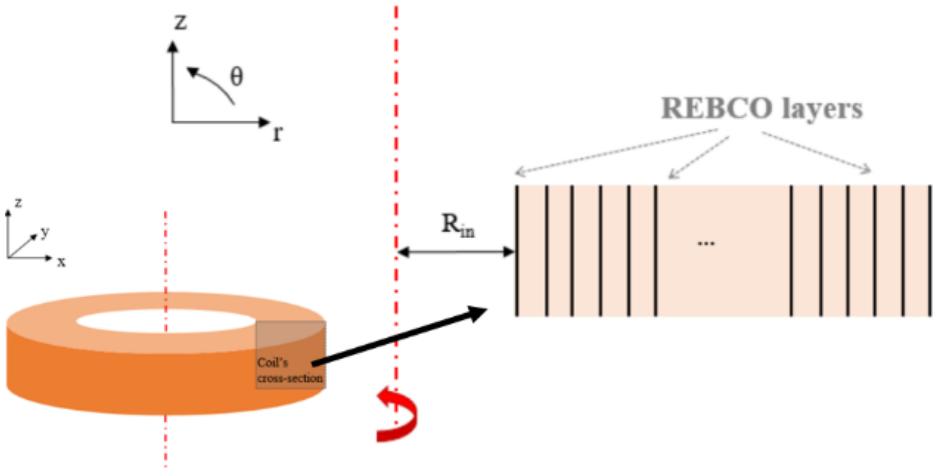

Fig. 53. Simplified coil geometry represented in a 2D axisymmetric view.

The current cycle that we used for the simulations reproduce as well as possible the experimental considering simulation constrains. It consists of successive ramps to 500 A in 25 s, with a 5 s plateau at the top and a very fast discharge (in 1 s) (Fig. 54).

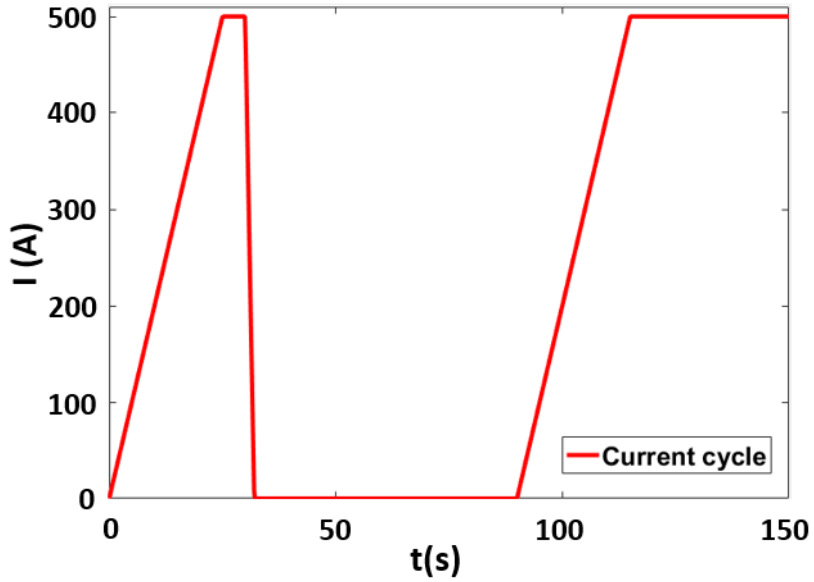

Fig. 54. Current cycle for the experiment and the modelling.

As mentioned above, using integral formulation leads to a significant reduction of the problem size. Indeed, the ratio of the REBCO layer cross-section to the overall coil volume is extremely high. Thin sheet hypothesis (the thickness is not discretized) can also be assumed as the tape aspect ratio is also large (about 6000 for a 12 mm wide tape). This simplifies drastically the model mesh.

The drawback of this method is that the field is only calculated on the conductor. When for post-processing purpose we need to evaluate the field distribution around the coil, FEM axisymmetric magneto-static simulations are conducted using COMSOL, for the given current density distribution calculated by Mipse. This in particular enables the calculation of the stored energy in the coil at any given moment.

II.3 Energy balance and transient voltages: comparison between modelling and experiments

The model mentioned above makes it possible to simulate the dynamic evolutions of the voltage across a REBCO coil (called V_{sc} for now on) during current variations. Good agreement was found in [61] for the coil total voltage, and was obtained as well in our work.

During ramp up, the voltage drift is clearly visible as expected (Fig. 55). It is not the same during the first ramp (in blue) and during the following ones (in black). When focusing on the voltage drift (Fig. 56), it is about 5 times higher during the first ramp than during the following ones. The pink dotted lines on both Fig. 55 and 56 are the simulated data. As in [61], a coefficient was applied to all critical current values taken from [71] to get a good agreement with the experiment. This coefficient relates to the difference between the measured short sample performances and the performance of the length of conductor wound in the coil. It is 0.59 in this case. The initial overvoltage observed on the blue curve is not found by the simulation. We will discuss this in section II.6.

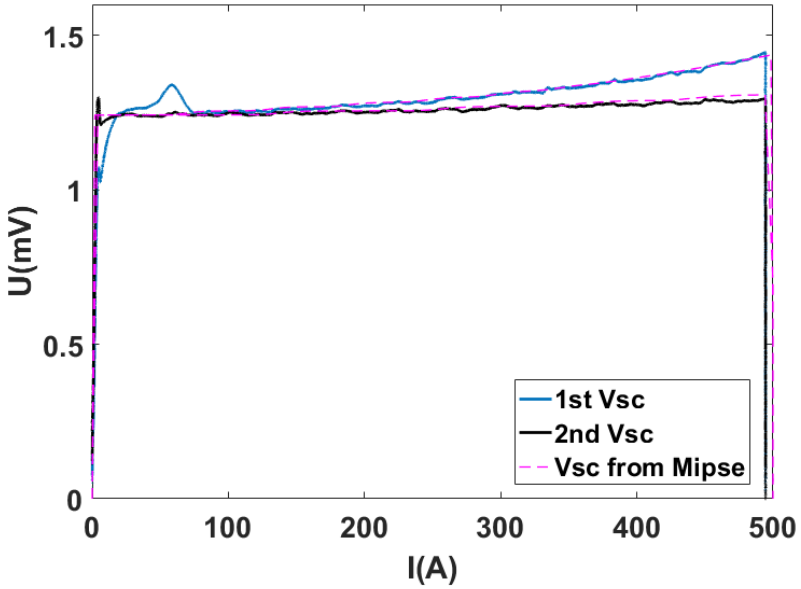

Fig. 55. Coil voltage for an experimental first and second current ramp up to 500 A compared to the modelling results.

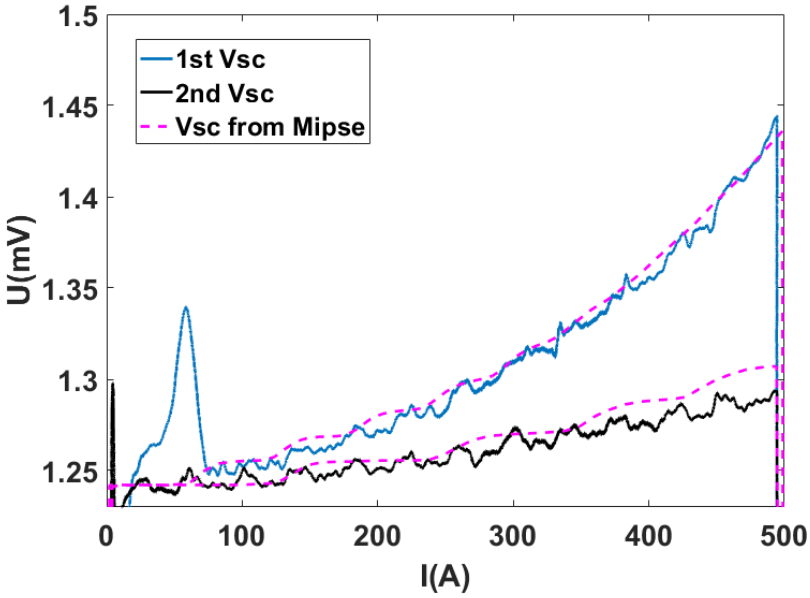

Fig. 56. Zoom on the inductive voltage drift for an experimental first and second current ramp up to 500 A compared to the modelling results.

II.3.1 Decomposition of the voltage across a REBCO magnet during transient

So far the model makes it possible to represent the total voltage, but not discriminate between its components. Proposing a meaningful decomposition of this voltage (v_{sc}) is tone of the objects of this chapter.

A large part of it is naturally the inductive voltage, but the correct definition of an inductance for such a coil with a wide non-linear conductor is not straightforward. Let us consider $L_{ref\ magnet}$ the inductance of the coil for a homogeneous current distribution. It is a constant, even if it may vary slightly due to changes of the geometry if the electromagnetic forces are very high. The voltage related to it is then $L_{ref\ magnet}\frac{di_t}{dt}$.

In addition to that component, a transient voltage component is due to the dynamic distribution of the current density in the conductor width when the coil current varies (and also if the background field varies). Intuitively, we can understand that it is related to the transient losses in the conductor, and thus represent a dissipation, let us call this voltage $v_{trans.\ dissip}$. But the fact that the current redistributes in the conductor width means that the coil inductance is also changing, so that part of this voltage is inductive: let us call it $v_{trans.\ induc}$. We will define these two voltage components in part II.3.3.1 and II.3.3.2.

The voltage across the magnet v_{sc} can then be written as (Eq. 7):

$$v_{sc} = L_{ref\ magnet}\frac{di_t}{dt} + v_{trans.\ induc} + v_{trans.\ dissip} + v_{defect}$$

Equation 7

i_t is the transport current.

With v_{defect} the voltage due to the local overstepping of the critical current: the component that we wish to detect.

$$v_{defect} = E_c \int_0^{\ell_{conductor}} \left(\frac{i_t}{I_c(l)}\right)^n dl$$

Equation 8

Where $\ell_{conductor}$ is the total length of the conductor used in the magnet.

In the next sections we will show that this decomposition of the signals has meaning and can be matched with experimental results. In this part, we want to validate quantitatively our decomposition of the REBCO coil voltage by establishing the energy balance of the coil in modelling and experiments.

II.3.2 Energy balance

The coil inductance is strongly related with the energy stored in its magnetic field. That is why we will focus here on the energy balance of the coil: listing the energy exchanged, dissipated and stored.

II.3.2.1 Input energy.

The one thing accessible from both modelling and experiment is the power supplied by the source, whose integration gives the input Energy W_{in}.

$$W_{in} = \int_t v_{sc}.i_t.dt$$

Equation 9

Fig. 57 compares the energy supplied in the experiment for a first and a second current ramp with the supplied energy calculated from the model. Similarly, to the voltage case, the modelling results are in good agreement with the experimental results.

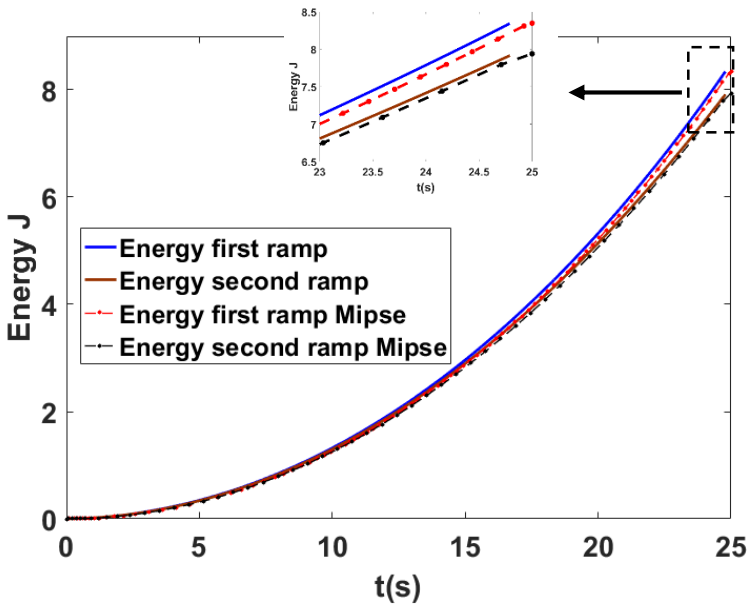

Fig. 57. Energy transfer from the power supply for a first and a second current ramp up to 500 A.

One can notice the energy delta between the two ramps. It is related to dissipative losses, which are bigger for a first current ramp than for the following ones, but also to the magnetic hysteresis of the REBCO coil, as some field remains trapped after the first current cycle.

II.3.2.2 Losses modelling results

In the model we estimate the losses locally based on the local equivalent resistivity (ρ_{equ}). We can then integrate over the whole geometry to get the dissipating power using (Eq. 10), with *n* the power law index, *J* the local current density, and J_c the local critical current density.

$$Pac = \int_V \rho_{equ}.J^2 dV = E_c \int_v \left(\frac{J}{J_c}\right)^n .J\, dV$$

Equation 10

This calculated dissipation Pac is what is commonly called AC losses. They correspond to all dissipative phenomena in a superconducting coil which occur during current or magnetic variations. They are mostly hysteretic losses in our case as we have a single tape conductor. These losses are represented Fig. 58. As can be expected, they are higher for a first ramp, from a magnetically virgin state, than for a second current ramp to the same current, by a factor of approximately 4.7.

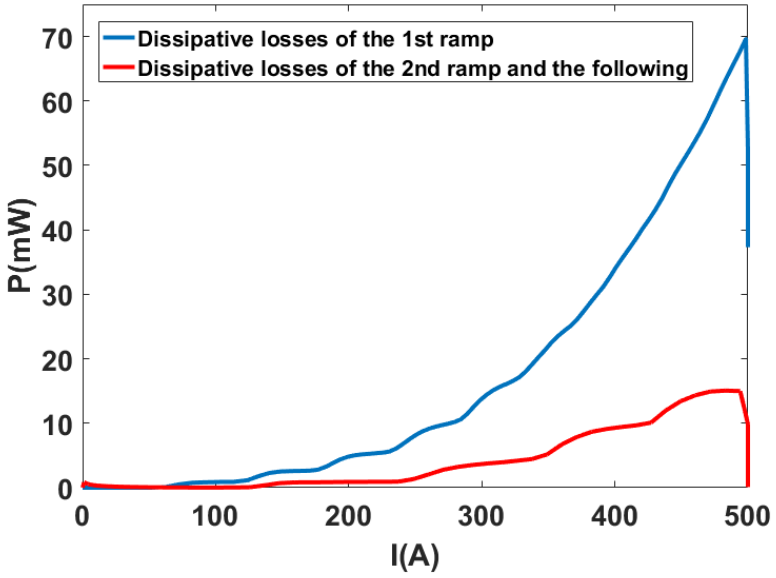

Fig. 58. Dissipative losses for the first, then the second and the following ramps up to 500 A (modelling results).

II.3.2.3 Simulated stored energy

By integration of the losses over time we can then get the dissipated energy during the two current ramps. By subtracting that dissipated energy from the energy injected by the source, we obtain the energy stored in the coil (Fig. 59). That stored energy can also be obtained by integrating the field generated by the current distribution in the coil conductor at any given time, as explained in section II.2.

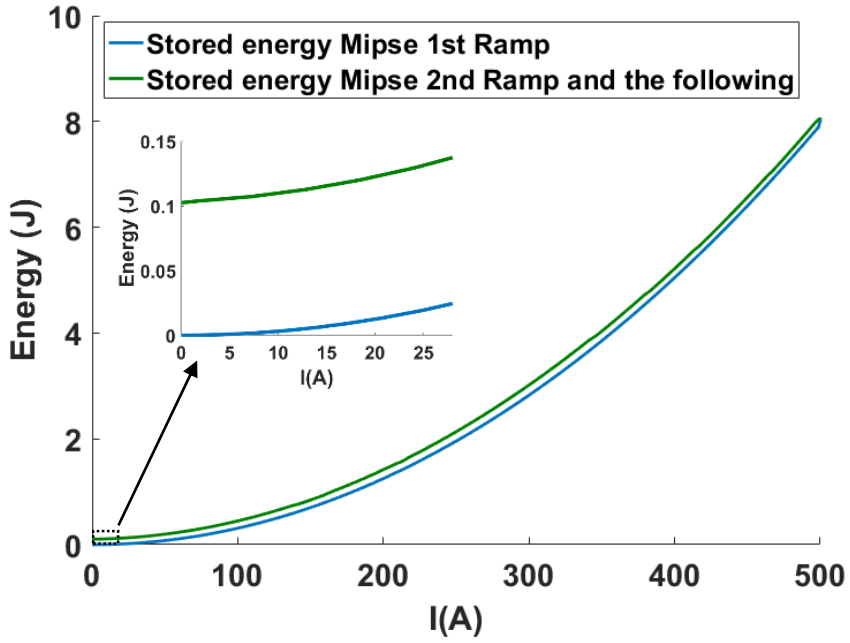

Fig. 59. Stored energy for the first and the second (and following) current ramps.

II.3.2.4 Trapped field and trapped energy

In Fig. 59 we can observe an offset to the stored energy at the beginning of the second ramp. It is due to the trapped field, which stores a small amount of energy.

In Fig. 60 shows the field distribution at the beginning of the second ramp (at t = 90 s, with zero source current), which is the trapped/remanent field. The integration over the volume gives a trapped energy after one charge and discharge cycle of 100 mJ. That is the energy at the starting of the second ramp.

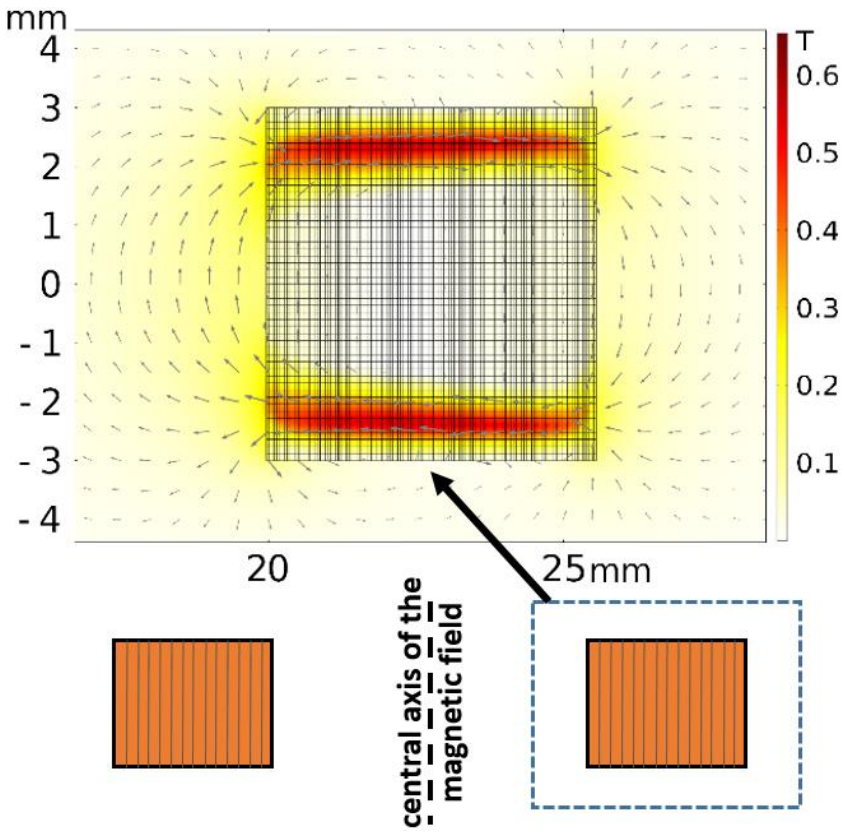

Fig. 60. Trapped field after one charge and discharge cycle. The arrows length corresponds to the log (B).

II.3.3 From energy balance to voltage components

II.3.3.1 Definition of coil inductance

As we said previously, precisely defining the inductance of a superconducting coil with a wide conductor (the REBCO tape) is not straightforward. Here we define an equivalent inductance L_{eq} for a given transport current I_t, related to the variation of the stored energy since the beginning of the ramp (Eq. 11).

$$L_{eq}(I_t) = \frac{2(W_{mag}(I_t) - W_{mag}(0))}{{I_t}^2}$$

Equation 11

where $W_{mag}(I_t)$ is the energy stored in the magnetic field for a transport current I_t.

The interest of that definition is that it can be used for the first ramp but also for the following ramps, at the beginning of which the stored energy is not zero due to the trapped field.

Fig. 61 summarizes the evolution of that equivalent inductance during the first (in black) and following (in blue) ramps of current.

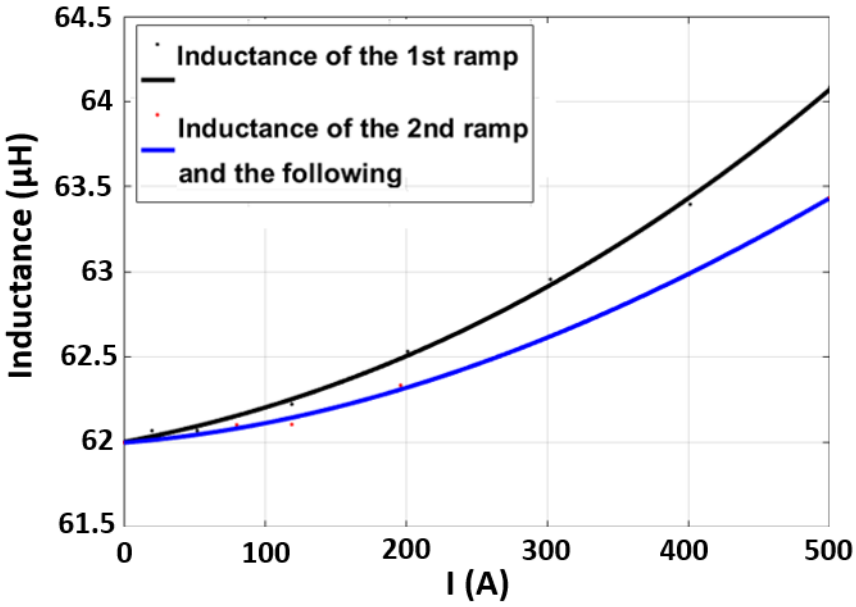

Fig. 61. Equivalent inductance definition based on the energy versus the time.

The rising trend of the inductance with current was expected. In this self-field coil configuration, the current is concentrated on the edges of the REBCO tape and gradually penetrates toward the center while the transport current rises (Fig. 62). This behavior increases the REBCO coil inductance.

Moreover, for the same current the equivalent inductance is smaller for the second current ramp (and following) than for the first. This can be understood: when reaching the maximum current $I_{t\,max}$ (here 500 A), the current density distribution and the magnetic stored energy $W(I_{t\,max})$ are the same for all the ramps, but for the second ramp (and following) there is a non-zero stored energy at the beginning, so that the energy variation during the ramp is smaller than for the first ramp.

The first ramp is unique, with higher losses and part of the energy trapped, so the inductance defined for that first ramp is not meaningful. It does not represent the usual behavior of the coil in operation, which usually consist in many ramps without warming up. During the second ramp and the following ramps, the initial inductance and its variation will remain the same.

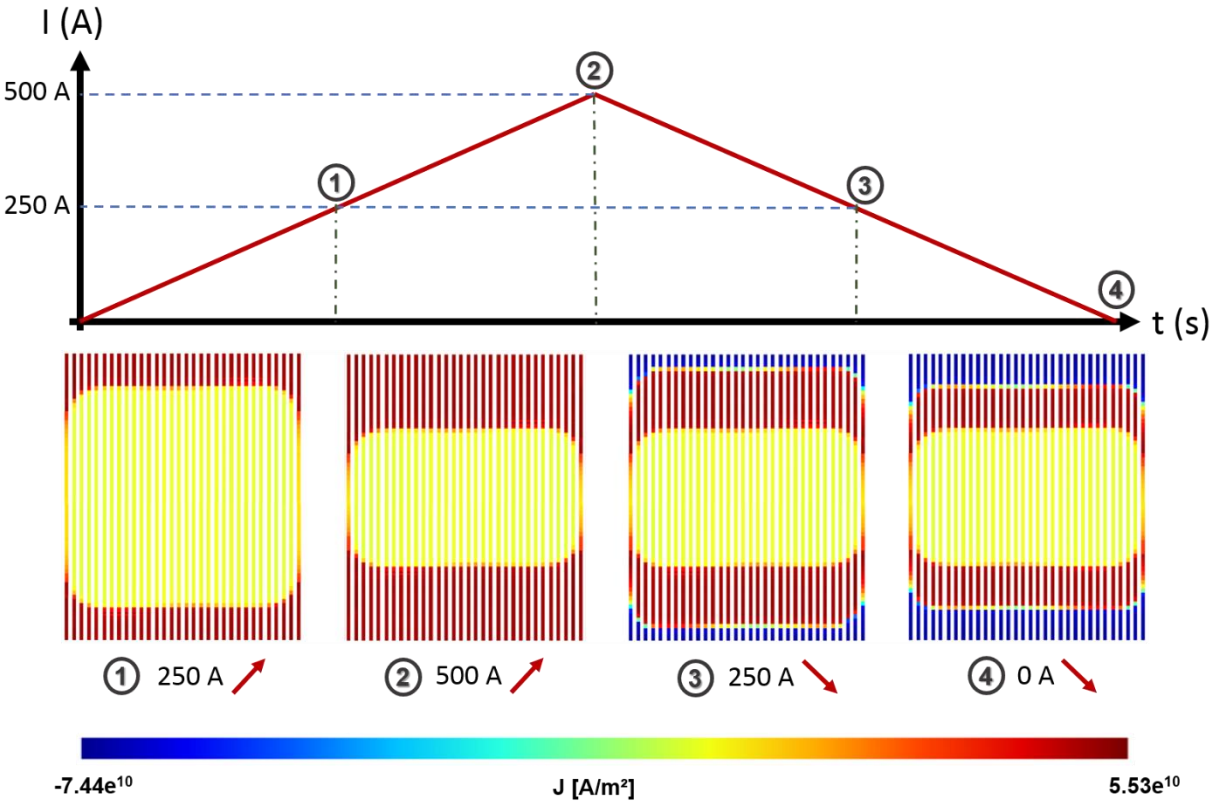

Fig. 62. Current density distribution along the tape width for the following current cycle: 0 A - 500 A; 500 A - 0 A.

The inductance drift confirms our assumption from section II.2: not all of the coil voltage drift is due to dissipation, some of it is inductive. If we regroup the inductive components of the coil voltage, equation 6 can be rewritten as follows:

$$v_{sc} = v_{inductance} + v_{trans.\ dissip} + v_{defect}$$

Equation 12

with

$$v_{inductance} = L_{ref\ magnet}\frac{di_t}{dt} + v_{trans.\ induc} = L_{eq}(t)\frac{di_t}{dt}$$

Equation 13

II.3.3.2 Decomposition of the coil voltage

We can now subtract $v_{inductance}$ from the total coil voltage to evaluate the voltage component representing the transient losses, which we referred previously as $v_{trans.\ dissip}$. The result is shown in Fig. 63 for the first and second ramps respectively.

The largest contribution to the coil voltage drift comes from that dissipative component. It represents about 79 % of the total voltage drift for the first ramp, and 62 % for the second and following. Note that the steps on the curves are due to the discretization of the conductor width in the model. Dotted lines are added to visualize the trends.

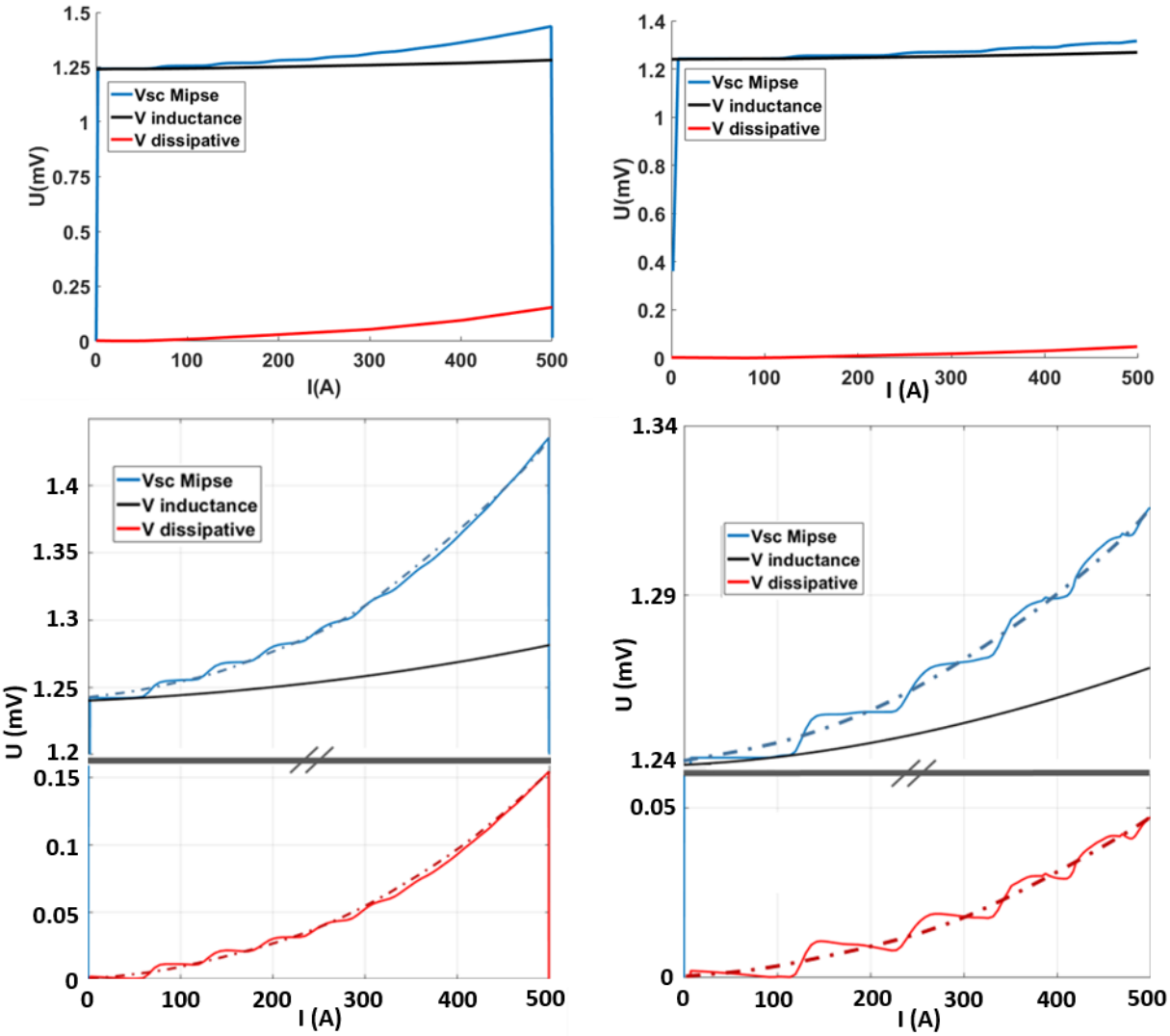

Fig. 63. Calculated voltages contribution for the first current ramp on the left and calculated voltages contribution for the second and the following current ramps on the right. The dotted lines are there to help visualize the trend of the curves.

II.3.3.3 Field hysteresis

As we saw previously in the Fig. 62 the model makes it possible to estimate the current density distribution inside each turns of the REBCO coil. With this information we can calculate the axial center magnetic field (B_{center}) generated by the coil and the magnetic field error (B_{error}) that corresponds to the difference between B_{center} value and the theoretical value if the current density was homogeneous ($B_{homogeneous}$).

$$B_{error} = B_{center} - B_{homogeneous}$$

Equation 14

Fig. 64 present the B_{error}-I curve calculated for the studied scenario, that is to say two current cycles up to 500 A. The curve does not follow the same path during the first cycle and the second, the trapped field being clearly visible.

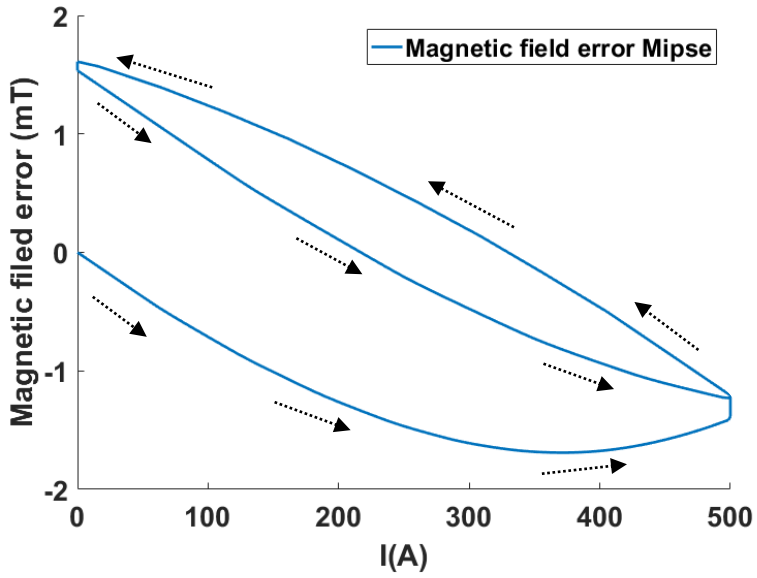

Fig. 64. Magnetic field error from Mipse corresponding to screening current field at the coil center.

This hysteresis cycle actually corresponds to the Screening Currents Induced Field [72]. In our case with only screening current fields in the width of the tape, the field hysteresis cycle is as expected counterclockwise.

II.3.4 Conclusion

In this part, we compared the simulations results with the experiment in terms of coil voltage and input energy, then we post process the modelling results to establish the energy balance of the coil, and from there derive the coil inductance variations. We were then able to propose a decomposition of the coil voltage in an inductive and a dissipative component. These decompositions give us two important information: First, the dissipative part represent the instantaneous losses, which are usually not accessible (AC losses evaluation are generally thought of for a whole current cycle). Second, the inductance variation is of the same order as the voltage due to dissipation, which means that efficiency estimation for SMES operation can only be done correctly if it is taken into consideration.

We will now examine the electromagnetic behavior of the REBCO coil in relation to the 3 different pickup coils and their compensated voltages.

II.4 Analysis of HTS coil behavior using pick-up coils

Let us now discuss the results obtained using pick up coils, both as additional experimental validation of the modelling results, and as a way to get effective thermal runaway detection.

II.4.1 Pick-up and compensated voltage discussion

When using pick-up coils for compensation, we subtract their voltage v_{pick} to the coil voltage v_{sc} to get the compensated voltage (Eq. 15), with *k* the adjustment factor of the compensation (representing the potentiometer).

$$v_{comp} = v_{sc} - k\, v_{pick} = v_{magnet} - k\frac{d\phi_{pick}}{dt}$$

Equation 15

For the Rogowski coil, ϕ_{pick} is the flux generated by the current flowing in the current leads, proportional to di_t/dt, and the compensated voltage is (Eq. 16). We expect it to remain constant throughout the ramp.

$$v_{pick} = M_{Rogowski}\frac{di_t}{dt}$$

Equation 16

For the two pick-up coils magnetically coupled to the HTS coil, ϕ_{pick} is the flux of the HTS coil passing through the pickup coil. Care must be taken when defining ϕ_{pick} in terms of mutual inductance. Even if the pickup coil inductance can be assumed constant, the HTS coil inductance is not, as we established in part II.3. We must then consider the variation of M_{pick} with the time to get v_{pick} , which will then be varying during a ramp (Eq. 17). M_{pick} can be expressed through (Eq. 18).

$$v_{pick} = M_{pick}\frac{di_t}{dt} + \frac{dM_{pick}}{dt}i_t$$

Equation 17

$$M_{pick}(t) = k_{coupling}(t)\sqrt{L_{sc}(t).L_{pick}}$$

Equation 18

where $k_{coupling}$ is the coupling coefficient, that may vary between 0 and 1.

Similarly, to what was done in section II.3 to evaluate the HTS coil equivalent inductance, we performed FEM magnetostatic simulations of the HTS coil and the two coupled pick-up coils for each time step in order to evaluate their mutual inductances with the HTS coil. A homogenous current distribution was assumed in the pick up coils. The results are summarized Fig. 65 for the partially and fully coupled pick-ups respectively. As we saw previously in Tab. 1 the two coupled pick up coils are much bigger (except for the co-wound Durnomag) in order to overcompensate the voltage REBCO coil. We find in Fig. 65 that the copper semi-coupled pick-up coil is higher than the REBCO coil (Fig. 61) as we desired.

The mutual inductance of the semi coupled coil is almost constant, which is explained by the fact that though the HTS coil inductance increase, the coupling coefficient actually decrease, from 0.363 to 0.357 during the ramp from 0 to 500 A.

On the contrary, for the fully coupled pick-up, the coupling coefficient increase during the ramp, from 0.97 at low current to 0.99 at 500 A.

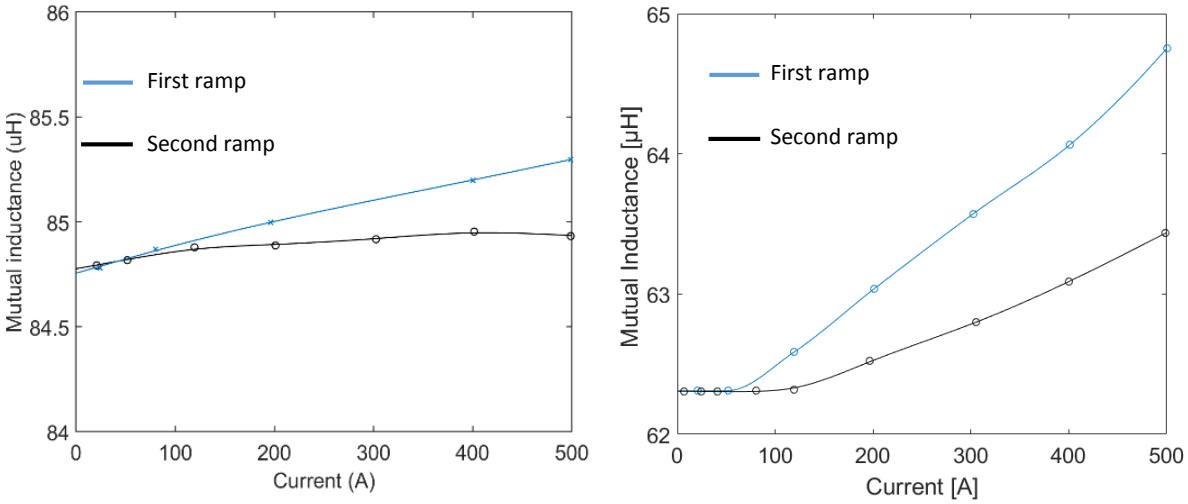

Fig. 65. On the left, the mutual inductance of the partially coupled pickup coil during first ramp (black) and second ramp (blue). On the right, the Mutual inductance of the very well coupled pickup coil during first ramp (black) and second ramp (blue). Estimation based on simulation results.

II.4.2 Experimental results

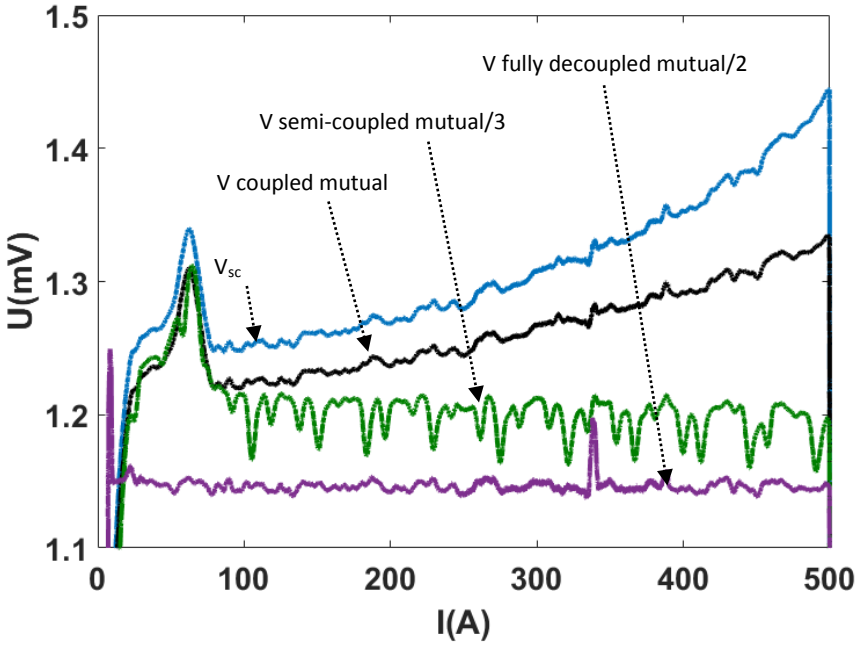

Fig. 66. Voltages from the REBCO pancake (V_{sc}, light blue) and the 3 pick-up coils (V coupled mutual in black, V semi-coupled mutual/3 in green and V fully decoupled mutual/2 in purple) for the first current ramp up to 500 A.

Fig. 66 compares the compensated voltages of the three compensation coils to the REBCO coil voltage V_{sc}. They are labelled as "V coupled mutual" for the voltage on the co-wound pick-up coil, "V semi-coupled mutual" for the copper solenoid pick-up coil placed below the REBCO coil and "V fully decoupled mutual" for the Rogowski coil. The graph does not start at zero to focus on the variation of the measured signals. For a better visualization we also divide the signals of the decoupled and the semi coupled pick-up coils by a factor of 2 and 3 respectively to match with V_{sc} at the start of the ramp, as they were wound with too many turns.

As expected, the voltage on the fully decoupled pick up is constant during the ramp. The partially coupled pick up voltage is also almost constant as expected from the mutual inductance evaluation. It is even slightly decreasing.

The voltage on the co-wound pick-up is increasing during the ramp following a trend similar to that of V_{sc}, as expected.

If we adjust the coefficient α of the compensation (Fig. 46) to cancel the REBCO coil voltage at zero current with the three pickup voltages we get the signals Fig. 67, where the drift of V_{sc} was also added for comparison.

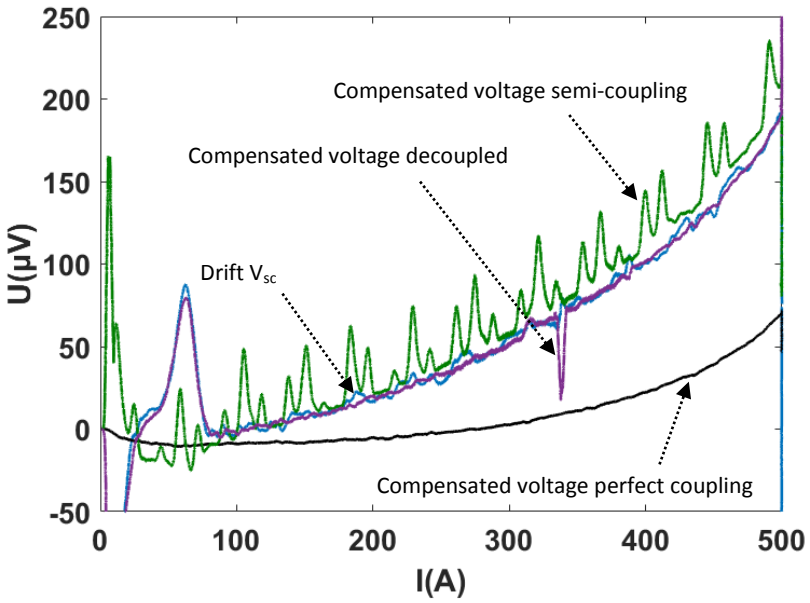

Fig. 67. Compensated experimental voltages compared to the inductive drift from the REBCO pancake for the first current ramp up to 500 A. The compensated voltage of the perfectly coupled mutual is in black. The compensated voltage of the semi-coupled mutual in green as well as the compensated voltage of the decoupled mutual in purple merge perfectly with the REBCO coil voltage drift in light blue.

As expected, the decoupled pick up coil does not compensate the drift of V_{sc}. The partially coupled pick up coil does almost the same.

The very well coupled pick up on the opposite does compensate this drift significantly. At first sight, knowing that the coupling is very close to perfect in this last case, we may assume that the REBCO inductance drift is fully compensated and that what is left is the dissipating voltage we identified section II.3. However, it is not exactly the case: we can observe for example that the compensated voltage (in black) actually become smaller than zero in the 100 to 200 A range.

The signals for the second ramp are showed Fig. 68 for the pick-up voltages and Fig. 69 for the compensated ones.

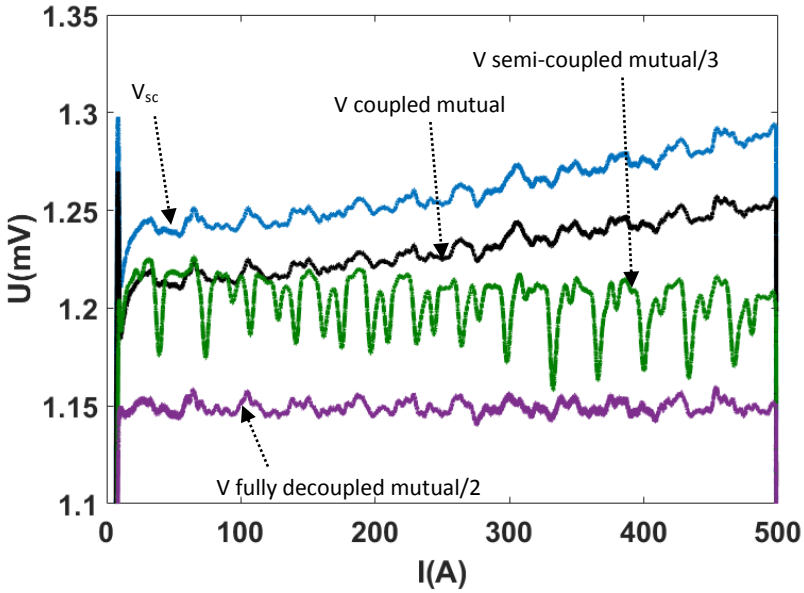

Fig. 68. Voltages from the REBCO pancake (V_{sc}, light blue) and the 3 pick-up coils (V coupled mutual in black, V semi-coupled mutual/3 in green and V fully decoupled mutual/2 in purple) for the second and the following current ramp up to 500 A.

For the second ramp the compensated voltages from the Rogowski and the partially coupled solenoid are still mostly confused with the superconducting voltage drift but their drift is divided by 4 compared to the first ramp (Fig. 69). The compensated voltage from the fully coupled mutual inductance is very close to zero, as can be seen in more details Fig. 70.

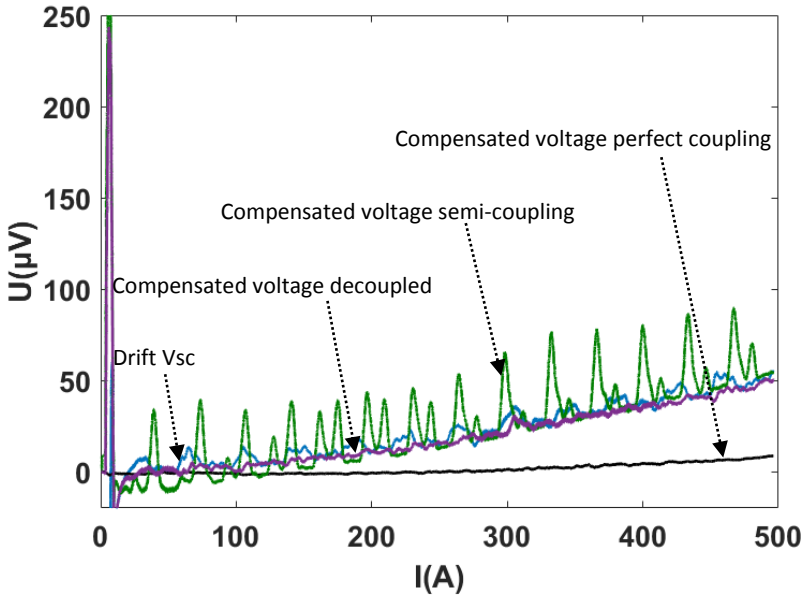

Fig. 69. Compensated experimental voltages compared to the inductive drift from the REBCO pancake for the second and following current ramps up to 500 A. The compensated voltage of the perfectly coupled mutual is in black. The compensated voltage of the semi-coupled mutual in green as well as the compensated voltage of the decoupled mutual in purple merge perfectly with the REBCO coil voltage drift in light blue.

From a practical protection point of view these results can be summarized as follows:

A partially coupled pick-up coil placed in the vicinity of the coil (with a 0.3 – 0.4 coupling coefficient) will compensate the REBCO coil transient voltage in the same way as an external Rogowski coil, but much easier to implement. The voltage drift of such compensated voltage is almost exactly that of the REBCO coil voltage itself, which we already discussed in section II.3.

A fully coupled co-wound pick-up coil compensate most of the REBCO coil voltage drift, especially for the second ramp (only 8 µV versus 70 µV for V_{sc}). It makes it much easier to detect early thermal runaway by mean of a low threshold. The signal also has much less perturbations. Its residual drift, though much smaller, is however not straightforward to interpret.

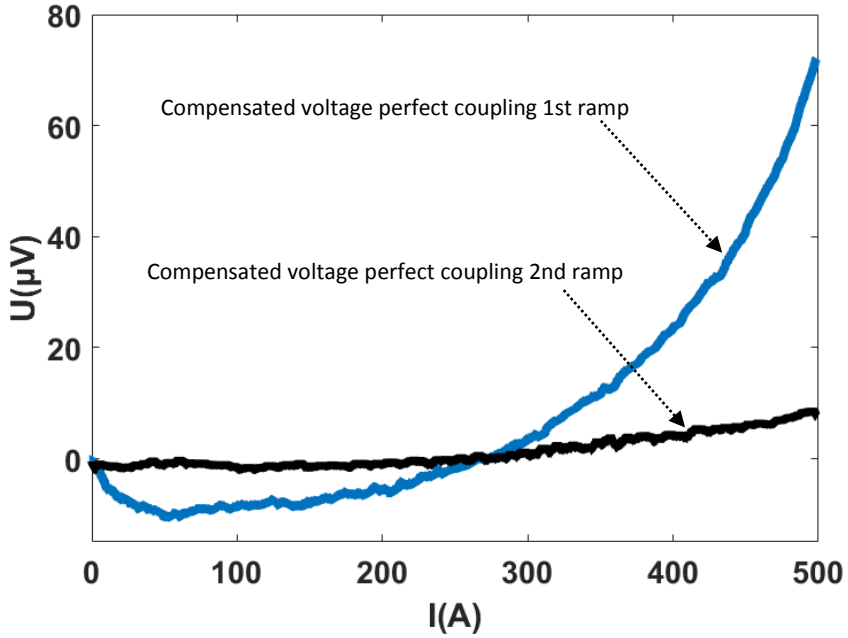

Fig. 70. Comparison of compensated experimental voltage with a perfect coupling for a first (light blue curve) and second (black curve) current ramp up to 500 A.

II.4.3 Prediction of pick-up coil voltages and model validation

Based on the mutual inductances we evaluated in II.4.1 and their time derivatives, we can predict the voltage of the coupled pick-up coils. Founded on our mutual inductance estimations, we expected the voltage for the semi-coupled pick-up to be constant. It is the case, though we did not predict the small decrease. The results for the fully coupled pick-up are more interesting. They are summarized Fig. 71, 72, 73. The rather good match between experimental and simulated voltages is a validation of our estimations for the pick-up coil mutual inductance and thus for the HTS coil equivalent inductance on which it is based.

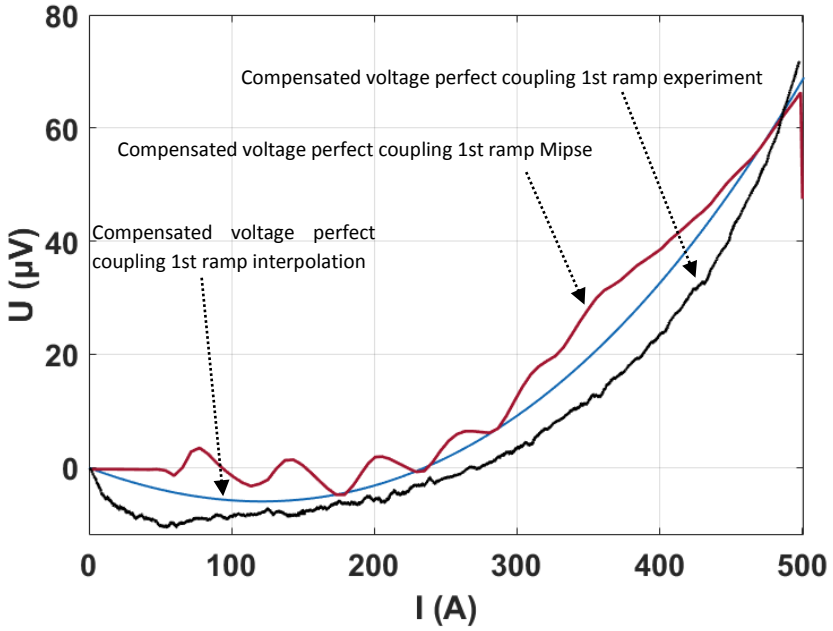

Fig. 71. Compensated experimental voltage with the "perfect" coupling for the first current ramp up to 500 A compared to the modelling results. Experimental curve in black, Mipse curve in red and the interpolation in blue.

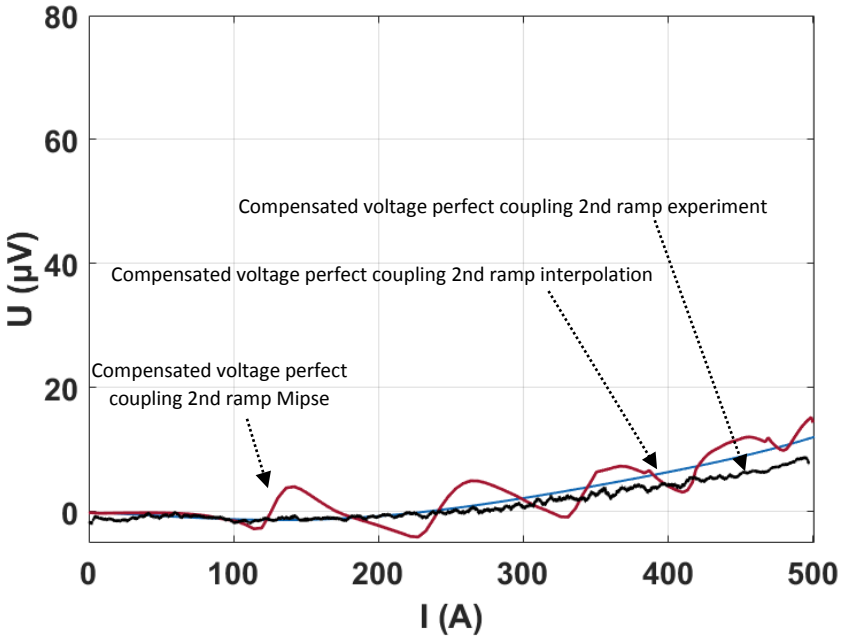

Fig. 72. Compensated experimental voltage with a "perfect" coupling for the second current ramp up to 500 A compared to the modelling results. Experimental curve in black, Mipse curve in red and the interpolation in blue.

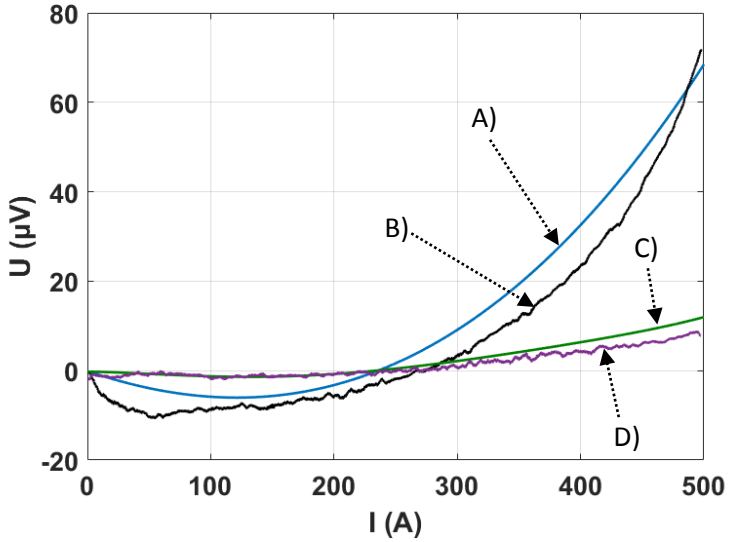

Fig. 73. Compensated experimental voltage with a perfect coupling for a first and second current ramp up to 500 A compared to the interpolations from the modelling. A) Compensated voltage perfect coupling 1st ramp interpolation B) Compensated voltage perfect coupling 1st ramp experiment C) Compensated voltage perfect coupling 2nd ramp interpolation D) Compensated voltage perfect coupling 2nd ramp experiment. 1st ramp experimental in black and its interpolation in light blue. 2nd ramp experimental in purple and its interpolation in green.

II.5 Thermal runaway experiment

We now study the behavior close or slightly above I_c to investigate practically the early detection capability. We can see easily the voltage runaway due to overstepping I_c at 638 A (Fig. 75). In terms of coil protection, we reach a high sensitivity: the threshold could have been set safely to about 150 μV for the Rogowski and the solenoid compensation pick-ups, and down to around 30 μV with the co-wound pick-up (Fig. 74-75).

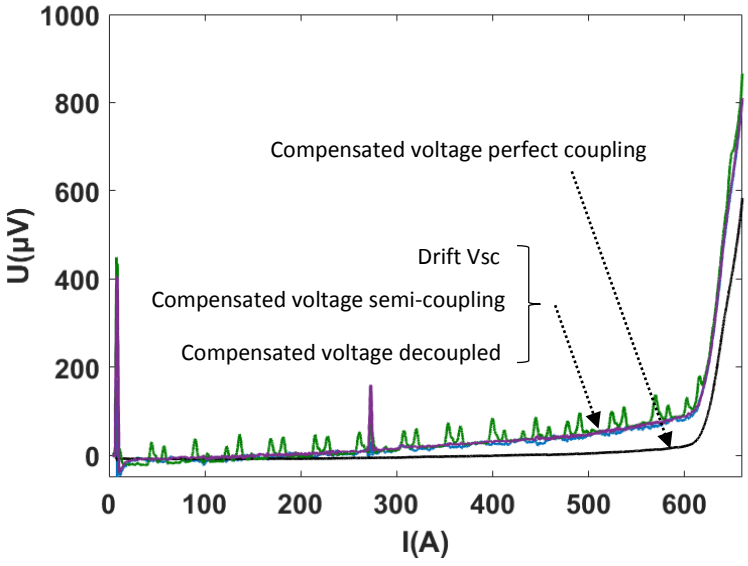

Fig. 74. Compensated experimental voltages compared to the inductive drift from the REBCO pancake up to a runaway. The compensated voltage of the perfectly coupled mutual is in black. The compensated voltage of the semi-coupled mutual in green as well as the compensated voltage of the decoupled mutual in purple merge perfectly with the REBCO coil voltage drift in light blue.

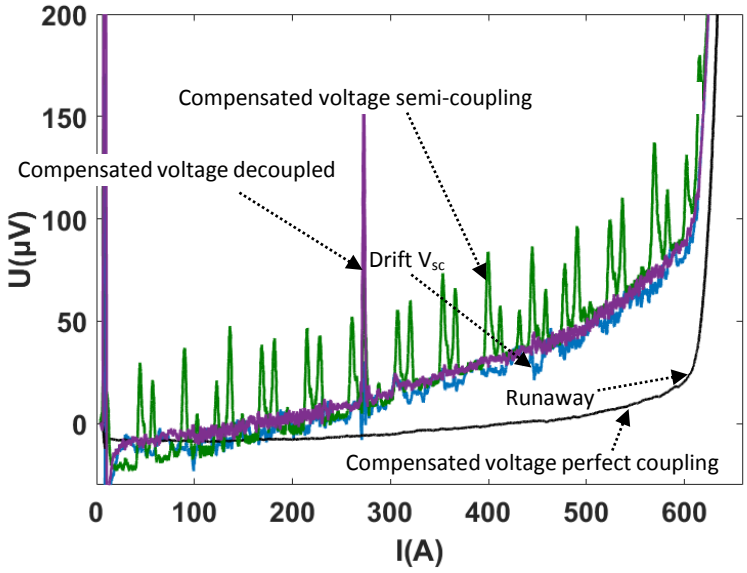

Fig. 75. Zoom on compensated experimental voltages compared to the inductive drift from the REBCO pancake up to a runaway. The compensated voltage of the perfectly coupled mutual is in black. The compensated voltage of the semi-coupled mutual in green as well as the compensated voltage of the decoupled mutual in purple merge perfectly with the REBCO coil voltage drift in light blue.

The sensitivity can be further improved for the semi-coupled and decoupled cases by adapting dynamically the threshold with the signal drift, as this drift is accurately predicted by simulations, and remains the same throughout the life of the coil. The limit in this case would be the spike noise on the signals especially the semi-coupled one.

If we simulate a continuous ramp using the Mipse model, the trend is similar to what was experimentally observed, with exponential voltage increase above 600 A. (Fig. 76). It demonstrates that the input data we used in the model are a good approximation of the tape that was used. The model, though not including thermal coupling predict accurately REBCO coil performances, at least if the dissipation level stays low.

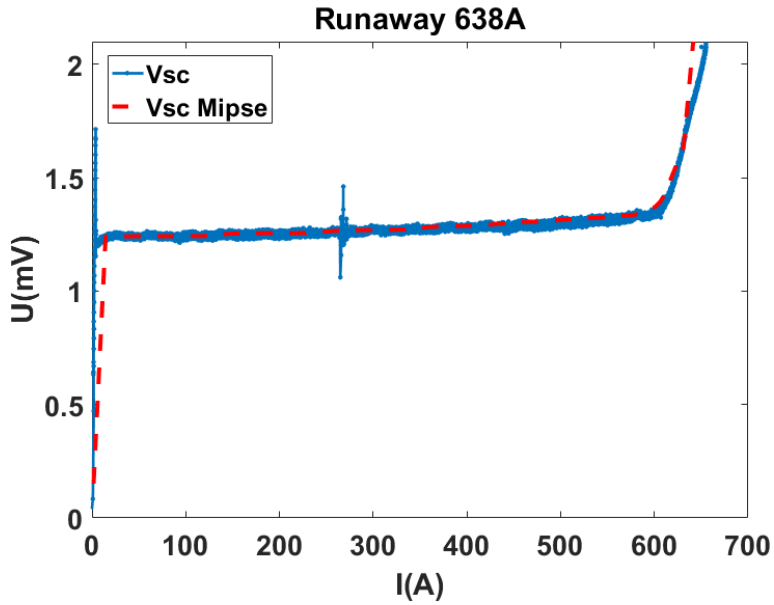

Fig. 76. Comparison between the experimental runaway and the modelling from Mipse.

II.6 Other magnetic behaviors

When we first evaluated the coil, we actually ramped first to 100 A then discharged, and then gradually increased the target current by 100 A steps, each time going back to zero, until reaching the target current 500 A. Each time the previous current is overstepped, the voltage jumps suddenly up to a level corresponding to that of a first ramp to 500 A from a "virgin" state, while below the current previously reached it corresponds to that of a "second" ramp as presented previously (Fig. 77).

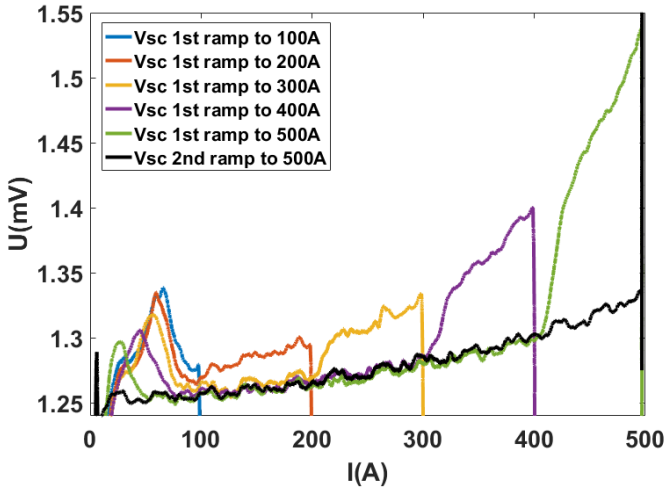

Fig. 77. First current ramps by making steps from 100 amps up to 500 amps by going back to 0 and a second ramp up to 500 A.

At the beginning of every ramps we also notice a spike or "bump" on the coil voltage. This bump is reduced as we ramp each time to a higher current, until disappearing when we reached a current close to the coil critical current (Fig. 78). Currently, we don't know exactly the origin of this behavior, which is not reproduced by the model. We can establish that it is magnetic since we can see similar bumps on the voltage of both the co-wound and the semi-coupled compensation coils. We will investigate this phenomenon on future test campaigns on other REBCO coils.

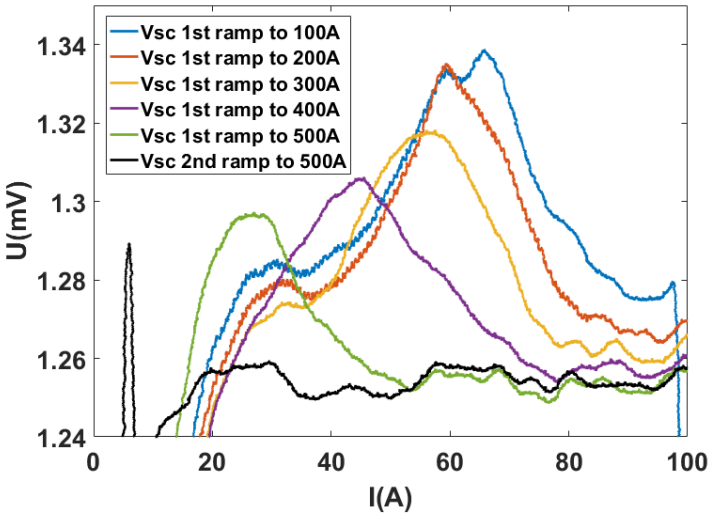

Fig. 78. Unknown magnetic bump decreasing as we get closer of the coil critical current.

II.7 Conclusion and prospect

In this chapter we studied the transient behavior of a small REBCO coil, thanks to three pick up coils whose magnetic coupling with the REBCO coil varies from zero to close to one. Using transient electromagnetic simulations, we were able to quantify the contributions of inductance variation and transient losses on the coil voltage during ramp up, and propose an estimation of the dynamic variation of the coil inductance. We were able to validate this estimation of the inductance, and thus the modelling approach, by using it to predict pick-up coil voltages.

From a practical point of view, we observed that a conventional pick up coil with partial coupling for compensation could be used to get a high thermal runaway detection sensitivity. The detection sensitivity increases if we adapt the threshold dynamically during the ramp based on the expected drift, which can be obtained from simulation results beforehand. This is the solution we consider for future large scale REBCO coils. This new understanding of the transient electromagnetic behavior of insulated REBCO windings will be of great value in interpreting the signals from the numerous Double Pancake and assembly tests performed in the framework of the BOSSE project which will be discussed in the next chapter.

It was established that the thermal runaway detection sensitivity can be much improved using a co-wound pick up coil, which reduces noise and drift. The solution tested here was a co-wound high strength / high resistivity tape. This solution is particularly appealing in applications where the mechanical stress is very large, like high field (or high flux) solenoids, where such tape is already used both as mechanical reinforcement and insulation [5, 73].

The possibility to use the co-wound metallic tape of metal-as-insulation (MI) coils as a type of pickup coil, in spite of the electrical contact with the REBCO tape, needs to be investigated as it could give access to small REBCO coil effective inductance variations and thus provide very early warning of the coil limits.

Chapter III: Superconducting Magnetic Energy Storage: The BOSSE project

Summary

SMES (Superconducting Magnetic Energy Storage) is an interesting energy storage solution for high power pulse operation. In the framework of the DGA BOSSE project, a SMES solenoid is being developed with the objective of reaching 1 MJ with a specific energy of 20 kJ/kg for the winding. To reach such performances, REBCO tapes are used in a liquid helium bath at 4.2 K. The BOSSE project is underway since 2015 and was the subject of the Jérémie Ciceron's PhD. He performed preliminary tests and designed the BOSSE solenoid, which consists in an assembly of 21 REBCO insulated Double-Pancakes (DPs).

In this chapter, SMES and the BOSSE project in particular are introduced. Then the test of each of these DPs at rated temperature in self-field up to its rated current is presented, before the realization and test of preliminary assemblies. These tests are performed safely thanks to a detection and protection system, whose development is presented in details. It relies on magnetic flux compensation and is based on the understanding obtain in chapter II.

III.1 What is a SMES?

Superconductors enable the realization of energy storage systems called SMES, interesting as a high power pulse current source and well adapted to electromagnetic launchers currently powered by capacitor banks (as it was studied in our group in the past [74]). The SMES energy density is limited by mechanical considerations to a rather low value, of the order of ten kJ/kg, but their power density can be extremely high. The heart of a SMES is its superconducting magnet, which must meet requirements such as a low stray field and a mechanical design to contain large Lorentz forces. REBCO high-temperature superconductors have expanded the application range of SMES due to their high current densities (even under a very strong magnetic field), thermal stability and mechanical strength, which are superior to conventional NbTi SMES. This facilitates cryogenics and improves the magnet's stability.

III.1.1 SMES concept

The energy storage concept of a SMES is simple: The idea is to store the energy in a magnetic field generated by a DC current flowing in a superconducting coil. The absence of resistivity in the superconducting state makes it possible to store energy in a superconducting coil short-circuited on itself. As the current is not dissipated by Joule effect, the magnetic energy is conserved almost indefinitely. Hence the name, Superconducting Magnetic Energy Storage. The big advantage of SMES is that there are no mechanical or chemical energy conversion for discharge, which maximizes the round-trip efficiency of the system. In addition, they are highly reactive and energy can be stored or released quickly.

The SMES coil can be defined by its inductance *L*. Therefore, the stored energy E_{mag} can be expressed not only as the integral in space of the product of the magnetic field *H* and the magnetic induction *B,* but simply as a function of *L* and *I* (Eq. 19).

$$E_{mag} = \frac{1}{2}LI^2 = \frac{1}{2}\iiint_{Space} BH dx dy dz$$

Equation 19

There is a strong similarity with the energy storage in a capacitor (Fig. 79): Where a superconducting inductance stores energy in magnetic field produced by a persistent current due to its zero resistance, the capacitor stores energy in electric field under a given voltage, due to its infinite inner resistance (Eq. 20). A SMES can be considered as a current source while capacitors are voltage sources.

$$E_{SMES} = \frac{1}{2}LI^2 \qquad E_{Capa} = \frac{1}{2}CV^2$$

Equation 20

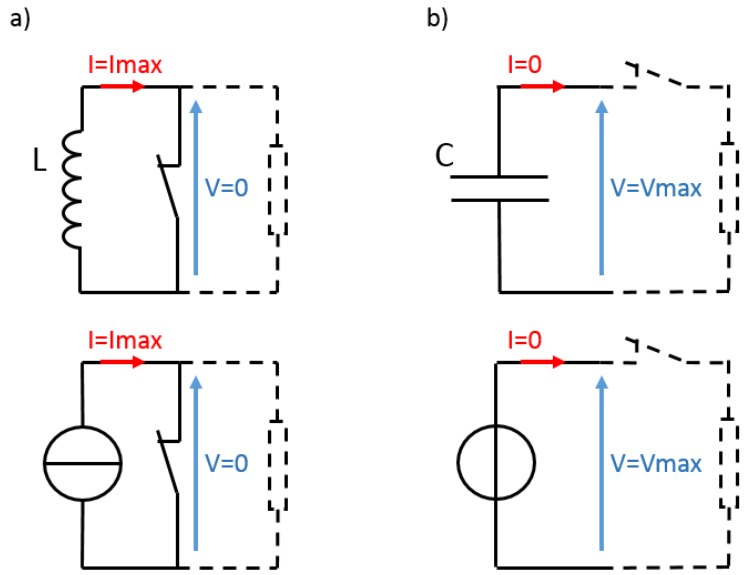

Fig. 79. Inductive (a) and capacitive (b) storage with discharge circuit.

The power output of a SMES is given by the product of its rated current and its maximum discharge voltage. Therefore, a large current is required to achieve high power outputs. Direct storage of electrical energy in a SMES can achieve cycle efficiencies greater than 96% under certain conditions. However, this energy balance does not take into account the energy needed to cool the system. Indeed, despite the high critical temperature of REBCO conductors (90 K), they are generally used below 20 K and most often at 4.2 K (liquid helium bath) because the lower the temperature, the higher the Ic. The efficiency is therefore quickly degraded for long term energy storage since the fixed costs prohibit their use as storage, and their use as a buffer is the only credible one. Therefore, SMES are best used as a pulsed energy source by performing continuous charging and discharging.

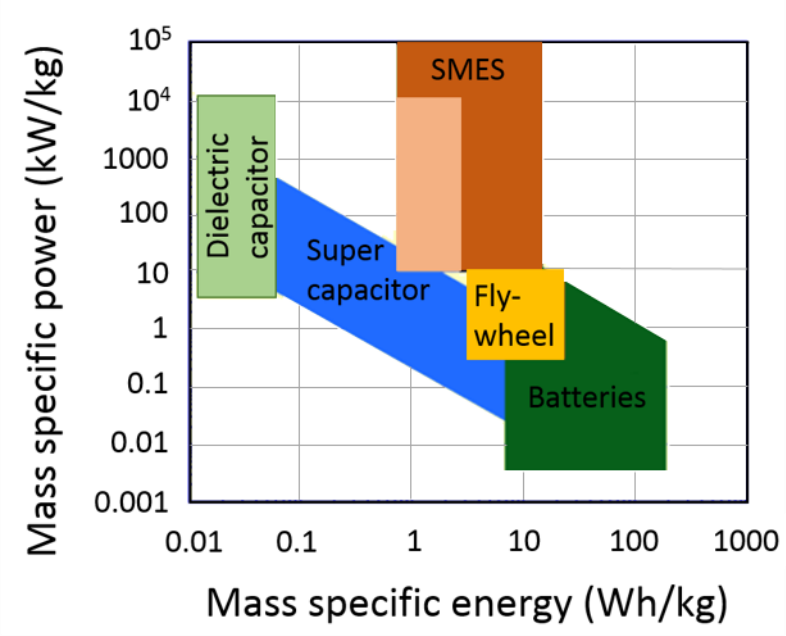

Fig. 80. Energy and Power densities for classical electric storage (Ragone chart) [75].

Fig. 80 compares the SMES to different storage devices, such as batteries and capacitors, in terms of specific mass energy and power. We can see that the energy density of inductive storage is limited. It is lower than batteries, but higher than capacitors.

III.1.2 HTS SMES and DGA project

The appearance of high temperature superconducting materials, and in particular REBCO conductors, makes it possible to consider very high energy density coils, because they can carry a high current density (more than 2000 MA/m² in average under 13 T at 4.2 K and still more than 1600 MA/m² under 21 T on short samples). They also have a very good mechanical resistance, which is an important feature as the magnet mechanical structure limits SMES energy per unit mass as for every electromagnet (see section I.2.5.5). For all these reasons, REBCO tapes enable to considerably improve the performances of SMES compared to other materials, in terms of weight, volume and thermal stability, and thus to enlarge their field of application.

Since 2004, a SMES program funded by the DGA (Direction Générale de l'Armement) has been launched at CNRS Grenoble to consider SMES as an energy buffer to supply electromagnetic launchers. The operating principle of an electromagnetic launcher is relatively simple (Fig. 81). It consists in accelerating a projectile by the Lorentz force. To do this, two electrically conductive rails are placed parallel to each other. Between these rails, a projectile with a sliding electrical contact is inserted. The circuit formed by the two rails connected by the projectile is then fed by a pulsed current source. The strong current flowing in this loop (rails + projectile) creates a magnetic flux density, thus creating a force and an acceleration of the projectile.

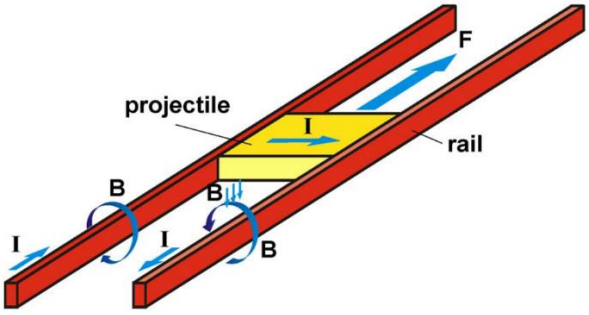

Fig. 81. Electromagnetic launcher principle.

The interest of these launchers is that the projectile can reach very high speed, higher than 2000 m/s. Such speeds cannot be reached with conventional methods. These launchers can be used for military purposes, such as guns and aircraft catapults. They could also be used to place nano-satellites in orbit. However, the current must be very high (from hundreds kA up to several MA) to obtain high output speeds of a few km/s.

Today, very large capacitor banks/inductances are used to power these launchers. The PEGASUS launcher of 10 MJ developed at ISL (Institut Recherches Franco Allemand St-Louis) uses this type of power supply and reaches a speed of 2000 m/s for a current of 1 MA (Fig. 82). However, these capacitor banks are very bulky, due to their low energy density on the one hand, and the low efficiency of the conversion chain

on the other hand. This is why a SMES, that is to say an inductive pulse source, is particularly well adapted to the supply of electromagnetic launchers.

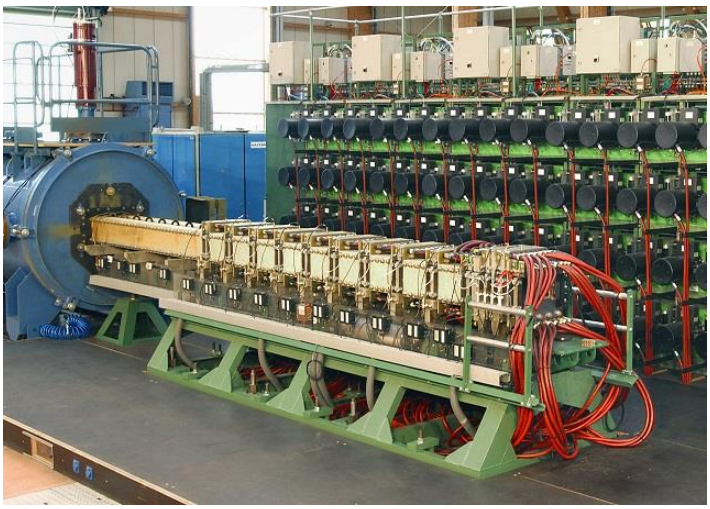

Fig. 82. Pegasus 10 MJ launcher (from ISL).

In Grenoble, a first SMES of 800 kJ composed of first generation HTS Bi-2212 tape was successfully tested in 2009. It was cooled by thermal conduction at a temperature of 20 K [76]. This work was continued through the BOSSE project with the design and realization of a new 1 MJ SMES made with second generation HTS REBCO tape. The conductor is one of the key components of the SMES. The high current transport capacity of REBCO tapes under strong magnetic field enables to improve considerably the mass and volume energy densities of SMES.

III.2 The BOSSE project

This PhD was conducted in the framework of the BOSSE project. This project started in 2015 and was already the subject of a previous PhD by J. Ciceron [60], at that time, I was in charge of the realization of the HTS REBCO superconducting windings at Neel Institute. In order to identify the contributions of each on this project, a brief history of the project as well as the work done by J. Ciceron will be described first in this chapter. This will also make it easier to understand the final design of this SMES and its evolutions considering the various constrains.

III.2.1 The history of the BOSSE project

Through the BOSSE project, one of the fundamental objectives was to develop the mastery and use of REBCO conductors in the manufacture of insulated high magnetic field magnets. To this end, J. Ciceron conducted a reflection to get the best out of REBCO tapes and determine the most suitable topology to achieve the objectives of the project. That is to say, to beat the current record of mass energy density of

13.4 kJ/kg [77] for a superconducting coil and reach 20 kJ/kg for a total energy of 1 MJ. In order to achieve these goals, the coil will be cooled by a liquid helium bath (4.2 K) to maximize the performance of the conductor and reduce the cost.

First, here are the constraints imposed on the design of such a magnet.

- The superconducting magnet must be designed to minimize the amount of superconducting material for a given magnetic energy in order to maximize its specific energy, but also to minimize the conductor cost.

- The operation of the magnet must be ensured by a good cooling to guarantee the superconducting state of the conductor and its design must ensure the mechanical support of the coil. Indeed, to reach such a high specific energy, high levels of stress and current density are required. Here, in order to maximize the specific energy, the large Lorentz forces will be contained by the conductor itself.

- The magnet must also be protected in case of hot spots to avoid its destruction. The difficulty lies in the fact that the thermal stability of a REBCO magnet as well as the high current density that flows through it requires a very fast reaction. For this purpose, J. Ciceron proposed and developed the protection strategy described in section II.1.2 of chapter II, which is based on a sensitive detection of the hot spot through pickup coils.

There are two main magnet topologies for a SMES: the solenoid and the toroid. At the beginning of the project, given the budgetary constraints and the high objectives, these 2 topologies were studied to determine which solution would minimize the amount of conductor used. The solenoid has a simple structure and the electromagnetic forces are easier to manage than in a toroid. A toroid is, in fact, subject to a large radial force toward the center axis, in addition to transverse and longitudinal forces. In addition, the solenoid has a higher specific energy than a toroid with a circular cross-section in the case of an isotropic conductor [78, 79]. However, since REBCO tapes have a strongly anisotropic behavior with respect to the orientation of the magnetic field B, a toroidal solution was also interesting since toroids have the advantage of having a low field in the radial direction.

For the project energy and energy density targets, the two solutions were of similar performances. The choice to finally design a solenoid using a conductor by SuperOx® was influenced by additional practical considerations:

- a solenoid is much easier and cheaper to manufacture (simpler support pieces and machining).

- a solenoid is much more modular than a toroid in case of pancake destruction. It can be shortened slightly without too much performance drop, while a toroid would be totally unbalanced, which would force to replace the pancake.

- for the electromagnetic and electromechanical characterization of the SMES elements, the solenoid pancakes are much easier to test individually in an external magnetic field.

- the toroid solution would have been beneficial only considering the specific properties of the REBCO tapes from the Fujikura® company, but these were out of budget. Its performances using SuperOx® tapes were lower

Before arriving at the final design of the solenoid on which I worked, several design iterations were conducted by J. Ciceron. Indeed, the designs studied have evolved in line with budget constraints related to the cost of REBCO conductor lengths. In the first designs, the solenoid was an assembly of several pancakes with multiple width. This concept adapts the coil ends by using wider tapes to compensate for the reduction in current-carrying capability due to the increased transverse field. It also enables all pancakes to be connected in series with a high current rating while matching the current density, and ultimately decreasing the cost of the conductor.

This led to a first version of the solenoid (Fig. 83) whose characteristics are as follows. An inner radius of 90 mm, a winding thickness of 30.5 mm and a height of 508 mm. It was composed of 48 pancakes with different conductor lengths: 36 pancakes made of 6 mm wide tape, then 8 of 8 mm and 4 of 12 mm. The rated current was 486 A which corresponded to an average current density in the winding of 600 A/mm² in the 6 mm pancakes. The maximum (longitudinal) field strength was 13.1 T and the maximum transverse field strength was 5.5 T. The hoop stress was 440 MPa. The total energy was 943 kJ and the specific energy is 21 kJ/kg.

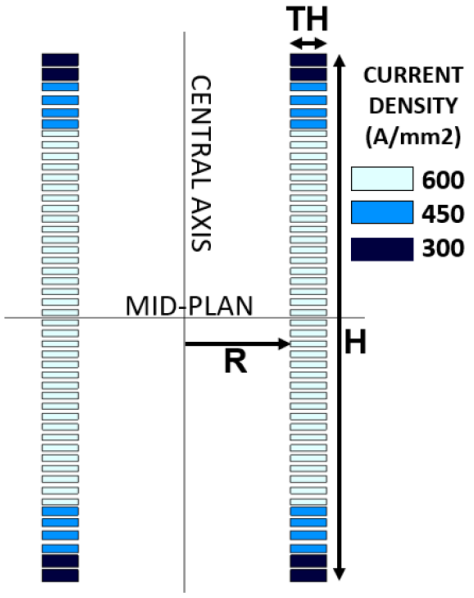

Fig. 83. Winding cross-section of the first BOSSE solenoid design using the MW method [60]

However, another constraint came in the way of the realization of this solenoid. The 6 mm wide conductor lengths were cut from 12 mm wide tapes. At the time, the slitting operation caused serious damage to the conductors and degraded their performance. As a result, the manufacturer had great difficulty in delivering the conductor lengths. Therefore, it was decided to make the solenoid entirely from 12 mm wide tape. A description of the adapted design made by J. Ciceron will be detailed more specifically in the next section III.2.2 since it is on this configuration of the solenoid that I carried out a part of my PhD work.

This change in configuration came very late in the project and J. Ciceron's PhD. A large part of his experimental work concerned the multiple width design of the solenoid. Therefore, he had already done several preliminary works, in particular the tests under external magnetic field of a pancake with a 6 mm wide conductor, in order to determine its limit performances and to validate the design of this SMES [65]. As

this validation was no longer valid for the new design, a new 12 mm DP prototype had to be realized and tested. It is at this level of project progress that my PhD began.

In the following parts this chapter will thus describe:

- The experimental validation of the SMES final design by testing the prototype DP in 12 mm.
- The transfer of competence to Sigmaphi and the industrialization of the DPs.
- Individual experimental tests of the SMES DPs.
- Experimental tests of the SMES sub-assemblies and their protection.

III.2.2 Final design of the BOSSE solenoid

As mentioned above, the final design of the BOSSE SMES is a solenoid made of 12 mm wide REBCO tapes. It will reach 1 MJ for a 850 A rated current, at which point the center field reaches 11.5 T. The magnet aims to achieve fast discharges under 5 kV (time constant of 1 second) which corresponds to a peak power of 4.2 MW. A first objective is to surpass the record for mass energy density, by reaching 14 kJ/kg. The final goal is to further increase the operating current further to reach 20 kJ/kg in the winding, which requires 890 A. Tab. 2 summarizes the different important quantities according to the objective in specific energy density to be reached.

TABLE 2: OBJECTIVES TO ACHIEVE

Energy	0.775 MJ 14 kJ/kg	1 MJ 18.1 KJ/KG	1.105 MJ 20 KJ/KG
I (A)	745	850	890
J (MA/m²)	460	523	550
B_z^{max} (T)	10.14	11.53	12.12
B_r^{max} (T)	3.7	4.2	4.4
Max. hoop stress (MPa)	306	396	421

III.2.2.1 BOSSE design

The coil is composed of a stack of 21 DPs, each with a soldered inner joint. They are manufactured by the SIGMAPHI company [80]. The total height of the solenoid is 814 mm and the inner and outer diameters of the solenoid are 188.5 mm and 240 mm respectively (Fig. 84). Since the multiple width method is no longer applied, its geometry is optimized at the coil ends by varying the spacing between pancakes: it is progressively increased in order to reduce the transverse field distribution and thus improve the critical current (Tab. 3). The important rated values of the SMES for the most ambitious operation point, 20 kJ/kg, are listed in Tab. 4. Thanks to these varying pancake gaps, the maximum transverse magnetic field on the conductor is 4.4 T. The central pancakes generate the greatest magnetic field and are therefore the most useful for energy storage. This is verified mechanically by the Virial theorem [81] since these pancakes have the highest circumferential stress to reach 421 MPa. Indeed, according to this theorem, the specific energy is proportional to the stress on the conductor. Therefore, to ultimately reach 20 kJ/kg, the BOSSE solenoid must operate at high levels of mechanical stress and current density.

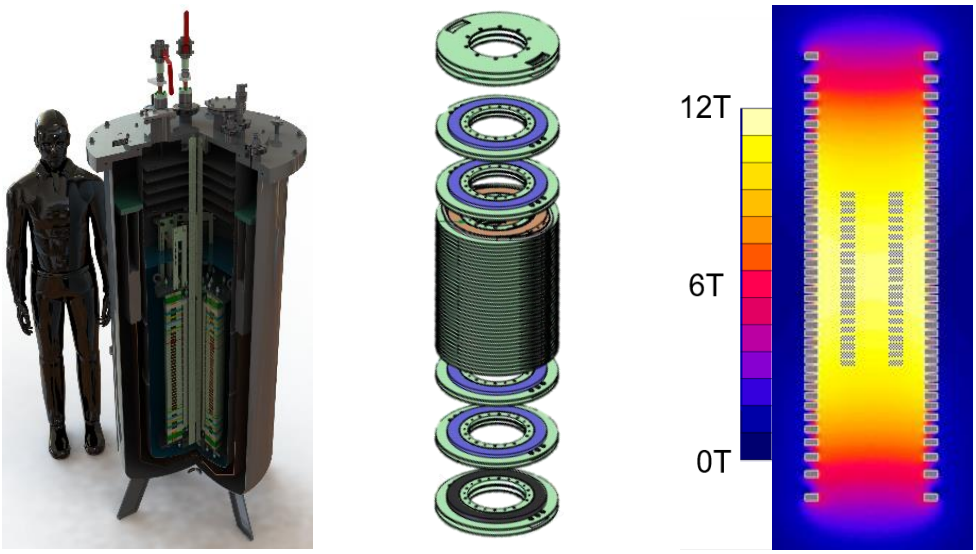

Fig. 84. Assembly of the solenoid and its magnetic field map.

The current margin of the solenoid was determined using data from a comprehensive characterization of $J_c(B,\Theta)$ at 4.2 K of SuperOx® tapes by T. Benkel [71]. The critical current of each tape is evaluated on the basis of the magnetic field value and its orientation measured over the tape width. Then, the "limiting» critical current of the SMES is equal to the critical current of the turn with the lowest critical current, due to the fact that the pancakes are all connected in series. With the SMES current rating fixed at 850 A to reach 1 MJ, the calculated current margin was 50 %. However, we will see that the value of this margin was rather optimistic thanks to the test up to the electromagnetic limits of the prototype DP, and that it is more in the range of 20 %. Indeed, the reference critical current data for these tapes [71] to estimate the current margin was for short samples with good performance. These data are not necessarily representative of a conductor's performance over longer tape lengths. The main characteristics of the BOSSE solenoid are shown in Table 2 and more details about the BOSSE project and the general coil design are presented in [60].

TABLE 3: GAP BETWEEN DPS

30 mm gap	2 x DPs
15 mm gap	2 x DPs
10 mm gap	2 x DPs
6 mm gap	2 x DPs
4 mm gap	13 x DPs

TABLE 4: RATED SMES OPERATION VALUES FOR 20 KJ/KG

Energy	1105 kJ
Height	814 mm
Inner diameter	188.5 mm
Outer diameter	240 mm
B_z^{max}	12 T
B_r^{max}	4.4 T
I operating	890 A
J_e	550 MA/m²
Max. hoop stress (full cond.)	421 MPa
Length of tape per pancake	121 m
Specific energy	20 kJ/kg
Pancake number	42
Inductance	2.79 H

III.2.2.2 Manufacturing of the Superconducting Double Pancake

III.2.2.2.1 The BOSSE conductor

As mentioned before, the REBCO superconducting tapes used to make the DPs are from the manufacturer SuperOx®. This manufacturer offered the best compromise between price and low temperature performance at the beginning of the project. The conductor (Fig. 85) is made of a 60 µm thick Hastelloy C-276 substrate on which buffer layers, the REBCO layer, as well as the silver layer are deposited. All these layers together form a thickness of about 5 µm. Copper is electrodeposited all around for thermal stability. In order to achieve a specific energy of 20 kJ/kg, the thickness of the copper stabilizer is limited to 30 µm in total (15 µm of copper on each sides of the tape). Finally, in order to perform fast discharges, SMES requires good electrical insulation. Another advantage of SuperOx tapes is that it is the commercial REBCO tapes insulated with a thin polyimide coating. In this way, the electrical insulation obtained is thinner and the average current density of the winding is less impacted. In order to guarantee a good dielectric performance but also not to degrade too much the mechanical strength of the coil, a thickness of 20 µm of polyimide is deposited on each side of the conductor. The total thickness of the conductor (insulating tape) is between 0.12 mm and 0.14 mm, with the thicknesses of the layers fluctuating slightly, particularly those of the polyimide coating and of the copper stabilizer.

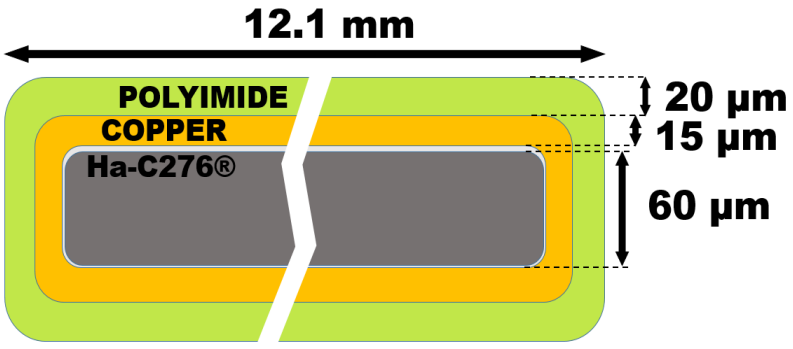

Fig. 85. REBCO conductor diagram used for the manufacture of the SMES of the BOSSE project.

REBCO tapes are not perfectly rectangular in cross section. They are curved slightly along the width, with "bone" shaped edges (Fig. 86). This is a disadvantage as the turns do not align perfectly during the winding, makes it less compact. This leads to variations of the number of turns per pancake. Even if it is not critical in this application as magnetic field homogeneity is not our main concern, this negatively affects the energy density. It can also affect the turn to turn redistribution of stress and thus the mechanical limit of the winding.

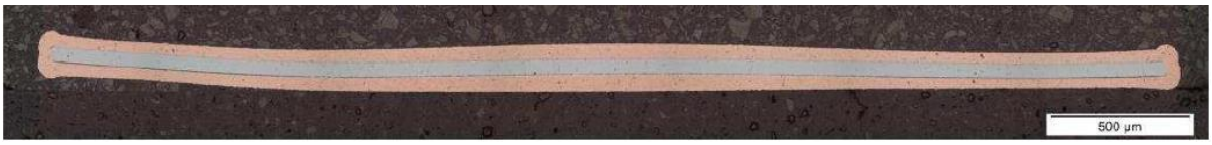

Fig. 86. Cross section of a REBCO tape with irregular copper deposition.

III.2.2.2.2 Description of the superconducting Double Pancakes

As mentioned before, the coil consists of a stack of DPs (Fig. 87). In principle, the term “Double Pancake” implies that a single length of tape is used to create the two pancakes, with a layer jump at the inner or the outer turn (most of the time at the inner turn). The idea is to limit the number of connections. In our case the winding is made of pseudo-DP: the winding process of the pseudo-DP starts from a bulk copper inner contact, on which the extremities of the two REBCO tape lengths forming the two pancakes are soldered. From there, the winding proceeds like that of a real DP. This technique allows us a better control of the soldering quality at the inner joints.

This technique was imposed by the fact that each pancake requires 120 m tape length, unit lengths twice that long were impossible to procure at the beginning of the project. The idea of having soldered joints in the winding was also not considered favorable. Inside a DP, the two pancakes are separated by a G11 flange. This flange is 4 mm-thick for the DPs at the center, and becomes gradually thicker for the DPs at the extremities as already discussed.

On the outer diameter, the winding ends with copper terminals, called “outer contact”, on which voltage taps are soldered to visualize the complete voltage (two pancakes + joint at the inner contact) of the DP during the tests. In total, there are about 180 turns per pancake depending on the overall thickness of the tape (from 0.12 to 0.14 mm).

Spacers are placed between the flanges at the outer diameter around the pancakes to support the axial forces of the solenoid [60]. These are not mechanically adjusted to the outer turns of the pancakes in order to let the pancakes move freely during the mechanical loading of the SMES, avoiding pinching and/or stress concentrations.

Finally, the electrical connections between DPs during solenoid assembly or intermediate assemblies are made via the outer contacts (Fig. 88). These connections are pressed contacts, assembled using screws, with a thin indium foil between each copper terminals to improve the electrical contact.

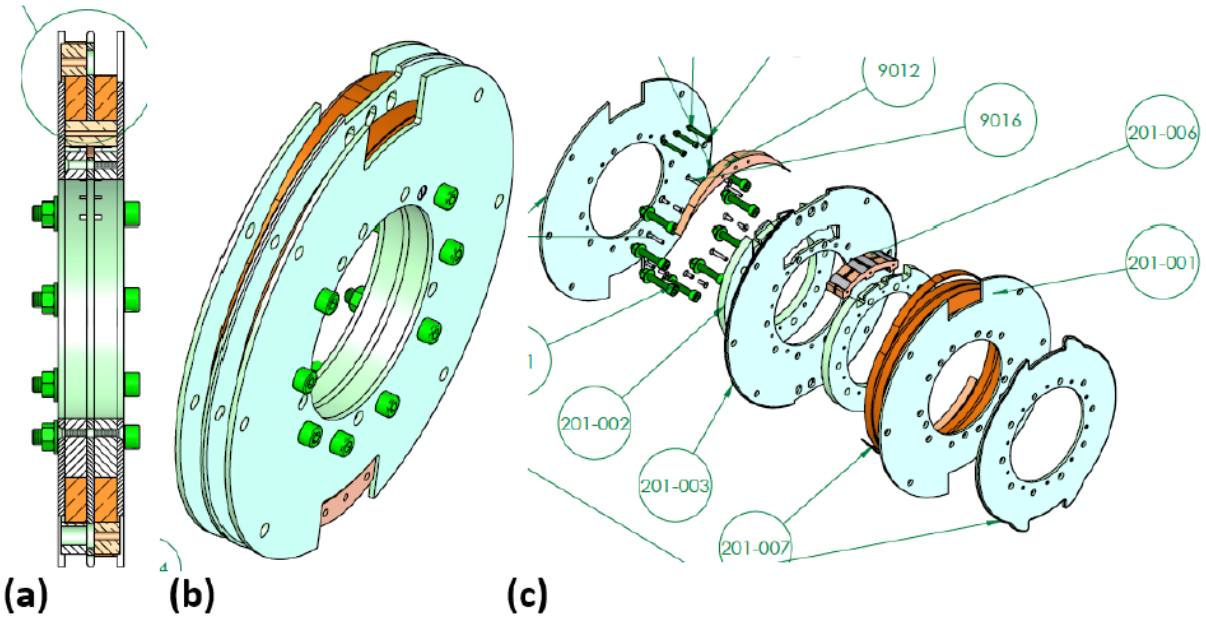

Fig. 87. a) Sectional view of a double pancake. b) Drawing view of a double pancake. c) Exploded view of a double pancake.

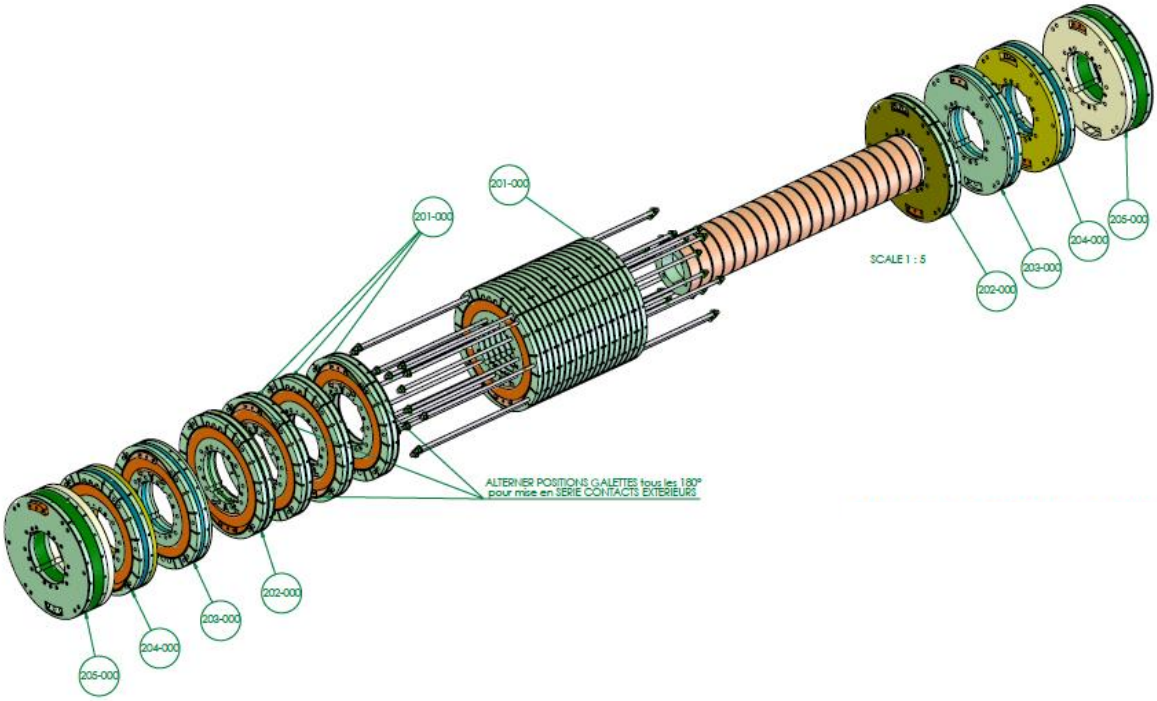

Fig. 88. Schematic view of the solenoid assembly.

III.2.2.2.3 Resistive joints: DPs inner and outer contacts

Soldering REBCO tapes is a delicate operation. As seen in section I.3.1.2, these tapes are sensitive to the temperature and duration of the heat treatment. Therefore, the soldering must be performed quite rapidly and under low temperature (< 200°C is recommended), otherwise the superconductivity of the conductor will be degraded. Moreover, due to their hastelloy substrate, they are stiff and difficult to hold in

place during soldering. In the framework of REBCO projects and prototypes developed at Neel Institute, this type of connection has been the subject of many tests over the years in order to find the best processes and obtain the lowest possible contact resistance. The design of the inner and outer contacts of the DPs is based on this know-how. One of the main difficulties is to obtain good contact resistances when soldering on a round surface. The pressure on the contact is more difficult to apply evenly when soldering, and it is necessary to avoid excess solder that would come out of the contact and flow onto the conductor or the mandrel. Once the solder has cooled and hardened, these droplets would considerably weaken the conductor mechanically.

The inner joints are soldered on an inner CuC1 copper contact to realize the inner electrical connection between 2 pancakes. The inner contact is both fixed angularly and axially to the mandrel and the middle flange, but it can slide radially to compensate the mandrel thermal shrinking. Good results had been obtained on the inner junction of 6 mm DPs with a resistivity of 60 nΩ.cm² per interface [60] (value in agreement with the literature [40]). Here, the interface of the 2 conductors of the pancakes was the copper part enabling the junction. Resistances of 85 nΩ were obtained. It was therefore decided to keep the same approach for the inner contacts of the 12 mm DPs. In addition to the copper junction piece, and still with the aim of improving the contact resistance and the connection of the 2 pancakes, 4 strips of 12 mm REBCO tape were added. This improved the contact resistance by a factor of 17 since resistances between 4 and 5 nΩ at 4 K under a rated current of 850 A have been measured during test campaigns. This know-how was transferred to the Sigmaphi company in charge of manufacturing the DPs, and the test campaigns carried out with them showed that this process was mastered with resistances obtained of the same order of magnitude and reproducible. At the other end of the pancake, the superconducting conductor is then soldered to the outside of a massive crescent-shaped piece of CuC1 copper. This crescent shape of the copper outer contact enables the addition of mechanical reinforcement towers, but also makes it possible to solder the copper crescent to the side of the conductor's REBCO layer in order to minimize the internal interfaces making up the conductor and to achieve better contact resistance. From a mechanical point of view, the ends of the crescent must be very thin and keep a certain flexibility to avoid stress concentrations on the conductor. Fig. 89 shows the inner and outer contacts of the DPs.

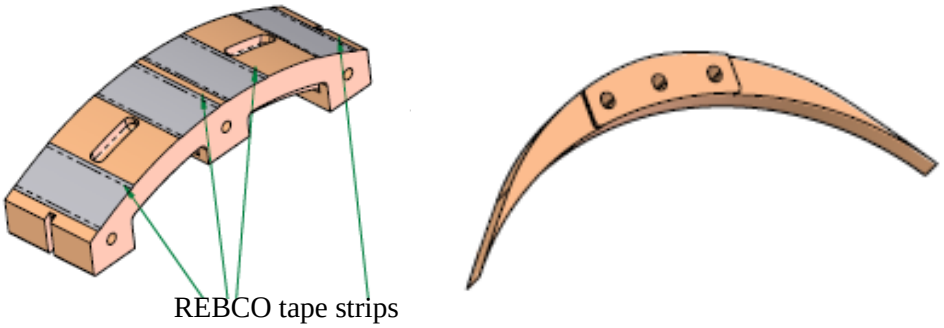

Fig. 89. The inner (left) and outer (right) contacts of the DPs.

One of the advantages of the contacts presented above is that they are removable. In this way a faulty conductor length can be easily replaced or a bad contact easily re-made. These are also long and wide enough to maximize the contact area and minimize contact resistance. In addition, they serve as thermal and mechanical stabilizers and provide low resistance and good contact reliability.

III.2.2.2.4 Double-Pancake manufacturing

The realization of REBCO windings is a real know-how of the laboratory. This process is not trivial and requires several key steps that need to be done with care. Several prototypes of pancakes, DPs, and even layer windings have been realized for more than ten years, either for the fabrication of magnets or superconducting fault current limiters. The dangerous steps for the realization of a REBCO winding are now clearly identified. As mentioned in the previous point, the realization of the connections between pancakes or between pancakes and current leads is the hard point of these windings. This crucial step can put the viability of an entire magnet at risk if it is poorly executed. However, the winding itself is also a difficult task. The turns must be aligned as closely as possible in order to get as flat a pancake as possible. Indeed, an inhomogeneous winding of the pancake could lead to a concentration of stress on the edge of the conductor and degrade it due to the axial electromagnetic forces undergone by the winding during its operation.

The removal of the insulation of the conductor is also delicate step. This operation requires manual handling of the tape during the winding process while maintaining the tension of the windings already made. Here, in the BOSSE project, the conductor insulation is coated. This is beneficial for the winding in terms of current density since the insulation is thinner but requires a chemical process to etch out the insulation layer, which makes this step even more complex. A first prototype of the BOSSE DPs has been realized at Neel Institute. Its manufacturing process will now be described. Once this one was successfully tested, the know-how concerning the realization of the DPs was transferred to the company Sigmaphi, partner of the BOSSE project, in charge of realizing the series DP of the BOSSE solenoid.

First of all, the ends of each length dedicated to the realization of the pancakes are uninsulated. Indeed, the polyimide must be removed in order to solder the REBCO tapes. For this a chemical solution heated up to 80°C is used (Fig. 90).

Fig. 90. Conductor de-insulation for soldering contacts.

Once the polyimide is removed, the conductor is carefully cleaned with ethanol to obtain a perfectly clean surface for pre-tinning the tape. The copper parts are also cleaned with ethanol and pre-tinned. A soldering flux (soldering water DIN EN 29454-1 from Felder) is also used to achieve a good wetting of the surfaces. Each tinning or soldering is always carefully cleaned with ethanol to remove any trace of flux that

could oxidize the conductor over time. As the performance of REBCO tapes is sensitive to heat, an indium tin alloy (InSn 42-58) with a melting point of 117°C is used. The solders are all made at 140°C.

Before starting the winding, the conductors of the 2 pancakes are soldered on the inner contact with the help of a heating cartridge inserted in a copper piece screwed on the inner contact (Fig. 91). Short strips of REBCO tape are also added in the grooves perpendicular to the conductors to improve the electrical resistance of the contact. The inner contact is blocked by the central flange and the mandrel.

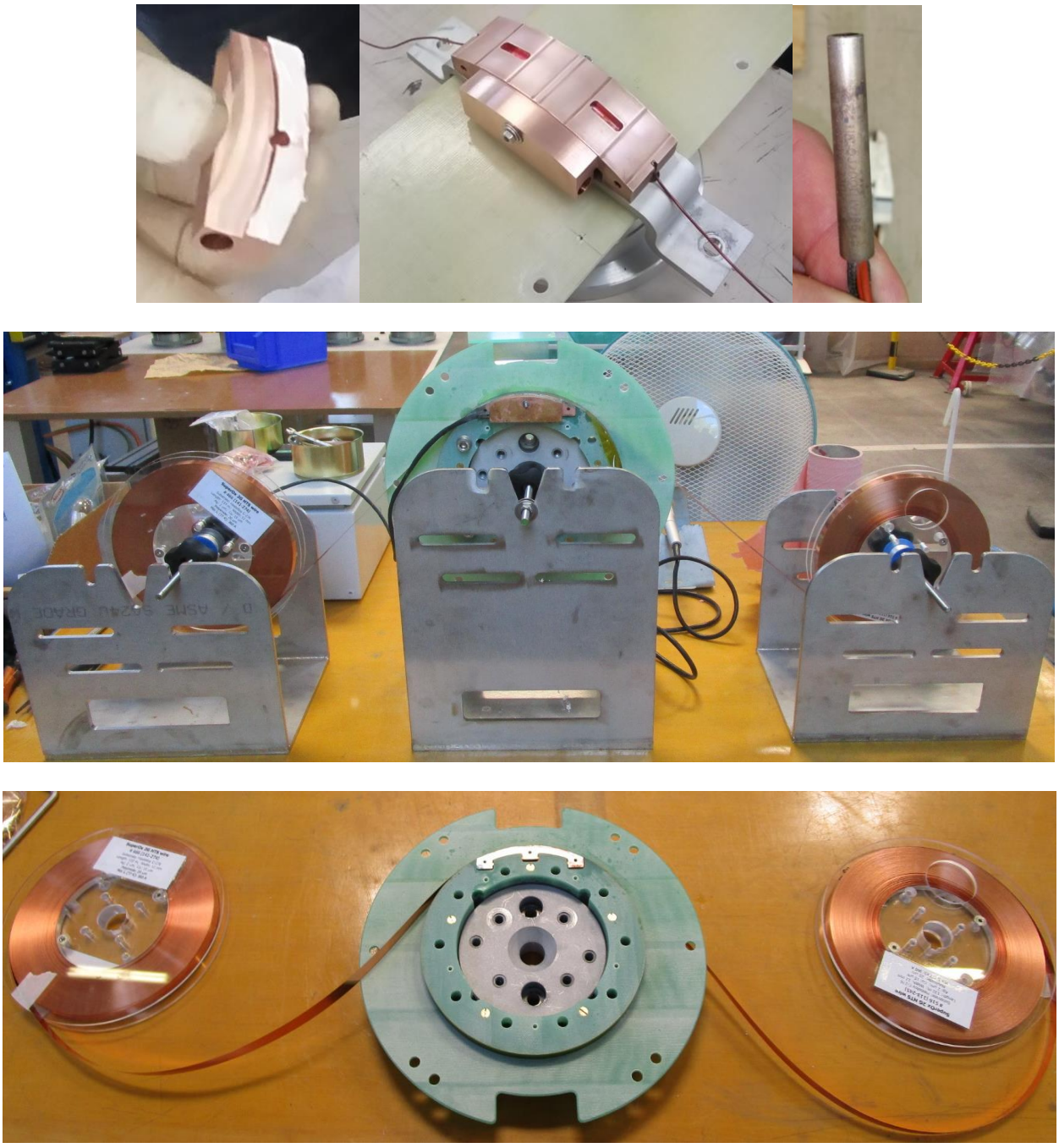

Fig. 91. Tooling and soldering of the inner contacts.

From there, one length is wound while the other, kept in reserve on a spool, is fixed as a “satellite” of the assembly. The winding machine of Néel Institute was used (Fig. 92). This one is motorized and equipped with a clutch/brake pack on the feeder, enabling the control of the winding tension. During the winding, the brake applies a constant torque of 0.70 N.m to the coil. The tension of the pancake varies from 0.7 kg at the beginning of the winding to 1.4 kg at the end. This winding tension was later increased to 2 N.m because of the turn movement of the coils during the tests.

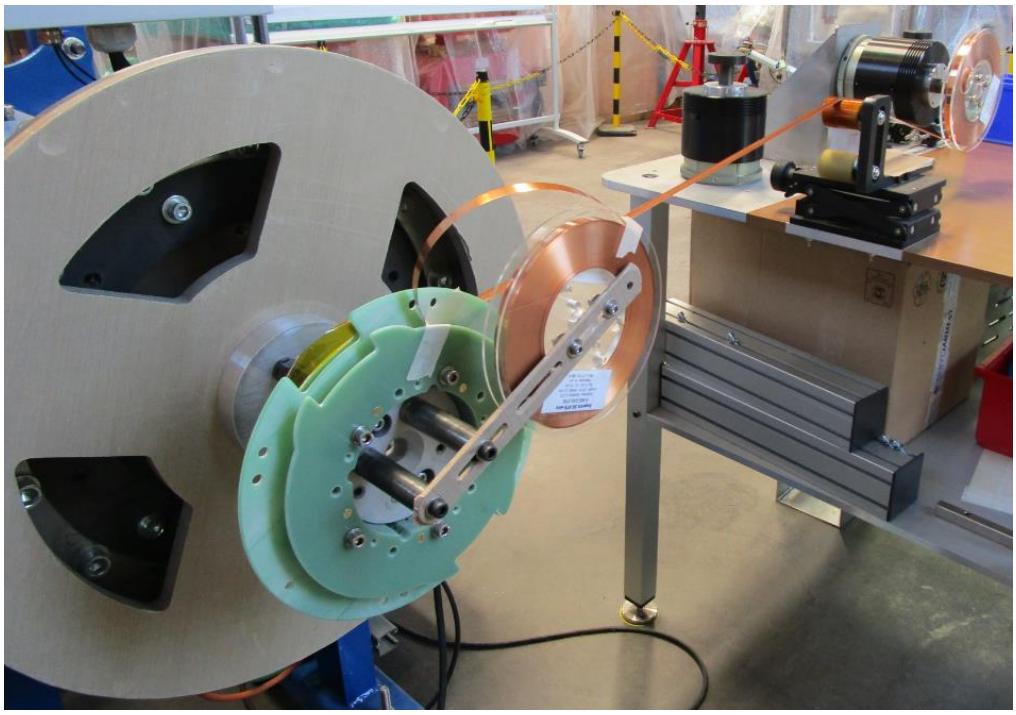

Fig. 92. Double-Pancake winding.

Once the outer diameter is reached the outer contact is soldered using the same protocol as for the inner contact. Namely, the insulation removal and the tinning of the parts to be soldered. The conductor is then soldered on the outer copper crescent. Then, the winding continues after the outer contact with 6 additional reinforcement turns, the last three of which are glued with small drops of Eccobond® epoxy (Fig. 93). This epoxy has good properties at low temperature. The quantity of epoxy deposited is small so that it does not overflow during the winding on the “active” turns of the pancake. This could cause delamination of the conductor. Concerning the 6 additional turns, where no current flows, they enable to balance the peripheral stress on the external contact. Finally, to finish the pancake, the conductor extremity is insulated with Kapton.

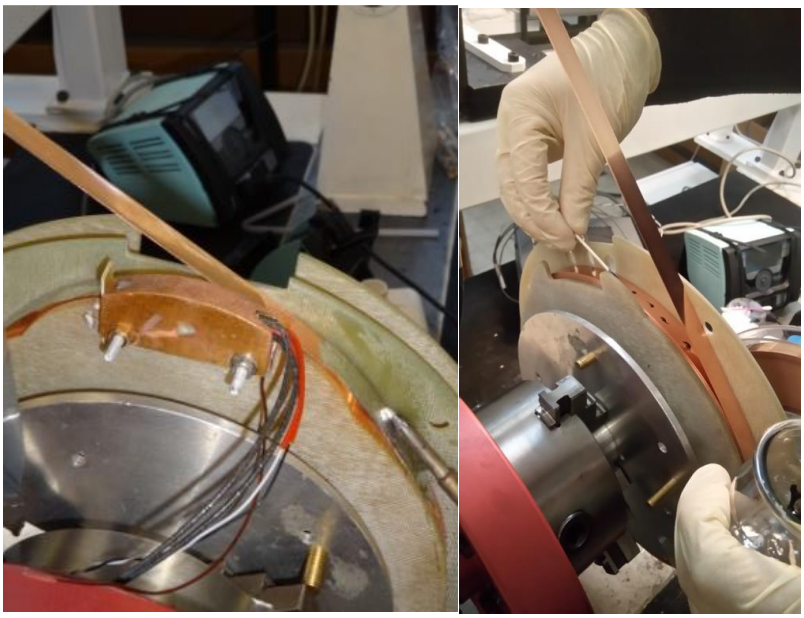

Fig. 93. Gluing of the last turns of the pancake with Eccobond.

After drying, the second pancake can then be wound in the same way as the first and the DP is finished (Fig. 94).

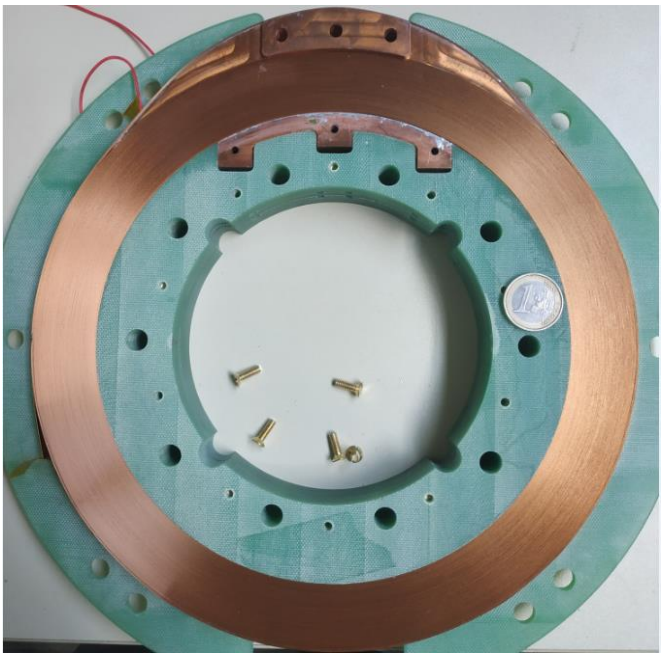

Fig. 94. Picture of a pancake winding (flange removed).

III.3 BOSSE protection

In principle, two voltage taps across the superconducting magnet and a single pickup coil for compensation are sufficient to ensure its protection, just as for a single DP. Nevertheless, the sensitivity is low: the hot spot relevant voltage remains the same whereas the other voltages and the noise increase. In addition, it is not possible to know which DP shows an issue.

In order to increase sensitivity and selectivity, it was decided for this project to equip each DP with voltage taps and an independent pick up coil. This makes it possible to protect the DPs either independently or by sub-assemblies. Individual protection of DPs also has the important advantage of accurately locating a faulty DP among the assembly in case of an early protection discharge event, making it possible to replace it or repair it.

As a result, the 21 DPs of the BOSSE solenoid each have their own respective pickup coils. Thus for the final assembly, the protection system described in section II.1.2 of chapter II, is multiplied up to 21 (Fig. 95). The voltage of each pickup coil is subtracted from the voltage of its corresponding DP. Exact compensation is obtained by means of a resistive voltage divider bridge on the each pick up coil signal. The 21 voltage measurements are monitored simultaneously in real time to detect the occurrence of a dissipative zone.

Note that since the BOSSE solenoid is used as a pulse source for the electromagnetic launchers, the pickup coils are only useful to protect the DPs in charge and storage mode. They are unnecessary during the discharges as the coil is always discharged rapidly down to 0 A.

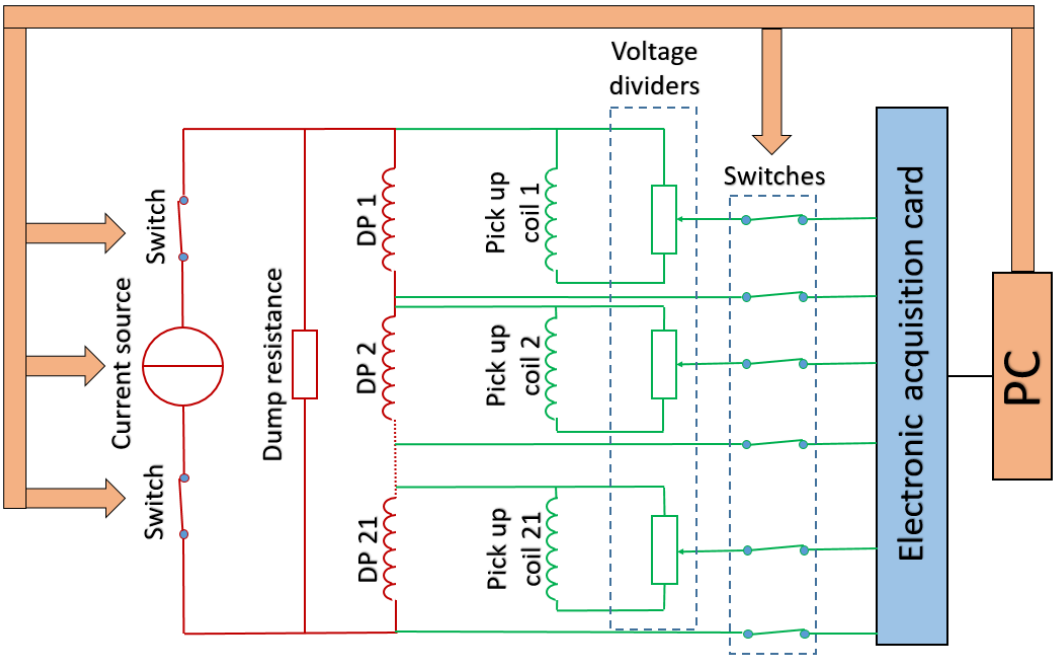

Fig. 95. Electrical circuit diagram of the BOSSE solenoid protection system.

The BOSSE solenoid should be discharged under 5 kV (5 kV terminal-to-terminal and ± 2.5 kV to ground) to get its rated power; the acquisition electronics is disconnected when the discharge is triggered to protect it from overvoltage, making it possible to operate without high voltage differential amplifiers that are costly and generate noise [82].

The signals from the DPs and subassemblies tested in self-field, which are presented in this chapter, were monitored using an oscilloscope controlling the protection switch through a 0 – 5 V TTL output. The compensated voltage signals were set to zero by manually adjusting the voltage divider bridges, in spite of the voltage drift observed and discussed in details in chapter II. This method is easily manageable for testing a single DP or "small" assemblies.

For future, larger assemblies, the signals will have to be treated automatically, taking into account the transient components of the signals as well as the voltage peaks due to winding movements. Indeed, individual and manual compensation of the 21 signals in real time is impossible. This must be managed digitally to ensure the protection of the solenoid. To this end, the addition of a small pickup coil will enable digital overcompensation of analog-compensated signals. Fig. 96 shows a schematic diagram of the DP protection. A first "coarse" compensation $V_{comp\ 1}$ will be made manually through the potentiometer (k1) between the DP and the pickup coil 1. The low voltage induced in the pickup coil 2 is directly measured by the acquisition system and the coupling coefficient k2 between $V_{comp\ 1}$ and $V'_{pickup\ 2}$ is calculated digitally. The subtraction of these two compensations (Eq. 21) makes it possible to digitally compensate the signal without losing sensitivity and while automating the protection. Consequently, the 21 pickup coils and potentiometers will only be used to perform "coarse" compensation of the signal and the sensitive compensation will be performed digitally.

$$V_{comp\ 2} = \left(V_{DP} - k1.V_{Pickup\ 1}\right) - k2.V'_{Pickup\ 2}$$

$$V_{comp\ 2} = V_{Comp\ 1} - k2.V'_{Pickup\ 2}$$

Equation 21

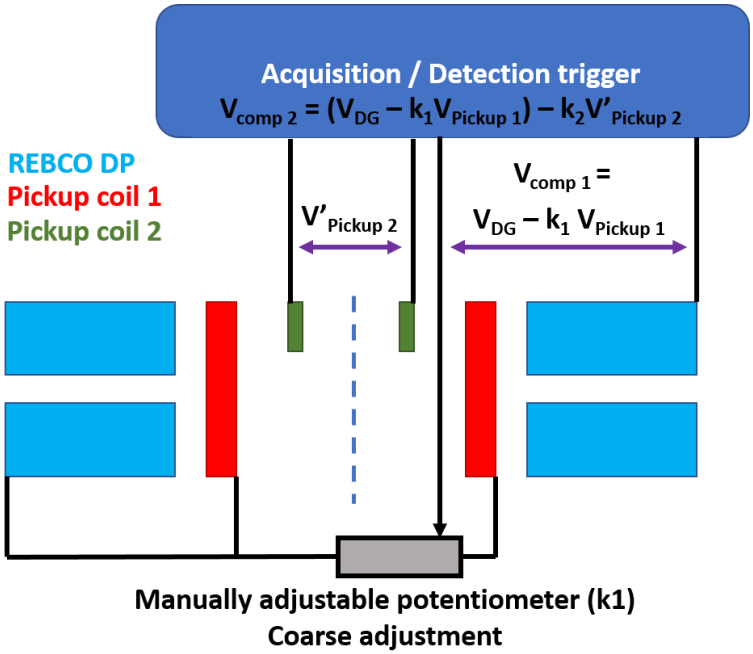

Fig. 96. Schematic diagram of digital overcompensation.

III.3.1 The BOSSE Pickup coils

The BOSSE pickup coils are inserted in the center of the solenoid (Fig. 97). This saves space and minimizes the size of the cryostat, at no cost for SMES application, as the center bore does not have to be clear for energy storage. They are however designed to be removable if the full magnet was to be used for other purpose in the future. They have 1200 turns of 0.36 mm diameter insulated copper wire with an inner radius of 56 mm, an outer radius of 63 mm and a height of 28 mm. These are all identical, and therefore the ratio of each divider is different since the DPs have all different couplings with each other [60].

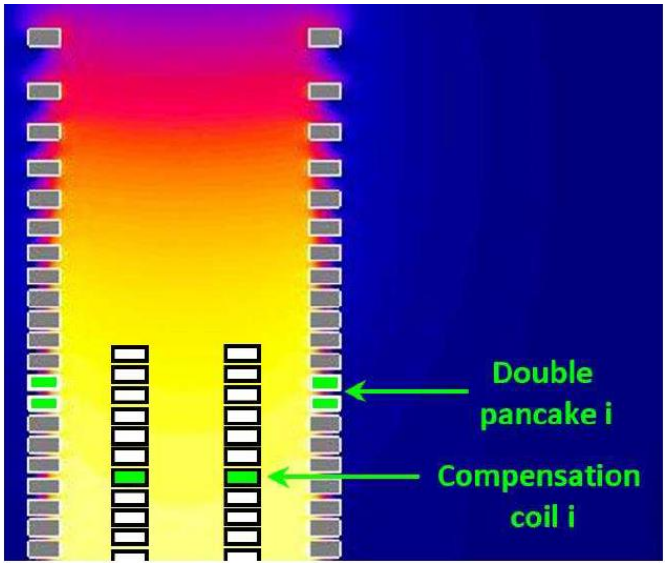

Fig. 97. The upper half of the BOSSE solenoid with its pick-up coils.

III.4 Experimental work

III.4.1 DPs test station

All the tests of DPs or sub-assemblies are carried out in liquid helium at 4.2 K. The individual tests of the DPs were performed in the cryostat developed for the EuCARD project (Fig. 98). It has an inner diameter of 298 mm which is large enough to test our DPs and has current leads optimized for current well over 1 kA. For the test of the sub-assemblies, the cryostat designed for the BOSSE project will be used.

The current source is a Sorensen® 1200 A / 10 V. We drive it with a LabVIEW® program in order to control the speed of the current ramps during the charge or discharge of the coils but also to maintain current plateaus. The discharge is triggered automatically as soon as the compensated voltage signal exceeds a predefined threshold value (see above the detection / protection scheme).

Real-time data processing is performed by a Yokogawa®-DL 850 oscilloscope or Dewetron® electronic cards. Electrical quantities such as winding voltage and current are monitored, but also the magnetic field (Arepoc® Hall effect probe) depending on the experiment. Digital filters are applied to the voltage signals,

such as sliding averaging low-pass filters with cut-off frequencies below 20 Hz. The temperature of the DPs and their copper contacts were measured using Cernox® sensors.

Fig. 98. Experimental set up of a DP test in self-field.

III.4.2 Experimental validations of the SMES design

Before launching the production of the 21 DPs, the manufacturing process of the DPs had to be confirmed by validation of its electromagnetic and mechanical performances. For this purpose, a prototype DP (Fig.99) corresponding to a central DP of the solenoid was made in order to conduct extensive tests. Indeed, the central DPs are those which will be subjected to the highest mechanical stresses and the self-field test of the prototype DP makes it possible to test its electromagnetic performance (I_c). The I_c of the magnet is defined by the transverse field (4.4 T) whereas the transverse field reaches 4 T for the rated current of a DP in self-field condition. These tests also make it possible to check the electrical resistance of the inner joint connecting the 2 pancakes.

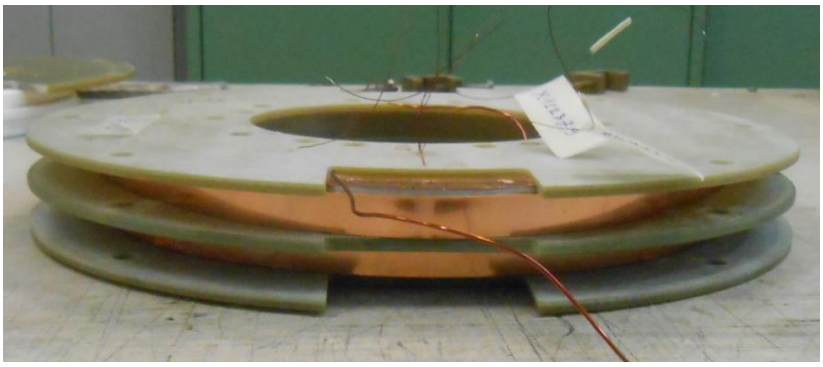

Fig. 99. Double Pancake prototype.

III.4.2.1 Electromagnetic design validation

III.4.2.1.1 Test up to rated current

The current was ramped up to 860 A followed by a plateau of 160 s. A current just above the rated current of the SMES (850 A) validating the first objective of this test. A 2D axisymmetric magnetic field map at 860 A of the central DPs performed on Comsol Multiphysics is shown in Fig. 100.

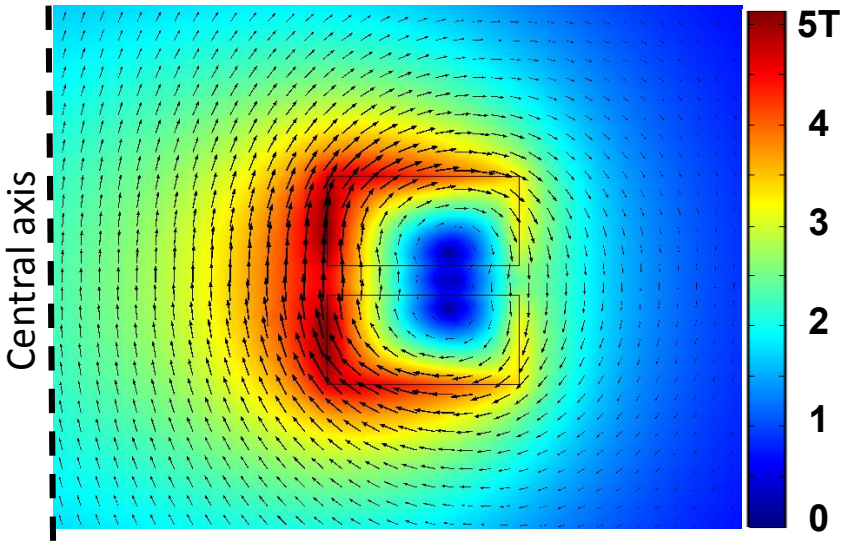

Fig. 100. Magnetic field map of a central DP with 4 mm pancake spacing.

Fig. 101 represents the current cycle (in red) carried out for this test with the compensated voltage signal (in black) of the DP used to protect the winding. The triggering threshold of the protection is set at 1.5 mV. This value is fixed based on simulations of the thermal runaway phenomenon developed in our group [82]. Of course, the lower the transition detection threshold, the longer and more comfortable the time for the protection to be triggered (see section II.1.1).

As seen in chapter II, the voltage drift observed from the beginning of the ramp on the protection signal is not due to a resistive component. It is due to the variation of the current density distribution in the width of the superconducting layer of the conductor as the current or the magnetic field varies, inducing a change of the superconducting coil inductance as well as AC losses. As such, it rapidly decays to zero during a current plateau (stabilization of the current density distribution). This explains the discontinuities in the protection signal curve Fig 101. Each of these discontinuities correspond to a readjustment of the compensation in order not to exceed the triggering threshold due to this signal drift.

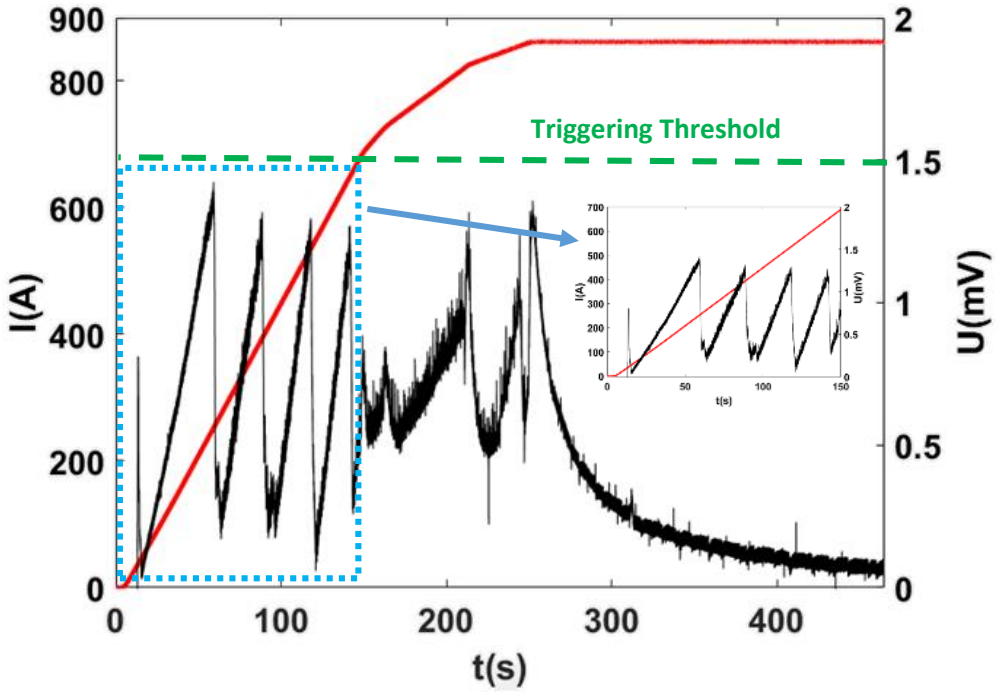

Fig. 101. The current cycle (in red) and the compensated voltage signal (in black) used to protect the winding during the prototype DP self-field test up to 863A.

III.4.2.1.2 Test up to the critical current

Once the rated current was reached, a test up to the critical current of the DP was performed to assess the current margin of the SMES and to maximize the transverse magnetic field seen by the conductor. This prototype DP reached the current of 973 A (Fig. 102). This value corresponds to 114 % of the SMES rated current (for 1 MJ) and an energy stored of 14.8 kJ. The overall energy efficiency can be calculated roughly taking into account the initial energy (1/2 L*I²) and calculating the integral of the product V x I during the discharge. It gives us a yield of 0.978.

Note that to reach this high current a very slow ramp of 0.18 A/s was applied to the prototype. This is to minimize the parasitic component due to AC losses and obtain a high sensitivity on the detection signal of a resistive transition. Indeed, fast ramps generate dissipation due to AC losses. These losses are not high enough to cause temperature increase and are thus not dangerous for the coil, but the voltage associated with them would force us to increase the detection system threshold, making it less sensitive.

In terms of magnetic field, 973 A corresponds to a maximum axial field of 5.7 T on the conductor (inner turn) and a maximum transverse field of 4.5 T (magnetic fields are calculated for a homogeneous current density distribution). This transverse field value is greater than the maximum transverse magnetic field of the SMES for 20 kJ/kg (4.41 T).

This test also validates the protection strategy in the worst case scenario with a current density of 600 A/mm² (854 A/mm² bare conductor), much higher than the rated value. We can notice in Fig. 102 that the compensated voltage is stable up to 950 A and the transition is clearly visible at 973 A where we can distinguish a break of slope on the detection signal which is characteristic of a transition from the superconducting state to the normal state for REBCO superconducting tapes. The protection of the magnet is thus triggered and its energy is discharged quickly (1 s) in the dumping resistance, preventing the thermal runaway.

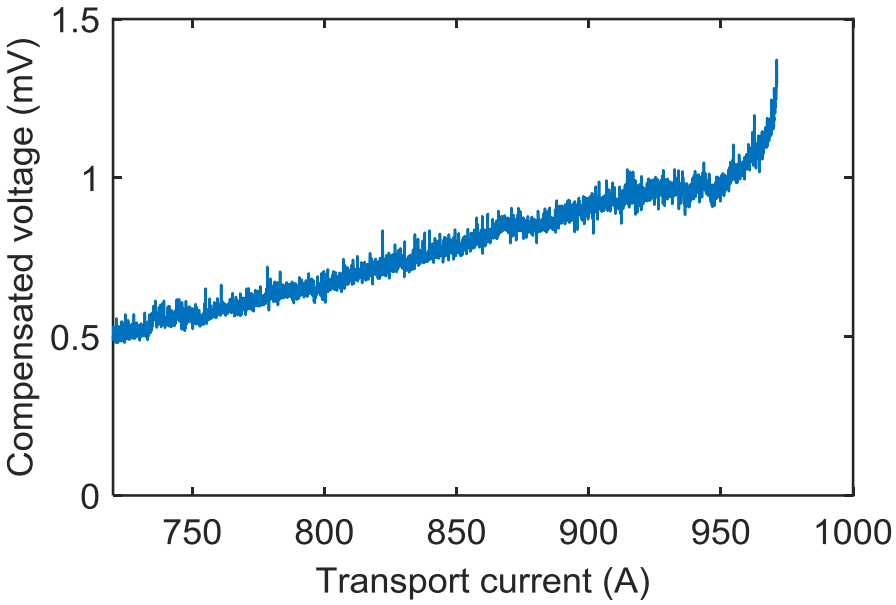

Fig. 102. Maximum current reached 973 A with a slow ramp of 0.18 A / s.

Moreover, it is important to add that this prototype was realized with the 2 lengths of conductor with the lowest critical currents (I_c 77 K = 379 A). This choice was made to ensure that no part of the coil have lower properties than the prototype. The conductor lengths with the best performance (I_c 77 K > 500 A) are intended for the DPs corresponding to the solenoid heads (extremities) were the transverse component of the magnetic field is highest. Therefore, the estimated margin is pessimistic and we can reasonably expect a larger margin on the full assembly. This further strengthen our confidence in the electromagnetic design of the solenoid.

The realization of the electrical contact connecting the two conductors was also validated by these tests. Its resistance was evaluated lower than 20 nΩ at 863 A, with no observed heating of the contact after a plateau of 180 s, proving the sound manufacturing process of the joint.

III.4.2.2 Mechanical design validation

Once the electromagnetic performance of the design was validated, the prototype DP was tested in an outer magnetic field to check its mechanical performance.

Fig. 103 shows the mechanical stress in a central pancake of the BOSSE solenoid calculated with the BJR and Wilson formulas [43, 44], as introduced in part I.3.2. For these calculations, the rated values of the SMES for 1 MJ were used. That is to say a current density of 525 A/mm² (850 A), a magnetic field of 11.55 T at the inner turn and a magnetic field of - 0.77 T at the outer turn. As expected the mechanical stress calculated with Wilson is smaller at the inner turn and larger at the outer turn than with the BJR formula. This can be explained by the fact that the inner turns are subject to much larger Laplace forces and are therefore supported by the outer turns. In a way we can say that the mechanical stress is homogenized over the width of the winding in this magnetic field configuration. The radial stress is negative and indicates a winding in compression. The stress calculated with Wilson is therefore closer to reality than the one

calculated with BJR. The maximum stress at the inner turn is then estimated at about 350 MPa. However, as we have seen in section I.3.2, Wilson's formula does not take into account the influence of the stiffness anisotropy and thermal contraction of the conductor. It is therefore important to take into account the conductor architecture in order to estimate more precisely the value of the hoop stress.

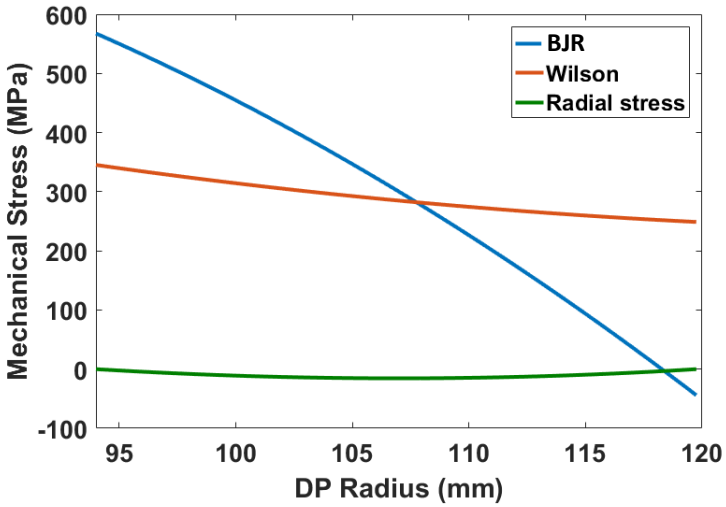

Fig. 103. Mechanical stress distribution in the central pancake of the BOSSE solenoid for a stored energy of 1MJ. Hoop stress and radial stress are calculated with the Wilson formula.

The polyimide insulation layer is soft and has a much higher coefficient of thermal expansion than copper or hastelloy (other materials in the conductor). As a result, the winding of these conductors is anisotropic from a mechanical and thermal point of view. The turns of the winding can separate under the influence of thermal contraction, creating gaps and hindering the stress redistribution. J. Ciceron [60] showed that this was the case for the BOSSE solenoid configuration and evaluated the impact on the mechanical behavior of the winding (Fig. 104).

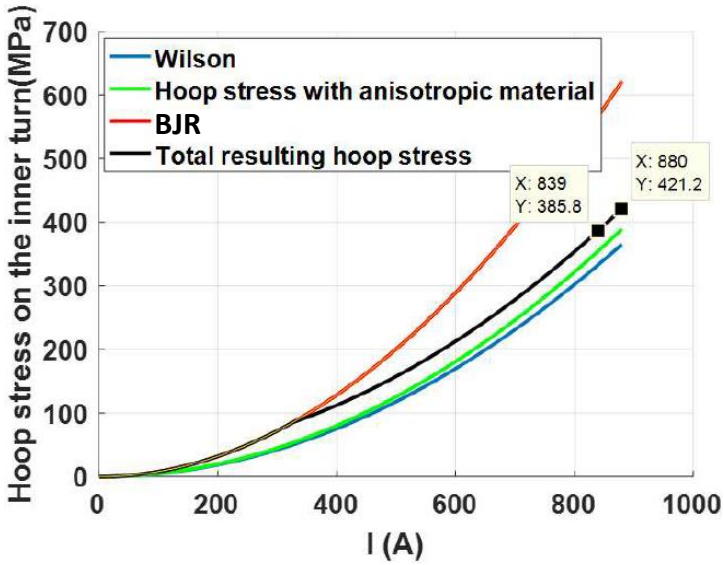

Fig. 104. J. Ciceron's estimate of the mechanical stress distribution in the winding of a DP at the SMES center for a stored energy of 1MJ [60]. Hoop stress and radial stress are calculated with the Wilson formula [43].

He proposed an estimation of the actual hoop stress inside the winding as a combination of several models [60]. Focusing on the inner turn of the central pancake of the BOSSE solenoid (highest stress), the hoop stress calculated by the Wilson formula is in blue, the Wilson formula for an anisotropic material is in green and the BJR formula is in red.

The conductor is coated with 40 µm of polyimide insulation. Therefore, when the winding is cooled to 4.2 K, the thermal contraction of the conductor leads to a shrinking of the winding. Each turn is therefore separated and we find ourselves in a configuration of mechanical stress calculation in "BJR" for a current below 330 A. At 330 A the gap due to thermal contraction of the conductor is filled. The turns are no longer independent and behave as a block (that is to say the Wilson model), thus following a trend similar to the green curve, but shifted upward (black curve).

The maximum stress at the inner turn can then be estimated more precisely, it reaches 421 MPa. The mechanical behavior is in between BJR and Wilson hypothesis. The turns behave first independently up to 330 A, then they behave as a block winding beyond that.

Calculations of the winding mechanical stress as well as the Young's modulus of the conductor are useful to estimate the conductor strain. The average Young's modulus of the conductor is estimated at 172 GPa. Note that only Hastelloy and copper are considered to evaluate the average Young's modulus of the conductor. Indeed, the mechanical properties of the polyimide insulating layer are so low (3 GPa) that they are neglected in the calculation. Thus, for the SMES to reach the first target of 1 MJ, the conductor elongation on the central windings of the solenoid will reach 0.345 %, and 0.38 % for 1.1 MJ, which corresponds to a specific energy density of 20 kJ/kg. This value is very close to the maximum permissible mechanical stresses for the conductor since irreversible degradation can occur above 0.4 % in conductors of this period [32].

For this reason, before launching the production of the 21 DPs, it was necessary to validate the design and manufacturing process by testing electro-mechanical performances. Therefore, after the test in self-field operating current limit (mentioned in introduction), the prototype DP already was also tested in background magnetic field under larger mechanical stress. As the pancake is large (240 mm outer diameter), the 376 mm diameter resistive magnet (12 MW/30 kA/10 T) from the LNCMI in Grenoble was used. Additional pick-up coils were added to this test in order to compensate the important electromagnetic noise (hundreds of mV) generated by the resistive background magnet and to keep a high sensitivity on the protection signal [65]. A photo of the prototype DP with its pick-up coils and the axisymmetric magnetic field map showing the positioning of each coil is shown in Fig. 105.

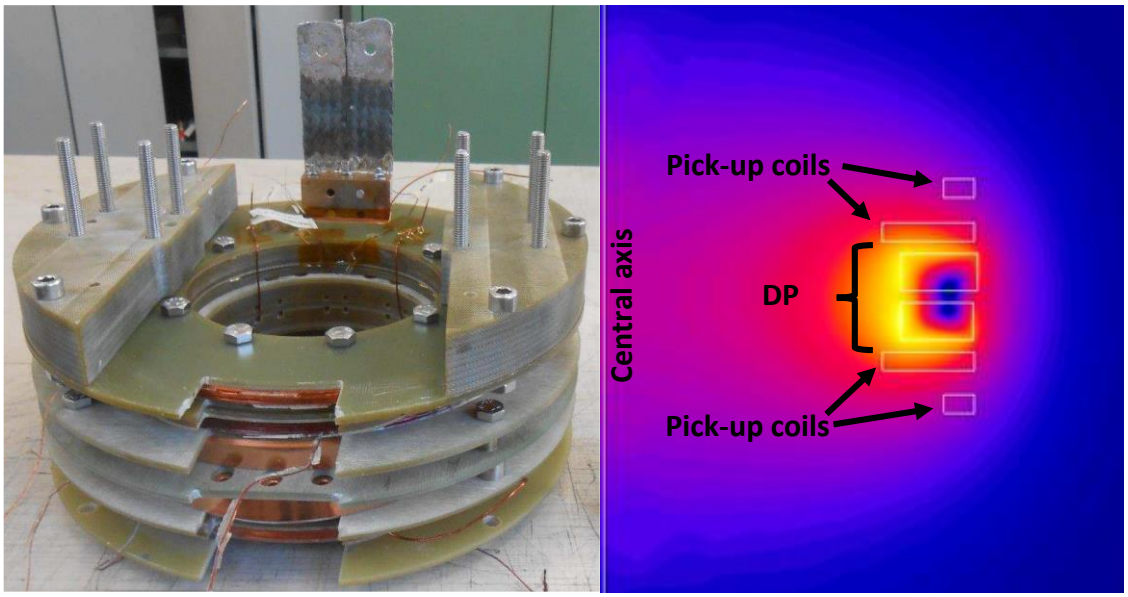

Fig. 105. On the left the DP prototype with its compensation coils ready to test in background field. On the right, the cross section of the DP and its compensation coils with its magnetic field map.

The prototype DP reached a current of 623 A under 6 T, for a total magnetic field at the center of the DP of 7.6 T, and 9.7 T on the conductor (Fig. 106).

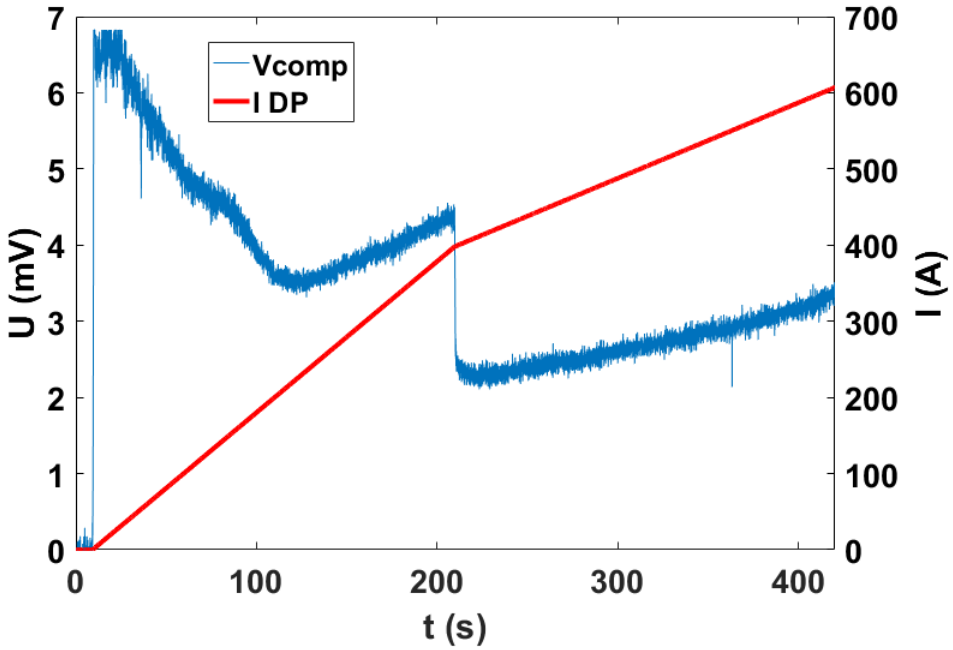

Fig. 106. The current cycle and the compensated voltage signal during the test under magnetic field background of 6 T.

We stopped the experiment at this value, as the stress on the outer diameter could become higher than in the final assembly, and the outer contacts are not designed for it [65], with a risk of stress concentration on the outer contact ends (Fig. 107). Still, under 623 A the stress reached 350 MPa on the inner

turns of the DP, corresponding to an elongation of 0.3% of the conductor. This represent already 83% of the maximum hoop stress at the rated current for the SMES solenoid.

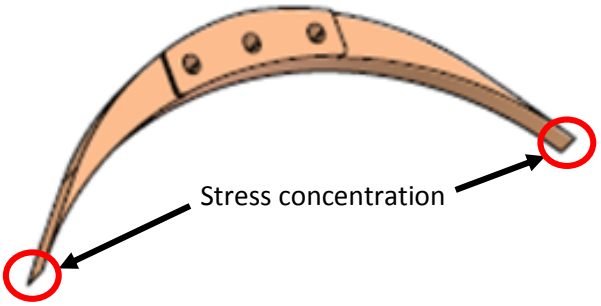

Fig. 107. Outer crescent contact structure.

III.4.3 Individual electromagnetic quality control of DPs

Once the solenoid design was validated by extensive tests of the prototype DP, the 21 DPs of the solenoid were produced by Sigmaphi, the industrial partner of the project. This project started in 2015 and all conductor lengths were procured at that time. Considering the uncertainty on tape performances from this period in low temperature/high field and the low critical current margin of the design (14 %), it was decided to test all DPs in liquid helium at 4.2 K at 860 A. This current value, just above the final rated current of the solenoid in the 1 MJ configuration (850 A), validates the DPs electromagnetic performance. Fig. 108 shows a solenoid DP ready for testing.

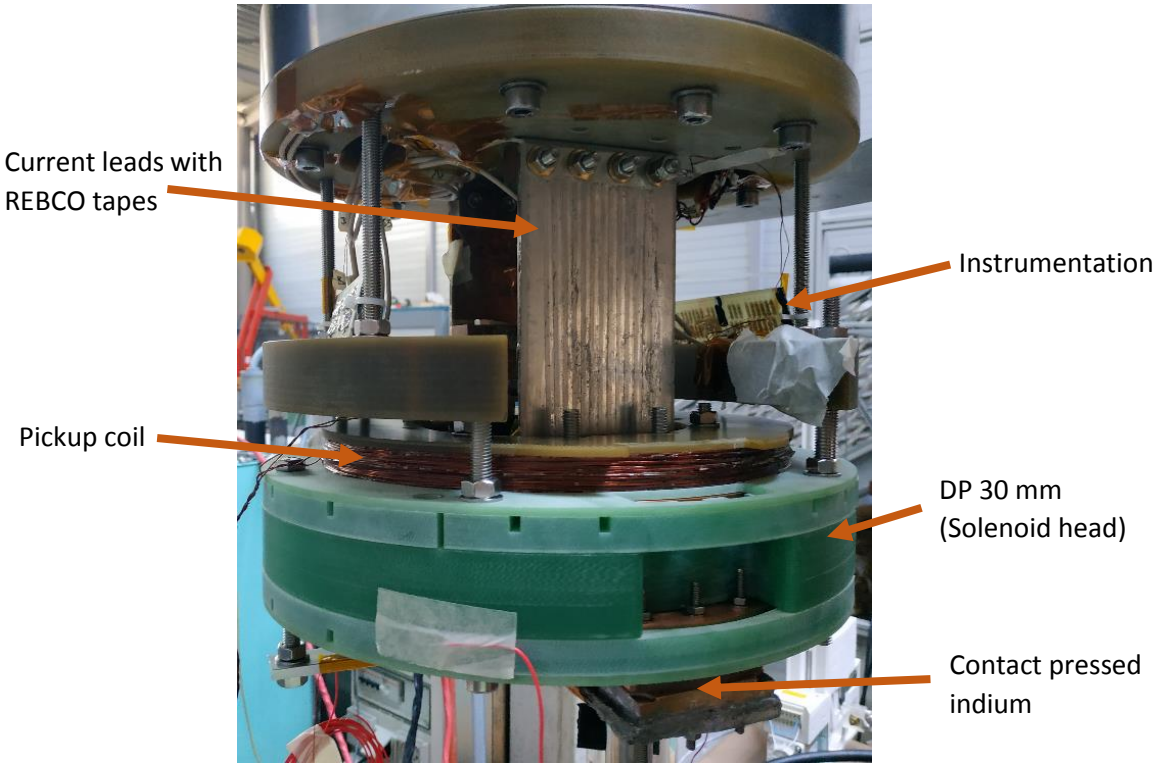

Fig. 108. DP individual test.

The main goal of these tests is to perform a quality control of all DPs in order to validate their good electromagnetic performances in operating conditions as close as possible to those of the final solenoid (transverse magnetic field of 4.4 T for 20 kJ/kg), but also to check the resistance of the inner joint between the pancakes. These tests are critical as we do not have much margin on the manufacture of the BOSSE solenoid. Indeed, we only had a few extra lengths of REBCO in addition to the 42 needed to manufacture the 21 DPs. If a DP shows insufficient performance or a resistive joint of too high a value, it must be rewound and retested until rated performance is achieved. Only mechanical stresses at the rated operating point of the solenoid cannot be achieved and validated with these stand-alone tests.

Another objective is to accumulate experience on protection about insulated REBCO magnets and increase the reliability of our detection approach. Moreover, by driving a large number of tests on almost similar REBCO coils we learn a lot about their electromagnetic behavior and its variations. These serial tests of the DPs provide a better understanding of the voltage signals and the factors that influence it. A summary table of the important quantities reached during their tests at a current of 860 A is shown in Tab. 5.

TABLE 5
VALUES REACHED DURING THE VALIDATION TESTS OF THE DPS

Gap between pancakes	4 mm	6 mm	10 mm	15 mm	30 mm
Average number of turns per pancake	180	180	180	180	180
L (mH)	39.32	38.51	37.1	35.6	32.36
I (A)	860	860	860	860	860
B_z^{max} (T)	4.96	4.9	4.61	4.51	4.19
B_r^{max} (T)	4	3.88	3.73	3.57	3.29
Calculated Max. hoop stress (MPa)	238	232	222	213	198

At this stage of the BOSSE project, 17 DPs have been successfully tested and validated up to 860 A in self-field (11/13 DPs with 4 mm gap, 1/2 DP with 6 mm gap, 1/2 DP with 10 mm gap, 2/2 DPs with 15 mm gap, 2/2 Ds with 30 mm gap). A current of 860 A flows through them for 180 s without showing any resistive voltage (except that of the inner joint resistance). There are still 4 to be remanufactured because of poor inner connections. Tab. 6 summarizes the status of self-field validation testing of DPs. Some DPs were defective during the first tests. After analysis of the defects they were rewound and tested again. In all, 26 cooling runs were performed with liquid helium. Knowing that about 90 L of helium were necessary for the cooling and the tests duration, this brings the total of liquid helium consumed to about 2340 L just for the DPs electromagnetic validation.

TABLE 6
SUMMARY OF ALL TESTS PERFORMED TO VALIDATE DPS IN SELF-FIELD

N° DPs	Gap between Pancakes	N° of cooling operations	Observations	Status
DP 1-1	4 mm	1	None	OK
DP 2-1	4 mm	2	1st Test: Pinched conductor / rewound 2nd Test: OK	OK
DP 2-2	4 mm	2	1st Test: Poor inner contact / rewound 2nd Test: OK	OK
DP 3-1	4 mm	2	1st Test: Winding failure (burned length) / rewound 2nd Test: OK	OK
DP 3-2	4 mm	1	None	OK
DP 4-1	4 mm	2	1st Test: Resistive / rewound 2nd Test: OK	OK
DP 4-2	4 mm	1	None	OK
DP 5-1	4 mm	1	1st Test: Winding failure (burned length)	On hold
DP 5-2	4 mm	1	None	OK
DP 6-1	4 mm	1	None	OK
DP 6-2	4 mm	1	None	OK
DP 7-1	4 mm	1	None	OK
DP 7-2	4 mm	1	1st Test: Resistive	On hold
DP 8-1	6 mm	0	Waiting for winding	On hold
DP 8-2	6 mm	2	1st Test: Resistive / rewound 2nd Test: OK	OK
DP 9-1	10 mm	2	1st Test: Resistive / rewound 2nd Test: insulation failure (burnt length)	On hold
DP 9-2	10 mm	1	None	OK
DP 10-1	15 mm	1	None	OK
DP 10-2	15 mm	1	None	OK
DP 11-1	30 mm	1	None	OK
DP 11-2	30 mm	1	None	OK

III.4.4 Lessons learned

Several imponderables affected the smooth running of the project. Several DPs had to be rewound because they did not fulfill our requirements. In the following parts we give a brief description of the more important issues we faced and the lessons learned from them.

- High DP inner resistance
- Deficiency in the winding process:
  - Soldering flux traces
  - Pinched conductor
  - Destructive localized resistive transition
- Conductor polyimide insulation defect

III.4.4.1 High DP inner resistance values

One of the main cause of concern for the series-produced DPs is the inner joint. The inner resistance of the prototype was very low (< 20 nΩ), but the resistance values obtained in series-produced DPs was much higher. This is surprising as a soldered-joints validation campaign was organized with the industrial partner prior to the winding phase, to define the procedure and tooling to be used (Fig. 109). During this campaign, joint resistance of 4 nΩ were routinely achieved, in good agreement with the prototype and literature [40]. It is suspected that a tension spike when starting the winding could be the origin, or an excessive time spent soldering the joint due to the more awkward position of the operator when soldering on an actual pancake. The average resistance of the 17 validated DPs reaches 367 nΩ, spreading from a minimum of 19 nΩ to a maximum of 700 nΩ. Several of them had higher values during their first tests and were rewound for this reason, and 4 are still waiting to be rewound.

Fig. 109. Testing an inner contact during the contact validation campaign.

III.4.4.2 Deficiencies in the winding process

Among the first 6 DPs performed, 2 of them showed resistive behavior and another one saw the appearance of a destructive localized resistive transition. These defective DPs were unwound in order to analyze the quality of the winding and identify the causes of the failure. In order to validate the diagnostics associated with the defects observed in the faulty windings, each length was then sent back to SuperOx to perform a continuous measurement of the tape critical current. This was done in order to compare the critical current distribution of the lengths before and after winding and correlate it with the degradations identified visually during the unwinding.

III.4.4.2.1 Soldering flux traces

On all 6 defective DPs (even the ones that worked for a time) traces of oxidation due to poorly cleaned soldering flux on the inner and outer contacts were observed (Fig. 110). On one of the DPs, the flux had flowed on the first 5 inner turns of the pancake, damaging the conductor. Some parts were corroded by the flux (Fig. 111). On the I_c continuous measurement (Fig. 112), we can see that the DP conductor's critical current has been degraded at the level of the flux traces that were corroding the tape as well as at the level of the turns stuck to the eccobond serving as a "fret". Note in Fig. 112 that winding and unwinding do not normally change the I_c of the tape within the accuracy of the measurement.

Fig. 110. Solder flux traces (green) on the inner and outer contacts of the DPs.

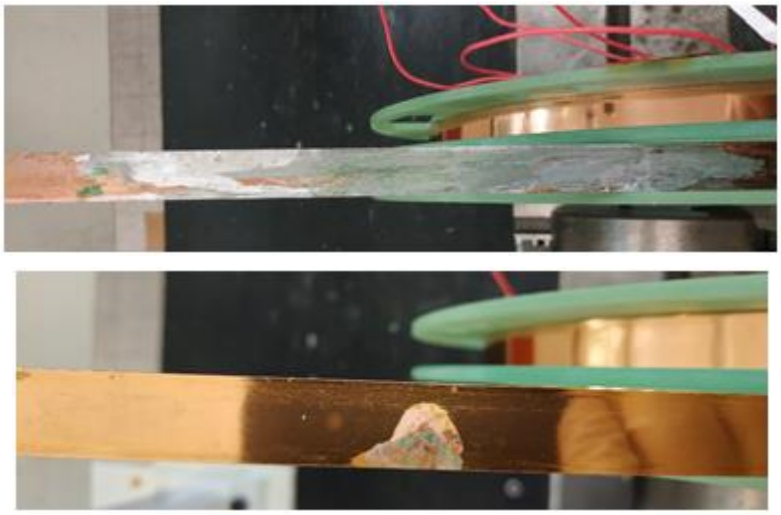

Fig. 111. Solder flux that has corroded the conductor.

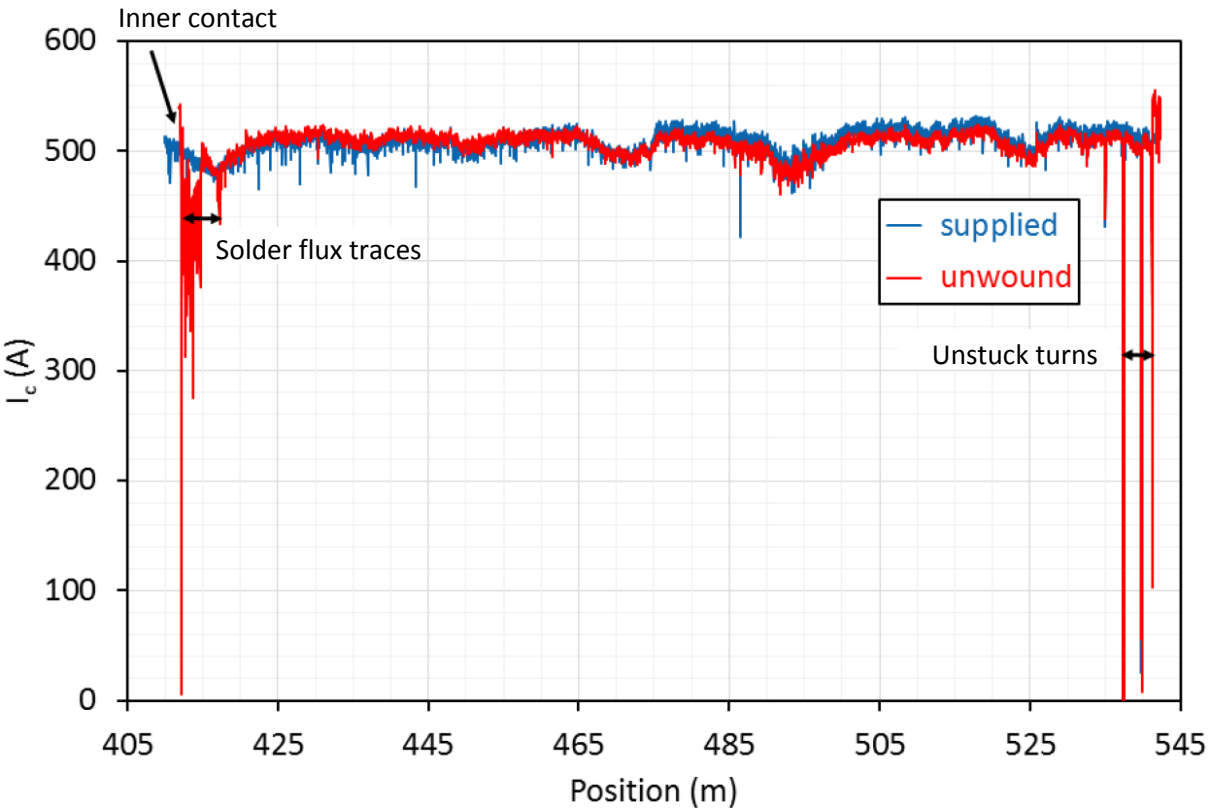

Fig. 112. Ic distribution of the conductor before and after winding. Correlation of critical current decreases with observed winding defects.

III.4.4.2.2 Pinched conductor

On another DP the tape was completely folded (Fig. 113). The measurement (Fig. 114) proves that the critical current of the DP tape has been degraded at the level of the pinch coming out of the inner contact.

Fig. 113. Pinched conductor at the exit of the inner contact.

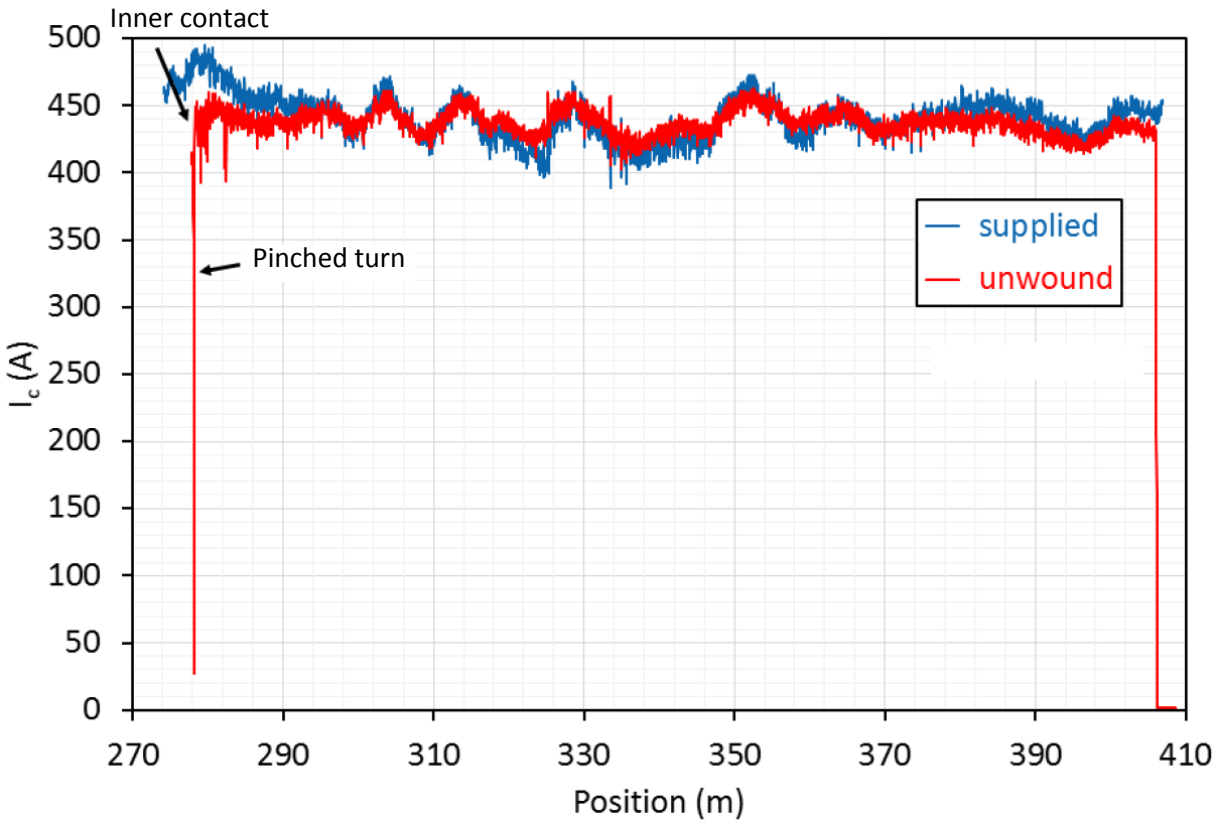

Fig. 114. I_c distribution along the conductor before and after winding. Correlation of critical current decreases with observed winding defects.

III.4.4.2.3 Destructive localized resistive transition

One of the DPs suffered a thermal runaway at a current of 840 A without the protective device having time to react. This transition damaged a large part of the conductor irreparably. We observed after unwinding that the hot spot has spread over about 50 turns (Fig. 115). The calculation in adiabatic condition of the maximum temperature of the hot spot maximum temperature is 740 K. However, this calculation does not take into account any heat exchange and is very pessimistic. Moreover, its critical current was still 200 A after the quench, it is very likely that the superconducting layer of the tape was not totally damaged. The I_c distribution post-mortem (Fig. 116) confirms that the critical current of the tape at the hotspot was still quite substantial. The heat also melted the polyamide and the unwinding of this pancake certainly amplified the damage of the conductor since the turns had stuck to each other.

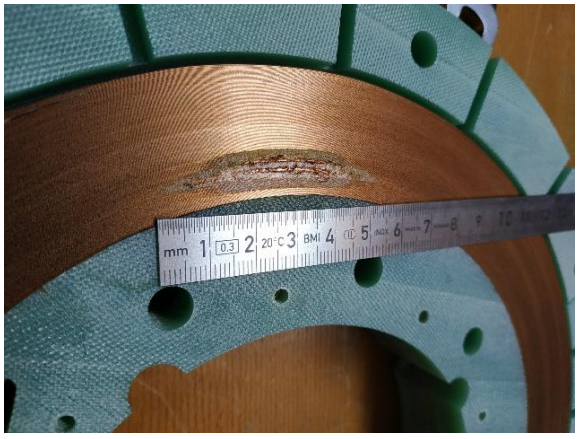

Fig. 115. Visualization of DP damage due to conductor transition.

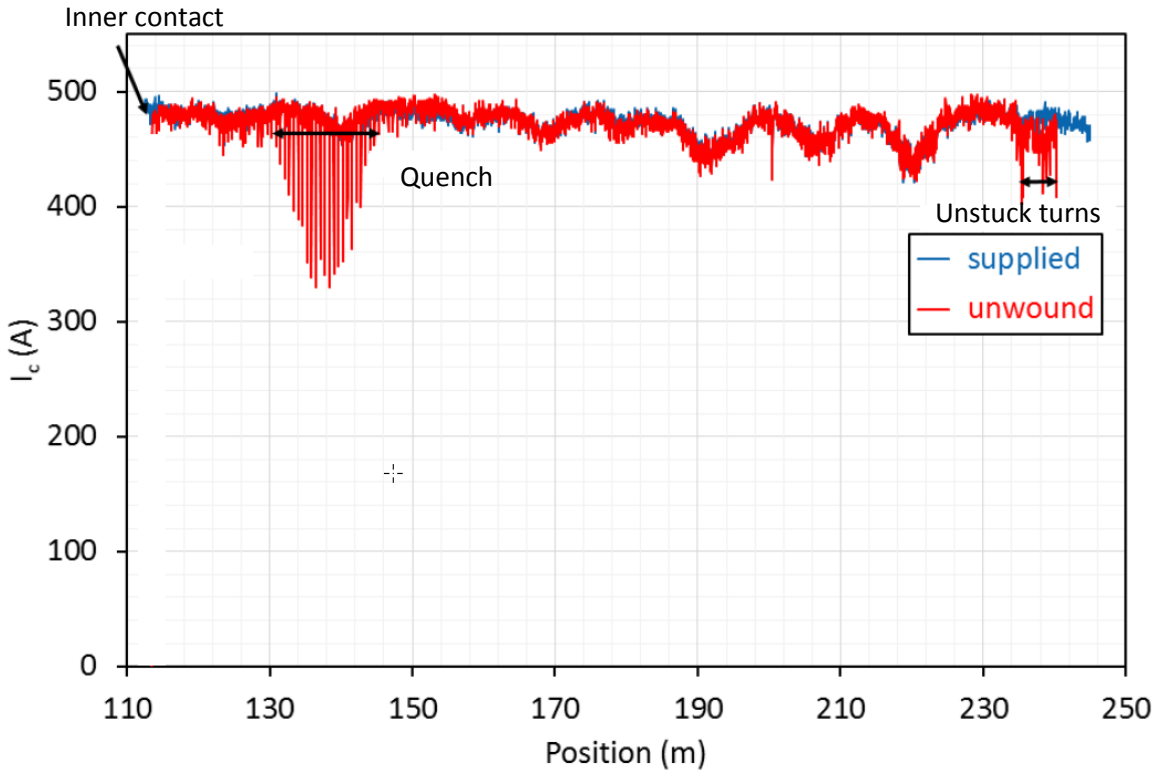

Fig. 116. Cryoscan of the conductor before and after winding. Correlation of critical current decreases with observed winding defects.

First of all, we questioned the reliability of the protection system in place to detect and quickly protect an insulated REBCO winding against the appearance of a hot spot. However, after analysis of the signals (Fig. 117), it can be seen that the detection voltage variation is very abrupt. This does not correspond to the dynamics of a thermal runaway due to degraded local I_c in a REBCO superconducting tape. We then suspected that this was due to a mechanical failure inside the winding. Indeed, after unwinding, indium-tin droplets coming from the outer contact soldering appeared to have ended up inside the winding (Fig. 118). With the binoculars, we can see grey balls of melted metal at the level of the damaged turns which seems to indicate the presence of solder (Fig. 119).

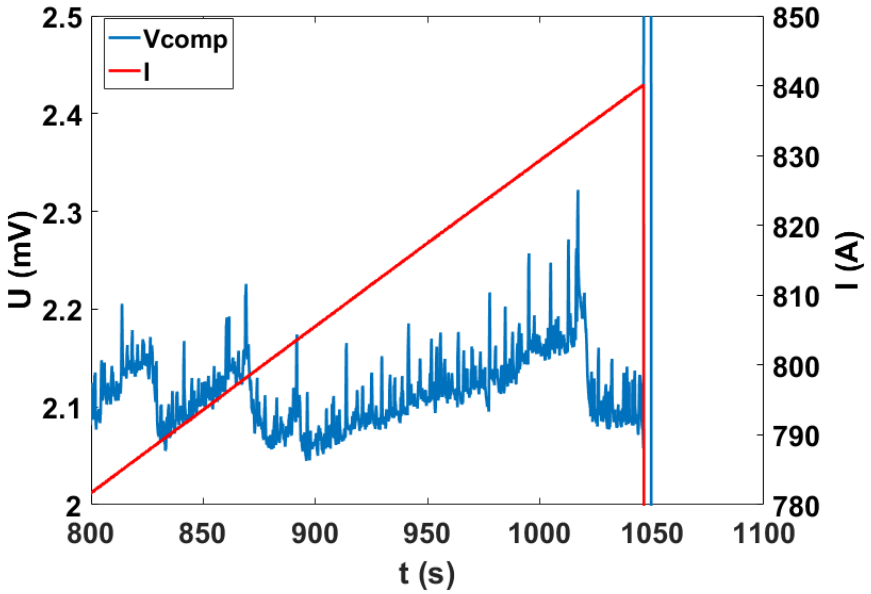

Fig. 117. Visualization of the current and compensated voltage signal during the sudden resistive transition at 840 A.

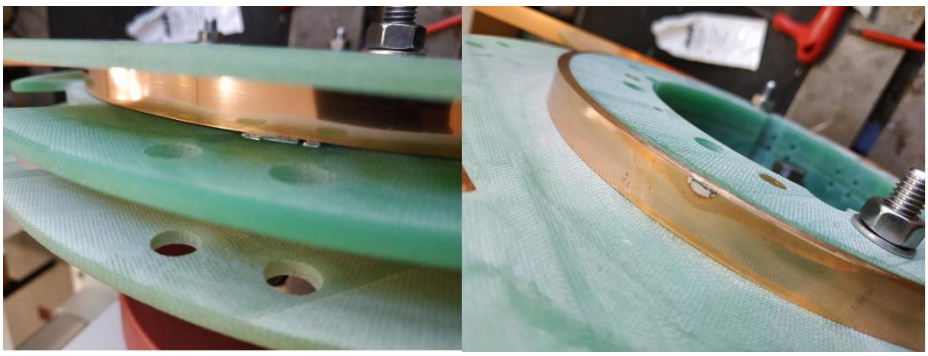

Fig. 118. Trace of indium tin inside the winding.

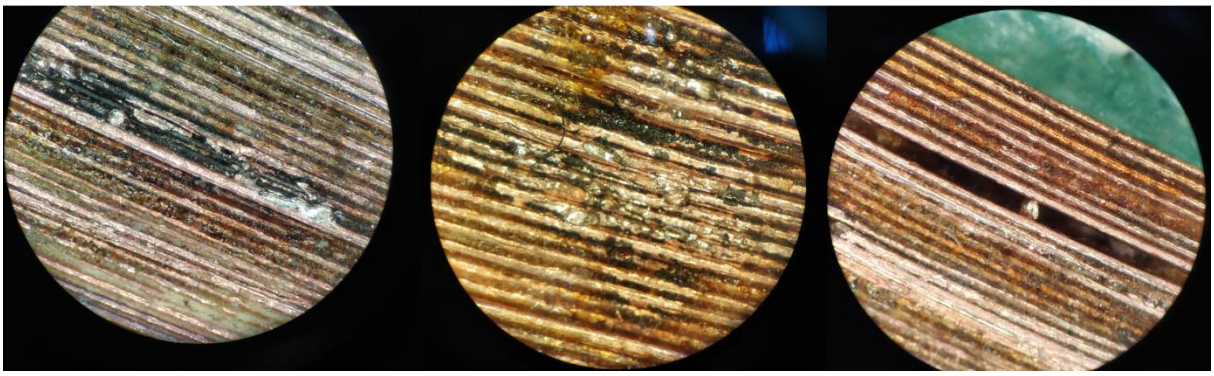

Fig. 119. Presence of indium tin balls in the winding at the level of the transited turns.

The electromechanical stress increasing with the current and the magnetic field, these droplets of solder inadvertently introduced in the winding created a concentration of stress inside the winding which led to sudden degradation of the superconducting layer and thus a hot spot.

III.4.4.3 Conductor polyimide insulation defect

The first lengths of conductor supplied by SuperOx had numerous insulation defects in the polyimide layer along their length. Dust of various materials was embedded in the polyimide and caused localized extra thicknesses in the winding (Fig. 120). These could cause a premature transition due to electromechanical stresses as described in the previous part (I.2.5.5). This greatly complicated the winding of some of the lengths because at each insulation defect including a foreign body, a chemical removal of insulation had to be performed to remove the extra thickness. Moreover, it was necessary to ensure that these local loss of insulation did not generate a short-circuit between turns.

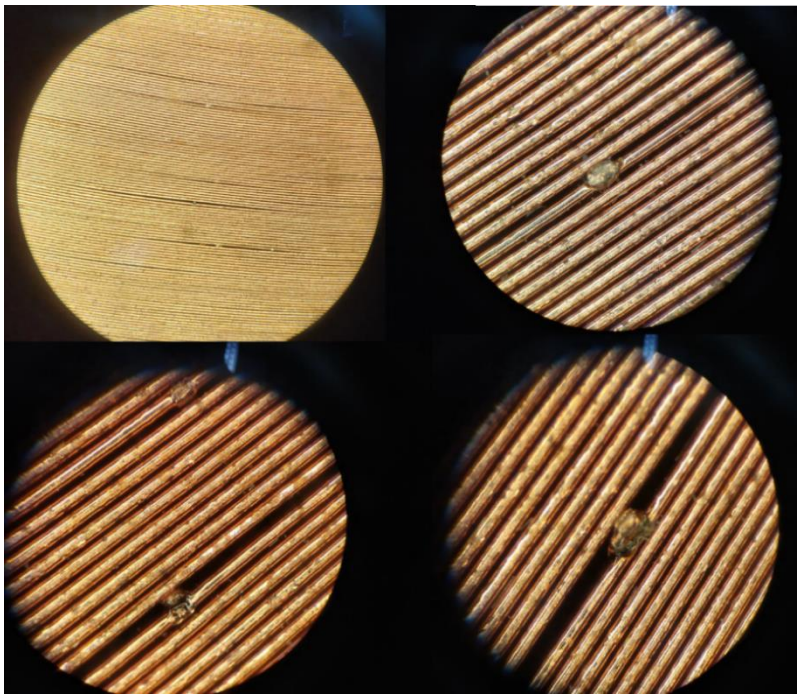

Fig. 120. Polyimide conductor insulation defects with excess thicknesses including foreign matter causing gaps in the winding.

Another polyimide conductor insulation defect caused the destruction of a pancake during an electromagnetic validation test of a DP. This time it was a lack of conductor insulation that was at fault. This was confirmed during the unwinding of the pancake thanks to a first visual analysis with binoculars (these insulation defects being very difficult to visualize with the naked eye for a non-experienced eye). A dielectric analysis showed that several lengths of about 20 cm had an inhomogeneous insulation coating where short circuit between the turns were identified (Fig. 121).

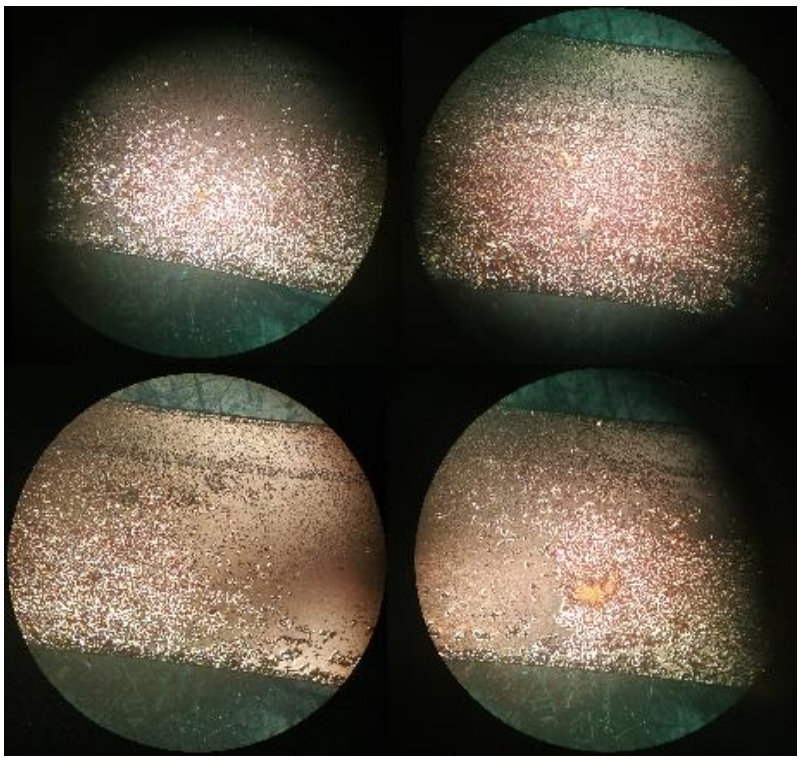

Fig. 121. Lack of polyimide conductor insulation.

During the test of this DP, the rated current was reached twice. However, the short-circuit between turns generated a high induced current, leading to the destruction of the conductor on several turns inside the winding during the second discharge (Fig. 122). After the analysis of the signals, we realize that the short circuit was already present from the beginning, because the energy efficiency of the DP was only 71% during the 1st charge and discharge cycle (recall τ = 1 s). Normally the energy efficiency is much higher and approaches 95% at least. Therefore, it is estimated that the first discharge only worsened the short circuit and the second discharge destroyed the pancake irreparably. The energy efficiency for this second discharge was 53% and 6.44 kJ were dissipated in this short circuit.

Fig. 122. Melting of the conductor on several turns due to a short circuit causing a hole in the winding.

This destroyed length of conductor as well as the lengths with too many insulation defects including foreign bodies have been kindly replaced by the manufacturer SuperOx.

III.4.4.4 Concluding Remarks

All these problems encountered have highlighted the multiple obstacles to be overcome in order to realize an insulated REBCO magnet. From the problem of resistive junctions between REBCO conductors, to the insulation defects of the conductor, to the winding difficulties, the main hard points have all been reviewed.

Despite these major setbacks, important lessons have been learned. Several actions were taken following these complications to ensure better quality control throughout the winding process. Namely:

- a better cleaning of the soldered parts to remove all traces of soldering flux.
- specific tooling for the soldered joints of the inner and outer contacts to improve their resistance and also to avoid solder to be inserted in the winding.
- Plexiglas flanges to check the good alignment of the windings and possible overthicknesses including foreign bodies to be removed.

These arrangements have greatly improved the quality of DPs. Only the junction resistances of the inner contacts could not be improved reliably.

Dielectric insulation defects of the conductor are also a critical point in case of short circuit between turns. These are very difficult to detect with the naked eye and checking all the 120 m lengths with binoculars would have been very time consuming and for an uncertain benefit. Therefore, it will still be necessary to be aware of this when testing with DP assemblies. Slow discharges are recommended in order to avoid any risk of irreversible conductor damage.

III.4.5 The BOSSE solenoid cryostat

The cryostat of the BOSSE solenoid (Fig. 123) has an inner diameter (helium chamber) of 497 mm and a height of 1600 mm. It has a capacity of 200 L. It is also equipped with a nitrogen guard of 70 L. The price of helium having greatly increased during the project (by a factor of 4), it was decided to implement ways to minimize the consumption of helium. For that, liquid nitrogen exchanger was set up in the cryostat in order to pre-cool the solenoid before transferring liquid helium. Also, blocks of H361 insulating PVC foam used for space launchers have been machined to fill the helium vessel's empty volumes. ALAT (Air Liquide Advanced Technologies) kindly provided the H361 cylinders. The cryostat is equipped with helium vapor-cooled AMI current leads. They minimize liquid helium consumption for a specific operating current and provide the most efficient means of transferring high currents from 300 K to 4.2 K. These are rated for 1000 A and run down to the last aluminum screen in the cryostat. They are then extended to the top of the solenoid by means of copper bars on which several REBCO tapes have been soldered to reduced heat dissipation. Then, Rutherford NbTi conductors take over to the ends of the solenoid to be connected thanks to a pressed contact indium with a large copper piece for interface. Concerning the instrumentation, 3 Pt100 probes are used to measure the temperature of the helium enclosure and of the solenoid during the pre-cooling of the helium gases through the liquid nitrogen exchanger. Then 5 carbon probes Allen-bradley 1/8 W are positioned at different heights of the solenoid and above to determine the level of liquid helium inside the cryostat. The voltage taps of the DPs and the pickup coils are made with high voltage enamelled copper wire. All this instrumentation goes up to the upper flange of the cryostat (room temperature) to be connected to several vacuum tight 12 pins connectors.

The effort to minimize helium consumption has clearly paid off for the subassembly tests. Indeed, even if precise measurements of consumption have not been made for the moment, between 100 and 120 L of liquid helium were necessary for these tests. The tests carried out lasted 4 hours and at the end of the tests the subassemblies were still bathed in liquid helium. As a comparison, the individual tests of the DPs carried out using the Eucard probe consumed 90 L each and they could not exceed 1 hour.

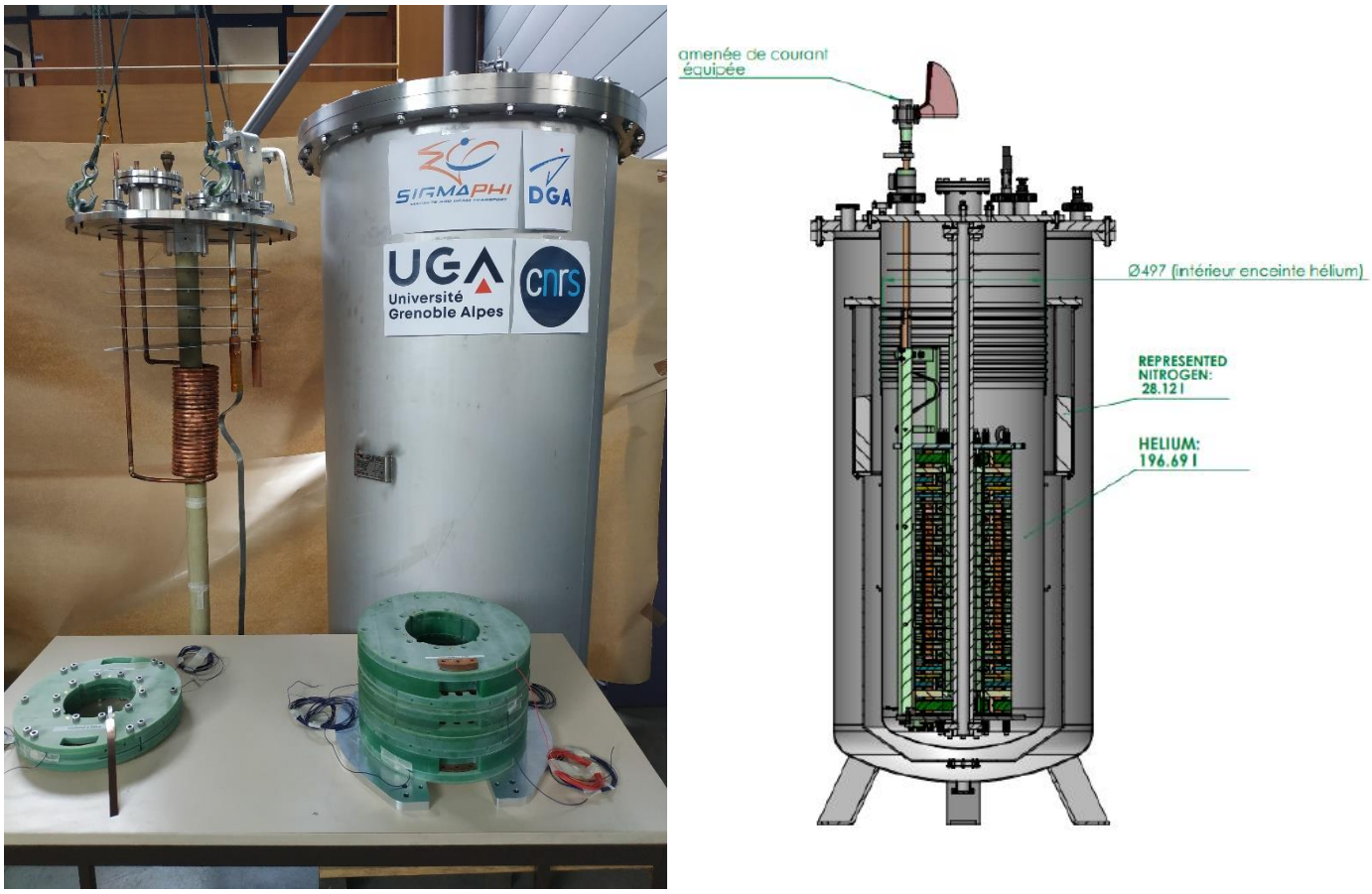

Fig. 123. Photo of the BOSSE solenoid cryostat and the cryostat section with its solenoid.

III.4.6 Assemblies of DPs

The assembly of the DPs is not difficult in itself but requires rigor and meticulousness. The DPs must be perfectly aligned to insert the 20 threaded fiberglass rods (8 mm in diameter) which sustain the assembly, and ensure a good alignment of the pressed electrical contacts between DPs. The stacking of the DPs also requires the use of adaptation flanges with varying thicknesses depending on the position of the DPs in the solenoid. During the change of flanges, the winding is completely exposed and care must be taken to ensure that no foreign bodies gets into the winding.

To ensure good pressed electrical connections, the DPs copper outer contact surfaces must be de-oxidized. This is done by grinding fine-grain abrasive paper. The dust is then vacuumed and the contact cleaned with ethanol. A protective sheet is placed on the winding during this phase. The flange serving as a spacer is also cleaned and blown with compressed air to remove any roughness that would come to press on the winding and degrade it. The winding protective sheet is then removed and the flange positioned. The next DP is then stacked and the external connection between crescent-shapes pressed contacts can be made. Between the cleaned contact surfaces, a thin indium foil is inserted to improve the electrical contact. The contact is then pressed through 3 stainless steel threaded rods of 4 mm. These steps are repeated until all DPs are assembled. Then comes the insertion of the pickup coils in the center of the solenoid. These are maintained and positioned in the center of the SMES with threaded rods also made of G11 fiberglass. The instrumentation is then carefully reassembled at the top of the magnet. The PVC foams to fill the dead volumes of the cryostat are then inserted around the solenoid. Finally, the whole assembly is sandwiched by two large fiberglass flanges and the 20 threaded rods are tightened with their respective nuts. To hold the

magnet inside the cryostat, a thick fiberglass tube attached to the cryostat head passes through the center of the solenoid and its pickup coil. The whole assembly is then maintained by the solenoid's bottom flange by means of pins inserted in the tube. This tube is also used for helium filling. Pictures of the different steps realized during the solenoid assembly are grouped in Fig. 124.

Fig. 124. Photos of the different stages of the solenoid assembly.

III.4.7 Test of a 3 DPs assembly

III.4.7.1 Assembly characteristics and test result

The main step left before the final magnet is to succeed in protecting several DPs in an assembly. Two partial assemblies were tested. The first one used 3 DPs. This assembly was made using DPs from the BOSSE solenoid heads, so they are separated by a larger gap than the central DPs. Moreover, these coil head DPs were wound with the tape lengths having the best average I_c at 77 K (>500 A) to keep sufficient current margins in transverse field. The 2 DPs at the ends of this assembly have a spacing of 30 mm between pancakes and the DP at the center a spacing of 15 mm. Between these three DPs a 15 mm spacing is chosen to homogenize the field distribution as well as possible. An axisymmetric magnetic field map of the assembly of these 3 DPs and their respective pick-up coils is shown in Fig. 125 as well as a picture of a DP pancake coil where the inner and outer contacts of the DP can be distinguished.

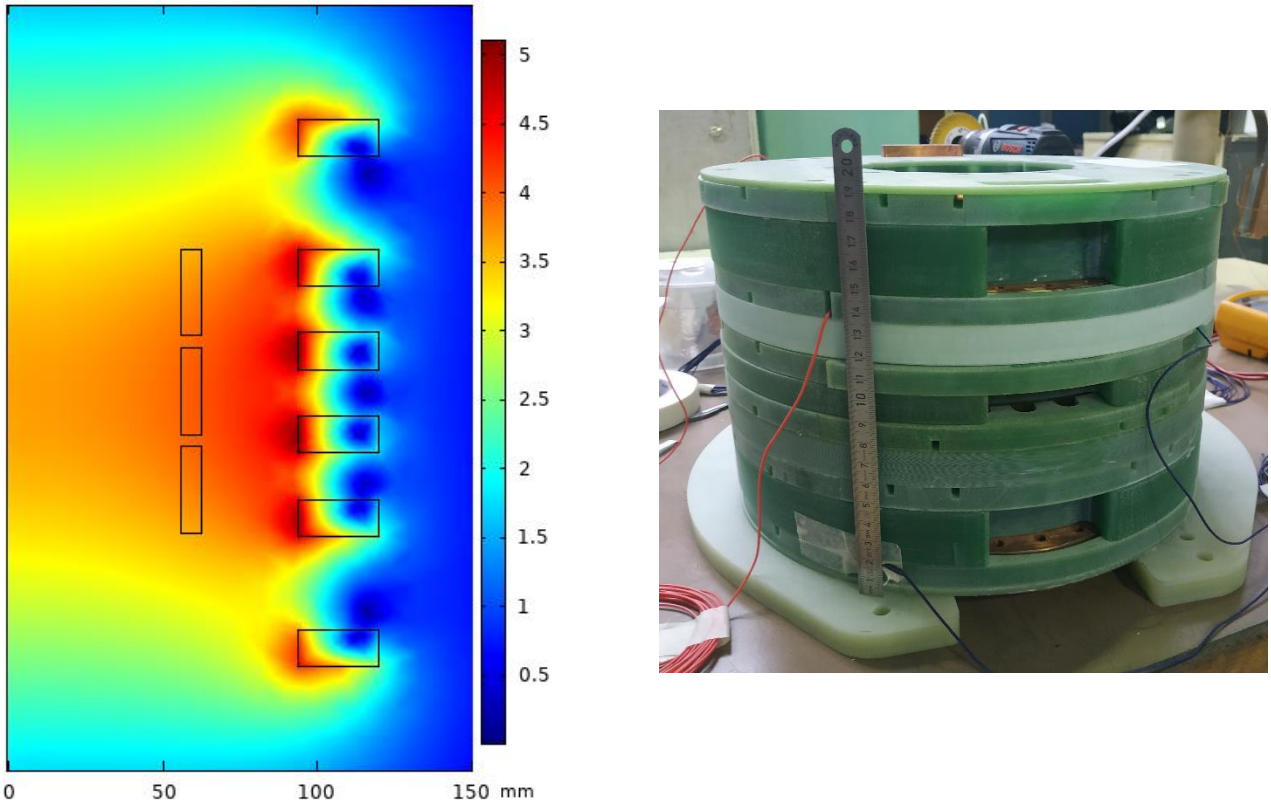

Fig. 125. The magnetic field map of the 3 DPs assembly and its pick-up coils as well as the picture of the real assembly.

For this first assembly, we evaluate the possibility to protect the three DPs together. Their three pick-up coils were connected in series in order to perform a global compensation of the assembly and analyze the sensitivity of the protection signal in such configuration. In order to minimize the risks of damage in this preliminary work, it was decided to limit the operating current to 745 A, corresponding to the first project target of 14 kJ/kg.

We exceeded the first target of 745 A and reached 763 A (see summary Tab. 7) which corresponds to a stored energy of 52.3 kJ and a specific energy density of 6.35 kJ/kg. A first current ramp at 2 A/s is performed

up to 600 A where a short plateau of about 100 s is maintained (to evaluate steady state dissipation), then the current ramp is increased with a ramp of 1 A/s up to 763 A where another plateau of about 160 s was achieved before the magnet discharge. During both current plateaus, the voltage returned close to zero, proving the safe operation of the assembly. Fig. 126 shows the total voltage of the 3 DPs connected in series and Fig. 127 shows the individual voltages of the 3 DPs and the current cycle for this test. The voltages of the DPs at the ends of the assembly are expected to be superimposed as they are identical and symmetrical. The slight difference observed in their voltage is due to a small variation in turn number: 360 for the upper one and 368 for the lower one. The voltage of the central DP is logically higher: its inductance is higher due to its smaller gap between pancakes (15 mm instead of 30 mm). It also has higher coupling with both others.

TABLE 7
DPS ASSEMBLY: MAIN DATA

Number of DPs	3
L (mH)	172
I (A)	763
B_z^{max} (T)	5.23
B_r^{max} (T)	3.4
Max. hoop stress (MPa)	203
Specific energy density (kJ/kg)	6.35

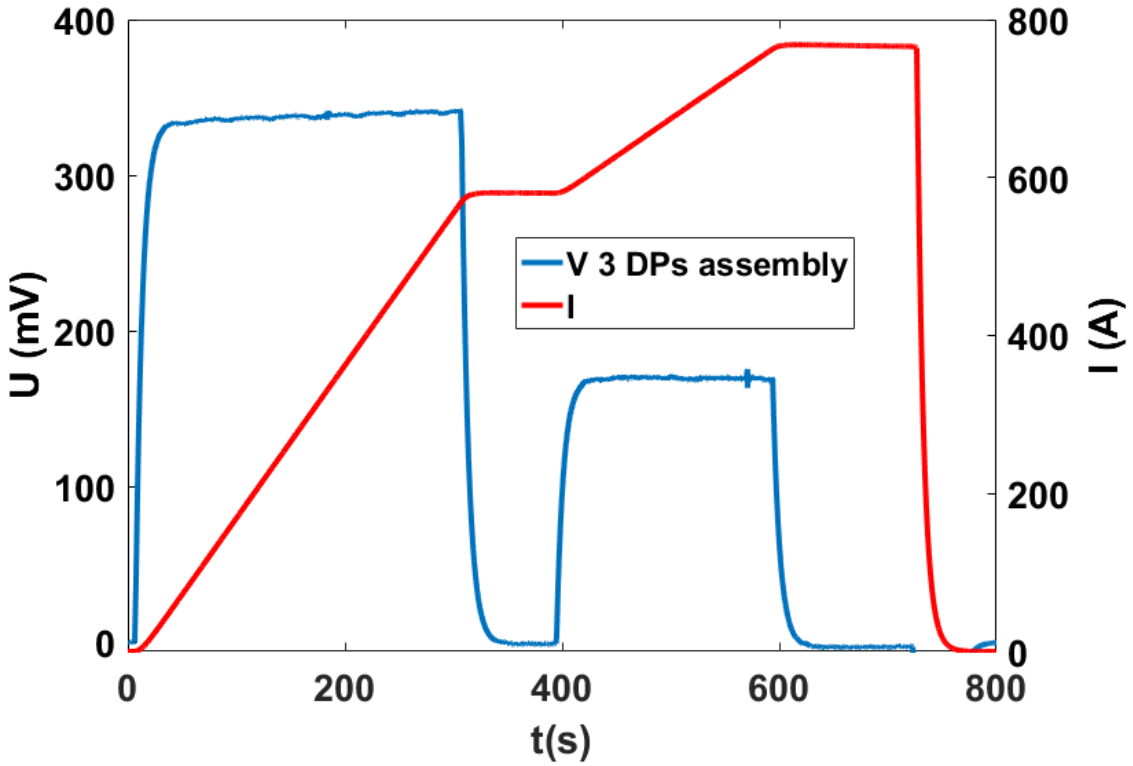

Fig. 126. The current cycle and the voltage measured across the 3 DPs assembly.

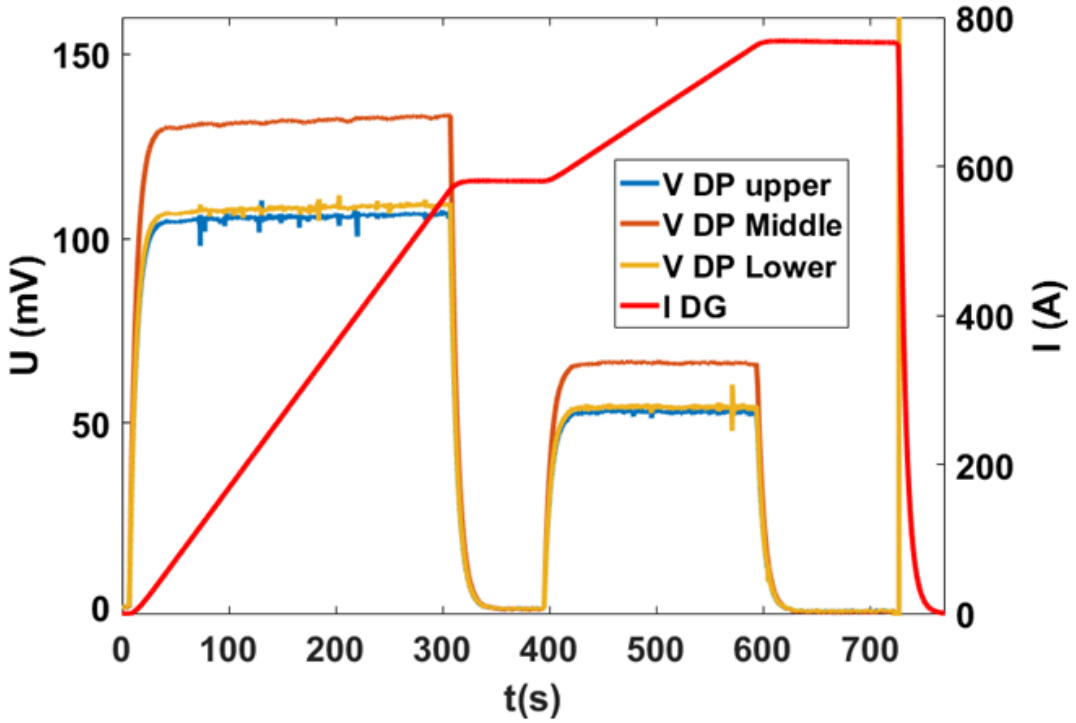

Fig. 127. The current cycle and the individual voltage across each DP.

Fig. 128 shows the compensated voltage signal of the assembly used to protect the winding (in blue).

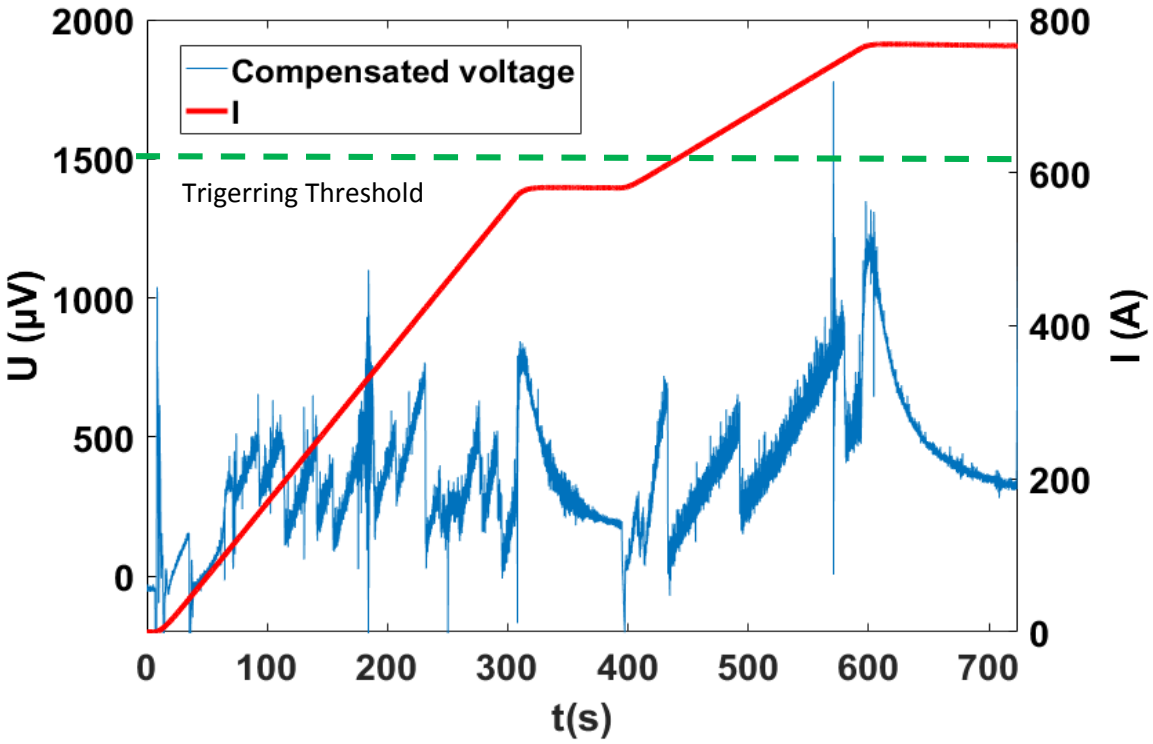

Fig. 128. The current cycle and the compensated voltage signal of the 3 DPs assembly.

The remaining voltage of about 250 µV at the end of the plateau at 763 A is due to the inner and outer connection of the windings which are resistive. This gives us a global resistance of the assembly of 327 nΩ at this operating current. The outer pressed contacts connecting the DPs together are very good and paradoxically better than the inner soldered contacts of the DPs. The latter are still satisfying, with an estimated resistance of about 60 nΩ in average.

The main result of this assembly test is that it was possible to reach sufficient sensitivity (well below 200 µV) in the thermal runaway detection system when observing a group of three DPs. This way the number of signals to monitor in a larger assembly can be reduced. Of course, the drawback of this solution is that identifying the defective DP is impossible if the protection triggers during a current transient.

Moreover, an excellent energy efficiency, 98.6 %, was obtained over the full charge-discharge cycle of this assembly (the discharge time constant was set to 6 s, slower than the 1 s target in the final configuration). The losses are AC losses and connection losses.

III.4.7.2 Inner contact damage and discussion

During a discharge of the 3 DPs assembly test, one of the inner contacts was degraded. Nevertheless, we reached several times this operating current of 763 A, showing that the superconducting winding itself was not damaged. As mentioned in part III.4.4.1, the inner contacts were a source of concern from the beginning of the series DP manufacturing, with joint resistance measured well above what was expected from the prototype. Still, this degradation occurred at the discharge and therefore neither at the maximum applied current nor stress. The reason may come from the inner contact structure (Fig. 129).

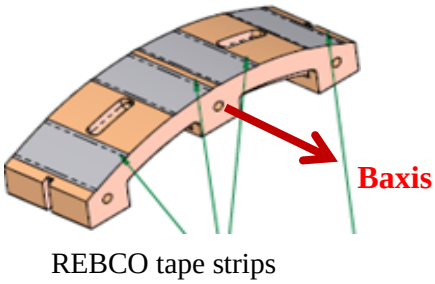

Fig. 129. Inner contact structure.

It was originally designed with large copper thickness to guarantee thermal stability, acting as a radiator in the helium bath. Eddy current heating during fast discharge was expected but the estimated temperature rise was acceptable. Indeed, with a linear variation of 11.57 T (rated magnetic field) in 1 second, the dissipated energy is 140 J by inner contact, estimated through FEM modelling. This corresponds to a rise in temperature of 39 K in adiabatic conditions (reasonable assumption in a few seconds timescale) [60]. Superconducting strips were added on the copper to reduce the joint resistance, but this may have been counterproductive. The improvement in terms of joint resistance was significant (III.2.2.2.3) but during transients, the induced current circulating in the copper contacts pass through these strips. When the transport current is decreased, this induced current is added to the transport current, with two potentially

detrimental effects. First, the total current may exceed the critical current of the strips. Second, this high current in the strips may cause abnormally high mechanical stress and the delamination of the conductor.

In consequence, simpler, thinner inner contact without REBCO tape strips will be considered in the future.

III.4.8 Test of a 5 DPs assembly

III.4.8.1 Assembly characteristics and test result

The main goal of the 5 DPs assembly was to test the possibility to monitor several protection signals at the same time, in this case with individual protection of each DP. The deterioration of the inner contact on one of the DPs was judged acceptable to perform tests with reduced operating current, and a good test case for the protection system. As for the previous assembly the DPs corresponding to the heads of the complete solenoid were used. Starting from the bottom, the stack included DPs with inner gaps of 30, 15, 10, 15, and 30 mm. The spacing between the DPs starting from the bottom was the following: 15, 11, 11 and 15 mm. The position of the DPs and their respective pick-up coils can be found on the magnetic field map Fig. 130, with a picture of the assembly.

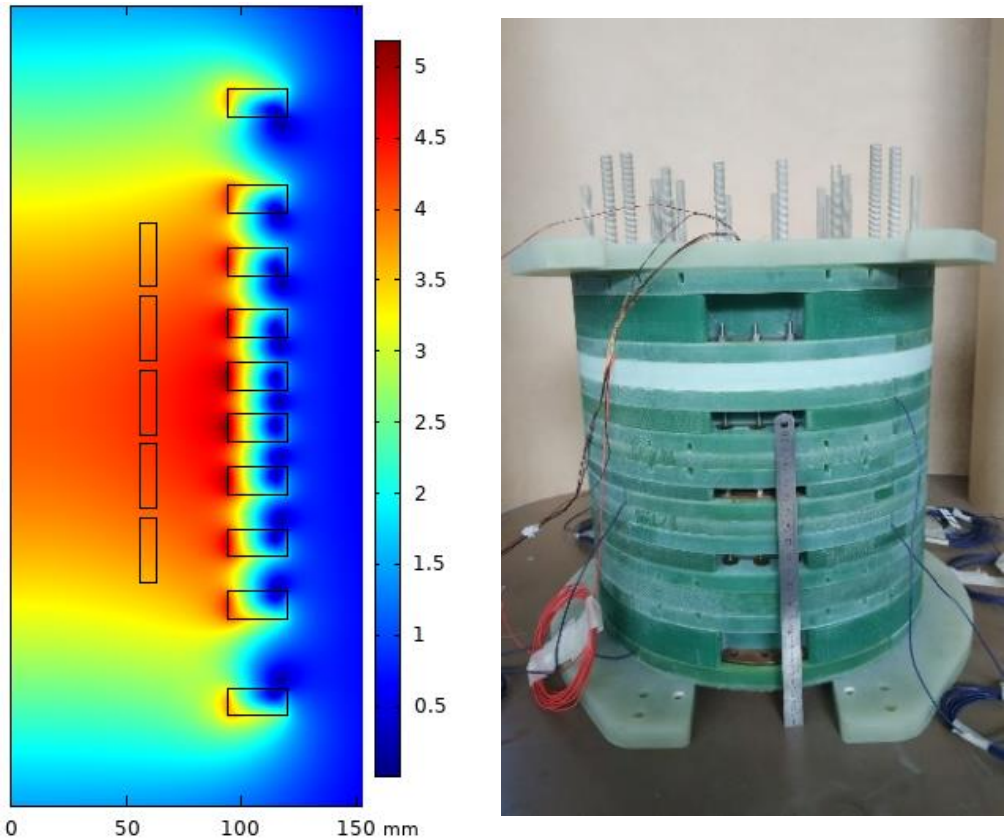

Fig. 130. The axisymmetric magnetic field map of the 5 DPs and their pickup coils as well as a photo of the assembly.

We did not set any current target for this experiment, but rather tested the coil up to the current for which the dissipation at the damaged contact appeared unstable. A current ramp of 8 A/s was performed up to 592 A where a plateau of about 300 s was achieved (Fig. 131). Tab. 8 summarize this tests parameters.

TABLE 8
5 DPs ASSEMBLY: MAIN DATA

Number of DPs	5
L (mH)	370
I (A)	592
B_z^{max} (T)	5.2
B_r^{max} (T)	3.5
Max. hoop stress (MPa)	140
Specific energy density (kJ/kg)	5

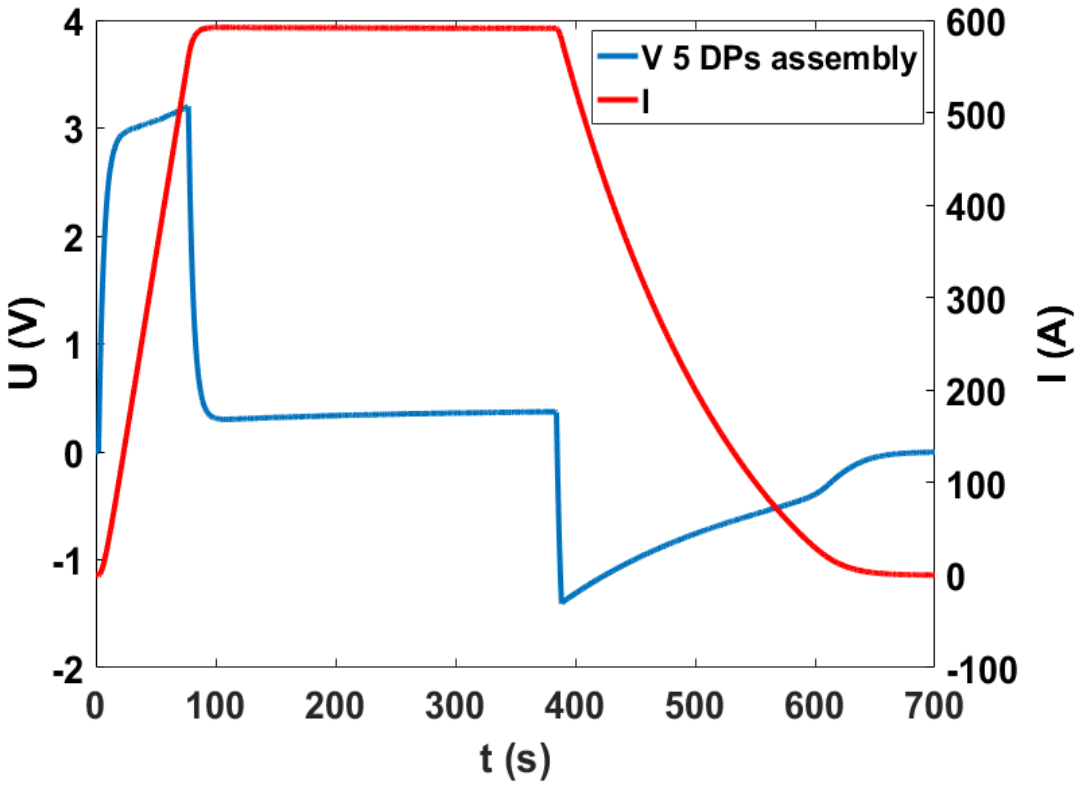

Fig. 131. The current cycle and the voltage measured across the 5DPs assembly.

In order not to degrade any other inner contact of DPs a very slow full discharge of 320 s was performed. The display of the compensated voltage signals of each DP is shown in Fig. 132. We can see that the signals of 4 DPs return to 0 V once the plateau has started except for one corresponding to the degraded DP of the previous assembly. The voltage is quite high and approaches 4 mV. Yet it remains stable, which means that it is due to the inner contact resistance of the DP. If a thermal runaway was occurring, it would have shown another dynamic. However, the dissipation of this contact was so high (2.37 W) that we considered it too dangerous to increase the current further.

The sensitivity of the individual DP compensation signals is very good: the noise envelops after compensation and filtering (numerical low pass with 15 Hz cut-off) is about 45 µV.

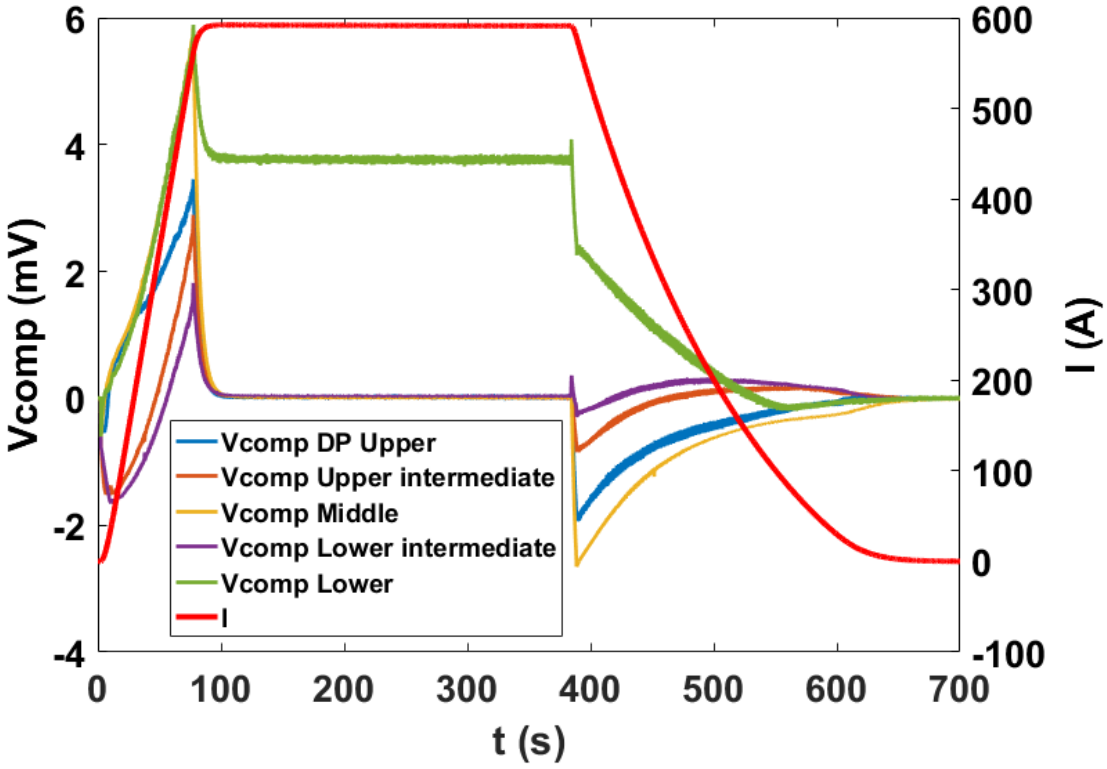

Fig. 132. The current cycle and the compensated voltage signals of the 5 DPs.

III.4.8.2 Discussion

In this assembly of 5 DPs, an individual protection of each DP has been successfully realized. We were able to perform several tests up to a current density of 365 A/mm² and this despite a degraded inner contact, which proves the robustness of the winding. The major benefit of this solution (in addition to the ability to clearly locate a defective DP) is the sensitivity level achieved below 50 µV. This advantage is all the more important as we are currently obliged to perform slow discharges. It is therefore of the utmost importance to have the finest possible transition detection sensitivity. This is why this protection solution will be adopted for the final solenoid protection.

III.5 Conclusion and Prospect

The BOSSE project has the ambitious objective of realizing a 1 MJ insulated REBCO magnet with a specific energy density of up to 20 kJ/kg for the winding. However, before reaching this goal, several intermediate steps were necessary. In this chapter, the solenoid design as well as the realization of a DP was presented first. Then, insulated REBCO windings being known to be difficult to protect in case of resistive transition, the system protecting each DP of the solenoid against the occurrence of a destructive thermal runaway is presented. Before starting the realization of each DP, a prototype DP was made and thoroughly

tested to validate the solenoid design. The electromagnetic validation tests demonstrate the reliability with a sensitivity of the thermal runaway detection system, with achievable thresholds as low as 400 µV, when high current density flows through the conductor (up to 600 A/mm², overall, and 853 A/mm² on the bare conductor). The magnet's electromechanical design was then validated through background magnetic field tests. 83% of the final device's mechanical stress, or 350 MPa, were reached.

With the prototype DP having passed the validation tests of the magnet design, the production process of superconducting DPs could begin. All series-produced DPs were tested at 4.2 K up to their rated current for quality control. Currently, 17 have been tested above the coil rated current (850 A) and have shown excellent electromagnetic performance. Each time a plateau at this current has been carried out and no voltage runaway corresponding to a thermal dissipation occurred. This was followed by a fast discharge without damage in a resistance to obtain the SMES time constant of one second. The number of validated DP shows that REBCO insulated pancakes work and can be protected. The collected results gave a lot of information about the electromagnetic behavior of these DP but also on their protection signal.

This test campaign study also highlighted the difficulty to obtain low resistance consistently in an industrial setting with the chosen inner contact design. Further work will be conducted on that point. These tests have also pointed out the various recurring difficulties in the manufacture of insulated REBCO coils and the damage they could cause.

An important step was the development and validation of a detection/protection system to protect an assembly of several DPs. It highlighted the benefit of monitoring DPs in small groups or individually using multiple pick-up coils to obtain high detection sensitivity. The high sensitivity we obtained practically during the 5 DPs assembly test – in the 50 µV range- makes us confident in the possibility to test the full assembly of the BOSSE solenoid reliably to its operation limits. However, even with a discharge time constant increased to 6 s, the discharge of the 3 DPs assembly degraded one of the inner contacts of a DP. The superconducting bridges added to the inner contact in order to improve the contact resistance are certainly the cause. A simpler and thinner inner contact, without REBCO strips, will be studied in the future.

There are still 4 superconducting DP to be manufactured and tested so that all are connected and give the SMES. The first important objective will be to overcome the magnetic energy storage record of 13 kJ/kg and reach 14 kJ/kg. For that, other DP assembly configurations will be tested to approach the mechanical constraints that the BOSSE solenoid will sustain that is to say 421 MPa, before the final assembly where the challenging objectives to reach the 1 MJ then 20 kJ/kg must be achieved.

Chapter IV:
High performance windings: Efficient and simplified winding structure for conduction cooled REBCO pancakes with high mechanical stress

Summary

In chapter II we first studied in detail the transient electromagnetic behavior of insulated REBCO windings for protection purposes. This study, applied to the BOSSE project, made it possible to perform the numerous DPs and assembly tests in a safer way as presented in chapter III. We also mentioned in chapter III the mechanical behavior of these coils and showed that estimating the mechanical stress of this kind of magnet is not straightforward. In this last chapter, we present solutions to improve the mechanics of insulated REBCO coils while ensuring a conduction cooling capacity.

REBCO Coated Conductors have high tensile strength along their length. They are however sensitive to delamination when traction force is applied on the tape surface, which in a (REBCO) solenoid corresponds to radial tensile stress. For this reason, most REBCO magnets are non-impregnated, which means they are dry-wound. One of the drawbacks of dry winding is that conduction cooling to low temperature (below 20 K) is inefficient due to the poor thermal conductivity at the pancake interface. Partial impregnation techniques were developed to mitigate this problem but the manufacturing process is complex and costly. First, we propose a simplified pancake structure with conduction-cooling capability, and test it under large background field to verify its mechanical performances. Then, based on the results of this first impregnated coil but also on our understanding of the electromagnetic and mechanical behaviors of REBCO windings, we propose in collaboration with the High Field Laboratory for Superconducting Materials (HFLSM) the design of a high performance conduction-cooled REBCO coil for a high magnetic field insert.

IV.1 Introduction

The effort to reach very high field (30 T and above), requires to operate REBCO inserts with large current densities and mechanical stresses. In other magnet applications such as energy storage, the trend is the same to gain performance and/or to reduce the conductor cost.

Although most high-field REBCO magnets are still designed to operate in a liquid helium bath, their conduction-cooled operation would facilitate the emergence of applications that require freedom from the constraint of using a cryogenic fluid and would also significantly reduce cooling costs due to the high price of liquid helium. As stated in the previous chapter, our research team has already worked on conduction cooled HTS windings. The first 800 KJ SMES consisting of first generation HTS tapes and cooled by conduction at 20 K was successfully tested in 2009 and proved the feasibility of an HTS coil with easy-to-use cooling. Nevertheless, for practical reasons this solution was put aside for the SMES of the BOSSE project and that is why it is cooled in a liquid helium bath at 4.2 K. Indeed, the conduction cooling conditions of a REBCO coil create several technical challenges.

To stably operate a REBCO coil in a cryogen-free system and enable efficient cooling of the winding, it is necessary to impregnate the coil. However, the anisotropic thermal contractions between the conductor, the insulator and the epoxy, lead to dangerous radial tensile stress. If this radial tensile stress in the winding locally exceeds the delamination resistance of the conductor, it leads to winding degradation. In addition, the effort to make very compact REBCO winding leads to designs using thick pancakes or double pancakes, with large thickness over diameter ratios. Impregnating such thick coils further increases the risk of delamination. The solution proposed in [83] is to use non-stick material to separate the turns in several blocks in radial direction, or even separate all turns from each other. This is the solution used successfully in recent magnets wound for HLFSM (High Field Laboratory for Superconducting Materials), where the insulation between turns is a co-wound thin polyimide tape with fluorine non-stick coating [56, 84, 85]. Using this technique, an impregnated pancake can behave essentially as a dry winding mechanically, while maintaining a good thermal conductivity required for conduction-cooling. However, this technique requires a complex winding process, very sensitive to the co-winding tension and alignment, as well as the impregnation application.

The use of a REBCO tape with thin (around 15 µm) polyimide coating already deposited was tested in Grenoble for dry winding. The first advantage of such a conductor is that the winding process is simpler. Only one feeder is needed and no complex co-winding process is required. The dielectric strength of coating insulation is much stronger than co-winding, in the same range as polyimide tape double wrapping while being much thinner. This is appealing for applications with very large voltages such as pulse SMES, but conduction cooling remains an issue.

The first idea proposed in this work is to use such simple winding using single coating-insulated REBCO tape as conductor, and then stick thin flanges with a cooling plate on the pancake surfaces. Thick epoxy compound with low curing temperature should be used so that the epoxy does not penetrate in the winding but glues the turns to the flanges.

In the framework of high magnetic field inserts developed at HFLSM, the second idea is to use this impregnation technique on a high performance conduction-cooled REBCO coil for a high magnetic field insert. The aim is to design a high current density and high mechanical stress winding.

IV.2 Simplified pancake structure with conduction cooling capability

IV.2.1 Test pancake structure and characteristics

The test pancake was wound at CNRS Grenoble. It is a single pancake wound using 6 mm wide SuperOx tape from 2015, it is 130 µm thick, including a 60 µm Hastelloy substrate, 20 µm-thick copper stabilizer on both sides, and 30 µm of insulation overall. Actually, it is exactly the same conductor as for BOSSE but in a 6 mm wide version. The inner and outer diameter of the pancake are 90 mm and 144 mm respectively for 195 turns. Initially the coil is dry-wound like BOSSE pancakes. A 0.2 mm thick FRP flange is glued by epoxy on each side of the pancake to make the thermal link between the turns and improve the rigidity of the coil. In this way, the coil turns are only glued to the flanges and not to each other. The potential radial tensile stress is therefore only transferred to the flanges, thus avoiding any risk of delamination. The thin thickness of the FRP flange provides a good compromise between the mechanical and thermal aspects of the coil. It keeps a certain flexibility and can be deformed under the stress due to the movement of the turns. This solution has already been approved by Toshiba developments. We find in Fig. 133 a 2D axisymmetric representation of the winding.

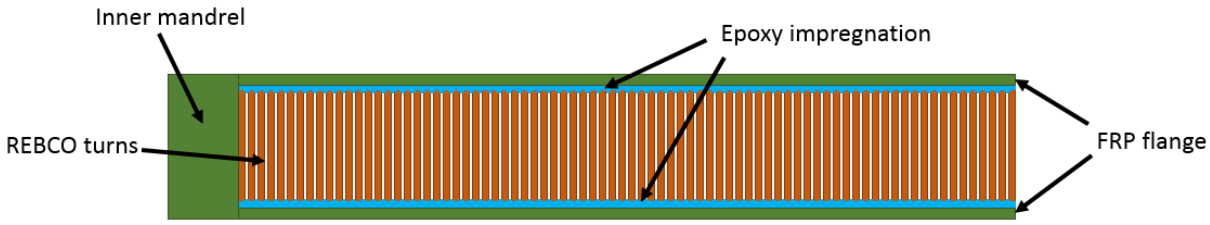

Fig. 133. 2D axisymmetric schematic of the edge-impregnated pancake.

For the epoxy, we use a HexbondTM 609 adhesive film. This type of high strength epoxy film is easy to handle and can cure at temperatures as low as 100ºC, a safe value for REBCO tapes. Here, a thermal cure of 120°C for 60 minutes was performed. In order to ensure the winding integrity, manipulations before adding the flanges must be limited. Moreover, the thickness of epoxy adhesive has to be controlled to ensure the geometry of the pancake, especially the homogeneity of its thickness (around 0.2 mm). Winding dimensions and properties are summarized in Tab. 9.

TABLE 9: TEST PANCAKE DIMENSIONS

SuperOx Tape 6 mm wide 130 µm thick with Polyamide insulation. 195 turns in series	
I_c (77 K sf (100 µV/m)	210 A
Inner diameter	90 mm
Outer diameter	144 mm
FRP flange thickness	0.2 mm

The radial stress of a coil depends on the outer diameter to inner diameter ratio for the given material properties. Above a ratio of 1.4, we enter the range where damage usually occurs during cooling in case of impregnation [83]. Thus, in order to validate this impregnation method, a ratio between the outer radius and the inner radius greater than 1.4 was deliberately chosen. This one is 1.6. In order to represent realistically the electrical connections to other pancakes in the case of a solenoid, the inner and outer terminals of the test single pancake are not directly soldered to the conductor, but connected to it using short REBCO strips, as shown Fig. 134. The goal is to reproduce the same constraints as in the high magnetic field inserts. Namely, little space for the connections between pancakes and no extra thickness of the winding. Photos of the different steps in the manufacturing of this pancake are shown in Fig. 135.

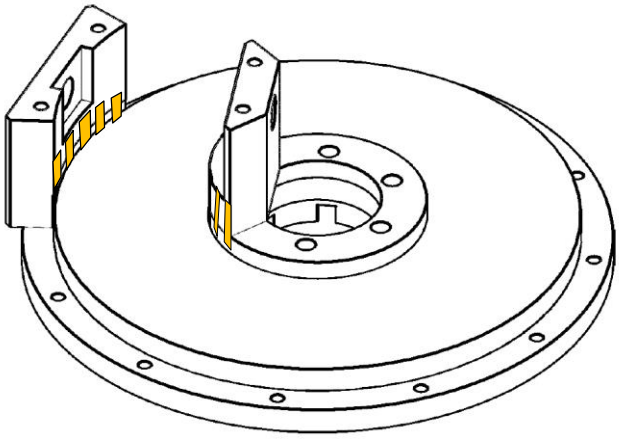

Fig. 134. Pancake structure with outer (left) and inner (center) copper current terminals connected to the winding with soldered REBCO strips (in yellow)

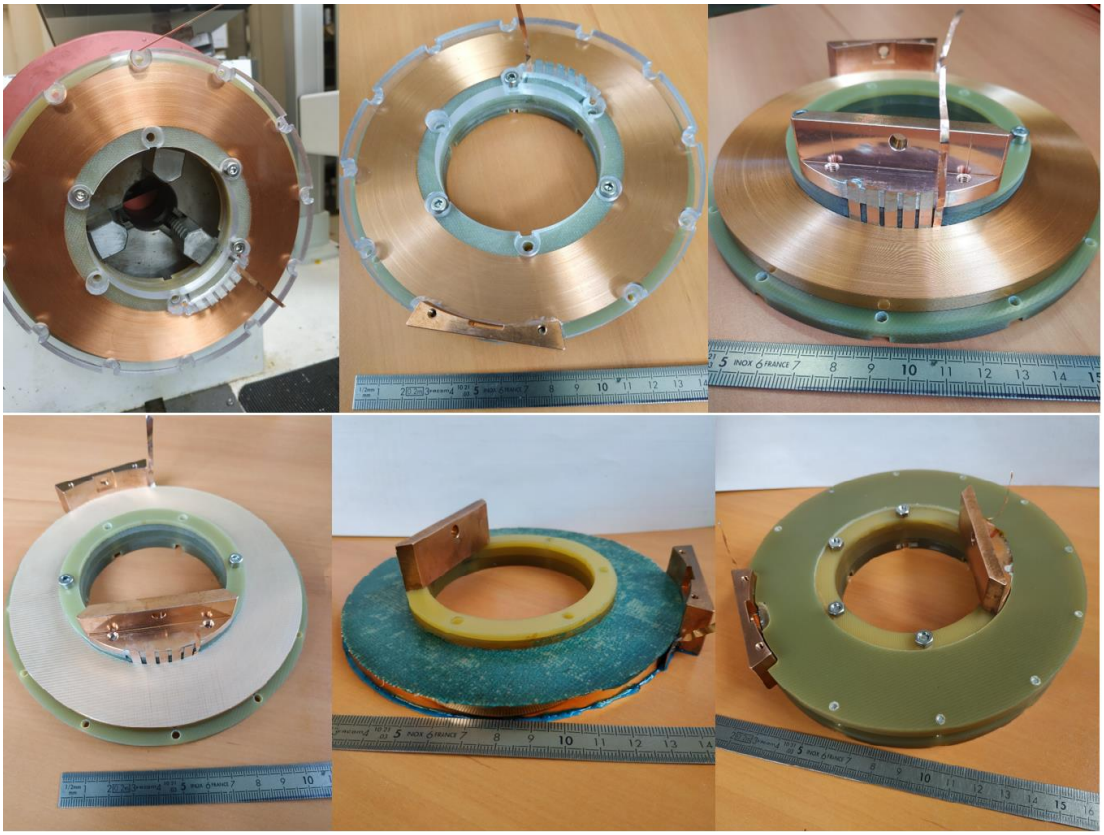

Fig. 135. The different steps to make a simple impregnated pancake.

IV.2.2 Test procedure and results

The winding was first tested up to 200 A in Grenoble in liquid helium to ensure that no degradation was induced by cooling down. The winding was then equipped at HFLSM with a 0.3 mm aluminum heat sink foil for conduction cooling and strain gauges on the outer turn. 5 strain gauges were installed but only three were functional during the tests. The tests were carried out at 20 K in a conduction cooling cryostat in background field generated by the 12 T Superconducting Magnet large bore magnet (360 mm room temperature bore) at HFLSM. The test magnet was ramped up to 370 A with no dissipation.

Fig. 136 represents the 2D axisymmetric modeling of the magnetic field generated by the pancake at a current of 370 A under 9 T of magnetic background field. The current distribution in the tape is assumed to be homogeneous. At this current level the pancake generates 2.3 T which gives us a maximum magnetic field of 11.3 T at the inner turn against 7.66 T on the outer one. The winding model is of course homogeneous and the turns are all the same.

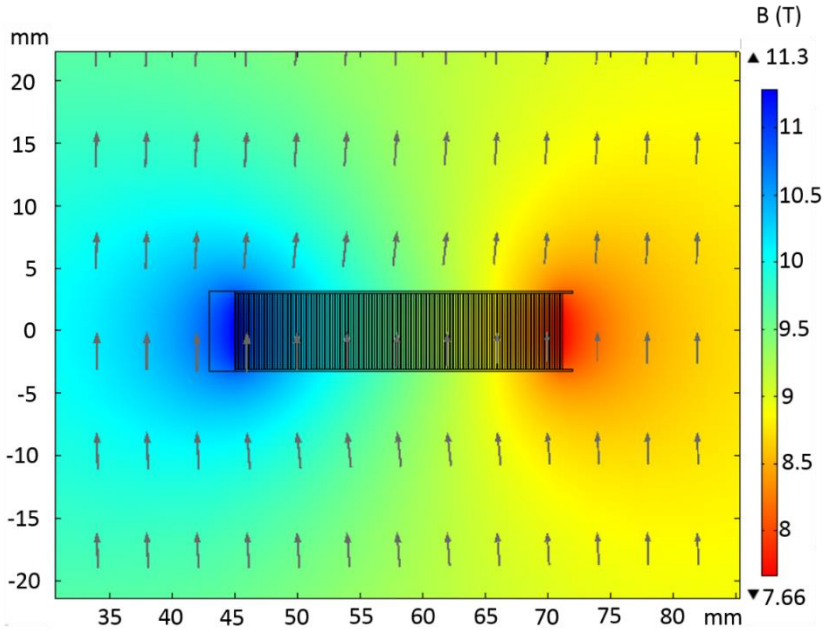

Fig. 136. 2D axisymmetric modeling of the magnetic field generated by the pancake at a current of 370 A under 9 T of magnetic background field. The differences in thickness between the turns as well as the periodic structures of the pancake turns that can be visualized are due to the graphic resolution of the image.

Fig. 137 shows the measured strain under 9 T, which reach 0.16 % in average at 370 A. We note the good correlation between the experimental measurement and the modeling result.

At 370 A, the test pancake reached its mechanical limit and we were not able to perform further tests on this pancake. In order to achieve inner and outer connections with the lowest possible contact resistances, the REBCO layer of the conductor was positioned on the outer side of the coil. With the hoop stress, the REBCO layer could not be supported on its hastelloy substrate, and it pulled away from its buffer layers.

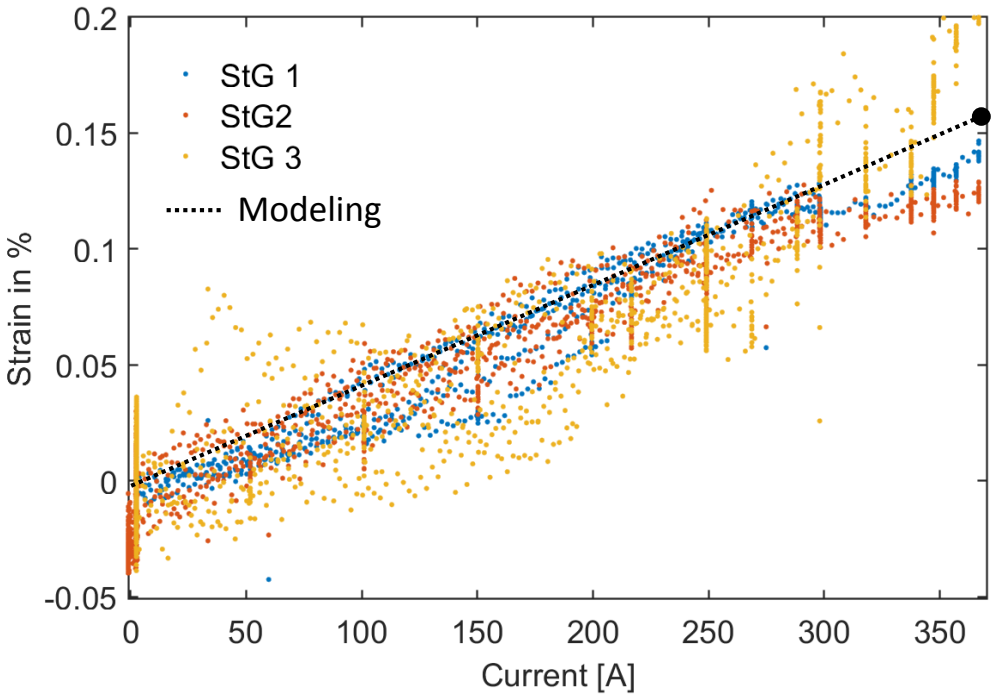

Fig. 137. Measured strain on outer turn of test pancake under 9 T background and up to 370 A. The black dotted lines represent the modeling results.

Considering the high stiffness of this tape, estimated at 170 GPa based on its layer's thicknesses, the measured stress on the outer turn reached 263 MPa. Due to the pancake structure, we will see that this value is however not the highest reached in the winding.

IV.2.3 Modeling the winding's mechanical behavior

As presented in chapter I, we can estimate the hoop stress in a coil with the following assumptions: dry winding, with tapes fully separated and stress following the BJR equation, and impregnated winding where the stress distribution follows the Wilson formula. Fig. 138 shows the stress distribution with these two calculation assumptions for the previously described experimental test. With edge-impregnation we can consider that the Wilson calculation is the most realistic. However, Wilson assumes a complete impregnation (turns glued together). If we look at the radial stress inside the winding (Fig. 139 and 140), we can see that the tensile stress between the turns would have exceeded 10 MPa.

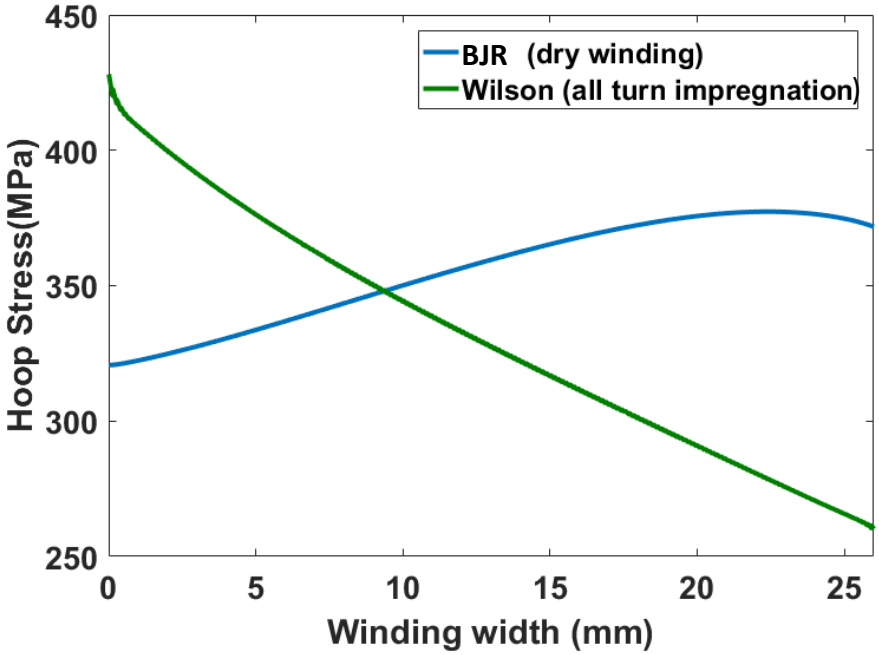

Fig. 138. Calculation in BJR and Wilson of the stress distribution along the pancake winding radius under a 9 T background and up to 370 A

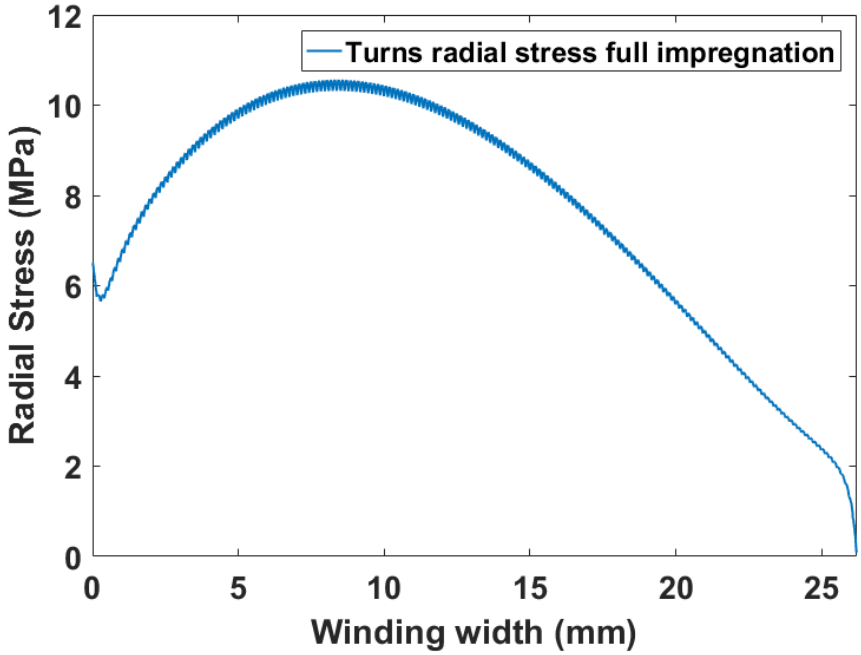

Fig. 139. Radial stress in full impregnation winding under 9 T background and up to 370 A (computed with Comsol).

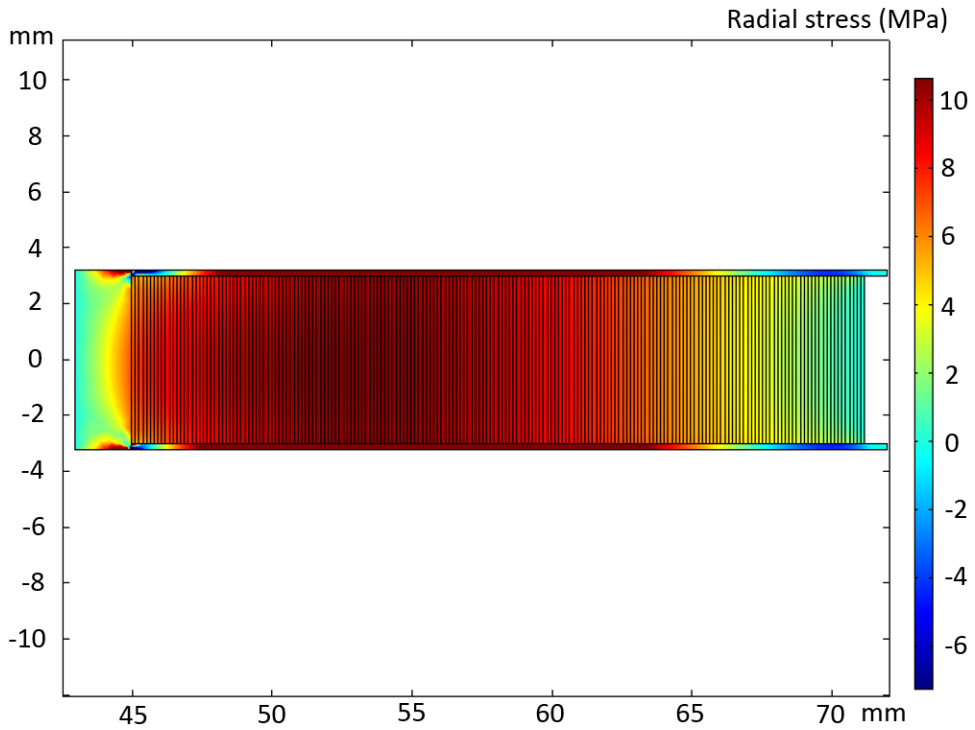

Fig. 140. Modeling the radial stress on this fully impregnated pancake under 9 T background and up to 370 A.

This radial tensile stress value of 10 MPa would likely have degraded the coil [86]. We can observe in Fig. 141 a statistical approach showing that for two different generations of conductors (one old and one new) the local degradation by delamination is unavoidable as soon as a radial tensile stress is applied. The probability of coil degradation increases as the maximum stress increases.

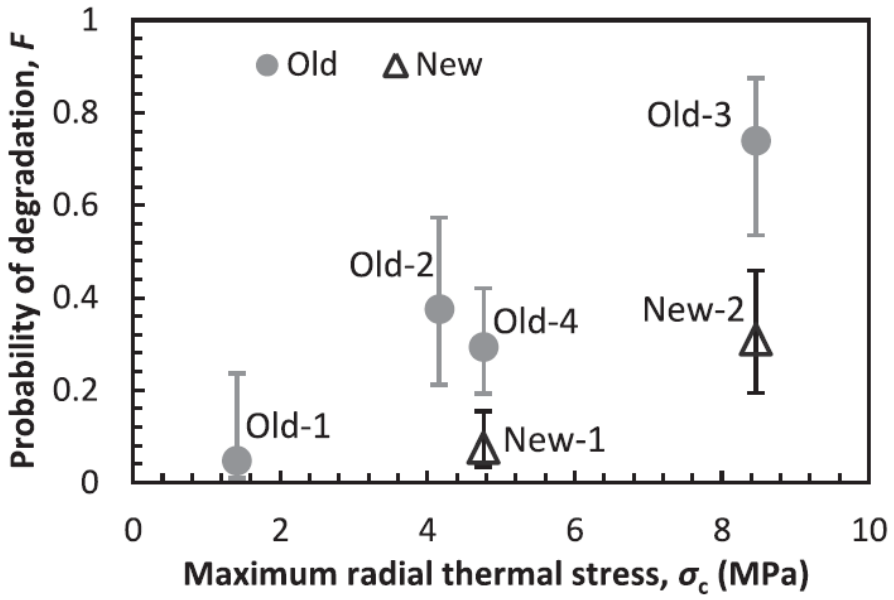

Fig. 141. Degradation probability F versus the calculated maximal thermal stress in the coil [86].

The calculations in BJR and Wilson are only valid for a homogeneous structure. Our case is more complex and requires FEM modeling. A multi-contact FEM modeling would be appropriate but is complex. To simplify the model, we use elastic interfaces. Fig. 142 summarize the stress distribution along the winding radius for: BJR equation, Wilson formula, and the most realistic case where FEM modelling was used to calculate the applied Lorentz forces and evaluate the stress in the actual pancake structure, including the tape edge bonding to the FRP flanges.

In order to model the mechanical behavior of this edge-impregnated pancake, the interface between each turn is represented by an elastic interface with a very low young's modulus (1 MPa) to represent a behavior of unglued turns. The epoxy between the conductor and the FRP flanges is represented by an elastic interface with a young modulus of 10 GPa. These interfaces can be seen in Fig. 133 in white and blue (white between turns and blue for the epoxy). Each turn is represented independently in this modeling. However, since the conductor contains 30 µm of soft polyimide insulation, a coefficient 130/100 corresponding to the ratio between the total conductor thickness and the conductor thickness useful for the winding mechanical support (copper + hastelloy layers), is used for the calculation of the hoop stress and the conductor strain.

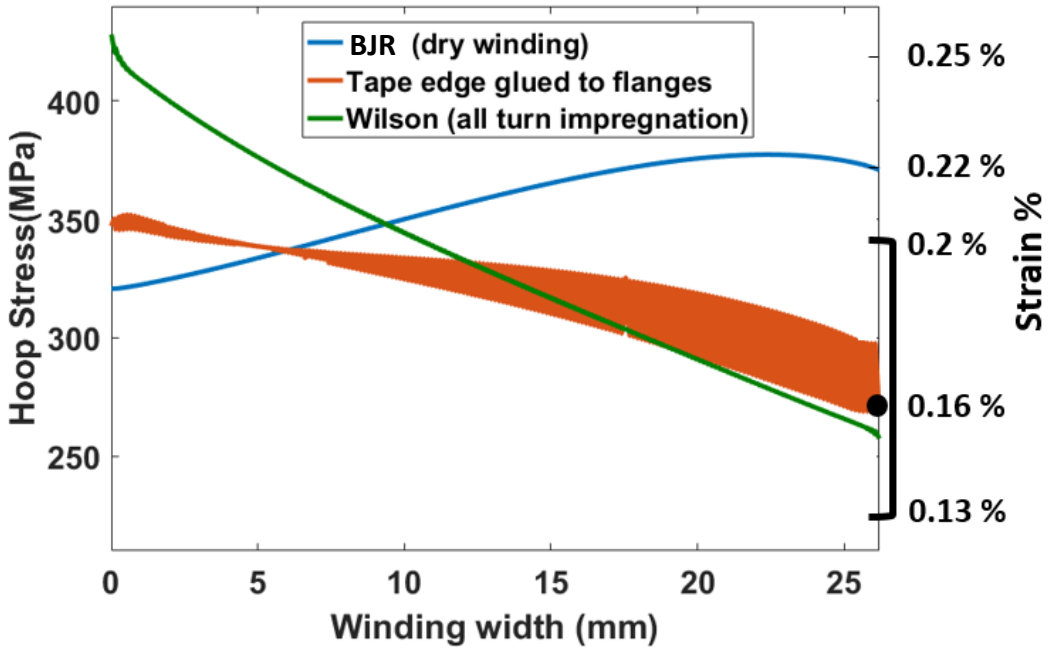

Fig. 142. Stress distribution along the pancake winding radius under 9 T background and up to 370 A. Black dot and bracket represent the mean value and spread of measured stress based on strain measurement at the outer turn.

The mean value of estimated hoop stress is in good agreement with the model of tape glued to flanges or with the full impregnation hypothesis. However, as said above, the hypothesis of turns stuck together is excluded because the radial stress is too high and would have damaged the pancake. We can also see that this edge-impregnated pancake structure also has the advantage of reducing the maximum hoop stress since it reaches 350 MPa at the inner turn against 425 MPa with a fully impregnated pancake. Fig. 143 shows the modeling of the conductor strain percentage as a function of the winding width. On the outer turn we find the 0.156 % conductor strain as the value measured in the experiment. The strain reaches 0.195 % at the inner turn due to the higher stress.

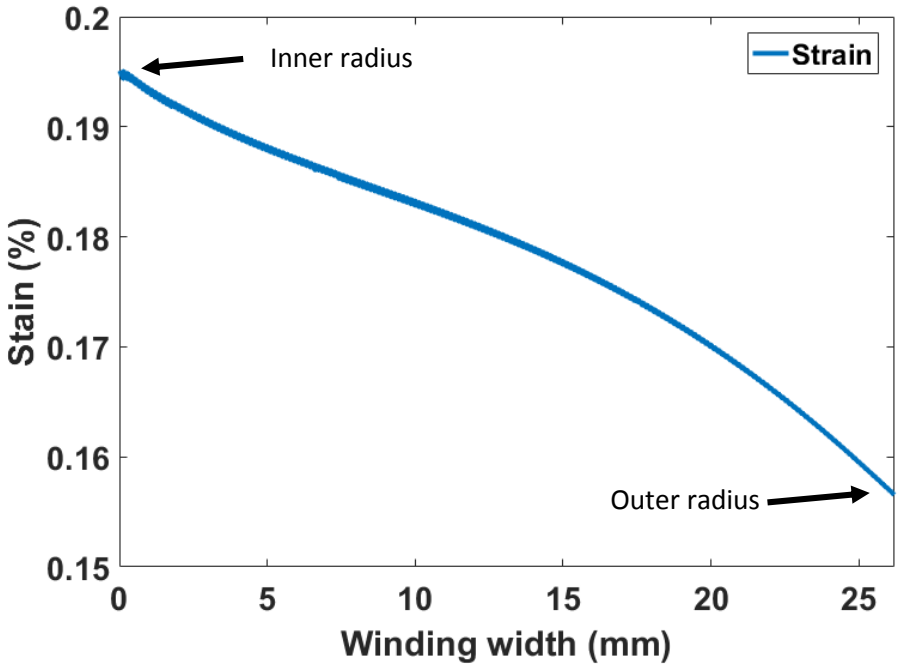

Fig. 143. Conductor strain across the winding under 9 T background and up to 370 A (computed with Comsol).

In our case, the radial stress is transferred in the FRP flanges as shown in Fig. 144 and 145. No radial stress is located inside the winding. The radial stiffness is defined by the thickness of the flanges since the turns are glued on. We see that their thickness can be very low with fiberglass, here 0.2 mm.

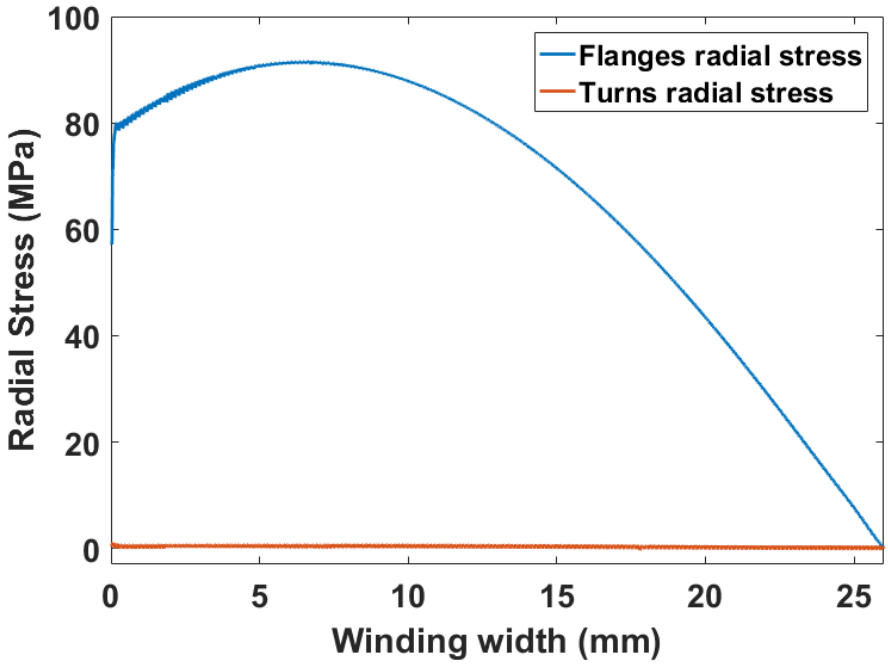

Fig. 144. The radial stress in the flanges and in the winding as a function of the winding width under 9 T background and up to 370 A.

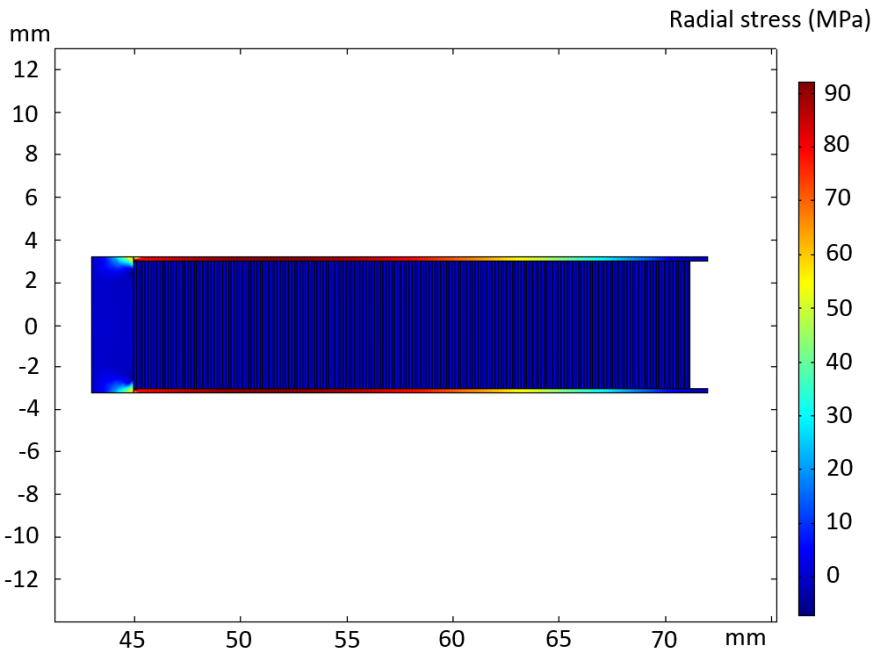

Fig. 145. Modeling the radial stress on the pancake impregnated by the edges under 9 T background and up to 370 A.

IV.2.4 Conclusion

Although the maximum stress achieved with this coil is moderate (about 350 MPa), this first result demonstrates that the proposed simplified coil cooling concept using edge-impregnated pancake structure can avoid coil degradation due to thermal stress. We find similar behavior to the more complex turn-by-turn separate impregnation concept used previously, as recently reported in [85]. Moreover, from a mechanical point of view, we find a behavior between BJR and Wilson, in other words a "soft" Wilson. This suggests that thin FRP plates bonded to the edges can help prevent coil deformation even with a soft polyimide insulation layer. In this way, the hoop stress is distributed more evenly across the winding, which is more desirable to take full advantage of the electromagnetic performance of the conductor.

IV.3 High performance impregnated pancake design

In order to obtain insulated REBCO windings with high current densities and high mechanical stresses, a new pancake design was developed.

The pancake structure with impregnated edges made it possible to dispense with a complex co-winding using thin polyimide tape with fluorine non-stick coating. In addition to the complexity of the winding, we have seen previously that this soft polyimide insulation layer is not optimal from a mechanical point of view. To go further, we have therefore studied the design of an insulated winding impregnated by the edges without soft polyimide insulation. A hard insulator must be used to homogenize the thermal and mechanical properties of the conductor. Indeed, the stress distribution in a "solid" winding varies only when the material layers are highly anisotropic. In addition, within the framework of the collaboration with the HFLSM, two REBCO tapes co-wound in parallel are added.

This laboratory specifically studies the co-winding of REBCO tapes for their future high magnetic field inserts [84].

In this chapter, the design of a simple pancake with two-tape bundle conductor with a face-to-back configuration with conduction cooled capability is presented. This conductor design enables redistribution of current between the tapes in case of local critical current degradation of one tape and reduces the risk of thermal runaway occurrence [56]. It also makes it possible to increase the current density of the winding since the amount of turns and thus the amount of insulation layers is reduced.

Moreover, in order to reinforce and homogenize the winding, it will be co-wound by means of a mechanical reinforcement made of hastelloy on which a layer of MgO is coated as an electrical insulator. As these materials have similar thermal shrinkage coefficients, the radial thermal stresses are reduced. Combined with the impregnation technique previously studied, this co-winding will make it possible to homogenize the mechanical stresses inside the winding and to avoid stress concentrations. In addition, co-winding may be used for sensitive quench detector.

IV.3.1 Pancake structure and characteristics

The pancake will be made with REBCO Fujikura FESC tapes with artificial pinning center. They are 4 mm wide and 0.15 mm thick. These tapes have a 50 µm hastelloy substrate and are surrounded by 2x40 µm thick copper stabilizer. The copper thickness reduces the hot spot temperature and reduces the risk of local degradation. Indeed, the delamination strength of REBCO tapes varies greatly depending on the stabilizer thickness, the conductor composition and the manufacturing process [83] To form the conductor, two of these tapes will be co-wound in a face-to-back configuration without insulation between them so that current sharing is provided in case of local degradation. The two conductors are soldered to the copper connections at the inner and outer diameter of the pancake. The electrical insulation will be provided by co-winding a 4 mm wide and 50 µm thick hastelloy tape on which a 5 µm insulating layer of MgO is coated (THEVA substrate). The inner and outer diameters of the pancake are respectively 163.2 mm and 267.3 mm for 148 turns. The outer/inner ratio is 1.64. As before, the winding will first be done dry. Once this is completed, two 0.2 mm thick FRP flanges will be glued by means of HexbondTM 609 adhesive films on each side of the pancake to make the thermal link between the turns, improve the rigidity of the coil and reduce the radial stress on the tapes. The stacking configuration of the tapes in the winding is shown in Fig. 146. Winding dimensions and properties are summarized in Tab. 10. The pancake CAD design is shown in Fig. 147.

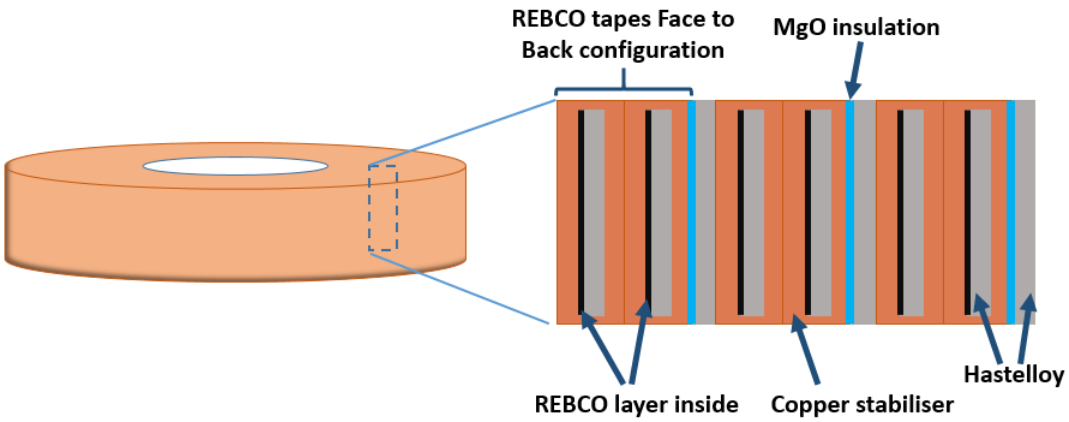

Fig. 146. The stacking arrangement of the tapes in the winding.

TABLE 10: PANCAKE DIMENSIONS

Tape dimension	4 mm wide / 150 µm thick
Substrate thickness	50 µm
Cu stabilizer thickness	2 x 40 µm
No. of bundled tapes	2 (face-to-back)
Tape reinforcement	50 µm (hastelloy)
MgO insulation thickness	5 µm
No. of turns	148
Inner diameter	163.2 mm
Outer diameter	267.3 mm
Outer/inner ratio	1.64
FRP flange thickness	0.2 mm

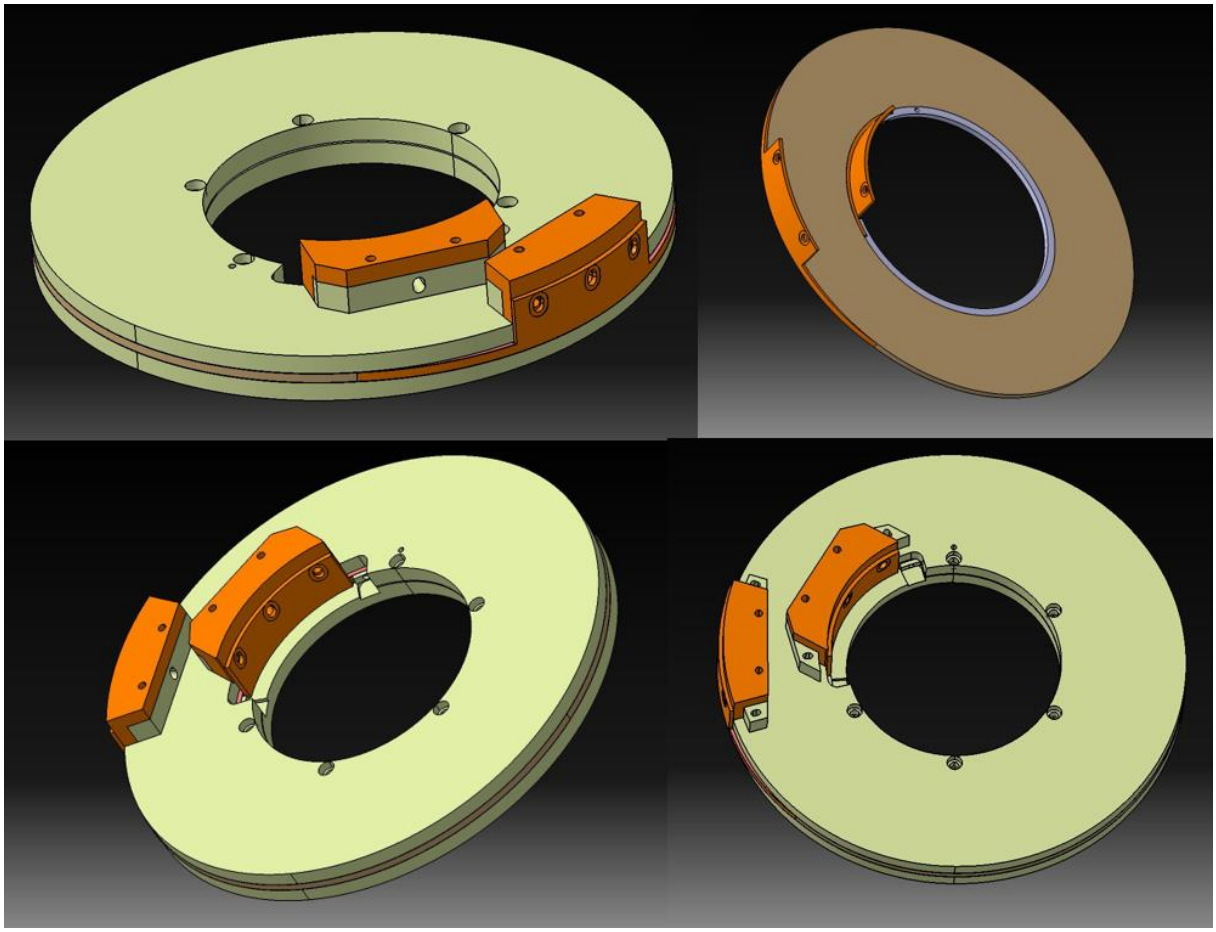

Fig. 147. Pancake CAD design.

IV.3.2 Pancake mechanical behavior modeling

The same modeling assumptions as for the previous pancake are taken. Except for the equivalent Young's modulus which is evaluated at 158 GPa taking into account the co-wound Hastelloy tape. As the winding has a hard insulator, no coefficient is applied in the calculation of the hoop stress and the strain.

In order to evaluate the maximum mechanical performance of the pancake, the limiting parameter for modeling is the conductor strain. For Fujikura FESC tapes with a 40 µm copper stabilizer the critical current drops off for a tensile strain greater than about 0.5% at 4.2 K (Fig. 148). We will therefore limit ourselves to 0.5% strain. Note that these curves do not take into account the mechanical fatigue of the tapes.

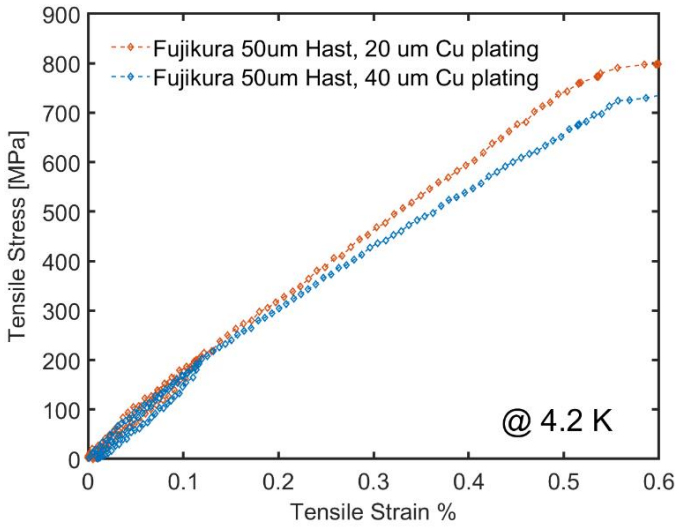

Fig. 148. Stress versus strain at 4.2 K of Fujikura conductors for 20 µm and 40 µm copper stabilizer [87].

In order to also estimate the pancake current margin, the critical current as a function of the magnetic field perpendicular to the Fujikura FESC tapes is plotted in Fig. 149 for different operating temperatures.

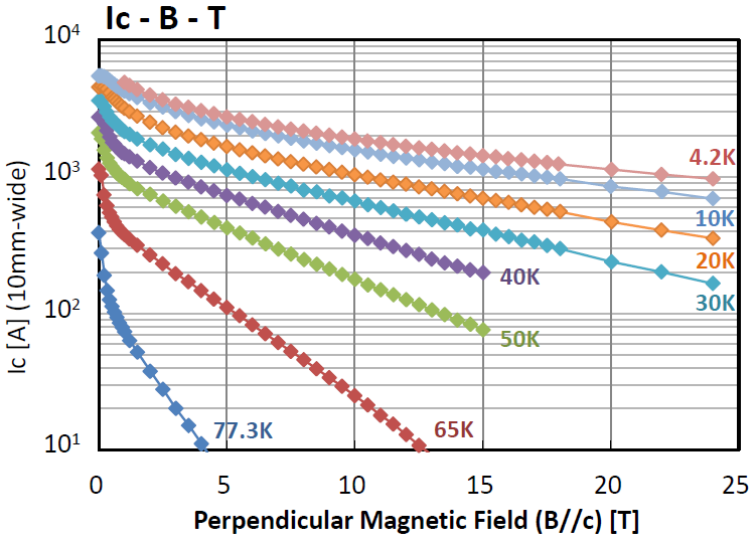

Fig. 149. The field dependence and angular dependence of I_c of the Fujikura FESC tapes [23].

IV.3.2.1 Modeling of mechanical behavior under 11 T

Meaningful test configuration can be obtained with background magnetic field of 11 T. To reach the 0.5 % strain level a current of 870 A should be injected in the coil. This corresponds to a current density of about 610 A/mm². Here on Fig. 150, the modeling of the 2D antisymmetric magnetic field map of the pancake for a current of 870 A. A magnetic field of 13.6 T is generated at the inner radius of the coil. The maximum transverse magnetic field inside the coil is relatively low and is 1.5 T. With operation at a temperature of 10 K the current margin is estimated to be 70 %.

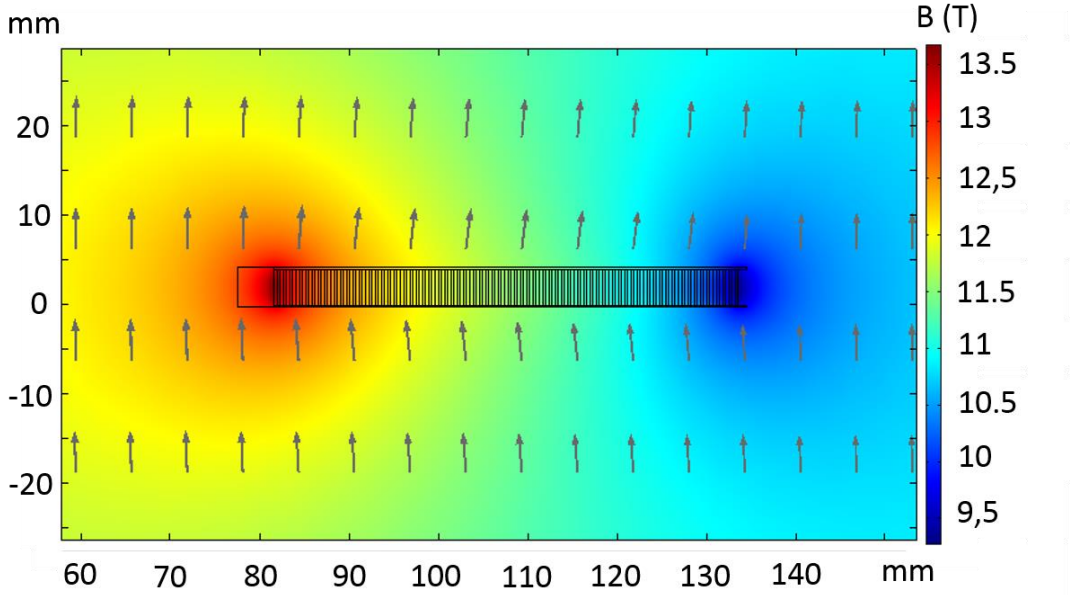

Fig. 150. 2D axisymmetric modeling of the magnetic field generated by the pancake at a current of 870 A under 11 T of magnetic background field.

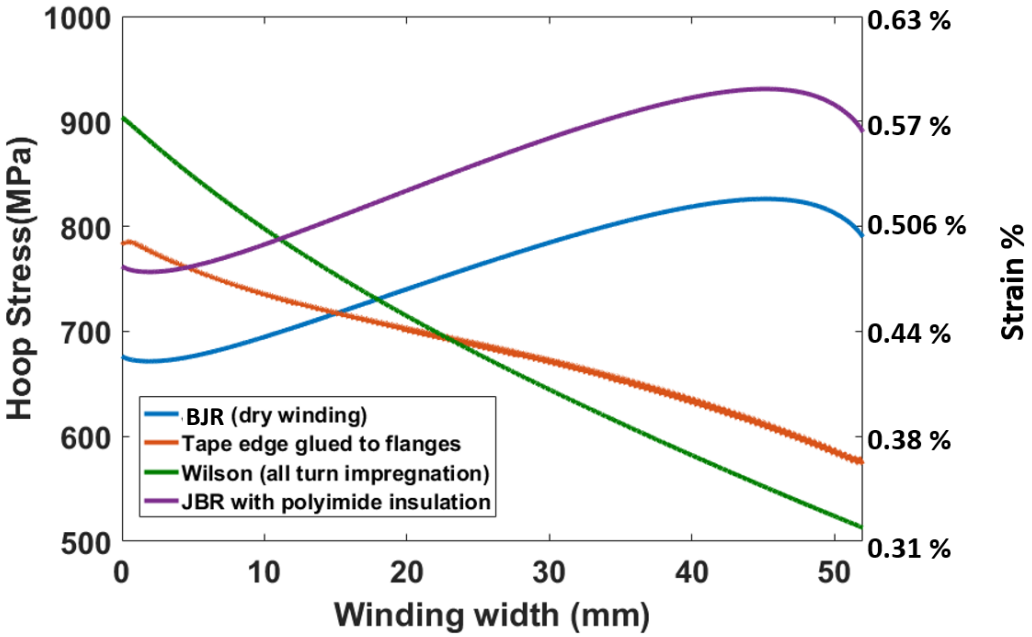

Fig. 151. Stress distribution along the pancake winding radius *in a background magnetic field of 11 T at a current of 870 A.*

Fig. 151 shows the mechanical stress distribution according to the different calculation assumptions. As before, we find an intermediate behavior between the BJR and the Wilson formula. The maximum hoop stress is located on the inner radius of the coil and reaches 785 MPa. Even if this hoop stress remains high, it is still lower than the maximum level reached by a mechanical behavior in BJR or Wilson. The hoop stress reaches 903 MPa for a Wilson behavior and 826 MPa for a BJR behavior. Note that at this current and magnetic field background value, a hoop stress of 930 MPa is reached for a non-impregnated winding with soft polyimide insulation. This corresponds to a strain of 0.59%. Fig. 152 shows the conductor strain as a function of the winding width for this test configuration.

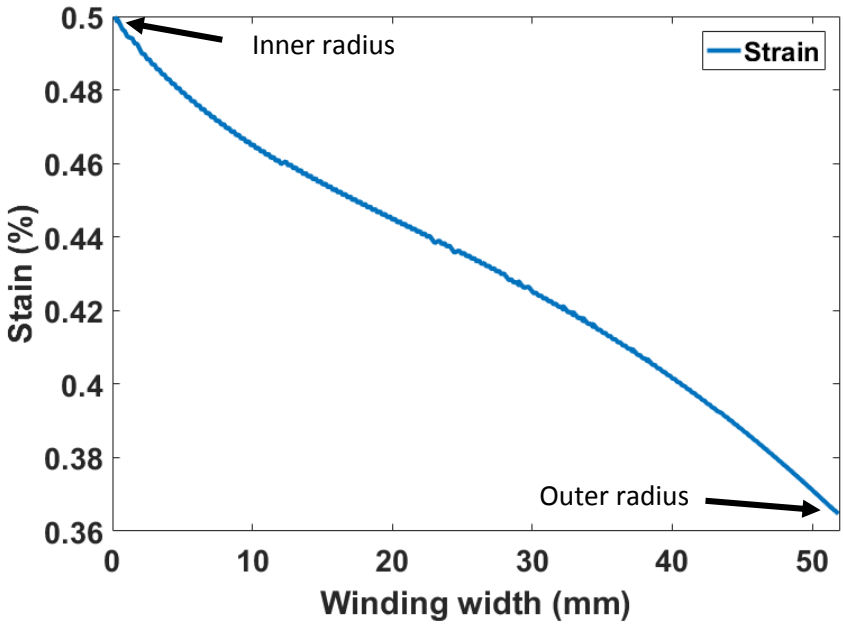

Fig. 152. Conductor strain across the winding for a current of 870 A in a background magnetic field of 11 T.

The thin FRP plates act slightly like a mechanical reinforcement. The radial stress is carried over into these plates and reaches about 350 MPa as shown in Fig. 153 and 154.

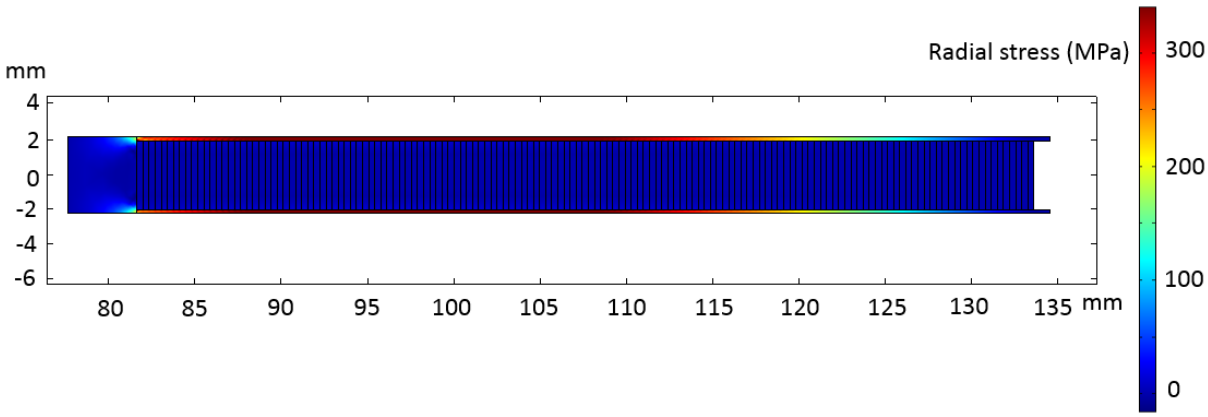

Fig. 153. Radial stress distribution in the pancake for a current of 870 A in a background magnetic field of 11 T.

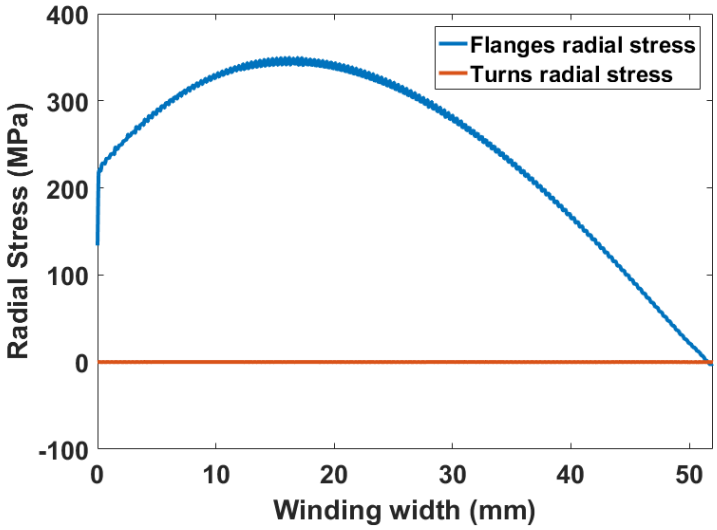

Fig. 154. Radial stress distribution between turns compare to radial stress in the FRP plates for a current of 870 A in a background magnetic field of 11 T.

The 350 MPa radial stress carried over in the FRP flanges is very high and is justifiably questionable. That said, the aggressive design of this high current density, high mechanical stress pancake is intentional. The design goal was to ensure that reaching the mechanical limit of the winding is possible with reasonable operating current so that reaching the mechanical limits during experiments is possible.

IV.3.2.2 Modeling of mechanical behavior under 5.5 T

Since the current leads of the HFLSM 12 T magnet test platform have a maximum current carrying capacity of 1500 A, another test configuration would approach this current. For this, a current of 1490 A would have to be injected into the coil in a background magnetic field of 5.5 T to reach the 0.5 % deformation. This corresponds to a very high current density of about 1050 A/mm². A magnetic field of 10 T is generated at the inner radius of the coil. The maximum transverse magnetic field inside the winding is 2.5 T. Still with an operation temperature of 10 K the current margin is estimated at 40 %. Fig. 155 shows the 2D antisymmetric magnetic field map modeling for this configuration.

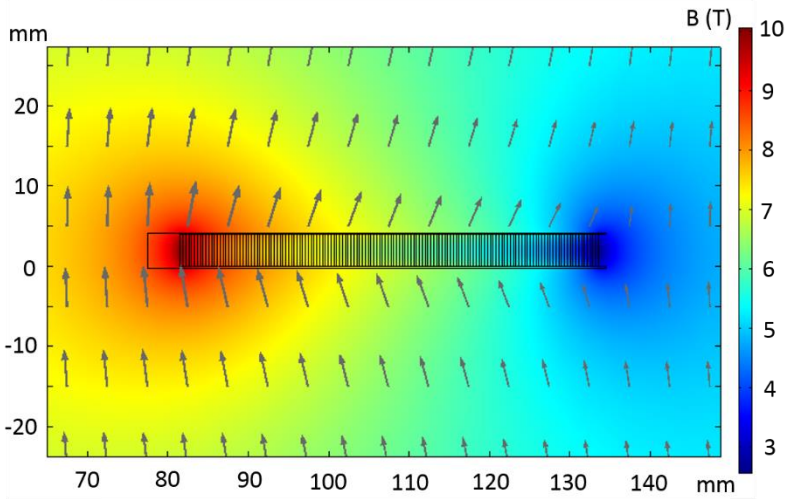

Fig. 155. 2D axisymmetric modeling of the magnetic field generated by the pancake at a current of 1490 A under 5.5 T of magnetic background field.

Fig. 156 shows the hoop stress distribution inside the winding for this test configuration. The maximum hoop stress achieved is 781 MPa compared to 831 MPa and 858 MPa for BJR and Wilson respectively. For a non-impregnated winding with a soft polyimide insulator the maximum hoop stress reaches 937 MPa which corresponds to an elongation of 0.59 %.

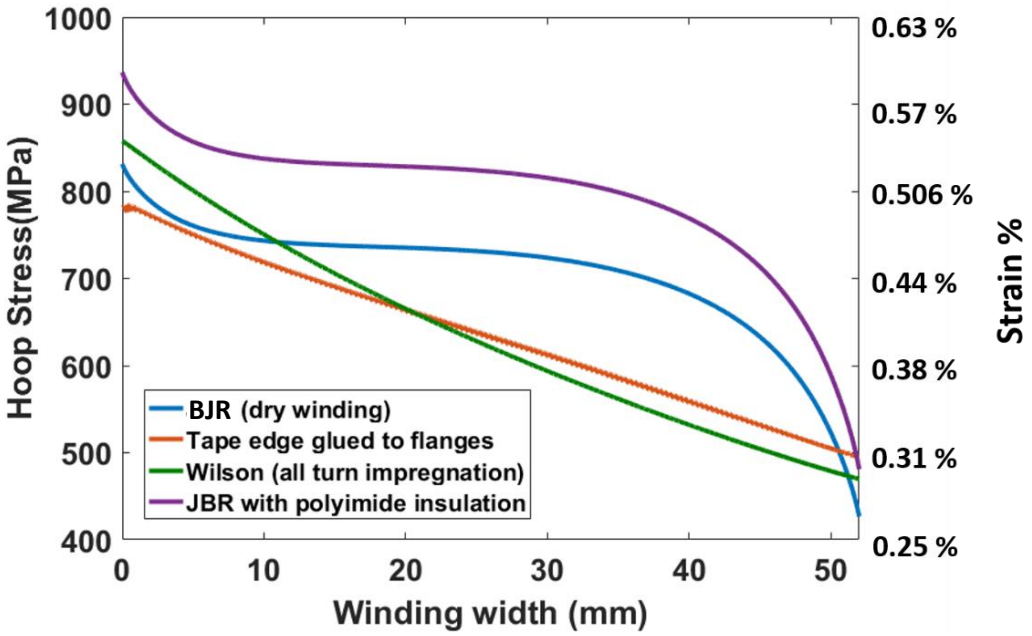

Fig. 156. Stress distribution along the pancake winding radius *in a background magnetic field of 5.5 T at 1490 A.*

Fig. 157 shows the conductor strain as a function of the winding.

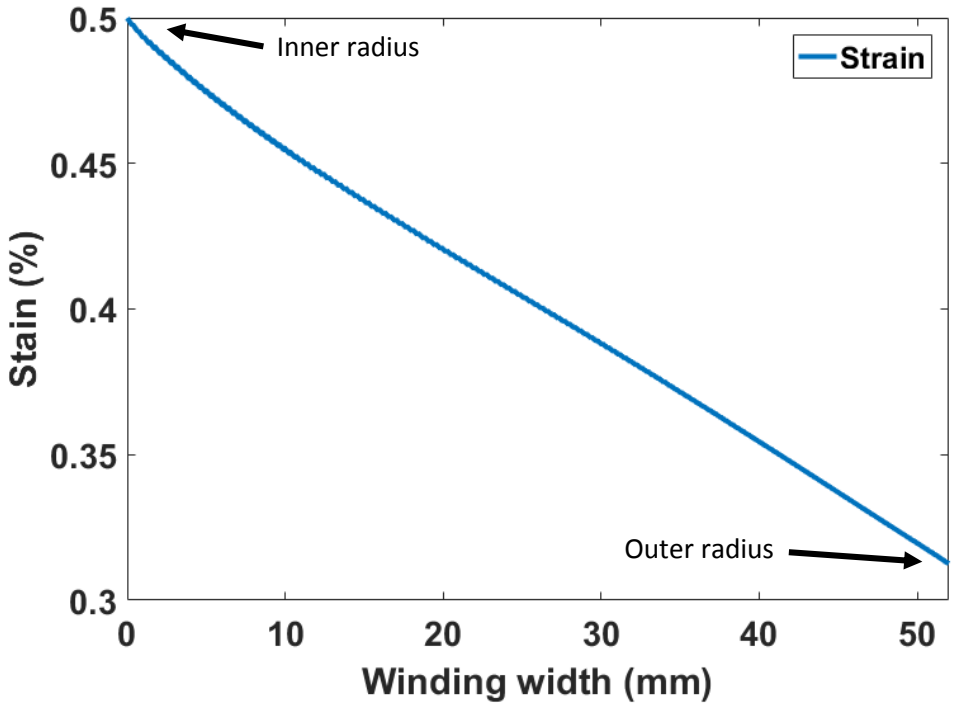

Fig. 157. Conductor strain across the winding for a current of 1490 A in a background magnetic field of 5.5 T.

Fig. 158 shows the radial stress on the FRP plates. The radial stress is still high and reaches 220 MPa.

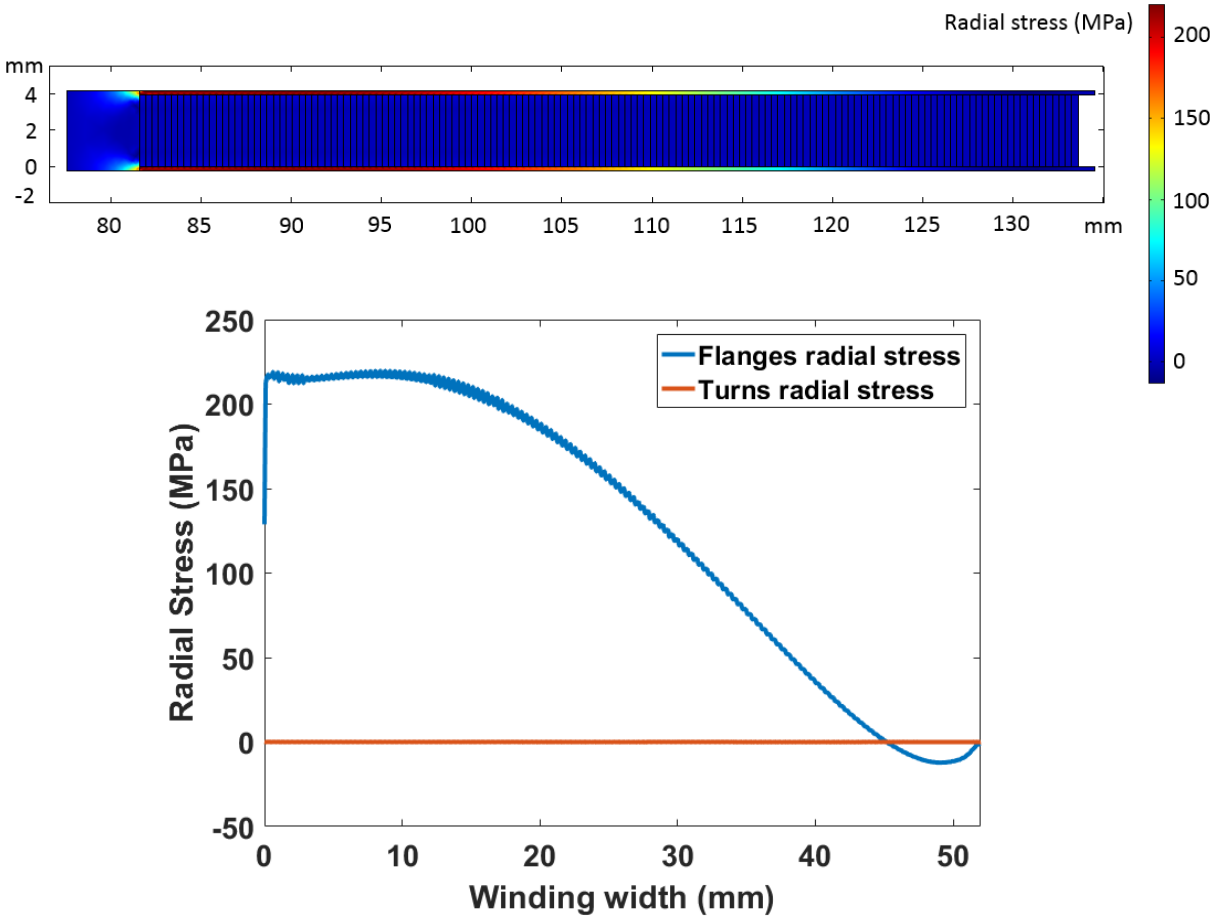

Fig. 158. Radial stress distribution in the pancake for a current of 1490 A in a background magnetic field of 5.5 T.

IV.4 Conclusion

A first preliminary study (using older generation tape) was conducted to test the behavior of a simplified pancake winding structure in terms of radial stress management and conduction cooling capability. This structure eliminates the need to separate the turns with a fluorine-coated polyimide tape to reduce the delamination stress of the REBCO windings. Instead, it uses film bonding to stick the flanges to the pancake, the viscosity of the film bonding preventing the glue to penetrate between the turns, hence the proposed name edge-impregnation. The conduction cooling capability was validated and tests in background field showed a mechanical behavior close to the one already obtained in the pancakes initially developed by HFLSM and Toshiba with a turn to turn separated impregnation. We obtained an intermediate behavior between fully impregnated and dry wound hypothesis without any delamination induced by radial stresses.

Within the framework of the collaborative project and in the light of these good results, the study and design of a high performance conduction cooled REBCO winding has been conducted. The two-tape bundle winding structure with a face-to-back configuration will be adopted to reduce the risk of thermal runaway due to critical conductor current drops or local winding degradation during winding. To obtain good mechanical performance and homogenized winding material properties, the

soft polyimide insulator is replaced by a 50 µm hastelloy tape on which a thin insulation layer of 5 µm of MgO is coated. The modeling results under 5.5 and 11 T make it possible to estimate a maximum hoop stress around 781 and 785 MPa for a maximum conductor strain equal to 0.5 % however at different current levels of 870 and 1490 A. The high performance of Fujikura REBCO tapes can operate at 5.5 and 11 T with extreme current densities such as 610 and 1050 A/mm² for the test configurations selected above. Such current densities still enable operation with large current margins of 40 and 70%.

The intermediate mechanical behavior between BJR and Wilson shows that thin FRP plates bonded to the edges can help prevent coil deformation. Modeling also showed that this winding structure without soft polyimide insulation was more favorable in terms of hoop stress than a dry non-impregnated winding. However, the high radial stresses of 350 and 220 MPa reported in the FRP flanges for the magnetic field configurations studied will need to be confirmed during tests.

Furthermore, as we discussed in chapter II, the co-wound MgO insulated hastelloy tape could also be used for protection purposes. This co-winding akin to a "perfectly" coupled pickup coil would provide even more sensitive hot spot detection. Experiments are expected soon.

General Conclusion

REBCO-coated conductors are extremely interesting for the generation of strong magnetic fields due to their very high current carrying capacity, even under strong magnetic field, as well as their outstanding mechanical properties. However, the implementation of REBCO HTS tapes still poses several technical challenges. Within the framework of the BOSSE project, this PhD thesis focused on improving our understanding on insulated REBCO windings behavior and finding credible solutions for the design of reliable high energy density insulated REBCO magnets. One of the issues with insulated REBCO magnets is their protection in the event of a hot spot. Reliable protection of insulated REBCO coils from thermal runaway is essential and can be achieved by very early detection of a dissipation regime. However, electromagnetic transients due to the variation of the current density across the width of the conductor influence the total coil voltage and make it difficult to detect a dissipative transition. The magnetization effects specific to superconducting materials are particularly visible on REBCO conductors whose width may be very large (12 mm).

A detailed experimental and numerical study of the transient electromagnetic behavior on a small insulated REBCO coil enabled a detailed understanding of the coil voltage and its transient. The validity of the electromagnetic model developed previously at G2Elab during the PhD of B. Rozier was confirmed. Using pickup coils with different magnetic coupling with the REBCO coil, in combination with numerical results, it was possible to discriminate and quantify the contributions of inductance variation and transient losses on the total coil voltage during magnet transients. The estimation of the dynamic variation of the coil inductance in particular is to our knowledge a first for REBCO magnets.

For practical purpose, we show that conventional pickup coils with partial coupling achieve high sensitivity of thermal runaway detection, provided that the threshold voltage is adjusted following the drift of the compensated voltage. We also established that pickup coil co-wound with the REBCO coil enable a voltage compensation with significantly reduced drift, making detection easier and improving the sensitivity.

This new understanding has been applied to the BOSSE project, and has led to a better apprehension of the testing and protection of the DPs. Before starting the realization of the 21 DPs composing the solenoid, a prototype DP was realized and successfully tested extensively in self-field and background field to validate the design of the solenoid. This important step enabled the launch of the DPs serial production. Each realized DP was then tested under the rated operating conditions of the SMES (4.2 K / 850 A) for quality control, and 17 out of 21 were validated. The successive tests of the DPs were very instructive from several points of view. First of all, the collected results gave a lot of information on the electromagnetic behavior of these DPs but also on their protection signal. But these tests have also highlighted the various difficulties involved in the manufacture of insulated REBCO coils. This leads us to improve the manufacturing process of the pancakes during the production run, and to draw some lessons for future realizations, in particular with regard to the realization of the inner contact. The inner connections between pancakes are a serious issue and will need to be studied further, to ensure reliability under mechanical stress and varying magnetic field, as well as low contact resistance.

Another important step was the development and validation of a detection/protection system for an assembly of several DPs. For this purpose, 2 preliminary assemblies of 3 and 5 DPs were tested using the same early detection approach but with two different monitoring philosophies: a global

monitoring of the 3 assembled DPs, and an individual monitoring of each DP for the 5 DPs assembly. The highest sensitivity was achieved by adopting individual protection of each DP in the 5 DP assembly test - in the 50 µV range compared to 200 µV for global protection -. This confirmed the initial protection approach that was chosen for the full solenoid assembly tests. However, before reaching the ambitious 20 kJ/kg winding goal, other DP assembly configurations will need to be tested. The first important goal will be to break the magnetic energy storage record of 13 kJ/kg and reach 14 kJ/kg.

Finally, based on the knowledge gained from these developments, a new high-performance REBCO coil design with conductive cooling capability is proposed, starting with the design and fabrication of a simplified partial impregnation insulated pancake with conductive cooling capability. This pancake consisted of a single REBCO conductor insulated with a polyimide coating and used the so-called edge impregnation concept: thin FRP flanges are glued to the pancake surfaces after their winding process, along with a cooling plate. In this way, the turn are not attached to each other but only to the flange, removing the risk of delamination. This pancake was successfully tested under a high background magnetic field in order to validate the edge impregnation process and to verify its mechanical performance.

Following this first promising result, we then presented the design of a larger high performance insulated REBCO pancake with conductive cooling capability for a high magnetic field insert. This pancake will consist of a single pancake with a two-tape bundled conductor, with a face-to-back configuration following the design previously proposed by HFLSM. This conductor design ensures current redistribution between the tapes in case of local degradation of the critical current of one tape and reduces the risk of thermal runaway. The insulation will be achieved by co-winding a Hastelloy® reinforcing tape with a layer of MgO deposited on top. This considerably improve the overall rigidity of the winding. Combined with the impregnation technique studied initially, this co-winding is expected to homogenize the mechanical stresses inside the winding and avoid stress concentrations. The possibility of using the reinforcement as a very sensitive quench detector will also be considered.

Perspective

The perspectives of this PhD work can be regrouped around 3 axes in the short, medium and long term.

- In the short term, work on the BOSSE project is continuing, and a lot of information can be obtained. Other configurations of "small" assemblies will be tested in order to progressively increase the mechanical constraints and the protection device will be developed. One of the important perspectives is to realize the automation of the protection system. An algorithm taking into account the electromagnetic behaviors studied in chapter II must be developed in order to obtain a reliable protection and to avoid triggering the protection system on false positives.

  The work presented in this PhD highlight the need to study in particular the inner contacts between the pancakes. It is important to identify the factors leading to possible degradations, through extensive experimental and numerical studies. Regarding the contact structure developed for BOSSE, induced currents in the solid copper contact pieces are suspected to cause abnormally high mechanical stresses and delamination of the conductor. Simpler and thinner internal contacts, without REBCO strips, are considered and will be tested soon on the prototype presented in chapter IV.

  Finally, systematic study of the magnetic field quality (linearity and stability) could be conducted to prepare for future projects with high field quality requirements.

- The detailed experimental and numerical study of the transient electromagnetic behavior has taught us a lot about the voltage variations that could be observed during the current transients. By evaluating the average critical current of the instrumented insulated REBCO coil, the model reproduces the evolution of the current density distribution inside the tape, which enables us to precisely predict the slope of the coil voltage. From there, it should be possible to evaluate the average performance of the REBCO lengths used in a coil (its limiting operating current) on the basis of the compensated voltage slope. It makes sense that qualitatively, in coils wound with REBCO lengths having a lower critical current in average, the current will penetrate more, causing a larger increase in inductance and generating more losses for a given operating current.

  This effect is well predicted using the transient electromagnetic model. However, experimental observation of that effect is not straightforward. Tests on BOSSE DPs do show differences in the compensated voltage slopes but no correlation between the slope magnitude and the average critical current of the REBCO tape lengths at 77 K self-field (I_c^{77K}) used for each DP could be established to date. This must be studied further: It could be due to the limited spread of average I_c^{77K} of the conductors used to wind the DPs, or to the fact that average I_c^{77K} is not predictive enough of the tape length performances at low temperature/high field.

  If it can be established without a doubt that the latter is true, that we cannot rely on the tape I_c^{77K} given by the suppliers to evaluate its practical performance, then this would have an important impact on tape requirements for future projects.

- The design of a high performance insulated REBCO winding presented in chapter IV is a good prospect for high magnetic field inserts. However, this concept remains to be validated in future experiments. Several points of interrogation remain regarding this innovative structure. First, regarding the high radial stresses carried in the thin FRP flanges and the possibility of shear stress on the tape edges glued to them. Then, regarding the thin MgO insulation layer and its dielectric strength and durability.

  Using the MgO-insulated hastelloy tape co-wound for protection purposes is an interesting prospect. Two of these tapes wound in a back-to-back configuration would be totally insulated from the REBCO winding. This way a similar configuration to that tested in chapter II would be obtained, with a pickup coil perfectly insulated from the REBCO tapes, which would definitely improve the detection sensitivity. These two co-wound hastelloy tapes would act as mechanical reinforcement, improving the overall mechanical performance of the winding by increasing the volume fraction of Hastelloy.

  Such reinforcement will in any case be necessary in future high field magnets to fully use the ever increasing current carrying capabilities of modern REBCO tapes.

  The possibility of using a single one-side MgO-insulated hastelloy tape as a sort of pick up coil can also be proposed. It is conceivable that such co-winding behaves, in certain conditions, as a pick-up coil despite the electrical contact with the REBCO tape on one side. The prototype presented in Chapter IV will be instrumented to test this idea.

- As mentioned in the previous point, modern REBCO tapes have such high current carrying capabilities that a lot of reinforcement is required to fully use their properties at low temperature. Another approach would be to take advantage of these performance to design very high field REBCO magnets with higher maximum operating temperature. For conduction-cooled magnets in particular it would reduce significantly the investment and the operating cost of the cryocooler. It would also enable rapid magnet charge and discharge, by tolerating higher AC losses thanks to the higher cooling power at higher temperature. This would also contribute to solve the problem of magnetic field relaxation due to the progressive current penetration in the width of the conductor. Indeed, the heating of the winding during its charge would bring a deeper current penetration in the conductor width by lowering its critical current. Then once a current plateau is reached and the AC losses disappear, the winding would cool down, the critical current of the magnet would increase again, causing the current penetration to stabilize, similarly to the current overshoot concept.

References

[1] Weijers H W et al. 2016 Progress in the development and construction of a 32-T superconducting magnet IEEE Trans. Appl. Supercond. 26 1–7

[2] Awaji S et al. 2017 First performance test of a 25 T cryogen-free superconducting magnet Supercond. Sci. Technol. 30 065001

[3] Yoon S, Kim J, Cheon K, Lee H, Hahn S and Moon S-H 2016 26 T 35 mm all-GdBa2Cu3O7–x multi-width no-insulation superconducting magnet Supercond. Sci. Technol. 29 04LT04

[4] Hahn S, Park D K, Bascunan J and Iwasa Y 2011 HTS pancake coils without turn-to-turn insulation IEEE Trans. Appl. Supercond. 21 1592–5

[5] Lécrevisse T and Iwasa Y 2016 A (RE)BCO pancake winding with metal-as-insulation IEEE Trans. Appl. Supercond. 26 1–5

[6] Philippe Fazilleau and al 2018 Metal-as-insulation sub-scale prototype tests under a high background magnetic field, Supercond. Sci. Technol. 31 095003

[7] H. K. Onnes, Further experiments with liquid helium, Communication from the physical laboratory of the University of Leiden, (1911)

[8] P. Jensen Ray, "Structural investigation of La2-xSrxCuO4+y: Following staging as function of temperature," University of Copenhagen, 2015

[9] R.G. Sharma 2015 Superconductivity Basics and Applications to Magnets

[10] D. Larbalestier, J. Jiang, U. Trociewitz, F. Kametani, C. Scheuerlein, M. Dalban-Canassy, M. Matras, P. Chen, N. Craig, P. Lee, and E. Hellstrom. Isotropic Round-Wire Multi_lament Cuprate Superconductor for Generation of Magnetic Fields Above 30 T. Nature Materials, 13(4):375{381, 2014

[11] A. A. Abrikosov, The magnetic properties of superconducting alloys (1957)

[12] P.Tixador, Les Supraconducteurs, Edition Hermes Paris, 39, (1995)

[13] "NHMFL." [Online]. Available: https://nationalmaglab.org/magnet-development/applied-superconductivity-center/plots

[14] J. Bednorz and K. Muller. Possible high-Tc superconductivity in the Ba-La-Cu-O system. Zeitschrift fur physik b-condensed matter, 64(2):189{193, 1986

[15] H. Maeda, Y. Tanaka, M. Fukutomi, and T. Asano. A new High-Tc Oxide Superconductor Without a Rare-Earth Element. Japanese Journal of Applied Physics Part 2-Letters, 27(2): L209{L210, 1988

[16] A. I. Golovashkin; et al. (1991). "Low temperature direct measurements of Hc2 in HTSC using megagauss magnetic fields". Physica C: Superconductivity. 185–189: 1859–1860

[17] Brown M et al 2017 Tensile properties and critical current strain limits of reinforced Bi-2212 conductors for high field magnets IOP Conf. Ser.: Mater. Sci. Eng. 279 012022

[18] M. Turenne, R. P. Johnson, S. Kahn, F. Hunte, L. Ye, and J. Schwartz, Characterization of REBOC coated conductors for high field magnets, in 1 st International Particle Accelerator Conference, IPAC 2010, p. 400-402

[19] SuperPower, "2G HTS wire."

[20] Pascal TIXADOR, Yves BRUNET. Superconductors - Environment and applications. Engineering techniques. Grenoble Electrical Engineering Laboratory - LEG, and the Very Low Temperature Research Center - CRTBT. May 2004. Grenoble, France. 18 pages

[21] SuperOx, "Recent advances in SuperOx 2G HTS wire manufacturing facilities,performance and customisation", ASC 2020

[22] Carmine Senatore, Matteo Alessandrini, Andrea Lucarelli, Riccardo Tediosi, Davide Uglietti and Yukikazu Iwasa, "Progresses and challenges in the development of high-field solenoidal magnets based on RE123 coated conductors", 2014 Supercond. Sci. Technol. 27 103001

[23] Fujikura, 2019 "Recent progress of 2G HTS wires and coils at Fujikura"

[24] Braccini V et al 2011 Properties of recent IBAD–MOCVD coated conductors relevant to their high field, low temperature magnet use Supercond. Sci. Technol. 24 035001

[25] Tsuchiya K et al 2017 Critical current measurement of commercial REBCO conductors at 4.2 K Cryogenics 85 1–7

[26] Y. Yanagisawa, H. Nakagome, D. Uglietti, T. Kiyoshi, R. Hu, T. Takematsu, T. Takao, M. Takahashi, and H. Maeda, "Effect of YBCOcoil shape on the screening current-induced magnetic field intensity," IEEE Trans. Appl. Supercond., vol. 20, no. 3, pp. 744–747, Jun. 2010

[27] Y. Yanagisawa, Y. Kominato, S. Matsumoto, K. Zaitsu, T. Hase, T. Miyazaki, M. Hamada, M. Hosono, and H. Maeda, "Magnitude of the screening field for YBCO coils," IEEE Trans. Appl. Supercond., vol. 21, no. 3, pp. 1640–1643, Jun. 2011

[28] Maeda H and Yanagisawa Y 2013 Recent developments in high-temperature superconducting magnet technology (review) IEEE Trans. Appl. Supercond 24 4602412

[29] Naoyuki Amemiya, Yusuke Sogabe, Satoshi Yamano and Hisaki Sakamoto, "Shielding current in a copper-plated multifilament coated conductor wound into a single pancake coil and exposed to a normal magnetic field", 2019 Supercond. Sci. Technol. 32 115008

[30] Wang Y et al. 2007 Detecting and describing the inhomogeneity of critical current in practical long HTS tapes using contact-free method Cryogenics 47 225–31

[31] Higashikawa K et al. 2017 Characterization of critical current distribution in Roebel cable strands based on reel-to-reel scanning hall-probe microscopy IEEE Trans. Appl. Supercond. 27 1–4

[32] Barth C et al 2015 Electro-mechanical properties of REBCO coated conductors from various industrial manufacturers at 77 K, self-field and 4.2 K, 19 T Supercond. Sci. Technol. 28 045011

[33] Chiesa L et al 2014 Electromechanical investigation of 2G HTS twisted stacked-tape cable conductors IEEE Trans. Appl. Supercond. 24 6600405

[34] MBARUKU, ABDALLAH L ; SCHWARTZ, JUSTIN: Fatigue behavior of Y‐Ba‐Cu‐O/Hastelloy-C coated conductor at 77 K. In: IEEE Transactions on Applied Superconductivity Bd. 18 (2008), Nr. 3, S. 1743‐1752

[35] Ilin K et al 2015 Experiments and FE modeling of stress–strain state in ReBCO tape under tensile, torsional and transverse load Supercond. Sci. Technol. 28 055006

[36] FLEITER, JEROME: Étude de l'implementation de supraconducteur a haute temperature critique dans les aimants d'accelerateur, Universite de Grenoble, PhD Thesis, 2013

[37] Markiewicz W D and Swenson C A 2010 Winding strain analysis for YBCO coated conductors Supercond. Sci. Technol. 23 045017

[38] Persistent current joints between technological superconductors, G D Brittles, T Mousavi, C R M Grovenor, C Aksoy and S C Speller, Published 11 August 2015 Supercond. Sci. Technol. 28 093001

[39] Jun Lu, Yan Xin, Brent Jarvis and Hongyu Bai 2021 Oxygen out-diffusion in REBCO coated conductor due to heating Supercond. Sci. Technol. 34 075004

[40] Jérôme Fleiter and Amalia Ballarino 2017 In-Field Electrical Resistance at 4.2 K of REBCO Splices IEEE Trans. Appl. Supercond. Vol. 27. 6603305

[41] Laser drilling: enhancing superconducting joint of GdBa2Cu3O7 – Δ coated conductors, Y J Park, M W Lee, Y K Oh and H G Lee, Published 2 July 2014, Supercond. Sci. Technol. 27 085008

[42] Ki Sung Chang, Hyun Chul Jo, Young Jae Kim, Min CheolAhn, and Tae Kuk Ko 2011 An Experimental Study on the Joint Methods Between Double Pancake Coils Using YBCO Coated Conductors IEEE Trans. Appl. Supercond. Vol 21. 3005

[43] WILSON, MARTIN N: SUPERCONDUCTING MAGNETS (1983)

[44] ARP, V: STRESSES IN SUPERCONDUCTING SOLENOIDS. IN: JOURNAL OF APPLIED PHYSICS BD. 48 (1977), NR. 5, S. 2026–2036

[45] Tara BENKEL, "Contribution to the design and realization of a high temperature superconductor insert superconducting insert for obtaining an intense magnetic field.", PhD, University of Grenoble Alpes, 18 Feb 2018

[46] Blandine ROZIER, "Contribution to electromagnetic and thermal modelling of High Temperature Superconducting REBCO coils for protection purpose", PhD, University of Grenoble Alpes, 24 octobre 2019

[47] Arnaud Badel et al, Modeling of 'quench' or the occurrence and propagation of dissipative zones in REBCO high temperature superconducting coils, 2019 Supercond. Sci. Technol. 32 094001

[48] Y. Iwasa, Case Studies in Superconducting Magnets : Design and Operational Issues Second Edition, Springer (2009)

[49] F Scurti, S Ishmael, G Flanagan and J Schwartz Quench detection for high temperature superconductor magnets: a novel technique based on Rayleigh-backscattering interrogated optical fibers Supercond. Sci. Technol. 29 03LT01

[50] Shin Hasegawa, Satoshi Ito, Gen Nishijima, and Hidetoshi Hashizume 2019 Fundamental Evaluations of Applicability of LTS Quench Detectors to REBCO Pancake Coil IEEE Trans. Appl. Supercond. Vol. 29. 9001305

[51] Marchevsky M, Xie Y Y and Selvamanickam V 2010 Quench detection method for 2G HTS wire Supercond. Sci. Technol. 23 034016

[52] H. W. Weijers et al., "Progress in the Development and Construction of a 32-T Superconducting Magnet," in IEEE Transactions on Applied Superconductivity, vol. 26, no. 4, pp. 1-7, June 2016, Art no. 4300807, doi: 10.1109/TASC.2016.2517022

[53] Christian Lacroix, Yannick Lapierre, Jonathan Coulombe and Frederic Sirois 2014 High normal zone propagation velocity in second generation high-temperature superconductor coated conductors with a current flow diverter architecture Supercond. Sci. Technol. 27 055013

[54] C. Lacroix, J.-H. Fournier-Lupien, K. McMeekin, and F. Sirois, "Normal zone propagation velocity in 2G HTS coated conductor with high interfacial resistance," IEEE Trans. Appl. Supercond., vol. 23, no. 3, p. 4701605, Jun. 2013

[55] Y. Yanagisawa, T. Fukuda, K. Sato, H. Nakagome, T. Takao, H. Kamibayashi, M. Takahashi, and H. Maeda, "Use of a thermal grid to increase thermal runaway current for REBCO pancake coils operated at 77 K," IEEE Trans. Appl. Supercond., vol. 23, no. 3, p. 4603505, Jun. 2013

[56] S. Awaji et al., Robust REBCO Insert Coil for Upgrade of 25 T Cryogen-Free Superconducting Magnet, IEEE Trans. on Appl. Supercond., 31(5), Art no. 4300105, 2021

[57] S. Hahn, D. K. Park, J. Bascnan, and Y. Iwasa, "HTS pancake coils without turn-to-turn insulation," IEEE Trans. Appl. Supercond., vol. 21, no. 3, pp. 1592–1595, Jun. 2010

[58] Hahn S, Park D, Voccio J, Bascunan J and Iwasa Y 2012 Noinsulation (NI) HTS inserts for >1 GHz LTS/HTS NMR magnets IEEE Trans. Appl. Supercond. 22 4302405

[59] T. Sung Lee et al., "The effects of co-wound Kapton, stainless steel and copper, in comparison with no insulation, on the time constant and stability of GdBCO pancake coils," Supercond. Sci. Technol., vol. 27, 2014

[60] Jeremie CICERON, "High energy density Superconducting Magnetic Energy Storage with second generation high temperature superconductors", PhD, University of Grenoble Alpes, 20 march 2019

[61] Rozier Blandine, Badel Arnaud, Ramdane Brahim and Meunier Gérard, "Calculation of the local current density in high-temperature superconducting insulated rare earth–barium–copper oxide coils using a volume integral formulation and its contribution to coil protection", Supercond. Sci. Technol. vol 32. 2019

[62] Arnaud Badel;Blandine Rozier;Kohki Takahashi;Satoshi Awaji, "Simulation of Local Dissipation Phenomena in the REBCO Insert of the 25-T CSM Magnet: Understanding and Preventing Destructive Thermal Runaway" ," IEEE TRANS. APPL. SUPERCOND., VOL. 29, 2019

[63] A. Badel et al., "Detection and Protection Against Quench/Local Thermal Runaway for a 30 T Cryogen-Free Magnet," in IEEE Transactions on Applied Superconductivity, vol. 31, no. 5, pp. 1-5, Aug. 2021, Art no. 4700705

[64] Vialle J, Badel A, Tixador P, Ciceron J, Forest F and Pasquet R 2021 Preliminary tests of pancakes from a 12 T REBCO insulated solenoid magnet IEEE Trans. Appl. Supercond. 31 4600805

[65] Ciceron J, Badel A, Tixador P, Pasquet R and Forest F 2018 Test in strong background field of a modular element of a REBCO 1 MJ high energy density SMES IEEE Trans. Appl. Supercond. 28 5701005

[66] Ariyama T, Takagi T, Nakayama D, Sasaki E, Takao T, Tsukamoto O and Matsuoka T 2016 Quench protection of YBCO coils: co-winding detection method and limits to hot-spot temperature IEEE Trans. Appl. Supercond. 26 4702205

[67] Martovetsky N N and Chaplin M R 1997 Detection of the normal zone with cowound sensors in cable-in conduit conductors IEEE Trans. Appl. Supercond. 7 451–4

[68] G2Elab 2018 MIPSE: Modeling of Interconnected Power SystEms https://g2elab.grenoble-inp.fr/en/platforms/mipse-modeling-of-interconnected-power-systems-1 (accessed 2 august 2021)

[69] Ruehli A E 1974 Equivalent circuit models for three-dimensional multiconductor systems IEEE Trans. Microw. Theory Tech. 22 216–21

[70] Wang T et al 2015 Analyses of transient behaviors of no-insulation REBCO pancake coils during sudden discharging and overcurrent IEEE Trans. Appl. Supercond. 25 4603409

[71] Benkel T, Miyoshi Y, Escamez G, Gonzales D, Chaud X, Badel A and Tixador P 2016 REBCO performance at high field with low incident angle and preliminary tests for a 10-T insert IEEE Trans. Appl. Supercond. 26 4302705

[72] Dilasser G, Fazilleau P and Tixador P 2017 Experimental measurement and numerical simulation of the screening current-induced field decay in a small ReBCO coil IEEE Trans. Appl. Supercond. 27 4900104

[73] Lu J et al 2012 Insulation of coated conductors for high field magnet applications IEEE Trans. Appl. Supercond. 22 7700304

[74] A. Badel, P. Tixador, M. Amiet and V. Brommer, "SMES to Supply an Electromagnetic Launcher," in IEEE Transactions on Applied Superconductivity, vol. 22, no. 3, pp. 5700204-5700204, June 2012, Art no. 5700204, doi: 10.1109/TASC.2011.2174549

[75] P.Tixador, Superconducting Magnetic Energy Storage: Status and Perspective, IEEE/CSC & ESAS EUROPEAN SUPERCONDUCTIVITY NEWS FORUM, No. 3, January 2008

[76] A. Badel, P. Tixador and P. Dedie, "Test of a Twin Coil HTS SMES for High Power Pulse Operation," in IEEE Transactions on Applied Superconductivity, vol. 21, no. 3, pp. 1375-1378, June 2011, doi: 10.1109/TASC.2010.2090321

[77] Yamamoto, A ; Makida, Y ; Yamaoka, H ; Ohmiya, H ; Tanaka, K ; Haruyama, T ; Yoshida, T ; Yoshimura, K ; U. A.: “A thin superconducting solenoid magnet for particle astrophysics”, IEEE Trans. Appl. Supercond. Bd. 12(2002), Nr. 1, S. 438–442

[78] Sviatoslavsky, I. N., & Young, W. C. (1980). Structural design features for commercial fusion power reactor magnet systems. Nuclear Engineering and Design, 58(2), 207-218

[79] Hassenzahl, W. (1989). A comparison of the conductor requirements for energy storage devices made with ideal coil geometries Magnetics, IEEE Transactions on, 25(2), 1799-1802

[80]"Nov. 2021. [Online]", [online] Available: https://www.sigmaphi.fr/

[81]F. C. Moon, "The virial theorem and scaling laws for superconducting magnet systems", J. Appl. Phys., vol. 53, no. 12, pp. 9112-9121, 1982

[82]Badel A, Rozier B, Ramdane B, Meunier G and Tixador P 2019 Modeling of 'quench' or the occurrence and propagation of dissipative zones in REBCO high temperature superconducting coils Supercond. Sci. Technol. 32 094001

[83] H. Miyazaki et al., Delamination Strengths of Different Types of REBCO-Coated Conductors and Method for Reducing Radial Thermal Stresses of Impregnated REBCO Pancake Coils, IEEE Trans. on Appl. Supercond., 25(3), 6602305, 2015

[84] H. Miyazaki et al., Testing of Stacked Pancake Coils for a Cryogen-Free 25-T Superconducting Magnet, IEEE Trans. on Appl. Supercond., 26(4), Art no. 4302004, 2016

[85] K. Takahashi et al., Electromagnetic Characteristics Study of Two-Ply REBCO Tapes Pancake Coils, IEEE Trans. on Appl. Supercond., 31(5), Art no. 4602305, 2021

[86] S. Muto, S. Fujita, K. Akashi, T. Yoshida, Y. Iijima and K. Naoe, "Evaluation of Actual Delamination Strength of REBCO-Coated Conductors Based on the Weibull Analysis Considering Size Effect," in IEEE Transactions on Applied Superconductivity, vol. 28, no. 4, pp. 1-4, June 2018, Art no. 6601004, doi: 10.1109/TASC.2018.2805859

[87] S. Fujita, Mechanical Properties of BaHfO3-doped EuBCO Coated Conductors Fabricated by Hot-wall PLD on IBAD Template, Fujikura, Vancouver, Canada, MT 2019

Vers des aimants isolés en Terre-Rare-BaCuO à très haute densité énergétique

Les matériaux supraconducteurs REBCO HTS permettent d'envisager des bobines à très haute densité d'énergie, car ils combinent des densités de courant critiques élevées sous fort champ magnétique et une très grande résistance mécanique. Cependant, la mise en œuvre de ces matériaux reste difficile, car ils présentent des inhomogénéités de performance à l'échelle microscopique qui ont un impact potentiellement destructeur à l'échelle du dispositif. Dans cette thèse, des solutions crédibles pour des aimants REBCO isolés à haute densité d'énergie sont proposées. Ce travail a été mené dans le cadre du projet BOSSE, qui vise la réalisation d'un aimant REBCO de 12 T / 1 MJ utilisé comme SMES.
Une protection fiable des bobines REBCO isolées contre l'emballement thermique peut être obtenue par la détection précoce de conditions dissipatives locales. Cependant, les tensions transitoires observées pendant les variations de courant rendent la détection difficile. Ce comportement électromagnétique transitoire des bobines isolées REBCO a été étudié expérimentalement et numériquement sur une bobine de test fortement instrumentée, permettant une interprétation détaillée des tensions mesurées.
Cette nouvelle compréhension a été appliquée au projet BOSSE, en commençant par les tests du prototype Double Pancake (DP) en champ propre et champ externe, pour atteindre en toute sécurité le courant critique et valider la conception du solénoïde. Chacun des 21 DP de série du solénoïde BOSSE est ensuite testé dans de l'hélium liquide jusqu'à son courant nominal pour le contrôle de qualité. Enfin, 2 assemblages préliminaires de 3 et 5 DP ont été testés en utilisant la même approche de détection précoce et de protection, validant ainsi les stratégies de protection du dispositif à l'échelle réelle.
Sur la base des connaissances acquises grâce à ces nouveaux développements, une nouvelle conception de bobine REBCO haute performance avec une capacité de refroidissement par conduction est proposée.

Mots clés : *Aimant REBCO isolé, SMES, tensions transitoires, protection contre le quench, aimant fort champ, semi-imprégnation.*

Towards very high energy density insulated Rare-EarthBaCuO magnets

REBCO HTS superconducting materials make it possible to consider coils with very high energy densities, because they combine high critical current densities under strong magnetic field and a very high mechanical strength. However, the implementation of these materials is remains difficult, as they present performance inhomogeneities at the microscopic scale that have a potentially destructive impact at the device scale. In this PhD, credible solutions for insulated high energy density REBCO magnets are proposed. This work was conducted in the framework of the BOSSE project, which aims at the realization of a 12 T / 1 MJ REBCO magnet used as SMES.
Reliable protection of insulated REBCO coils against thermal runaway can be achieved by early detection of local dissipative conditions. However, the transient voltages observed during the current variations makes the detection challenging. This transient electromagnetic behavior of REBCO insulated coils was studied experimentally and numerically on a heavily instrumented test coil, enabling a detailed interpretation of the measured voltages.
This new understanding was applied to the BOSSE project, starting with the tests of the prototype Double Pancake (DP) in self and background magnetic field, to safely reach the critical current and validate the design of the solenoid. Each of the 21 series DPs of the BOSSE solenoid are then tested in liquid helium up to their rated current for quality control. Finally, 2 preliminary assemblies of 3 and 5 DPs were tested using the same early detection and protection approach, validating the protection strategies of the full-scale device.
Based on the understanding gained from these new developments, a new high-performance REBCO coil design with conductive cooling capability is proposed.

Keywords: *Insulated REBCO magnet, SMES, transient voltages, quench protection, high field magnet, edge-impregnation.*